SYNTHESIS AND BIOLOGICAL EVALUATION OF PYRIMIDINE AND ISOQUINOLINE INHIBITORS AS POTENTIAL ANTIMALARIAL ANTIFOLATES AND TRANSMISSION-BLOCKING AGENTS

by

Khonzisizwe Somandi

(1153883)

Degree of Doctor of Philosophy:

A thesis submitted to the Faculty of Science, University of the Witwatersrand, Johannesburg, in fulfilment of the requirements for the degree of Doctor of Philosophy

Supervisor: Professor Amanda Rousseau

24 April **2023** in Johannesburg

Declaration

I declare that this thesis has been written and compiled by myself and confirm that the work presented in this thesis is my own, except for the biological testing, which was performed by colleagues at BIOTEC in Thailand and at the University of Pretoria and the CSIR. The work presented in this thesis was carried out by myself under the supervision of Professor A.L. Rousseau. This thesis is being submitted for the Doctor of Philosophy Degree in Science in the University of the Witwatersrand, Johannesburg and I declare that the work has not be submitted before for any other degree or professional qualification in any other university.

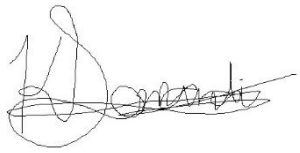

_____

Khonzisizwe Somandi

24th day of April 2023 at Johannesburg.

ABSTRACT

Malaria continues to be a serious threat, in particular to the African region. According to the World Health Organisation, in 2021, 247 million malaria cases were reported globally of which 95 % and 96 % of malaria related deaths were in the African region. The persistence of the disease, amongst it being difficult to treat and kill, is also attributed to its resistance to currently used antimalarial agents, including class II antifolate drugs such as pyrimethamine, which are used to target the *P. falciparum* dihydrofolate reductase (*Pf*DHFR) enzyme. However many other drugs have lost activity because of mutations in the active site of the enzyme.

The first component of the research described herein has been to synthesise 2,4-diaminopyrimidine analogues that work by disrupting folate metabolism by inhibiting *Pf*DHFR. In a four step synthetic approach we have successfully prepared a series of pyrimidine-2,4-diamines possessing a flexible four atom linker at the 5-position of the pyrimidine ring (in yields of 33-96 %), which could prove advantageous in avoiding clashes with mutant amino acids in the enzyme active site. Enzyme inhibition assays of the compounds have shown successful inhibition of the wild-type (WT) and quadruple mutant (QM) *Pf*DHFR in nM ranges (*K*i-WT; 1.27 – 242.72 nM and K_i-QM; 13.01 – 208.23 nM). A moderate antiplasmodial activity *in vitro* was observed for all compounds assessed against the drug sensitive strain IC_{50} (TM4/8.2) 0.42 – 28.0 µM and the drug resistant strain IC_{50}(V1S) 3.72 – 53.7 µM.

The second component of the research focuses on the synthesis of transmission-blocking analogues that target the sexual stage of the malaria parasite life cycle and work by inhibiting stage IV/V gametocytes which prevents the transmission of the parasite from the human host back to the feeding mosquito. A series of 3-substituted-isoquinolin-1-yl benzamides, derivatives of the hit compound MMV1581558, have been successfully prepared in a synthetic protocol that involves only two steps from relatively simple precursors, in yields ranging between 14 – 68 %. All analogues are undergoing biological assessment against stage IV/V gametocytes and currently we have only received the results of the asexual blood stage activity assay, with most analogues displaying only moderate activity (IC_{50} 1.18 – 7 µM). Additional biological assays are still underway.

DEDICATION

In Loving Memory

Mxolisi Somandi

1962 - 2019

This thesis is dedicated to my late father, Rev. Mxolisi Somandi. A man who believed in me when I most doubted myself. In one of our final conversations before you passed on, you urged me to take on this journey and promised to support me in any way until its end. I am where you inspired me to be now-where I desired to be; and although you may not be living amongst us anymore, your spirit lives amongst and your spiritual support has been heartfelt throughout this journey.

ACKNOWLEDGEMENTS AND THANKS

First and most importantly, I would like to thank Professor Amanda Rousseau for the major role you have had in my postgraduate journey. From being supervised by you in a semester project in my Honours year to being supervised by you in my Masters and PhD research, I consider myself blessed to have been around someone who is a fountain of knowledge, compassionate and always pushing me to perform at my absolute best. Your words of encouragement and constant catch-up chats have truly made this journey much more fulfilling.

To the Wits Organic group, Prof. de Koning, Prof. Bode, Prof. Jo Michael, Dr Kennedy, Dr Zimuwandeyi, Dr Ntsimango, thank you for your support and gruelling questions and suggestions especially during our group presentations, these have truly groomed me into a better scientist and communicator. To my lab mates, Sandile, Lebo, Aneesa, Nafisa, Cecilia, Alex, Matthew, Bianca and both Kabelo's, thank you for making the lab a fun and exciting place to be and an environment where we can freely share ideas and learn from each other.

A special thanks to my colleagues, Dr Kamo Butsi, who co-supervised me in my Honours and worked with me in my Masters and PhD years, although we were working on separate projects your advice and suggestions were invaluable. Matthew Maree, a special thanks to you for your constant availability and assistance with the molecular modelling part of my research, thank you for patience and tremendous help. Similarly to Edward Chavalala and Kabelo Dilebo, thank you as well for also being available to help with the molecular modelling part of my research. To Lebogang Tefu, it was a pleasure working with you in my second project, your hard working and charismatic nature made the project much more enjoyable.

A special thanks to the CSIR for allowing me to use the CHPC system for molecular modelling.

Dr Zimuwandeyi and Dr Kotzè, a special thanks for the NMR training and also keeping the instruments performing optimally for us to run our experiments.

Dr Zimuwandeyi and Dr Selepe (University of Pretoria), my special gratitude goes to you for running the variable temperature NMR for me. Without you, this project would have not been possible.

To Dr Eric Morifi, thank you for the HRMS training and ensuring that the HRMS instrument is also in peak condition.

Professor Fernandes, thank you for running countless crystal structures for me, this truly helped in the progression of my research.

To the collaborators who conducted biological assays; Dr S. Kamchonwongpaisan and the team at BIOTEC in Thailand. The University of Pretoria and the CSIR in teams led by Professor L-M. Birkholtz and Dr M. van der Watt. I thank you for your efforts in performing biological assays for my compounds and ensuring that the results reported are of a high standard.

A special thanks to the University of the Witwatersrand for providing the facilities to do my research and for offering me the Postgraduate Merit Award which aided me financially and a huge thank you to the National Research Foundation (NRF) for the financial support.

To my mother (Nomfundo Somandi) thank you for your constant prayers and support throughout my research and to my siblings, thank you for always encouraging and motivating me.

To a very special person in my life, Lutho Zono. Thank you for always been there. You have witnessed this journey first hand and you have supported, inspired and encouraged me throughout. I truly thank you for always being there for me.

Most importantly, I am thankful to God, for the constant protection, guidance and wisdom. I am where I am today because of your grace and mercy.

LIST OF ABBREVIATIONS

µM	Micromolar
ABS	Asexual blood stage
AcOH	Acetic acid
ACTs	Artemisinin Combination Therapy
AP2-G	Apetala 2-G
ATP	Adenosine triphosphate
CDI	1,1'-Carbonyldiimidazole
CSIR	Council for Scientific and Industrial Research
CSP	Circumsporozoite protein
DCC	*N, N′*-Dicyclohexylcarbodiimide
DCE	Dichloroethane
DCM	Dichloromethane
DDT	Dichloro-diphenyl-trichloroethane
DHA	Dihydroartemisinin
DHF	Dihydrofolate/ Dihydrofolic acid
DHFR	Dihydrofolate reductase
DHNA	Dihydroneopterin aldolase
DHPS	Dihydropteroate synthase
DMSO	Dimethyl sulfoxide
DNA	Deoxyribonucleic acid
DNDi	Drugs for Neglected Diseases Initiative
DVI	Dengue Vaccine initiative
EtOAc	Ethyl acetate
EtOH	Ethanol
EVI	European Vaccine Initiative
FIND	Foundation for Innovative New Diagnostics
GSK	GlaxoSmithKline
GTP	Guanosine triphosphate
HRMS	High resolution mass spectrometry
IFD	Induced fit docking

ITN	Insecticide treated nets
IPM	International Partnerships for Microbicides
IR	Infrared
IRS	Indoor residual spraying
KO^tBu	Potassium tertiary butoxide
LAH	Lithium aluminium hydride
MCR	Multicomponent coupling reaction
MeOH	Methanol
MMV	Medicines for Malaria Venture
MTHFR	Methylene tetrahydrofolate reductase
n-BuLi	n-Butyllithium
nM	Nanomolar
NMR	Nuclear magnetic resonance
OSM	Open Source Malaria
p-ABA	*p*-Aminobenzoic acid
PDPs	Product Development Partnerships
Pf	*Plasmodium falciparum*
PfHda2	*P. falciparum* histone deacetylase 2
PfHP1	*P. falciparum* heterochromatin protein 1
PLP	Pyridoxal phosphate
PPPK	Pyrophosphokinase
PRB	Pandemic response box
PYR	Pyrimethamine
QM	Quadruple mutant
RNA	Ribonucleic acid
SAM	*S*-adenosylmethionine
SAR	Structure activity relationships
SDX	Sulfadoxine
SHMT	Serine hydroxymethyltransferase
TBAB	Tetrabutylammonium bromide
TCAMS	Tres Cantos Antimalarial
THF (biology)	Tetrahydrofolate

THF (chemistry)	Tetrahydrofuran
TLC	Thin layer chromatography
WHO	World Health Organisation
WT	Wild-type
XP	Extra precision

TABLE OF CONTENTS

PREFACE

INTRODUCTION-A brief overview of malaria

Malaria distribution and mortality

Malaria continues to be a growing health burden in Africa. The *Plasmodium* parasite causes malaria, and transmission to humans occurs by inoculation from a female *Anopheles* mosquito that is infected.[1] There are several known parasite species that cause malaria in humans, including, *P. vivax, P. malariae, P. ovale, P. knowlesi* and *P. falciparum*.[2] *P. falciparum* is prevalent in Africa, causes the most fatalities,[1] and is the focus of this research project.

The malaria disease distribution is very climate and socio-economic specific. The disease is common in developing regions where the humidity and temperatures are high. Some of these regions include Africa, South/South East Asia, Central/South America, Dominican Republic and Oceania to name a few.[3] The African region, however, continues to have disproportionally high malaria infections.[1] According to the World Health Organisation, in 2021 there were 247 million malaria cases recorded globally, with 95% of those cases being caused by *P. falciparum* infections in the African region. Over 50% of all malaria deaths globally occur in four African countries, namely, Nigeria, the Democratic Republic of the Congo, United Republic of Tanzania, and Mozambique.[1] Other African countries that are also a concern in malaria related cases and deaths include Angola, Uganda and Burkina Faso.[3] Additionally, 80% of global malaria deaths were of children under the age of 5 years.[1]

These alarming statistics clearly indicate that this disease is largely an African problem and is lethal amongst very young children, despite the fact that malaria is treatable. There is therefore a need to find more effective ways of treating malaria.

Over the past 20 years, scientists have been dedicated to reducing malaria deaths in affected African populations. A steady decline in child (below 5 years) and population mortality has been observed since 2000, **Figure 1** and **Figure 2** are illustrations of this.[3,4] Notably, the global annual deaths have decreased from about 900 000 to 630 000 and of this, the African region has decreased its annual death toll from about 840 000 to 602 000, **Figure 1**.[4] Child mortality has also declined, as illustrated in **Figure 2**, where some regions have eliminated child mortality due to malaria infections.

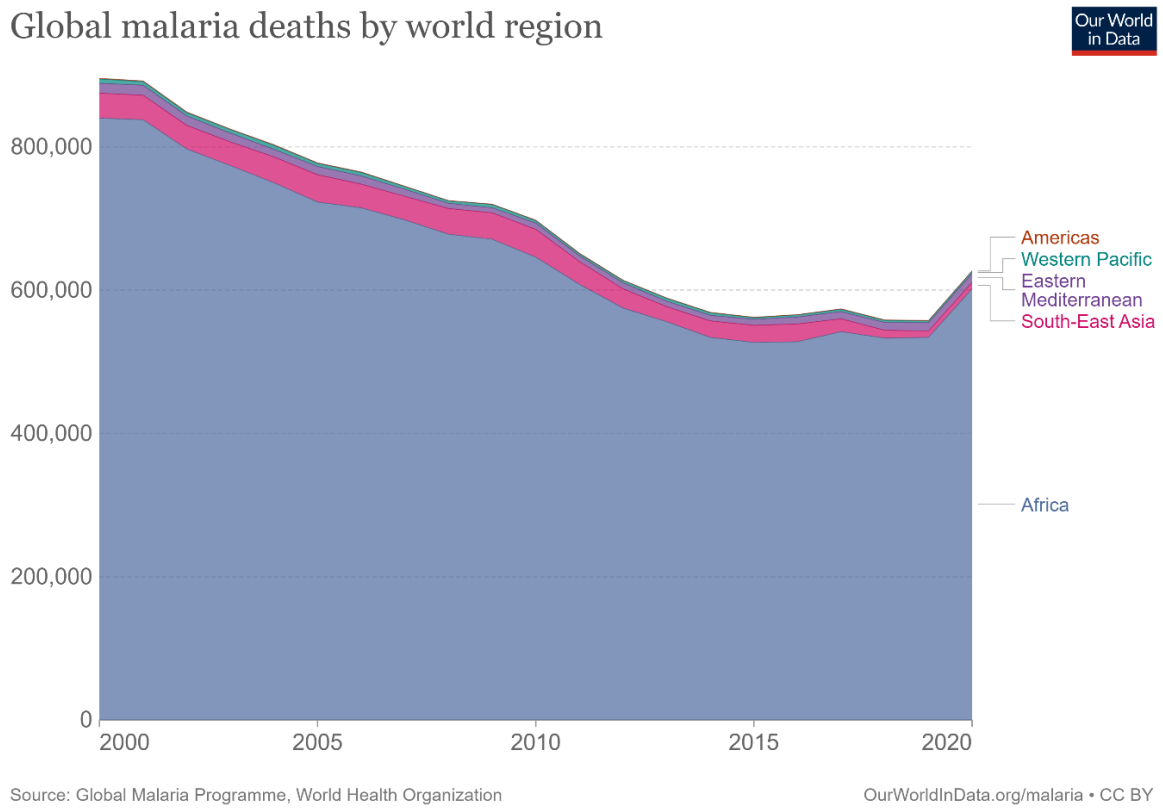

Figure 1: Global annual malaria deaths from 2000 to 2020 in regions with high malaria infections.[4]

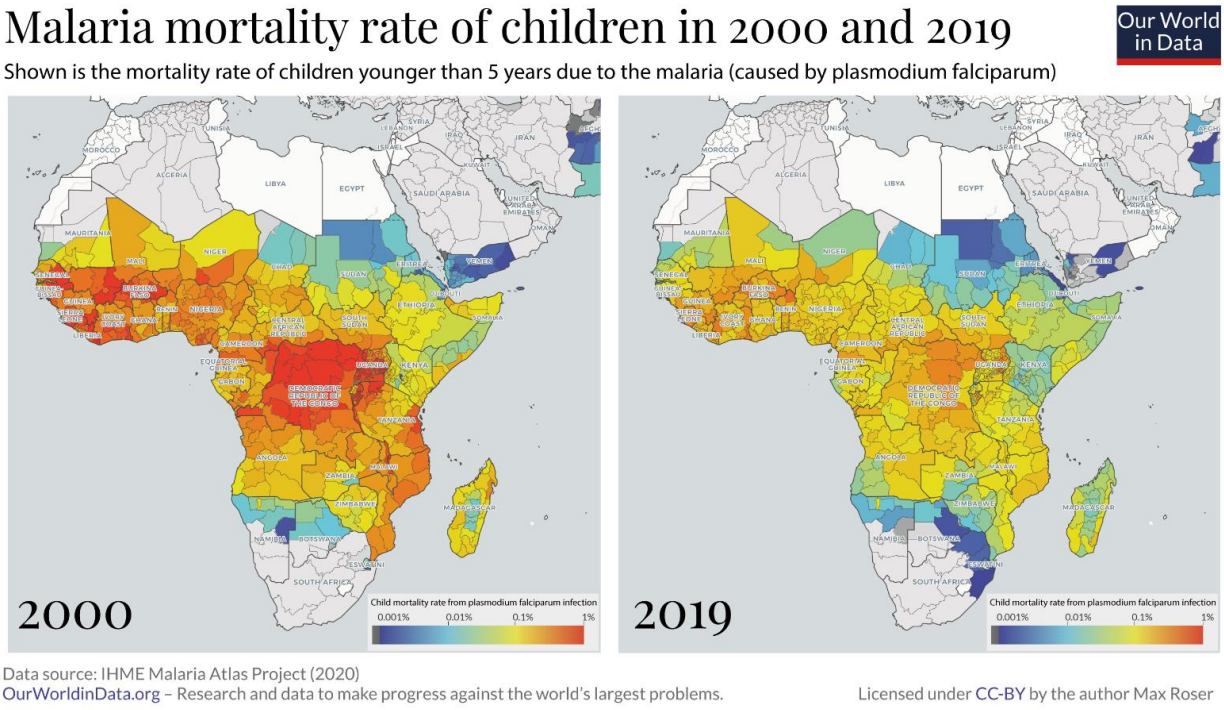

Figure 2: Mortality rate of children under the age of 5 years from 2000 to 2019 in the African region.[4]

This is promising progress for the eradication of malaria as this highlights how preventative measures for malaria, which is discussed below, are key components to the eradication of the disease. However, it is also observed that there has been a stagnant period from about the year 2015, with an increase in malaria related deaths in 2020 which could be attributed to disruptions caused by the Covid-19 pandemic,[3] **Figure 1**. This is indicative that more still needs to be done to alleviate the malaria burden and eventually eradicate the disease.

Malaria parasite life cycle

An in-depth knowledge of the malaria parasite life cycle remains a key component in the potential success of drug design and the development of antimalarial agents, as understanding the life cycle provides much needed information regarding potential novel targets within the parasite which can be exploited to synthesise a desirable and potentially effective drug.

An overview of the life cycle of the malaria parasite is given in **Figure 3**.

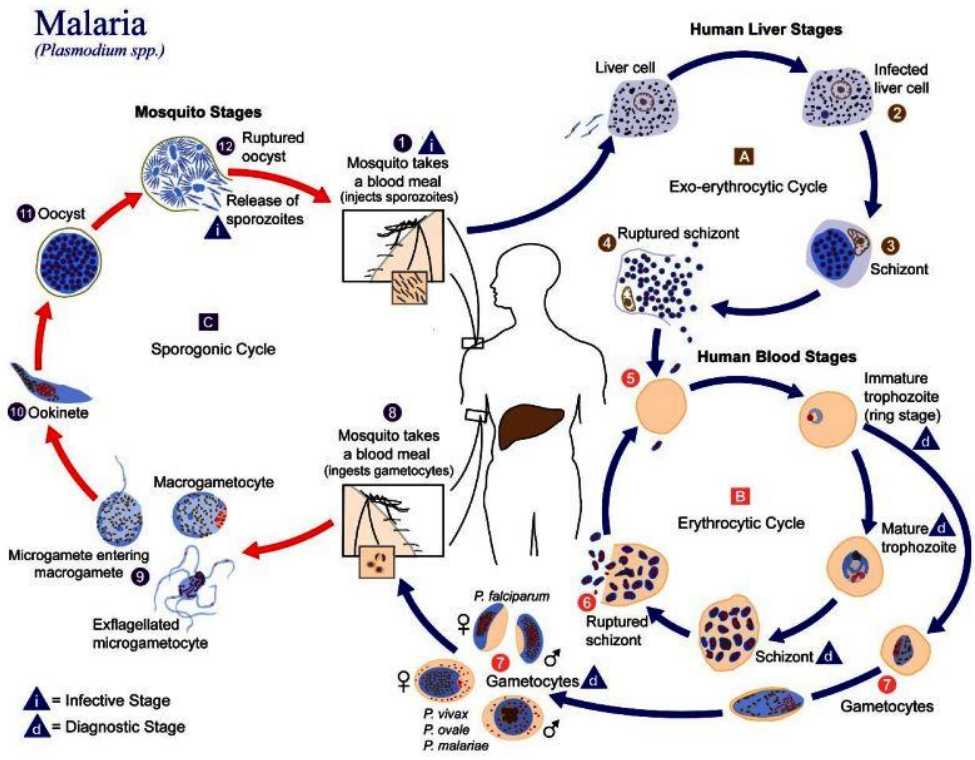

Figure 3: Illustration of the malaria parasite life cycle.[5]

The malaria parasite utilises two hosts to complete its life cycle: the human and the mosquito. When taking a blood meal, an infected female *Anopheles* mosquito injects sporozoites into the human host (Figure 3, annotation 1). The liver cells are infected (Figure 3, annotation 2) and mature into schizonts (Figure 3, annotation 3) that rupture and release merozoites (Figure 3, annotation 4), which infect red blood cells (Figure 3, annotation 5). Note that the species *P. ovale* and *P. vivax* have a dormant stage [hypnozoites] that can stay in the liver for weeks or years and causes relapse by delayed bloodstream invasion,[5] however this is absent from our species of interest, *P. falciparum*. The initial replication of the parasite in the liver (exo-erythrocytic schizogony (Figure 3, annotation A)) is followed by an asexual multiplication in the erythrocytes (erythrocytic schizogony (Figure 3, annotation B)). Immature trophozoites develop and form schizonts that rupture and release more merozoites (Figure 3, annotation 6). Some evolve and form gametocytes (Figure 3, annotation 7), which are the sexual erythrocytic stages of the parasite.[5]

During a blood meal on a human host, an *Anopheles* mosquito then ingests these female (macrogametocytes) and male (microgametocytes) gametocytes (Figure 3, annotation 8). Male gametocytes penetrate the female gametocytes forming zygotes in the mosquito (Figure 3, annotation 9) which then become ookinetes that are elongated and motile (Figure 3, annotation 10) and invade the mosquito's midgut wall, developing into oocysts (Figure 3, annotation 11).[6] The oocysts develop, rupture, and release sporozoites (Figure 3, annotation 12) that migrate to the salivary glands of the mosquito. Injecting these sporozoites (Figure 3, annotation 1) into a new human host continues the malaria parasite life cycle. The multiplication of the parasite which occurs within the mosquito is called the 'Sporogonic cycle' (Figure 3, annotation C).[5]

As sexual reproduction occurs in the mosquito, the mosquito should be called the "host" and humans the vector. However, throughout literature, the mosquito is referred to as the vector, and humans, the host, and this is the approach adopted in this thesis.

Preventative measures for malaria

Malaria prevention strategies are key components in the fight against the disease. These strategies can either prevent malaria infections entirely, i.e., (i) vector control (in this case of the *Anopheles* mosquito), or these strategies can help cure malaria and reduce mortality and transmission, i.e. (ii) vaccines and (iii) chemotherapy.

i) Vector control

The two main vector control interventions are indoor residual spraying (IRS) of insecticides and the use of insecticide treated nets (ITN).[1] These strategies can be used together to achieve the best malarial control results.[6] Both these strategies employ the use of insecticides to kill the mosquito that bites or rests indoors.[7] One of the earliest used synthetic insecticides was DDT **1** (dichloro-diphenyl-trichloroethane), developed in the 1940's, **Figure 4**.[8] This insecticide achieved great success in the prevention and control of malaria, however it had to be discontinued in most countries because of its negative impact on wildlife, its adverse environmental effects, its persistence in the environment and because of its risk as a probable human carcinogen.[8] In some developing countries, however, DDT is still used for essential public health purposes, e.g. its use in African countries for malaria vector control. Currently, pyrethroids, of the general structure **2**, are the most commonly used insecticides, **Figure 4**.[7] These are synthetic derivatives of naturally occurring pyrethrin insecticides found in the extract from the flowers Chrysanthemum cinerariaefolium.[9] They work by binding to and disrupting the voltage-gated sodium channels of insect nerves.[9] Unfortunately, several species of *Anopheles* mosquito have been reported to have developed resistance against this class of insecticides.[3] The WHO also reports that 78 countries have found insecticide resistant mosquitoes to at least 1 of the 4 commonly-used insecticide classes in the period 2010–2019, these include, pyrethroids **2**, carbamates **3**, organophosphates **4**, and organochlorines, e.g. DDT **1**, **Figure 4**. Additionally, 29 countries have reported mosquito resistance to all main types of insecticides.[1,10]

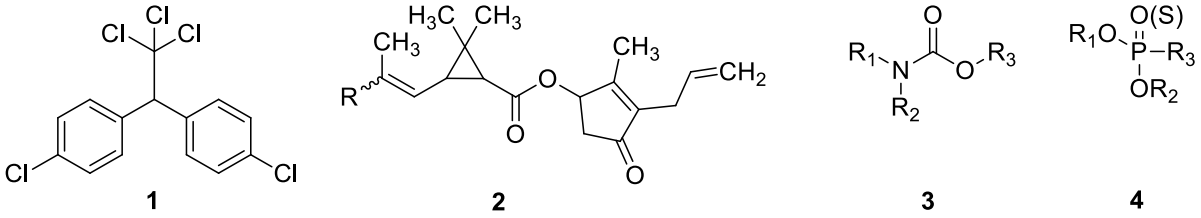

Figure 4: Structure of DDT (1) and general structure of commonly used insecticides pyrethroids (2), carbamates (3) and organophosphates (4).

ii) Vaccines

One of the most noticeable interventions to help control malaria has been an effective malaria vaccine. Very few vaccine candidates have demonstrated sufficient efficacy. The most notable vaccine to date is the RTS,S/AS01 vaccine produced by GlaxoSmithKline (GSK).[11] This is the only vaccine that has gone to phase III trials and has reproducible efficacy in different populations. RTS,S/AS01 is a recombinant protein vaccine that targets the circumsporozoite protein (CSP) of *P. falciparum*, expressed at the pre-erythrocytic stage of infection.[3] Although considered efficacious, the vaccine displayed a low efficacy in phase III trials with 36 % efficacy against clinical malaria.[11] This was observed in children 5 and 17 months old within 4 years after being vaccinated and receiving a booster 21 months later.[11] It was also reported that the RTS,S/AS01 efficacy peaked at ~60–70% in the initial 6 months of receiving a vaccination, but rapidly declined in efficacy, and had limited or non-significant efficacy by 18 months.[3] The WHO and partners aim to achieve a malaria vaccine with efficacy >75% by the year 2030.[3]

Despite the lower than anticipated efficacy, the vaccine significantly reduces the severity of malaria in young children. As a result of this, in October 2021 the WHO recommended that the RTS,S/AS01 malaria vaccine be used more broadly among children living in regions with moderate to high *P. falciparum* malaria transmission.[1]

Another promising vaccine candidate is the novel R21/Matrix-M pre-erythrocytic malaria vaccine candidate, originally designed and developed at the University of Oxford.[12,13] Similar to RTS,S/AS01, R21 is also a recombinant protein vaccine.[12] Both vaccines possess the protein HBsAg, which is fused to the C-terminus and central repeats of the CSP, which self assemble into virus-like particles in yeast. A key difference however, is that R21 does not have excess HBsAg, whereas RTS,S does.[12] Additionally, in R21 only fusion protein moieties are present, whereas RTS,S comprises 20% with 80% being HBsAg monomers expressed individually, this therefore likely diminishes CSP coverage of the virus-like particle surface.[12]

The R21/Matrix-M vaccine displayed high immunogenicity in preclinical studies and therefore was selected for clinical development. Phase IIb trials have been conducted by Datoo *et al.* for the R21/Matrix-M vaccine for children aged 5–17 months in Nanoro, Burkina Faso, which is a malaria hotspot.[12] The vaccine was administered and the efficacy monitored after 6 months and 12 months respectively, after which, a booster was administered and similarly the efficacy analysed over a 6 month and 12 month period. Essentially, two groups (group 1 and group 2)

were treated with different compositions of adjuvant Matrix-M of the vaccine, i.e. for group 1, 5 µg R21/25 µg Matrix-M and for group 2, 5 µg R21/50 µg Matrix-M. The third group (group 3) was a control and received Rabivax-S. Each group had 150 participants. The findings reported that for the primary vaccine administration, group 1 showed an efficacy of 74 % in a period of 6 months and 71 % after 12 months. Group 2 showed 76 % (6 months) and 76 % (12 months).[12] After a booster shot was administered, results showed that for group 1 the efficacy was unchanged at 74 % in a period of 6 months and 71 % after 12 months. For group 2 however, an improvement of 78 % (6 months) and 80 % (12 months). Furthermore, a Cox regression model that compares group 1 and group 3 resulted in vaccine efficacy of 74% and a comparison of group 2 with group 3 resulted in 77% efficacy.[12] Only mild adverse effects were observed with the most common being a fever. These results therefore render the R21/Matrix-M vaccine a promising candidate.

In April 2023, Oxford University reported that the R21/Matrix-M vaccine has ongoing phase III clinical trials in Burkina Faso, Kenya, Mali and Tanzania with 4800 children enrolled.[13] Reports also state that the recent phase III trial data is also displaying high-levels of efficacy by the vaccine and a good safety profile.[13] These phase III trial results are expected to be reported later in the year.[13]

iii) Chemotherapy for malaria infections

Antimalarial agents are an essential tool to combat the effects of the growing malaria disease burden. The current antimalarial drugs used are split into three categories. These include aryl aminoalcohol compounds (such as quinine **5** and chloroquine **6**), antifolate compounds (such as pyrimethamine **7** and proguanil **8**) and artemisinin compounds (such as dihydroartemisinin (DHA) **9** and artesunate **10**), **Figure 5**.[2] Although most of these drugs are effective, in some regions the resistance towards each of these classes of drugs has been observed.[2] Artemisinin resistance is well characterised in Southeast Asia [14,15] and more recently in some regions outside Southeast Asia, including the Greater Mekong Subregion which extends from Cambodia to parts of Vietnam, Laos, Thailand, Myanmar, and China.[14] Chloroquine-resistant *P. falciparum* initially occurred in the 1950s in three to four areas in Southeast Asia, South America and Oceania. To date, the resistance to chloroquine has spread to almost every area worldwide where *P. falciparum* malaria is present.[15] Resistance to antifolates was initially observed in South America and Southeast Asia in the 1970s, shortly after their introduction.

Antifolate resistance in Africa was noted in the early 1980s in East Africa and in the late 1980s for West Africa. [16]

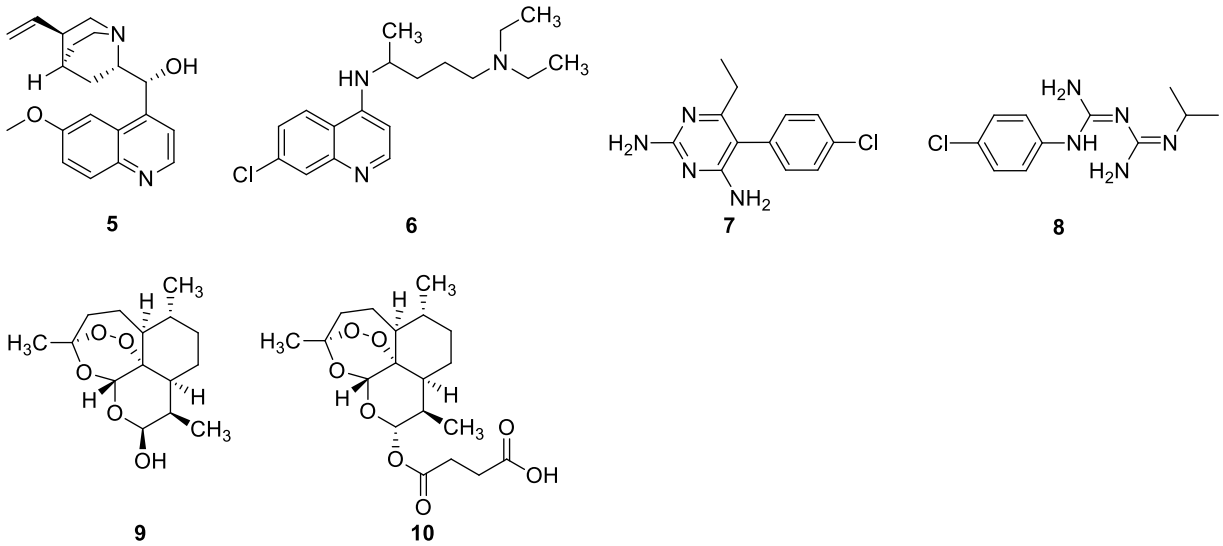

Figure 5: Antimalarial agents quinine (5), chloroquine (6), pyrimethamine (7), proguanil (8), dihydroartemisinin (9) artesunate (10).

The use of transmission-blocking agents as a more novel approach to eliminating the malaria disease by blocking the transmission from the infected human host to the feeding *Anopheles* mosquito is also being investigated.[17] There have been no clinically approved transmission-blocking drugs yet, however, some drug candidates are undergoing preclinical (e.g. MMV183 **11**); human volunteer (SJ733 **12**); and human exploratory (e.g. MMV390048 **13**) phases (**Figure 6**).[17]

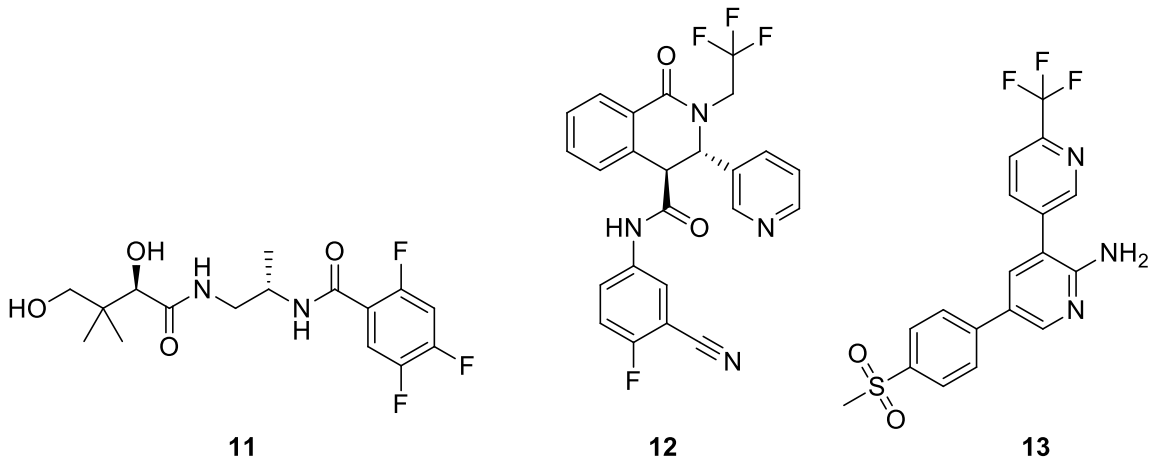

Figure 6: Some transmission-blocking candidates under development MMV183 (11), SJ733 (12), MMV390048 (13).

iv) Product Development Partnerships (PDPs) for malaria

PDP's are international, not-for-profit organisations that focus on the development of vaccines, drugs and diagnostics for neglected and poverty-related diseases, making them available at affordable costs.[18]

As research and development for new medicinal therapies is time consuming, expensive and risky, typically diseases affecting low and middle income countries are neglected as developing products for these diseases does not a have financial incentive for the pharmaceutical sector. The consequences of this are the gaps and restrictions in the global health innovation pipeline.[18]

Fortunately, the support of PDPs from bodies such as the German Federal Ministry of Education and Research have helped in bridging those gaps and restrictions in the global health innovation pipeline.[18] PDPs work similarly to the pharmaceutical sector in the way in which they develop drugs and vaccines. However, differences in PDPs from private companies is in their funding sources and partners involved, that is, funding will typically come from either governments or philanthropic donors.[18,19] Furthermore, PDPs promote and coordinate the collaborative research between partners from the public, private, academic, and philanthropic sector.

Some PDPs include Medicines for Malaria Venture (MMV), PATH Malaria, Dengue Vaccine initiative (DVI), Drugs for Neglected Diseases Initiative (DNDi), European Vaccine Initiative (EVI), Foundation for Innovative New Diagnostics (FIND) and International Partnerships for Microbicides (IPM).

The MMV and PATH organisations have played a major role in finding new antimalarial treatments. The MMV, founded in 1999, is based in Geneva, Switzerland.[19] MMV pave the way for innovation by allowing open collaborations with standard research and development processes which include compound screening and hit-to-lead identification, lead optimization, preclinical development and candidate selection, clinical phase 1, 2, and 3 trials, and drug registration and launch. MMV has collaborated with pharmaceutical companies such as Novartis, in the development and launch of a combination treatment for malaria, Coartem® Dispersible at an affordable cost.[19] This treatment is typically used for adults, however it is highly effective and well accepted by children as well.[19]

PATH was founded in the mid-1970s and has become one of the world's largest non-profit technology organizations that focuses on health concerns in developing countries.[19] PATH has

performed research on vaccine work and in the malaria field, the PATH Malaria Vaccine Initiative has collaborated with GlaxoSmithKline (GSK) Biologicals in developing a malaria vaccine which was in Phase 3 trials in African countries in 2011.[19]

There have also been open source efforts for malaria research. Open Source Drug Discovery is governed primarily by six laws; i) all data are open and all ideas are shared, ii) anyone can take part at any level, iii) there will be no patents, iv) suggestions are the best form of criticism, v) public discussion is much more valuable than private email and vi) an open project is bigger than and is not owned by any lab.[20] Pharmaceutical research organisiations such as GSK Tres Cantos and Novartis St. Jude's Children's Research Hospital have contributed to the open source movement and have released large data sets of antimalarial compounds derived from phenotypic high throughput screening. The GSK Tres Cantos Antimalarial (TCAMS) data set contained numerous hit compounds and provided many starting points for various research groups, which included independent groups, academic groups in collaboration with GSK or internal groups at GSK. Highly potent antimalarial compounds have been discovered by this Open Source Malaria (OSM) initiative, which include the potential antimalarials shown in **Figure 7** as starting points since they possess desirable pharmacokinetic properties and high ligand efficiency.[20]

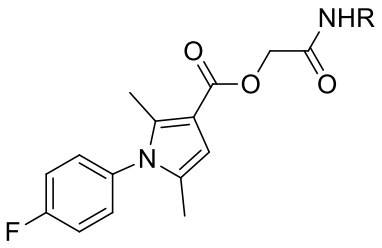

TCMDC-123812 (OSM-S-5)	R = H	IC_{50}, 177 - 610 nM (3D7 drug sensitive strain of *Pf*) $IC_{50,}$ 375 nM (K1 chloroquine resistant strain of *Pf*)
TCMDC-123794 (OSM-S-6)	R = 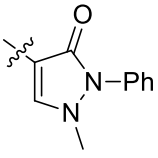	IC_{50}, 245 - 387 nM (3D7 drug sensitive strain of *Pf*) $IC_{50,}$ 152 nM (K1 chloroquine resistant strain of *Pf*)

Figure 7: Potent hit compounds from open source malaria research efforts.[20]

Open source has also greatly inspired a part of this research project as the hit compound MMV1581558, was identified from the MMV Pandemic Response Box and screened by researchers at the University of Pretoria. These efforts found this compound to be active against stage IV/V gametocytes and as part of a collaborative effort, we will be developing the MMV1581558 compound. This will be explored more in detail in the chapters that follow.

This open source effort has the potential to increase the efficiency of drug discovery and will allow for more cost effective treatments in diseases associated with low-income regions.

Aims of the project

This project will look at two aspects of the malaria parasite life cycle for intervention strategies: i) the liver and blood replication stage and ii) the gametocyte transmission stage from human to mosquito. In Part 1, the focus will be on the replication stage and disruption of folate metabolism in the parasite using antifolates.[21] Antifolate drugs are antimetabolites with antagonistic properties, which largely target the asexual stages of the malaria parasite.[22] Antimalarial antifolates work by inhibiting the folate metabolic enzymes dihydrofolate reductase (DHFR) and/or dihydropteroate synthase (DHPS).[21] In this project, we will focus on inhibition of DHFR, which will stop the parasite's cellular replication. Pyrimidine-based antifolates with this potential will be synthesised. In Part 2, the focus will be on the human to host transmission stage, by inhibition of the stage IV/V gametocytes. To this end, isoquinoline derivatives with potential transmission-blocking ability based on a hit molecule, MMV1581558 identified from the MMV pandemic response box, will be synthesised.[22] These compounds target the sexual stage gametocytes and will potentially display transmission-blocking activity, by death or inactivation of the gametocytes.[22]

PART 1-THE REPLICATION STAGE

CHAPTER 1: Folates and folate metabolism

In the malaria parasite life cycle in humans, replication occurs at the liver stage and at the blood stage. This replication is essentially dependant on folates and folate metabolism. Therefore, understanding the mechanism of action of antifolates is best achieved when understanding the important roles folates play in mammalian cells. Folates are responsible for the synthesis of nucleotides and certain amino acids. They achieve this by their important role in acceptance, redox processing, and transfer of one-carbon units. [23,24] The inability of humans to synthesise folate derivatives [24] makes it essential to include folates in our diet, along with other important nutrients such as vitamin B12 and B6.[23] Therefore, without folate derivatives, cell replication cannot take place.

1.1. Folate metabolism

Folate metabolism in the malaria parasite is a complex set of enzymatic processes in which folate derivatives are synthesised: the *de novo* pathway; or in which folates derivatives are recycled: the salvage pathway.[24] The metabolic processes differ between humans and the *Plasmodium* parasite in that humans can only salvage folic acid from nutrient sources. By comparison, malaria parasites are able to perform the *de novo* synthesis of folate cofactors, as well as recycle them via the salvage pathway. [24]

One-carbon metabolism reactions are folate requiring and include the synthesis of pyrimidines and purines. Additionally, these reactions include the metabolism of amino acids and the formation of the key methylating agent, *S*-adenosylmethionine (SAM), **Figure 8**. The polyglutamyl form of tetrahydrofolate (THF) has the role, in the one-carbon cycle, as the central folate acceptor.[23] This folate coenzyme principally functions to donate one-carbon units in key metabolic pathways.

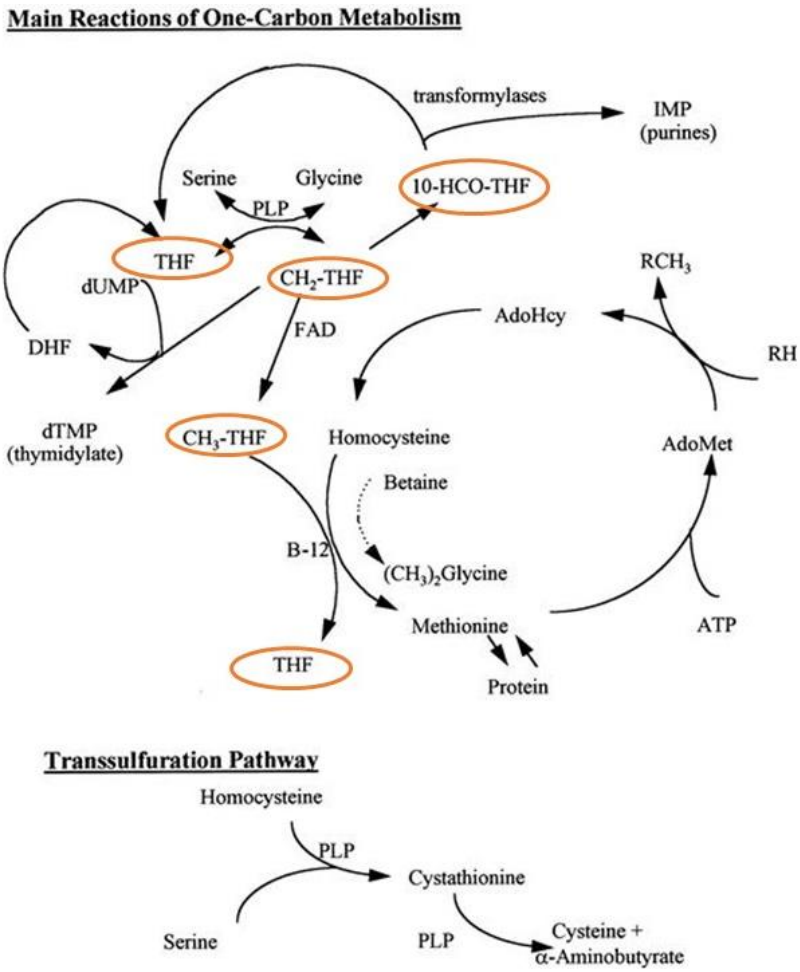

Figure 8: Main reactions of one carbon metabolism and the transsulfuration pathway in folate metabolism.[23] The central folate acceptor, THF is highlighted.

The cycle begins by converting THF to 5,10-methylene THF and glycine and the main carbon source of this reaction is the 3-carbon of serine. The enzyme that is important for this one carbon transfer is pyridoxal phosphate (PLP)-dependent serine hydroxymethyltransferase (SHMT).[23] A portion of the resulting 5,10-methylene-THF produced undergoes conversion, forming 5-methyl-THF via an irreversible enzymatic reduction, catalysed by the enzyme methylene tetrahydrofolate reductase (MTHFR).[25] The 5-methyl-THF has an N-5 group that is solely metabolically utilised for transfer to homocysteine. A removal of the methyl group from the 5-methyl-THF occurs by a methionine synthase reaction and transfers it to the vitamin B12 coenzyme before homocysteine, consequently forming methionine.[25] The methionine produced also has a role in protein synthesis and additionally it functions by donating a methyl group via conversion to SAM,[24] which takes part in over a hundred methyltransferase reactions with a diverse range of acceptor molecules.[25]

The methionine synthase reaction is also responsible for the regeneration of the THF needed for forming 5,10-methylene-THF and 10-formyl-THF which have direct utilisation in thymidylate and purine synthesis.[23] The thymidylate synthase reaction involves the 5,10-methylene-THF donating its CH_2 unit to become the thymidine methyl group, forming dihydrofolate (DHF), (**Figure 9**).[26] The DHF is used as a substrate by DHFR, the enzyme responsible for the reduction of DHF to THF in a NADPH-dependent reaction, **Figure 9**. The resulting THF is then reused in one-carbon metabolic processes already described.

As described above, DHFR is a key enzyme in folate metabolism, and it is ubiquitously expressed in all organisms.[27] Fortunately there is sufficient difference in amino acid sequences in the tertiary structures of DHFR enzymes in different organisms to get selectivity, for example, in the malaria parasite DHFR exists as a bifunctional dimer with thymidylate synthase. Due to the important role in nucleoside biosynthesis, DHFR has become a drug target in disease classes including malaria, cancer and for the treatment of bacterial infections. Inhibition of this enzyme with folate antagonists or antifolates, stops cell replication.[28]

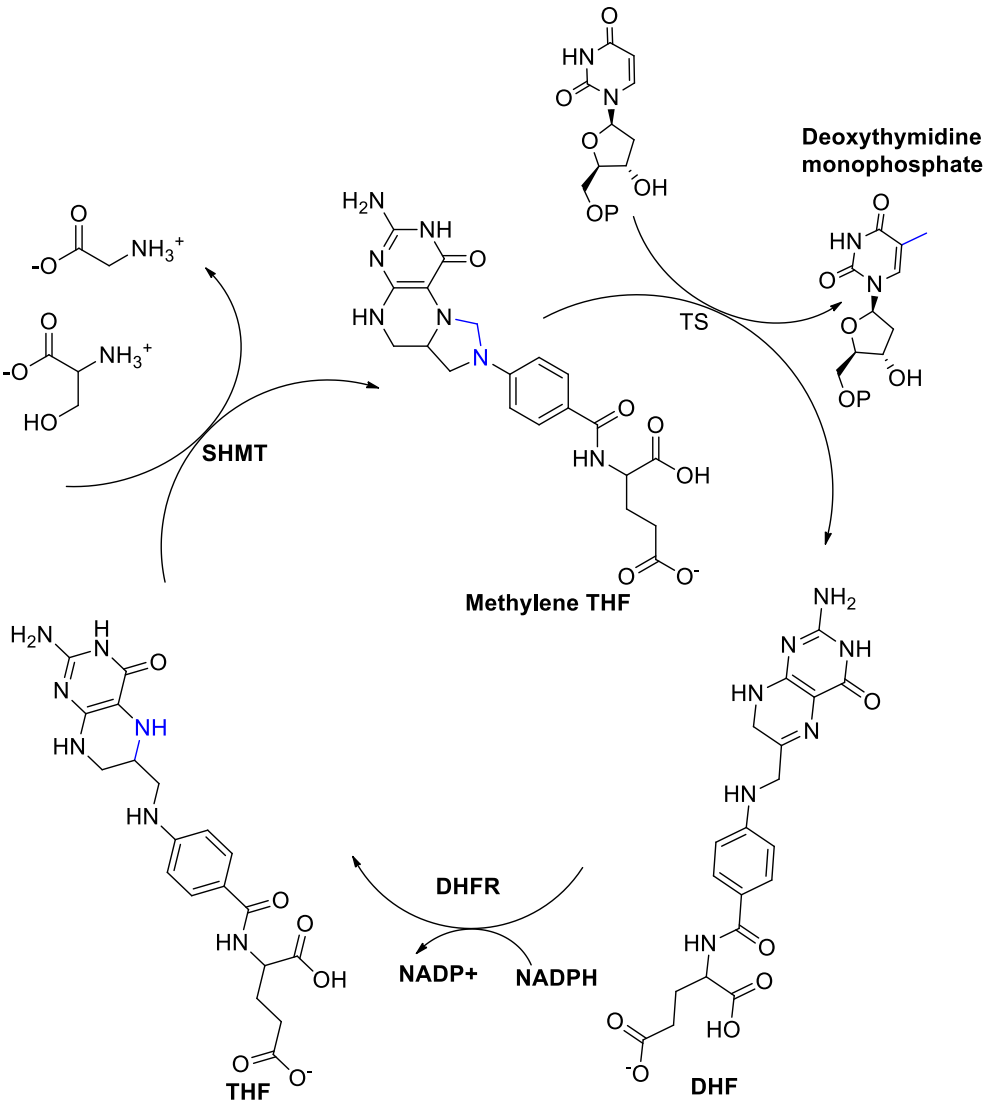

Figure 9: Representation of the key components in the folate salvage pathway.

SHMT: serine hydroxymethyltransferase; THF: tetrahydrofolate; DHFR: dihydrofolate reductase; DHF: dihydrofolate; NADP+/(H): nicotinamide adenine dinucleotide phosphate.

The *de novo* synthesis of folates present in some organisms utilises GTP in the initial step, **Figure 10**. This is followed by the removal of a triphosphate group prior to conversion to 6-hydroxymethyl-7,8-dihydropterin catalysed by dihydroneopterin aldolase (DHNA). This is thought to occur via non-enzymatic loss of pyrophosphate and subsequent removal of the last phosphate via non-specific phosphatase activity.[26] The host's salvage pathway is responsible for the synthesis of *p*-aminobenzoic acid (*p*-ABA), a substrate for dihydropteroate synthase,

however it can also be synthesised via the shikimate pathway.[26] Preceding complex enzyme specific reactions seen in **Figure 8**, the enzyme DHPS catalyses the condensation of *p*-ABA with dihydropteridine pyrophosphate in the *de novo* folate biosynthesis pathway, hence forming 7,8-dihydropteroate, which is a precursor of DHF.[24] The enzymes in the folate pathway prefer the polyglutamated forms of the substrates. There is still uncertainty as to whether the new folate that is synthesized in *P. falciparum* is polyglutamated, at the THF or DHF stage or both, however Yuthavong *et al*.[24], for simplicity's sake, displayed the process happening at the THF stage (see large brackets) [24] **Figure 10**.

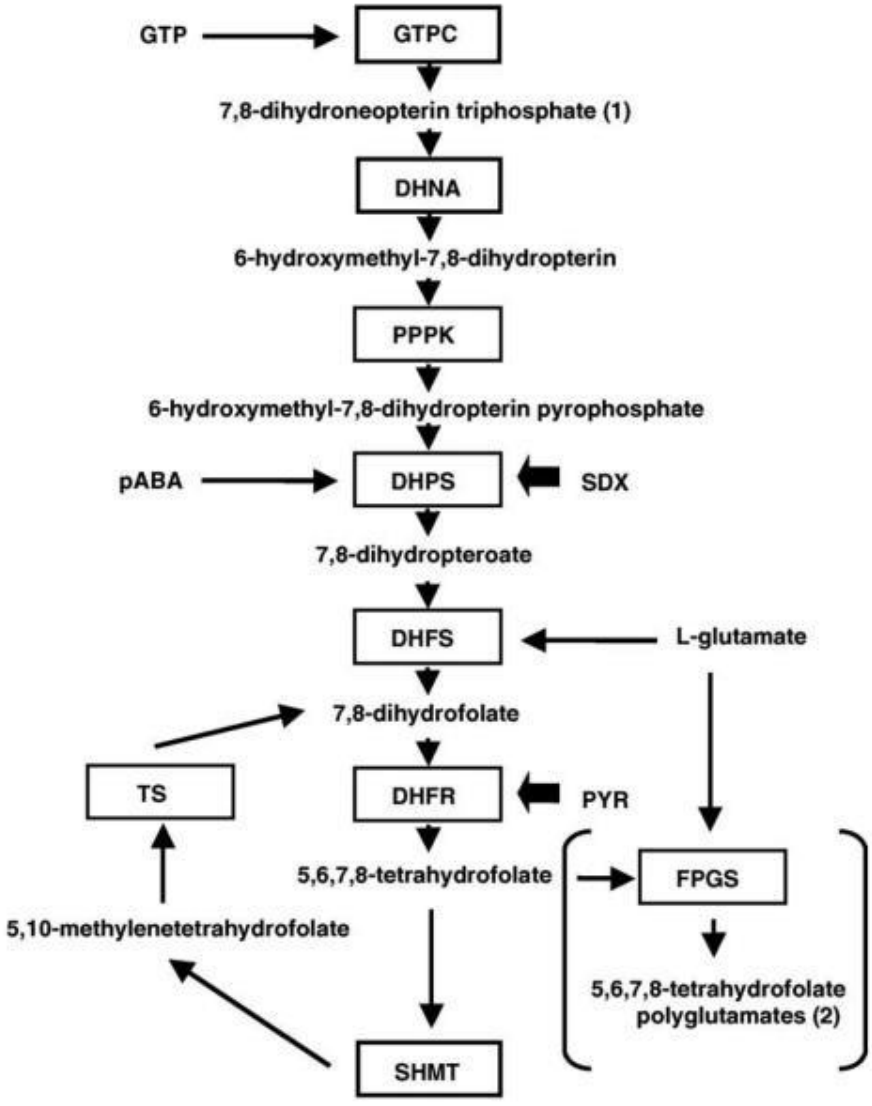

Figure 10: Illustration of the use of the key enzymes in the *de novo* pathway. [24]

GTPC: GTP cyclohydrolase I; DHNA: dihydroneopterin aldolase; PPPK: hydroxymethyldihydropterin pyrophosphokinase; DHFS: dihydrofolate synthase; FPGS: folylpolyglutamate synthase; TS: thymidylate synthase.[24]

Displayed above in **Figure 10** are essential substrates and enzymes required in the folate pathway to form THF and its use in the thymidylate cycle for the malaria parasite, using both the DHPS enzyme in the *de novo* pathway and the DHFR enzyme in the salvage pathway.[24] Antifolates target enzymes in these pathways and fall under two classes: class I antifolates, which inhibit dihydropteroate synthase (DHPS), and class II antifolates, which inhibit dihydrofolate reductase (DHFR).[29] Using both DHPS and DHFR inhibitors is synergistic, therefore they are often used in combination in the treatment of malaria. The class I antifolate, sulfadoxine (SDX) and its target DHPS as well as the class II antifolate, pyrimethamine (PYR) and its target DHFR are shown in **Figure 10** above.[24]

1.2. Antifolates and *P. falciparum* resistance

With the acquired knowledge of folate metabolism and the function of folate derivatives in cells, antifolates were developed. Antifolates have been studied for more than 50 years.[21] They are a class of anti-metabolites that act as antagonists and competitive inhibitors of the DHFR and DHPS enzymes.[23] By targeting folate metabolism, antifolates stop DNA/RNA synthesis and repair, cell division and protein synthesis.[24]

Antimalarial drug resistance, however, is a grave concern as it has resulted in an increase in the mortality and morbidity rate of the disease in recent years.[30] Drug resistance is observed globally for *P. falciparum*, *P. vivax*, and *P. malariae* parasites. *P. falciparum* has been reported to be resistant to various antimalarial drug classes, including class I antifolates.

1.2.1. Class I antifolates and *P. falciparum* resistance

Class I antifolates are classified as DHPS inhibitors. Currently used class I antifolates are sulfa-containing compounds.[24] The discovery that sulfa-drugs disrupt the *de novo* pathway led to the use of this class of compound as antimalarial agents.[29] These sulfa-drugs mimic *p*-ABA (*para*-aminobenzoic acid) **14** and inhibit DHPS by forming sulfadihydropteroate products which further disrupt folate metabolism.[24] Examples of class I antifolates include sulfadoxine **15** and dapsone **16**, **Figure 11**.[24,29] Dapsone **16**, is the most potent DHPS inhibitor synthesised. Sulfadoxine **15** and dapsone **16** differ from *p*-ABA **14** by the replacement of the carboxylic acid (red) functional group with a sulfonamide or sulfoxide functional group (blue), **Figure 11**.

Previous attempts to use class I antifolates as a monotherapy were unsuccessful due to their low efficacy and unacceptable toxicity.[29] The low efficacy could be attributed to the fact that the folate salvage pathway ensures adequate levels of folate derivatives, despite inhibition of

the *de novo* pathway by these drugs. Interest in this class of antifolates remained however, since it was demonstrated that they acted synergistically with DHFR inhibitors. This prompted their use in antifolate combination therapies.[29]

The long-acting class I antifolate, sulfadoxine **15**, has been used with pyrimethamine **7** (will be discussed later), a DHFR inhibitor in a combination therapy which is known as Fansidar®. The short acting class I antifolate, dapsone **16**, is also used with pyrimethamine **7** in a combination therapy which is known as Maloprim®. The use of Fansidar® is very common in most malaria endemic regions for malaria prevention in pregnancy.[31]

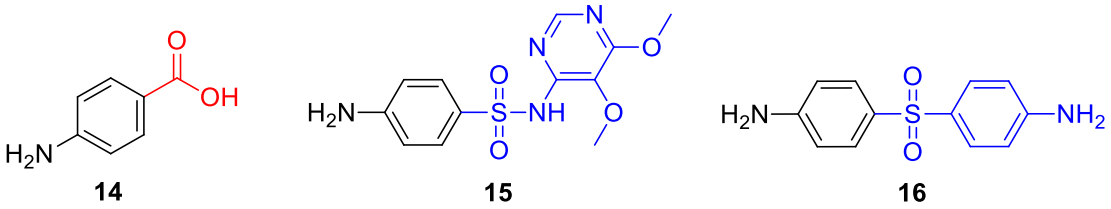

Figure 11: Structure of *p*-ABA (14) and class I antifolates; sulfadoxine (15) and dapsone (16).

Recent studies have shown that point mutations S436A, A437G, K540E, A581G, and A613S cause resistance to class I antifolates and therefore reduce the effectiveness of these drugs. [30,32]

1.2.2. Class II antifolates and *P. falciparum* resistance

Class II antifolates are a class of compounds that target DHFR.[29] Aminopterin (4-aminopteroyl-glutamic acid), (**17**, **Figure 12)**, was the first clinically accepted folate analogue. It was first clinically used in 1947 by Sydney Farder and co-workers, in the treatment of children with leukaemia.[29,33] Aminopterin's success was short-lived however, due to a developed toxicity [29] and it was also observed that within a few months of treatment, leukaemia cells grew again, and the newly growing leukaemia cells were resistant to aminopterin **17**.[33] This influenced the development of methotrexate (4-amino-10-methylpteroyl-glutamic acid) (**18**, **Figure 12**), which resulted in a better therapeutic index, hence receiving huge success in the treatment of certain cancers and autoimmune disorders.[21] Both aminopterin **17** and methotrexate **18** mimic the natural substrate of DHFR, dihydrofolic acid (DHF) **19**. Both compounds, aminopterin **17** and methotrexate **18**, respectively, replace the carbonyl functional group (red) of DHF **19** with an amine group (blue). In methotrexate **18**, the amine group (green) of DHF **19** is substituted with a methyl group (purple), **Figure 12**.

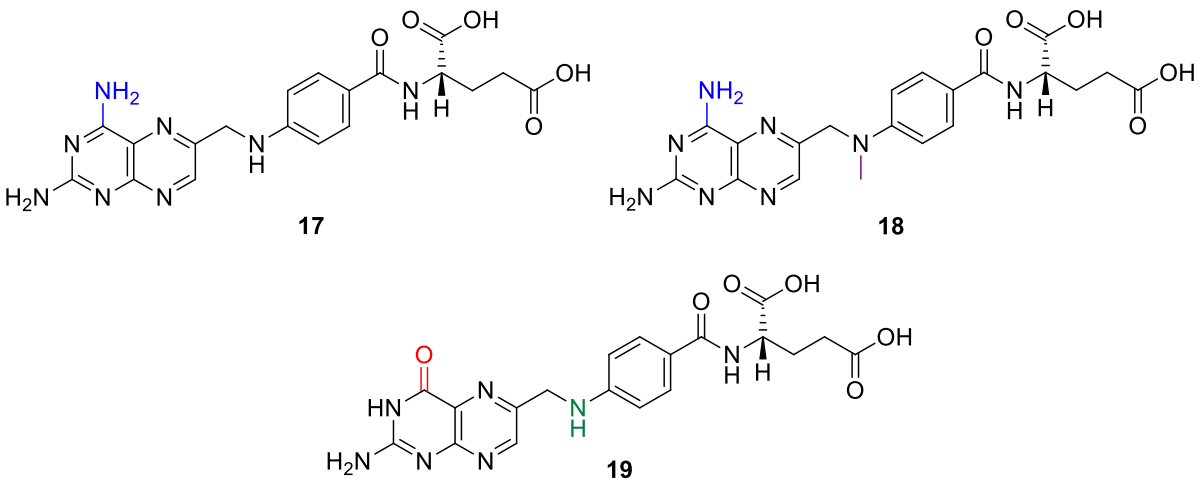

Figure 12: Structural comparison of aminopterin (17), methotrexate (18) and dihydrofolic acid (DHF) (19).

The first reported class II antimalarial antifolate was proguanil **8**, which was discovered in 1945, **Figure 13**. Its better activity and higher therapeutic index than quinine (**5**, **Figure 14**) against avian malaria in animal models prompted its use in humans.[29] Proguanil **8** is a prodrug which inhibits the DHFR enzyme after being metabolised *in vivo* to its dihydrotriazine form, cycloguanil **20** (**Figure 13**).[34] Proguanil **8** has been used as a prophylactic agent in monotherapy and synergistically with atovaquone **21**, **Figure 14** an inhibitor of electron-transport to the cytochrome bc1 complex (coenzyme Q) in a combination therapy called Malarone®.

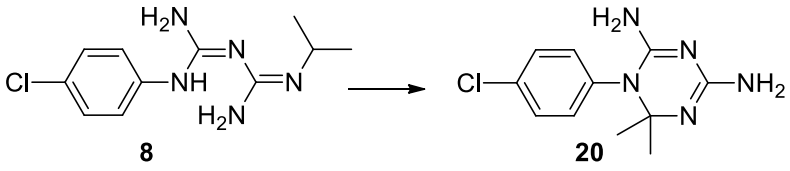

Figure 13: Structures of proguanil (8) and cycloguanil (20)

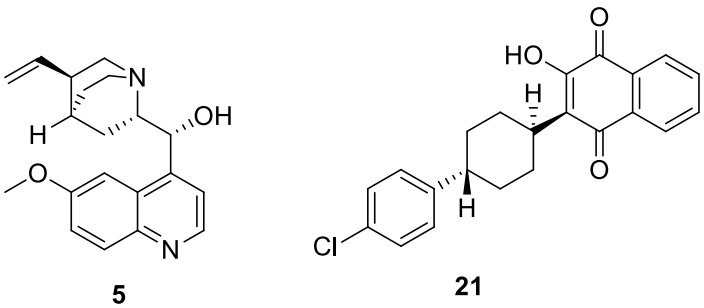

Figure 14: Structures of quinine (5) and atovaquone (21)

The success of proguanil **8** initiated the search for dihydrotriazine analogues. These findings made way for the discovery of chlorproguanil **22**, which cyclizes to its dihydrotriazine form chlorcycloguanil **23** *in vivo* (**Figure 15**). Chlorproguanil **22** comprises of a dichlorinated phenyl ring in contrast with the monochlorinated phenyl ring of proguanil and as previously mentioned, is also metabolised to the active metabolite, chlorcycloguanil **23**. The higher potency of chlorproguanil **22** compared to proguanil **8** has prompted its recommended use as a prophylactic agent at lower doses.[29] However, research has later demonstrated an inadequate prophylactic protection from this drug. This antifolate has been used in combination therapy with dapsone **16** under the name Lapdap®.[29]

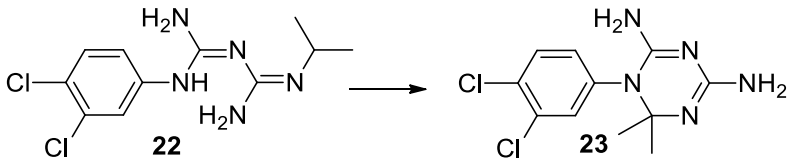

Figure 15: Structures of chlorproguanil (22) and chlorcycloguanil (23).

Clociguanil (BRL 50216) **24**, **Figure 16**, was also discovered. This is a derivative of chlorcycloguanil **23** and differs by possessing a methylene-oxy linker between the dihydrotriazine and the phenyl ring. The clinical evaluation of this compound, conducted in Africa, demonstrated that clociguanil showed good antimalarial properties, however it had an erratic bioavailability and was short acting,[29,35] which was not seen as an advantage over pyrimethamine **7** and proguanil **8**, hence the drug was abandoned.[29,35]

Other discoveries included BRL 6231 (WR 99210) **25**, **Figure 16**. This is a triazine derivative and possesses a five-atom linker between the dihydrotriazine ring and the chlorinated phenyl ring. In the early 1980s, WR 99210 **25** showed selective inhibition of parasite growth *in vitro*,[36] however, because of its low bioavailability, the biguanide pro-drug of WR 99210 **25**, PS-15 **26** (**Figure 16**) was developed. PS-15 **26** demonstrated improved bioavailability and a better potency than WR 99210 **25** in an *in vivo* model, which revived interest in this molecule for clinical use.

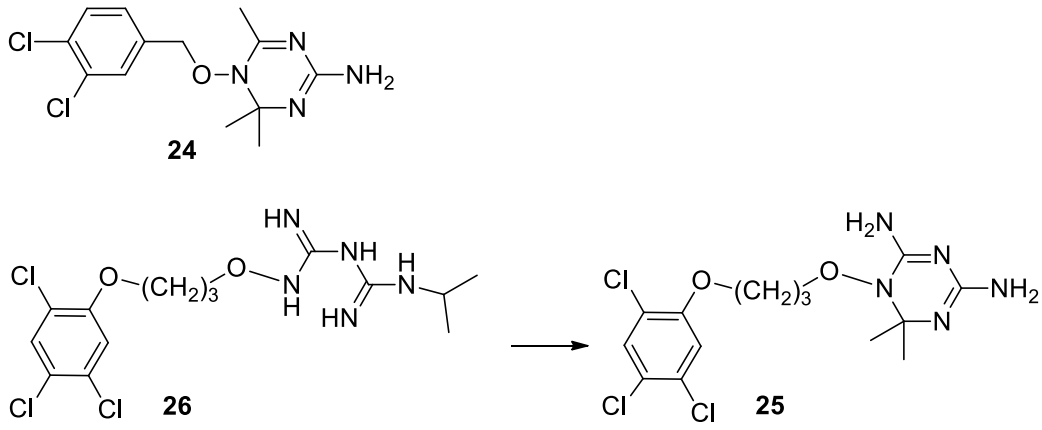

Figure 16: Structures of flexible class II antifolates; clociguanil (24) WR 99210 (25), and PS-15 (26).

Researchers attributed the increase in the potency of the cycloguanil analogues to the increase in chlorines in the phenyl rings as well as the increase in the length of the linker between the dihydrotriazine ring and the phenyl ring, which later become important in attempting to combat *P. falciparum* resistance.[29,37]

Pyrimethamine (**7**, **Figure 17)** is a class II antifolate belonging to the 2,4-diaminopyrimidine family.[38] Interest was initiated in these compounds when they were synthesised as folic acid analogues and evaluated in the treatment of tumours.[29] Falco *et al*.[39] observed the similarity of these compounds to proguanil (**8**, **Figure 13**) and hypothesised their potential antimalarial activity. A successful screening of these 2,4-diaminopyrimidines led to the identification of the antimalarial pyrimethamine **7**. It is the most utilised antimalarial antifolate agent to date. As previously mentioned, pyrimethamine **7** is used mostly in combination with sulfadoxine **15** or dapsone **16**, **Figure 11**, known as Fansidar® and Maloprim® respectively.[29,38] However it has also been used in monotherapy, but to a lesser extent and is sold under the brand name Daraprim.[29]

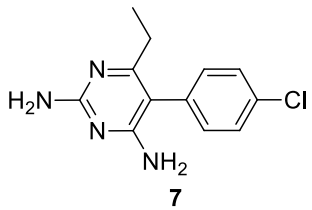

Figure 17: Structure of pyrimethamine (7)

As discussed previously, class II antifolates target the *Pf*DHFR enzyme. Research has shown that the following point mutations; N51I, C59R, S108N, and I164L cause drug resistance.[30,32] These mutations in the *Pf*DHFR enzyme have caused previously potent drugs such as pyrimethamine **7** and cycloguanil **20** to lose activity with IC_{50} values of > 90 μM against parasite strains bearing mutant forms of DHFR.[40] Mutations, S108N and C59R cause steric clashes with inhibitors in the DHFR active site, while mutations, N51I and I164L shift the chains around the active site, causing the binding affinity of small analogues to be reduced.[40]

When the *P. falciparum* resistant strain bearing quadruple mutant DHFR was observed and studied by researchers, findings showed that the N108 side chain of the mutant enzyme had steric clashes with the *p*-Cl atom of pyrimethamine **7**, causing decreased affinity to the mutant enzyme. However, on the contrary, this mutant strain was sensitive to WR 99210 **25**.[41] This can be attributed to the structure of WR99210 **25**. Unlike smaller molecules, such as pyrimethamine **7** or cycloguanil **20** that bear a rigid bi-aryl axis that restricts their conformation, WR 99210 **25** possesses a flexible five-atom linker chain. This is important because the inherent flexibility of WR 99210 **25** allows the molecule to avoid steric clashes due to mutant amino acids and the flexible side chain adopts a conformation which fits well in the active site, therefore contributing to binding.[42] This is illustrated in **Figure 18 (A-D)** by a molecular model representation of pyrimethamine **7** and WR99210 **25** binding to the active sites of both the wild type and quadruple mutant *Pf*DHFR. Furthermore, **Figure 18 (E-F)** shows how the binding position of pyrimethamine **7** changes poses in the active site of wild-type *Pf*DHFR (blue) and quadruple mutant *Pf*DHFR (red), this change in position may attribute to a reduced binding affinity in the quadruple mutant *Pf*DHFR. As for WR99210 **25**, the triazine core maintains its position and only the flexible linker changes conformation for facilitate favourable binding in the respective active sites.

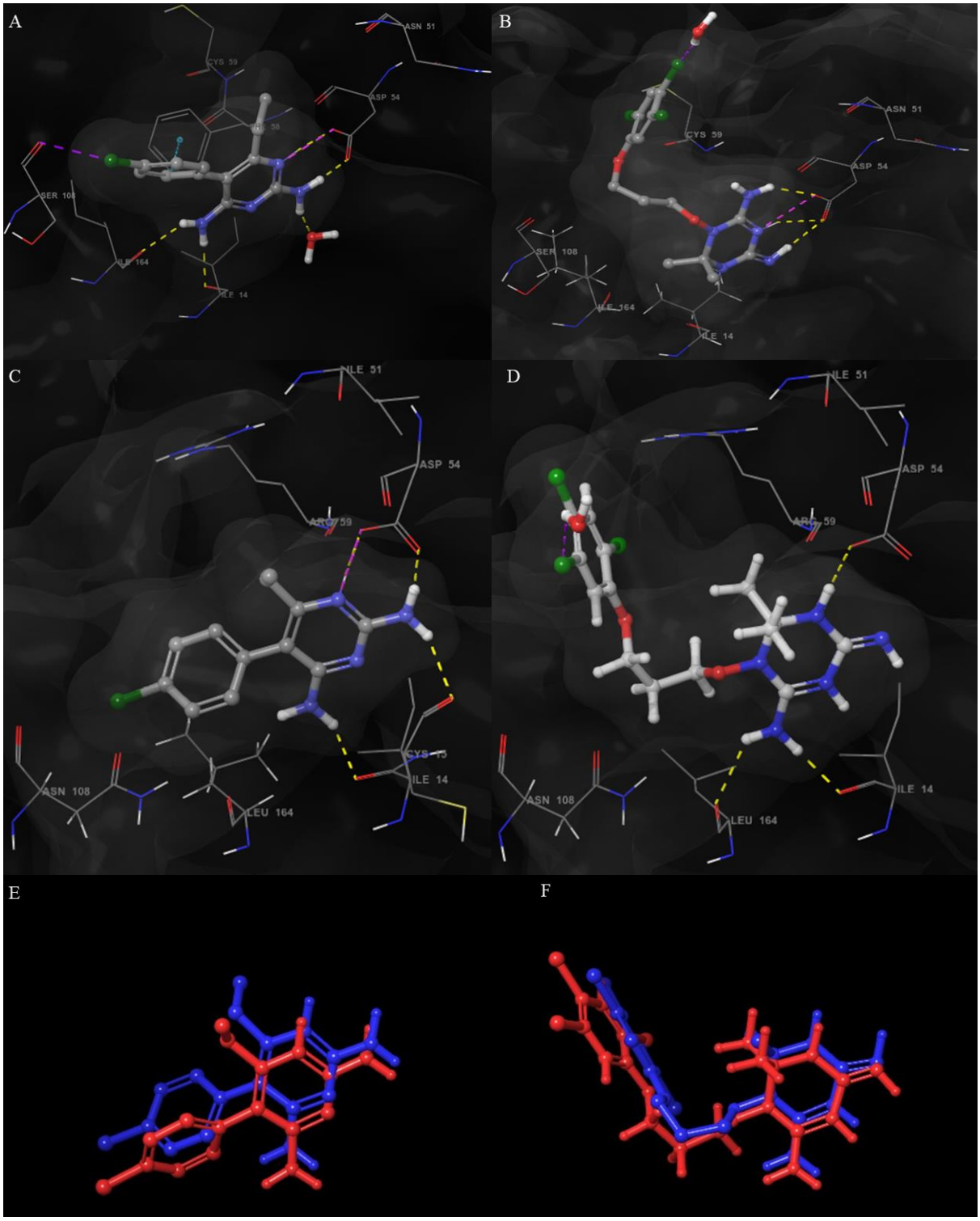

Figure 18: Molecular model illustrating the rigid binding of pyrimethamine (7) and the flexible binding nature of WR99210 (25) in both the wild-type and quadruple mutant *Pf*DHFR active sites. A-B: Comparison of pyrimethamine (A) and WR99210 (B) binding to wild-type *Pf*DHFR. C-D: Comparison of pyrimethamine (C) and WR99210 (D) binding to quadruple mutant *Pf*DHFR bearing the following point mutations, N51I, C59R,

S108N, and I164L.[43] **E-F: Overlay of pyrimethamine (E) and WR99210 (F) in active site of wild-type *Pf*DHFR (blue) and quadruple mutant *Pf*DHFR (red).**

The emerging antimalarial drug-resistant parasite threatens the malaria control efforts achieved thus far. This has prompted researchers to look for new and improved treatment regimens to treat and control the disease.

1.3. Synthesis of 6-substituted-2,4-diaminopyrimidine-5-phenethylamines as inhibitors of *Pf*DHFR

The first component of this research project aims to synthesise class II antifolates bearing a pyrimidine core. This part of the research is a continuation of a bigger project which was initiated by Prof. Rousseau while working at the CSIR. Active antimalarial dihydrotriazine analogues of general structure **27** were synthesised and shown to be inhibitors of *Pf*DHFR, **Figure 19**. These triazine compounds also mimic the natural substrate DHF **19**. Key functional groups that are important for activity have been highlighted. These include: the nitrogen backbone (purple), which is key for binding to the active site; the four atom linker chain (blue), which is essential for flexibility of the compound and finally the substituted phenyl ring (orange), which is important for additional binding in the active site (**Figure 19**).

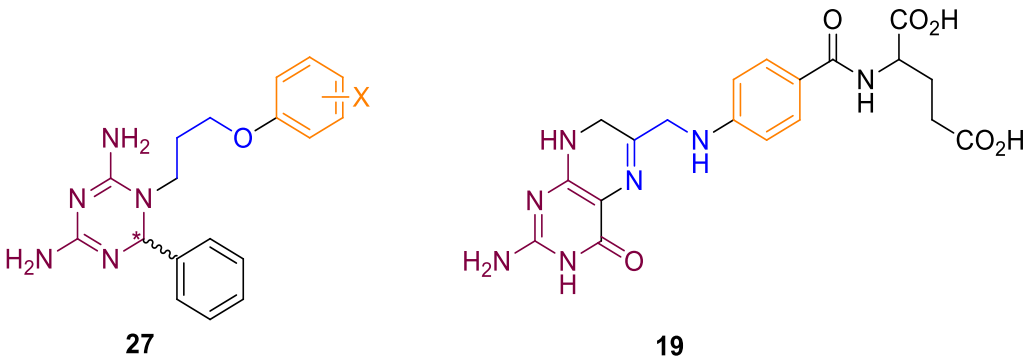

For X = 4-Cl:
IC_{50} 33 nM (FCR-3 drug resistant)
IC_{50} 80 nM (D10 drug sensitive)
Ki 4.9 nM (WT); 8.2 nM (FCR-3)

Figure 19: Substituted dihydrotriazine (27) prepared previously alongside DHF (19).[44]

A series of analogues bearing flexible linkers ranging in length of two up to six atoms between the dihydrotriazine and the phenyl ring was synthesised. The rationale behind the synthesis of compounds **27** bearing flexible linkers is that this allows the compound to adopt conformations

that can avoid steric clashes in mutant amino acids in the active site, due to its inherent flexibility. This flexibility is also advantageous in that the compound **27** can adopt conformations that can find new binding sites in the active site of the enzyme, similar to what is observed for WR99210 **(25)**, **Figure 18**. Rousseau *et al*. reported that analogues bearing the four atom linker showed the best antiplasmodial activity.[44] However, the presence of a chiral centre in the resulting product gave racemic mixtures, which was not desirable, and an enantioselective synthesis was not possible.[44] Our work over the past three years has provided a solution to the latter by synthesising pyrimidine derivatives (**28**, **Figure 20)**, which lack the chiral centre and hence allow for a single product to be synthesised. These compounds are structural derivatives of the earlier antifolate, pyrimethamine **7**, which has lost activity against drug resistant malaria strains. We proposed a synthetic route to compounds of general structure **28** as shown in **Scheme 1**. The difference in *in vitro* antiplasmodial activity when R is a phenyl, cyclohexyl or cyclopropyl group and X is OMe, F or Cl, will be determined. In this manner we hope to establish structure-activity relationships (SAR) for antiplasmodial antifolates bearing a pyrimidine core substituted with a flexible side chain.

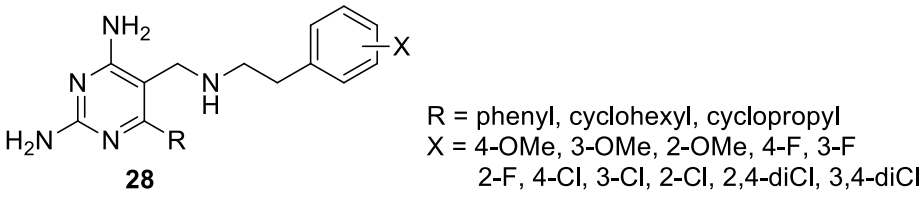

Figure 20: General structure of pyrimidine analogues proposed in this work.

Scheme 1 shows the disconnection from 6-substituted-2,4-diaminopyrimidine-5-phenethylamines which are of interest in this project. As mentioned previously, these compounds are structural derivatives of pyrimethamine **7**, and structural modifications include replacing the rigid bi-aryl bond of pyrimethamine **7** with a more flexible 4-atom linker chain in the C-5 position of the pyrimidine ring and varying the R groups. This characteristic has been proven to be advantageous in that when point mutations occur in the *Pf*DHFR active site, the flexibility of the linker chain allows the compound to position itself to avoid steric clashes with mutant amino acid residues, or alternatively find additional binding regions.

As represented in the disconnection in **Scheme 1**, a multicomponent coupling reaction between suitably substituted aldehydes **29**, malononitrile and guanidine hydrochloride under basic conditions forms a substituted 2,4-diaminocyanopyrimidine **30**. Compound **30** can be subjected

to a reduction reaction to afford the aldehyde **31**. Compound **31** can then undergo a reductive amination reaction which will give the desired substituted amine **28**.

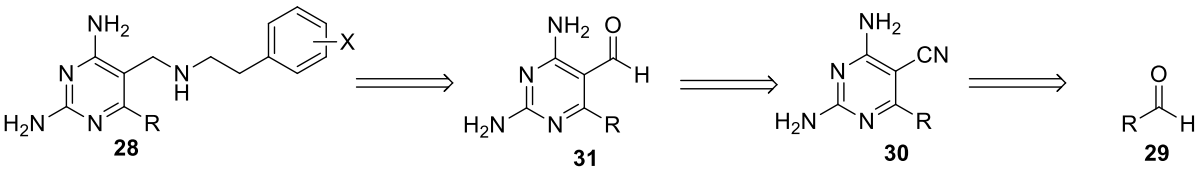

Scheme 1: Disconnection from target compound (28)

The analogues synthesised will be subjected to *Pf*DHFR enzyme inhibition assays against both the wild type and quadruple mutant *Pf*DHFR to test for inhibitory activity. Selectivity will be assessed by determining inhibition of human DHFR in an enzymatic assay. Analogues yielding promising inhibitory results will then be assessed in whole cell *P. falciparum* assays *in vitro* against both drug sensitive and drug resistant strains to assess the antiplasmodial activity. Compounds will also be assessed in standard *in vitro* cytotoxicity assays.

CHAPTER 2: RESULTS AND DISCUSSION

The first component of the research project focuses on the synthesis of 2,4-diaminopyrimidines **28**, **Scheme 2**, as potential antiplasmodial antifolates. The synthesis will be achieved following the protocol shown in **Scheme 2**.

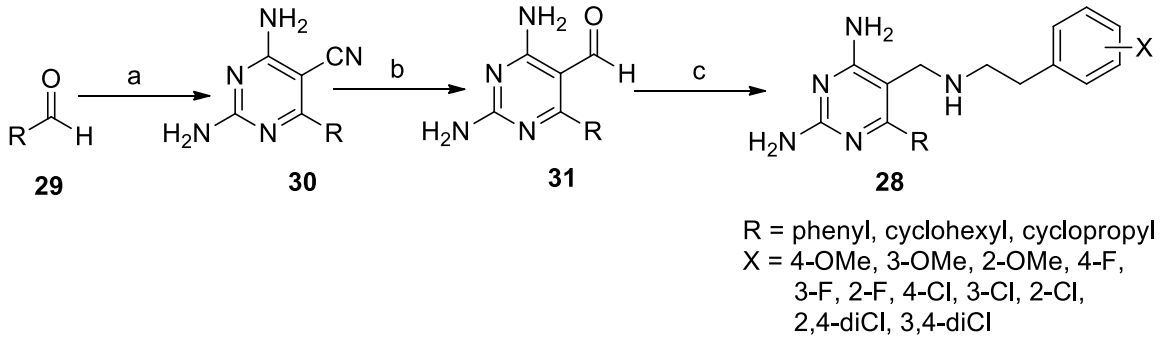

Scheme 2: *Reagents and conditions*: a) Malononitrile, guanidine hydrochloride, NaOAc, H_2O/EtOH, reflux, N_2, 2.5-3h; b) Raney Ni, 81% aq. Formic acid, reflux, N_2, 1 h; c) $NaBH(OAc)_3$, 1,2-DCE, glacial AcOH, substituted phenethylamine, reflux, N_2, 3h.

Previous work has been done by Professor Amanda Rousseau, while working at the CSIR, on a similar set of analogues, where active dihydrotriazine compounds **27**, **Figure 21**, were synthesised. These dihydrotriazine compounds **27** showed antiplasmodial activity *in vitro* against both the wild-type and drug resistant parasite strains.[44] The drug resistant parasite strain that compounds **27** were assessed against was the *P. falciparum* cycloguanil resistant mutant (*Pf* FCR-3). These compounds **27** were highly active against the *Pf* FCR-3 strain showing IC_{50} values in the range of 2.66-171 nM, some examples of which are included in **Figure 21**, with the most active compound of the series being **27** when X = 2,4-diCl (IC_{50}, 3 nM). The compounds were also shown to be potent inhibitors of both wild type (*K*i 2.3 – 29.5 nM) and quadruple mutant (*K*i 4.9 – 29.1 nM) *Pf*DHFR. Although these compounds showed promising activity, they contain a chiral centre, which gave rise to racemic mixtures. This was not desirable as a stereoselective synthesis was not readily accessible, and purification of the racemates proved challenging resulting in low yields of product. To avoid these issues, pyrimidine analogues **32**, **Figure 21**, of these active dihydrotriazines **27** were synthesised in an earlier project by Seanego *et al.*[45] These pyrimidine analogues **32** eliminated the chiral centre at C-6 (denoted as an * in **27**) and hence solved the issues mentioned previously. Unfortunately, these pyrimidines **32** were less potent than the dihydrotriazines **27** against the same strain of the parasite *in vitro* and displayed IC_{50} values in the low micromolar range (0.9-27 µM, *Pf*

FCR-3),[45] with compound **32** where X = 3,5-diCl demonstrating the best activity of the series, **Figure 21**. This significant drop in activity could potentially be attributed to compounds **32** possessing different pharmacokinetic properties, or the introduction of a rigid sp^2 hybridised biaryl axis now present at C-6 between the phenyl substituent and the pyrimidine ring in **32**, which replaced the sp^3 hybridised C-6 observed in the dihydrotriazines **27**. Enzyme inhibition activity of these compounds **32** against *Pf*DHFR, however was not assessed.

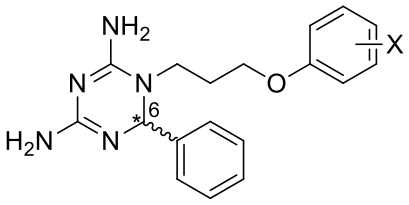

27

	(*Pf* FCR-3)
X = 4-Cl,	IC_{50} 55 nM
X = 3,4-diCl,	IC_{50} 40 nM
X = 2,4-diCl,	IC_{50} 3.0 nM
X = 4-F,	IC_{50} 39 nM

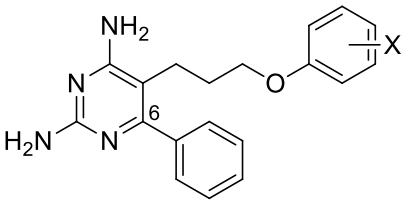

32

	(*Pf* FCR-3)
X = 4-Cl,	IC_{50} 4.0 μM
X = 3,4-diCl,	IC_{50} 15 μM
X = 3,5-diCl,	IC_{50} 0.9 μM
X = 3-F,	IC_{50} 27 μM

Figure 21: Selected general structures and IC_{50} values of previously prepared 2,4-diaminopyrimidines (32) and dihydrotriazine compounds (27).[44,45]

As a continuation of the previous work, the effect of the 6-phenyl substituent of compounds **32** on inhibitory activity against *Pf*DHFR is being determined in a separate project, where compounds **33**, **Figure 22**, where the ether linker chain is maintained and R varies by having more flexible alkyl substituents, are being synthesised and assessed. This research project however, will focus on synthesising 2,4-diaminopyrimidines of general structure **28**, **Figure 22** that possess an amine (-NH) group in the linker chain of compounds **28**, which may have a role in the binding of the compounds. The free NH may improve the pharmacokinetic properties of the compounds and may have a positive influence on LogD values of these compounds. We will synthesise analogues with a 6-phenyl substituent to determine if the change in linker has any effect in the biological activity; but will also introduce an sp^3 hybridised cyclohexyl substituent and a smaller cyclopropyl substituent at R to determine the effect of these cycloalkane substituents on the inhibitory activity against *Pf*DHFR. These substituents will provide information about the effects of having a rigid aromatic group, that is, the phenyl ring, in comparison to an sp^3 hybridised alkyl group like the cyclohexyl ring on the activity of the compound. Furthermore, having the smaller cyclopropyl group will assist in

comparing how effective smaller cycloalkanes in comparison to larger cyclohexyl and phenyl groups are when it comes to the compound's activity. Should these variations be feasible, as a continuation of the work, we might consider the use of non-classical bioisosteres such as cubane as an R substitient.[46] Bioisosteres are reported to have an advantage over aromatic substituents, such as phenyls, in that they are reported to improve solubility.[46] To this end, this thesis will report our efforts towards the synthesis and biological evaluation of compounds **28**.

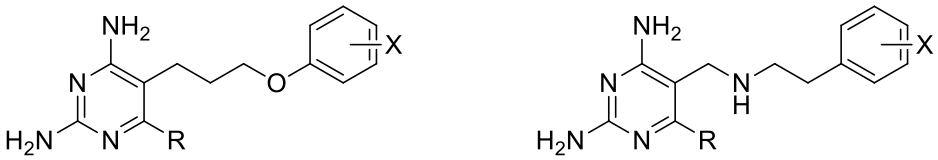

33 **28**

Figure 22: General structures of diaminopyrimidines (33) and (28) being prepared.

2.1. *In silico* molecular modelling - induced fit docking of proposed analogues (28)

In silico molecular modelling of compounds **28** in the active site simulation of *Pf*DHFR was performed using Schrodinger software and the crystal structure of our target enzyme DHFR. The model used (1J3K) had the known compound WR99210 **25** and a co-factor bound in the active site and were removed prior to docking. **Figure 23** shows the compounds whose predicted binding ability was assessed using induced fit docking (IFD) on Schrodinger.

An induced fit docking (IFD) study was performed on compounds **28** bearing 6-phenyl, 6-cyclohexyl and 6-cyclopropyl substituents respectively, with X = OMe, F, Cl (from readily commercially available phenethylamines). This study assessed the binding ability of compounds **28** against the quadruple mutant *Pf*DHFR (PDB structure 1J3K[47]) which possesses the following mutations: N51I, C59R, S108N, and I164L.

This study incorporated docking constraints in the form of forced hydrogen bonds to the backbone of residues Ile14 and mutant Ile164 and to the Asp54 side chain. This was done to ensure the ligands adhered to the known conserved binding mode. For the initial Glide docking and Prime refinement steps, the default settings were used, while for the redocking step, the more rigorous Glide XP algorithm was used for the glide redocking step.

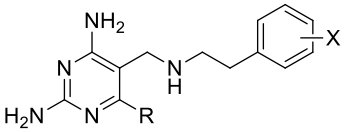

28

28a R = phenyl, X = 2-OMe	28l R = cyclohexyl, X = 2-OMe	28w R = cyclopropyl, X = 2-OMe
28b R = phenyl, X = 3-OMe	28m R = cyclohexyl, X = 3-OMe	28x R = cyclopropyl, X = 3-OMe
28c R = phenyl, X = 4-OMe	28n R = cyclohexyl, X = 4-OMe	28y R = cyclopropyl, X = 4-OMe
28d R = phenyl, X = 2-F	28o R = cyclohexyl, X = 2-F	28z R = cyclopropyl, X = 2-F
28e R = phenyl, X = 3-F	28p R = cyclohexyl, X = 3-F	28a' R = cyclopropyl, X = 3-F
28f R = phenyl, X = 4-F	28q R = cyclohexyl, X = 4-F	28b' R = cyclopropyl, X = 4-F
28g R = phenyl, X = 2-Cl	28r R = cyclohexyl, X = 2-Cl	28c' R = cyclopropyl, X = 2-Cl
28h R = phenyl, X = 3-Cl	28s R = cyclohexyl, X = 3-Cl	28d' R = cyclopropyl, X = 3-Cl
28i R = phenyl, X = 4-Cl	28t R = cyclohexyl, X = 4-Cl	28e' R = cyclopropyl, X = 4-Cl
28j R = phenyl, X = 2,4-diCl	28u R = cyclohexyl, X = 2,4-diCl	28f' R = cyclopropyl, X = 2,4-diCl
28k R = phenyl, X = 3,4-diCl	28v R = cyclohexyl, X = 3,4-diCl	28g' R = cyclopropyl, X = 3,4-diCl

Figure 23: Compounds that were subject to IFD studies using Schrodinger.

Compounds **28** were then subjected to the IFD experiments and each compound generated several docking scores, including the XP GScore (calculated for the final glide XP docking step) the Prime energy (approximates the overall energy of the binding pose) and the IFDScore (combines the Prime energy and docking score into a single term). For all docking scores, the lower the calculated energy is, the better the binding of the compound. **Table 1** shows the results produced by the study.

The IFD results shown in **Table 1** predicted a high binding ability (low energies) of the series of compounds **28** to the target enzyme with IFD scores for compounds **28a-g'** ranging from -2471.36 to -2464.66 cal.mol^{-1}. These results compared well with the known ligands pyrimethamine (PYR) **7**, WR99210 **25** and the natural substrate dihydrofolic acid (DHF) **19** with IFD scores of -2466.26, -2462.52 and -2470.90 cal.mol^{-1} respectively. Encouragingly, our series of compounds mostly generated better IFD scores than WR99210 which was reported to be active against *P. falciparum* strains bearing (quadruple mutant) DHFR.[41]

Table 1: Induced Fit Docking results of compounds 28a-g' into the active site of *Pf*DHFR (1J3K).

Entry	XP GScore[a]	Prime energy[a]	IFD Score [a]	Entry	XP GScore[a]	Prime energy[a]	IFD Score [a]
28a	-13.027	-49146.7	-2470.36	**28s**	-11.239	-49167.7	-2469.62
28b	-13.874	-49154.1	-2471.58	**28t**	-10.425	-49162.0	-2468.53
28c	-11.004	-49166.1	-2469.31	**28u**	-8.926	-49148.6	-2466.36
28d	-11.890	-49132.3	-2468.50	**28v**	-11.196	-49155.4	-2468.96
28e	-12.331	-49142.0	-2469.43	**28w**	-11.028	-49159.7	-2469.01
28f	-10.758	-49155.7	-2468.54	**28x**	-10.993	-49167.4	-2469.36
28g	-7.883	-49135.6	-2464.66	**28y**	-11.231	-49159.6	-2469.21
28h	-12.331	-49142.0	-2469.43	**28z**	-10.998	-49157.5	-2468.87
28i	-12.091	-49128.8	-2468.53	**28a'**	-11.356	-49131.9	-2467.95
28j	-11.019	-49150.1	-2468.52	**28b'**	-10.122	-49168.2	-2468.53
28k	-11.991	-49139.3	-2468.96	**28c'**	-10.192	-49164.5	-2468.42
28l	-9.542	-49187.5	-2468.92	**28d'**	-11.386	-49154.8	-2469.13
28m	-10.945	-49162.6	-2469.08	**28e'**	-10.726	-49168.0	-2469.13
28n	-11.692	-49149.3	-2469.16	**28f'**	-11.483	-49167.2	-2469.84
28o	-10.769	-49161.1	-2468.82	**28g'**	-10.967	-49165.8	-2469.26
28p	-11.283	-49144.6	-2468.51	**DHF**	-15.891	-49100.1	-2470.90
28q	-10.171	-49160.2	-2468.18	**WR99210**	-9.257	-49065.3	-2462.52
28r	-10.358	-49167.0	-2468.71	**PYR**	-8.827	-49148.7	-2466.26

[a] All docking scores given in units cal.mol^{-1}.

When comparing the binding ability of the compounds **28**, a trend in the binding ability of the substituents X was observed. Compounds bearing methoxy substituents generally displayed better IFD docking scores in the ranges of (-2471.58 to -2468.92 cal.mol^{-1}). Compounds possessing 2,4- and 3,4-dichloro substituents (-2469.84 to -2466.36 cal.mol^{-1}) followed, then the chloro substituents (-2469.43 to -2464.66 cal.mol^{-1}) and finally the fluoro substituents in the ranges of -2469.43 to -2467.95 cal.mol^{-1}. Additionally IFD results predicted that the position of the X-substituent on the phenyl ring had a significant influence on binding, with the 3-position being clearly favoured to the 4-position and 2-position respectively. No clear trend was observed for the 6-R substituents, however, on average the 6-cyclopropyl series **28w-g'** displayed the best results with an IFD score average of -2468.97 cal.mol^{-1} followed by the 6-phenyl series **28a-k** (IFD score average of -2468.89 cal.mol^{-1}) and the 6-cyclohexyl series **28l-v** with an average IFD score of -2468.62 cal.mol^{-1}.

Surprisingly, the 6-phenyl series produced better IFD data than we had anticipated, especially for compounds **28a-c**, which had the best IFD scores for our series of compounds. The reported

biological assay results on a similar set of compounds **32**, **Figure 21**, discussed above, gave us the expectation that the 6-phenyl series may display much weaker binding than the 6-cyclohexyl and 6-cyclopropyl series. We would have attributed this to the sp^2 hybridised 6-phenyl substituent which we expected to have unfavourable clashes in the active site, however this was not confirmed by the IFD scores in our modelling study.

Conserved binding interactions observed between our series of compounds **28** and the active site included strong pi-cation and pi-pi interactions with Phe58. Hydrogen bond interactions were also observed for Cys15, Ile14, mutant Leu164 and mutant Asn108, with Asn108 behaving as both a hydrogen bond donor and acceptor from the secondary amine present in the linker chain, (**Figure 24 B**). The NH in the linker region however does not seem to be essential in terms of interactions with the protein as interactions observed for the compound in **Figure 24 B** are not commonly observed with the other compounds, as displayed in **Figure 24 A** and **Figure 24 C**. Hydrogen bonds to Cys15 were commonly observed for compounds bearing the 6-cyclopropyl substituent (**Figure 24 C**, compound **28 w**). The close proximity to this residue is most likely owed to the small cyclopropyl group possessed by these compounds. Further interactions were observed with the oxygen of the methoxy group of **28a** acting as a hydrogen bond acceptor to the Tyr170 residue, (**Figure 24 A**) and the chlorine of the dichloro-phenyl substituent of **28v** having halogen bonds to Ser167, (**Figure 24 B**), which highlights the advantage offered by the different substituents on the phenyl ring. Furthermore, the IFD results demonstrated that at physiological pH, the nitrogen in position-1 (**Figure 24 A and B**) in the pyrimidine ring can undergo protonation and engage in electrostatic interactions with nearby residues, with a salt-bridge interaction to the charged residue Asp54 being especially significant, **Figure 24** demonstrates these findings.

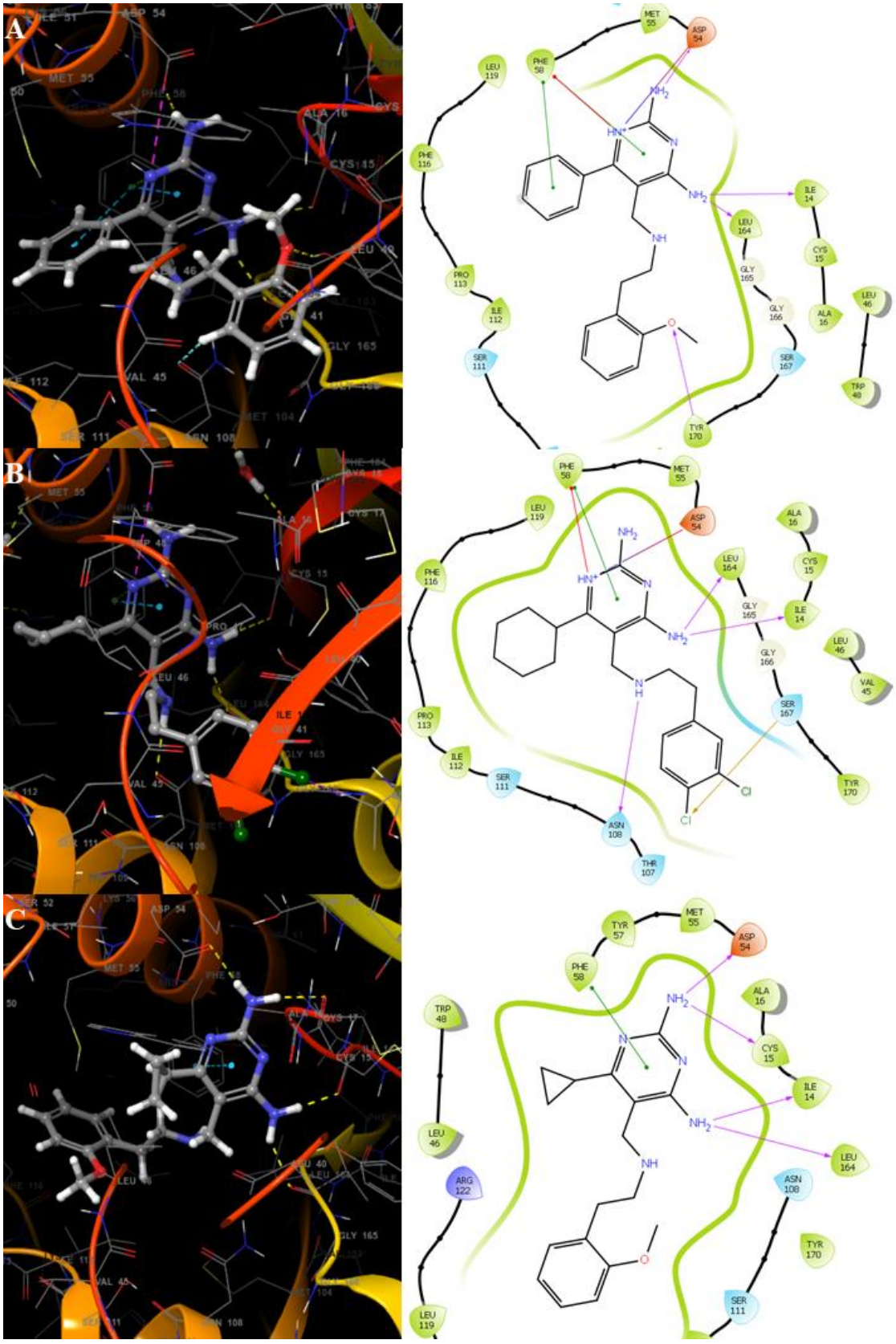

Figure 24: An illustration of A: 28a; B: 28v, and C: 28w bound in the active site of *Pf*DHFR (PDB: 1J3K) and the corresponding 2D interaction diagram for each compound.

Compounds **28l-v** and **28w-g'** bearing the 6-cyclohexyl and 6-cyclopropyl groups respectively both displayed a tightly conserved binding mode of the pyrimidine ring, with the position of the pyrimidine core maintained between ligands while the linker chain and the terminal phenyl rings displayed more variability in position, **Figure 25A**. Notably, when comparing with the binding mode of the 6-phenyl substituted compounds **28a-k**, it is observed that these compounds occupy a slightly offset binding position with slightly different binding interactions, **Figure 25B**. These findings are likely caused by the rigid biaryl axis at the C-6 position present in these compounds, and may be the reason for the reduced potency of compounds **32** bearing a 6-phenyl substituent (**Figure 21**).

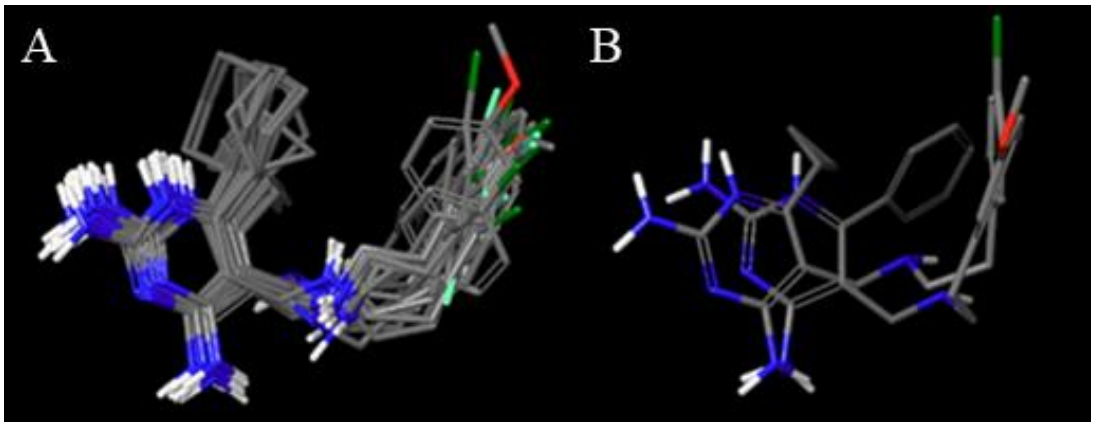

Figure 25: (A) 6-Cyclohexyl (28l-v) and 6-cyclopropyl (28w-g') analogues superimposed to show the conserved binding mode. (B) 6-Phenyl (28i) and 6-cyclopropyl (28x) analogues superimposed to demonstrate offset binding mode of the 6-phenyl analogues.[40]

2.2. *In silico* molecular modelling – qikprop pharmacokinetic property predictions of proposed analogues (28)

QikProp prediction of the pharmacokinetic properties of compounds **28a-g'** was also assessed for this series of analogues and compared to the known antifolates PYR **7**, WR99210 **25** and the natural substrate DHF **19**. **Table 2** summarises the predicted pharmacokinetic properties.

Table 2: Qikprop predictions for pharmacokinetic properties of 28a-g' and known antifolates PYR (7), WR99210 (25) and DHF (19).

Entry	#stars [a]	CNS [b]	MW[c]	dipole [d]	donor HB[e]	accept HB[f]	QPlogPo/w [g]	QPlogS[h]	QPPCaco[i]	QPlogBB[j]	#metab[k]	QPlogKhsa[l]	HOA[m]	%HOA[n]	PSA[o]	RO5 [p]	RO3 [q]
28a	0	0	349.435	2.151	5.000	5.250	2.223	-1.861	187.489	-0.613	4	-0.074	3	80.643	88.591	0	0
28b	0	-1	349.435	1.618	5.000	5.250	2.483	-2.812	131.575	-0.899	4	0.039	3	79.416	91.732	0	0
28c	0	-2	349.435	4.480	5.000	5.250	2.306	-2.887	75.682	-1.168	4	0.038	3	74.079	93.904	0	0
28d	0	-1	337.399	2.403	5.000	4.500	2.417	-2.974	81.473	-0.992	3	0.029	3	75.303	87.500	0	0
28e	0	-2	337.399	1.016	5.000	4.500	2.550	-3.269	78.844	-1.008	3	0.067	3	75.825	87.872	0	0
28f	0	-2	337.399	3.805	5.000	4.500	2.549	-3.267	78.843	-1.008	3	0.067	3	75.820	87.874	0	0
28g	0	-1	353.853	3.296	5.000	4.500	2.707	-3.012	121.468	-0.715	3	0.075	3	80.104	83.219	0	0
28h	0	0	353.853	3.033	5.000	4.500	2.814	-3.125	133.799	-0.640	3	0.094	3	81.481	82.889	0	0
28i	0	-1	353.853	3.798	5.000	4.500	2.799	-3.625	78.833	-0.969	3	0.133	3	77.284	87.875	0	0
28j	0	-1	388.299	1.558	5.000	4.500	3.431	-4.371	107.614	-0.720	3	0.275	3	83.404	84.184	0	0
28k	0	0	388.299	3.883	5.000	4.500	3.230	-3.699	133.906	-0.516	3	0.189	3	83.924	82.848	0	0
28l	0	0	355.48	1.499	5.000	5.250	2.678	-3.079	170.171	-0.682	5	0.214	3	82.552	88.10	0	0
28m	0	0	355.482	2.719	5.000	5.250	2.212	-1.624	215.902	-0.385	5	0.082	3	81.674	90.023	0	0
28n	0	-2	355.482	1.810	5.000	5.250	2.583	-3.694	100.075	-1.047	5	0.224	3	77.871	93.469	0	0
28o	0	-1	343.446	1.327	5.000	4.500	2.691	-3.519	122.930	-0.748	4	0.216	3	80.102	84.421	0	0
28p	1	0	343.446	0.805	5.000	4.500	2.579	-3.208	117.647	-0.674	4	0.176	3	79.107	83.042	0	0
28q	0	0	343.446	1.979	5.000	4.500	2.739	-3.554	132.052	-0.677	4	0.215	3	80.938	84.378	0	0
28r	0	-1	359.901	4.650	5.000	4.500	2.669	-3.265	113.959	-0.708	4	0.221	3	79.387	81.804	0	0
28s	1	0	359.901	0.808	5.000	4.500	2.828	-3.555	118.076	-0.630	4	0.240	3	80.590	83.026	0	0
28t	0	0	359.901	2.003	5.000	4.500	2.983	-3.901	131.909	-0.634	4	0.280	3	82.363	84.323	0	0
28u	0	0	394.346	3.434	5.000	4.500	3.158	-3.986	113.996	-0.565	4	0.327	3	82.253	81.757	0	0
28v	0	0	394.346	6.385	5.000	4.500	2.825	-2.446	137.151	-0.267	4	0.274	3	81.739	83.990	0	0
28w	0	0	313.402	1.898	5.000	5.250	1.465	-0.956	137.631	-0.518	4	-0.162	2	73.803	88.195	0	0
28x	0	-2	313.402	2.091	5.000	5.250	1.781	-2.828	94.967	-1.059	4	-0.096	3	72.771	93.151	0	0
28y	1	-2	313.402	0.664	5.000	5.250	1.788	-2.855	95.743	-1.062	4	-0.096	3	72.875	93.612	0	0

Table 2: Qikprop predictions for pharmacokinetic properties of 29a-g' and known antifolates PYR (7), WR99210 (25) and DHF (19) continued.

Entry	#stars [a]	CNS[b]	MW[c]	dipole[d]	donor HB[e]	accept HB[f]	QPlogPo/w [g]	QPlogS[h]	QPPCaco[i]	QPlogBB[j]	#metab[k]	QPlogKhsa[l]	HOA[m]	%HOA [n]	PSA[o]	RO5 [p]	RO3[q]
28z	0	0	301.366	2.238	5.000	4.500	1.804	-2.361	129.049	-0.653	3	-0.141	3	75.288	84.538	0	0
28a'	0	0	301.366	1.612	5.000	4.500	1.733	-1.900	130.843	-0.521	3	-0.149	3	74.976	84.581	0	0
28b'	0	0	301.366	2.304	5.000	4.500	1.937	-2.666	120.683	-0.696	3	-0.099	3	75.544	84.880	0	0
28c'	0	0	317.820	2.007	5.000	4.500	1.765	-2.007	102.881	-0.614	3	-0.117	3	73.297	82.426	0	0
28d'	0	0	317.820	1.708	5.000	4.500	1.978	-2.213	136.648	-0.469	3	-0.090	3	76.747	84.466	0	0
28e'	0	0	317.820	2.286	5.000	4.500	2.185	-3.006	121.337	-0.650	3	-0.036	3	77.037	84.905	0	0
28f'	0	0	352.266	2.959	5.000	4.500	2.206	-2.591	102.659	-0.468	3	-0.026	3	75.864	82.423	0	0
28g'	0	0	352.266	4.683	5.000	4.500	2.078	-1.693	210.630	-0.080	3	-0.099	3	80.702	83.874	0	0
DHF	4	-2	441.402	11.864	6.250	12.750	-0.381	-3.944	0.033	-5.176	6	-1.066	1	0.000	249.823	2	1
WR99210	1	-1	394.687	5.114	4.000	6.450	3.030	-5.159	395.962	-0.968	1	-0.055	3	91.180	88.642	0	0
PYR	0	-2	248.714	1.972	3.000	4.000	1.775	-2.905	389.391	-0.784	1	-0.245	3	83.7	74.965	0	0

Key for **Table 2**: [a] Number of parameters falling outside of a 95% similarity range for known drugs, [b] Central nervous system activity [c] Molecular weight [d] Calculated dipole moment, [e] Number of H-bond donors, [f] Number of H-bond acceptors, [g] Octanol/water partition coefficient, [h] Water solubility, [i] Caco-2 cell permeability in nm/s (model for gut-blood barrier, only non-active transport is considered), [j] Blood – brain barrier permeability, [k] Number of likely metabolites, [l] Human serum albumin binding coefficient, [m] Human oral absorption: Measure of human oral absorption combing serval factors, [n] Percentage Human oral absorption: Predicted human oral absorptivity percentage scale, value is used in the calculation of HOA, [o] Polar surface area, [p] Number of violations of Lipinski's rule of 5, [q] Number of violations of Jorgensen's rule of 3.

Qikprop predictions suggested good pharmacokinetic properties for our series of compounds **28**. #Stars is a descriptor value that demonstrates the number of properties of the compound that fall outside the 95 % range of similar values for known drugs, a recommended range is 0-5. Our series of compounds therefore showed excellent results with only three compounds (**28p**, **28s** and **28y**) showing 1 star and the rest of the compounds showing 0 stars, meaning that very few properties fall outside the 95 % range of similar values for known drugs. These compounds compared well with the known inhibitors WR99210 (**25**) and PYR (**7**) which showed 0 and 1 star respectively and performed better than the natural substrate DHF which showed 4 stars. None of the compounds violated either Lipinski's rule of 5 or Jorgensen's rule of 3. Lipinski's rule of 5 takes into account the following factors: molecular weight (MW) < 500, log P (QPlogPo/w) < 5, number of H-bond donors (donorHB) ≤ 5, number of H-bond acceptors (accptHB) ≤ 10; and Jorgensen's rule of 3 considers these factors: predicted aqueous solubility (QPlogS) > -5.7, predicted apparent Caco-2-cell permeability (QP PCaco) > 22 nm/s and the number of primary metabolites < 7. This therefore means that the compounds were all predicted to be drug-like and more likely to be orally available. Other properties such as the predicted central nervous system activity (CNS) with -2 (inactive) and +2 (active) predicted that none of our compounds were active against the central nervous system and this data compared well with the known inhibitors WR99210 **25** and PYR **7** and the natural substrate DHF **19**. QPlogKhsa which predicts binding to the human serum albumin also predicted all our compounds to be in the recommended range -1.5 – 1.5. Percentage human absorption (% HOA) predicted compounds **28** to be in the recommended range (<25 % poor; >80 % high) with values in the range of 72.8 – 82.9 %, with compound **28k** showing the highest % HOA (83.9 %). None of our analogues performed better than WR99210 (91.2 %). Generally the percentage human absorption is predicted to be the highest for the 6-cycohexyl series **28l-v** (77.9 – 82.6 %), followed by the 6-phenyl series **28a-k** (74.1 -83.9 %) then finally the 6-cyclopropyl series **28w-g'** (72.8 – 80.7 %).

The mean value and percentage compliance for the series of analogues **28a-g'** was also calculated for each of these properties and the results are summarised in **Table 3** below.

Table 3: Average values of pharmacokinetic properties as well as the acceptable range (95 % range for similar drugs), and the percentage compliance our series of compounds 28a-g' assessed.

Property	Mean value	Acceptable range	Percentage compliance (%)
#stars[a]	0.09	0 – 5	100
CNS[b]	-0.58	-2 (inactive), +2 (active)	100
MW[c]	356.38	130 - 725	100
dipole[d]	2.51	1 – 12.5	90.9
donor HB[e]	5.00	0 - 6	100
accept HB[f]	4.70	2 - 20	100
QPlogPo/w[g]	2.43	-2 – 6.5	100
QPlogS[h]	-2.90	-6.5 - -0.5	100
QPPCaco[i]	123.23	<25 poor; >500 great	100
QPlogBB[j]	-0.70	-3 – 1.2	100
#metab[k]	3.60	1 – 8	100
QPlogKhsa[l]	0.070	-1.5 – 1.5	100
HOA[m]	2.97	1 low; 2 medium; 3 high	100
%HOA[n]	78.33 %	<25 % poor; >80 % high	100
PSA[o]	86.18	7-200	100
RO5[p]	0	Max 4	100
RO3[q]	0	Max 5	100

Key for **Table 3**: [a] Number of parameters falling outside of a 95% similarity range for known drugs, [b] Central nervous system activity [c] Molecular weight [d] Calculated dipole moment, [e] Number of H-bond donors, [f] Number of H-bond acceptors, [g] Octanol/water partition coefficient, [h] Water solubility, [i] Caco-2 cell permeability in nm/s (model for gut-blood barrier, only non-active transport is considered), [j] Blood – brain barrier permeability, [k] Number of likely metabolites, [l] Human serum albumin binding coefficient, [m] Human oral absorption: Measure of human oral absorption combing serval factors, [n] Percentage Human oral absorption: Predicted human oral absorptivity percentage scale, value is used in the calculation of HOA, [o] Polar surface area, [p] Number of violations of Lipinski's rule of 5, [q] Number of violations of Jorgensen's rule of 3.

As illustrated by **Table 3** above, our compounds are predicted to display pharmacokinetic properties within acceptable ranges of known drugs. This is promising for the potential antiplasmodial activity of these compounds which will be assessed.

The results of this study therefore confirmed the rationale in synthesising the 2,4-diaminopyrimidine compounds bearing a 6-cyclohexyl, 6-cyclopropyl or 6-phenyl substituent for biological testing.

2.3. Approaches to the synthesis of 2,4-diaminopyrimidine core

The 2,4-diaminopyrimidine core has an essential role in the binding of the analogues to the active site, as previously shown with the *in silico* molecular model, **Figure 24**. There have been various synthetic protocols reported to synthesise 2,4-diaminopyrimidine derivatives bearing an aromatic substituent at the C-6 position. These protocols however, do not always involve the synthesis of the 2,4-diaminopyrimidine core as the first step. Previous work reported by Seanego *et al*. included a four step synthesis, (**Scheme 3**) to synthesise 2,4-diaminopyrimidines **32**.[45] Initially, commercially available substituted phenols **34** were alkylated with 1,4-dibromobutane to afford substituted ethers **35**. The resulting ethers **35** undergo a functional-group interconversion by reaction with potassium cyanide to generate pentanenitriles **36**. An α-cyanoketone **37** is then generated by reacting the nitrile **36** with ethyl benzoate in the presence of base. The formation of the 2,4-diaminopyrimidine was achieved in the final step, where **37** was reacted with diazomethane to form the intermediate enol ether, which was subsequently reacted with guanidine hydrochloride to afford the 2,4-diaminopyrimidine derivatives **32** in low yields (9-11 %).[45]

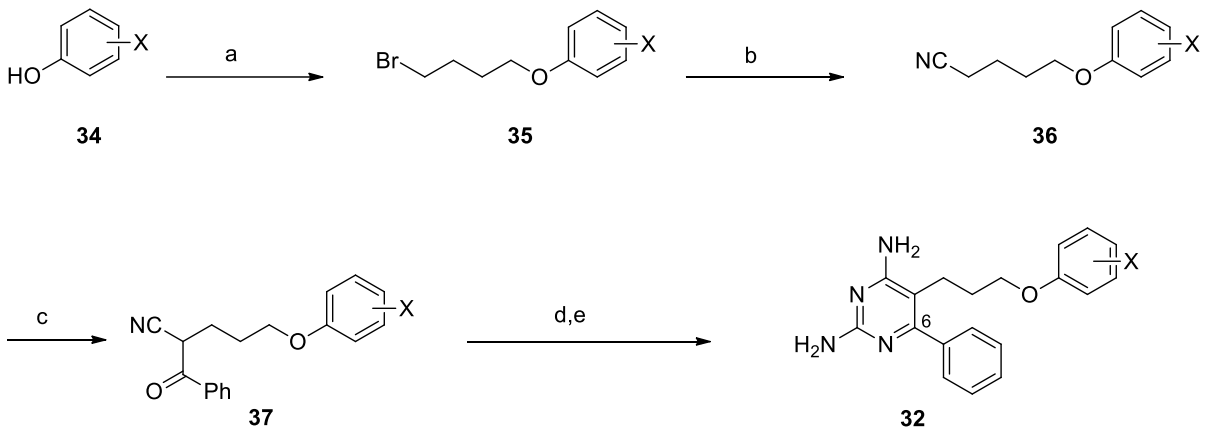

Scheme 3: Reagents and conditions: (a) 1,4-dibromobutane, K_2CO_3, CH_3CN, reflux, 20 h; (b) KCN, EtOH/H_2O, reflux, 48 h; (c) ethyl benzoate, KOtBu, THF, rt, 18 h; (d) diazomethane, CH_2Cl_2, rt, 18 h; (e) guanidine HCl, DMSO, NaOMe, 90 °C, 24 h.[45]

We could employ the same method for the synthesis for our desired compounds **28** by starting with substituted anilines instead of phenols **34** in step *a*. However, the same method was attempted for the synthesis of 2,4-diaminopyrimidines **32** bearing a non-aromatic substituent (cyclohexyl and cyclopropyl) at C-6, and was not successful. The formation of the essential α-

cyanoketones **38** by reacting the nitriles **36** with either methyl cyclohexane carboxylate or methyl cyclopropane carboxylate, was unsuccessful as mainly starting material was recovered (**Scheme 4**). The reaction therefore could not be continued to afford the desired pyrimidine derivatives **33**. We therefore did not attempt this method in the synthesis of our desired compounds **28**.

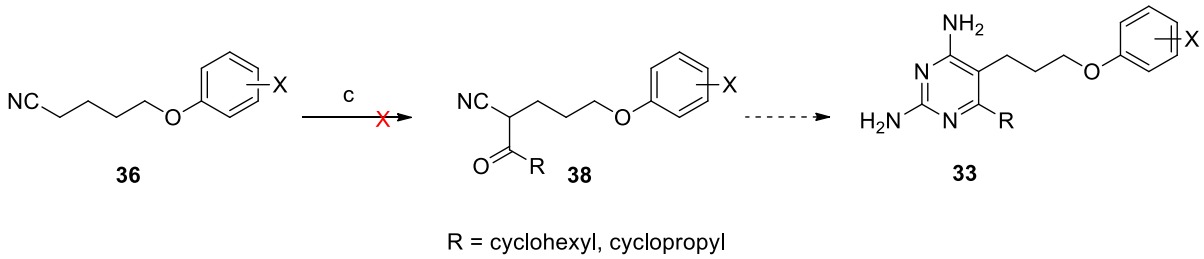

Scheme 4: Attempted synthesis of analogues 33 bearing non-aromatic substituents at C-6 using previously reported methodology.

The limitations posed by the methodology in **Scheme 4** on the synthesis of analogues bearing smaller, more flexible cycloalkyl R groups, encouraged further investigation into alternative approaches for the synthesis of these compounds, including the synthesis of the pyrimidine ring as the first step. To synthesise the 2,4-diaminopyrimidine core in the first step**,** multicomponent coupling reactions (MCRs) are commonly used. MCRs are one-pot reactions where three or more compounds are reacted together to form one target compound. [48] These reactions are commonly used in heterocyclic and combinatorial chemistry. MCR methodologies to form the pyrimidine ring reported by Wang *et al*. shown in **Scheme 5**, were achieved by treating a 1,3-dicarbonyl derivative with an amidine or guanidine to form a 4-chloro-6-substituted pyrimidin-2-amine intermediate **39** which was subsequently treated with a substituted primary amine to afford the 6-substitued pyrimidine-2,4-diamine derivatives **40**.[49] Although this method was selective for both aromatic and alkyl substituents at C-6, it did not functionalise the C-5 carbon, which is essential for achieving our target compounds **28** (**Figure 22**) as this carbon, (C-5) will possess the flexible linker chain.

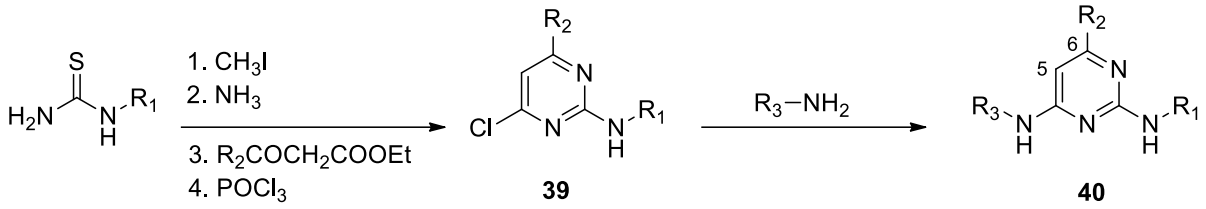

R_1, R_2, R_3 = alkyl or aryl

Scheme 5: Synthesis of 6-substituted pyrimidine-2,4-diamine derivatives with non-functionalised C-5 atom.[49]

Wang *et al*. also prepared the 6-phenyl-pyrimidine derivatives by a Suzuki coupling reaction, using 2-methylthio-4,6-dichloropyrimidine **41** as the starting material to afford the 4-chloro-2-(methylthio)-6-phenylpyrimidine intermediate **42**, which was then treated with amines in the presence of hydrogen peroxide to afford the 6-phenyl-pyrimidine derivatives **43**. Presumably, the Suzuki coupling is done first to ensure displacement of thioether (-SMe) in the subsequent step. Similar to the method in **Scheme 5**, the methodology in **Scheme 6** did not functionalise the key C-5 carbon which will contain the flexible linker in our compounds of interest, **28**.

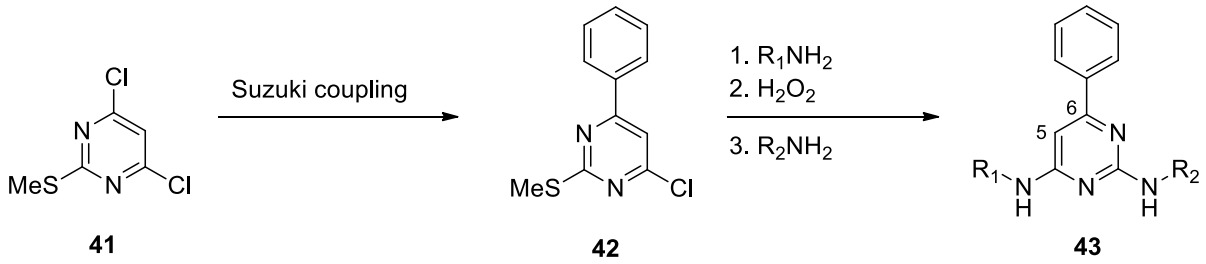

R_1, R_2 = alkyl or aryl

Scheme 6: Synthesis of 6-phenyl-pyrimidine derivatives.[49]

2.4. Approaches to the synthesis of 2,4-diaminopyrimidine-5-carbonitriles

MCRs that functionalise the pyrimidine C-5 with a nitrile substituent, which we could later utilise to incorporate our flexible side chain, have also been reported. The C-5 nitrile group could readily be converted to an aldehyde, which could be used in a reductive amination reaction to afford our desired products **28**. These MCR methods, however, are reported to successfully synthesise 2,4-diaminopyrimidines with substituted phenyl substituents at C-6. We hoped to successfully optimise one of these methods for the synthesis of 2,4-diaminopyrimidines with non-aromatic substituents at C-6 as well.

For example, Deshmukh *et al*. reported an environmentally friendly MCR method for the synthesis of 2,4-diaminopyrimidine-5-carbonitriles where C-6 substituents are substituted phenyls, as shown in **Scheme 7**.[50] In this method an aromatic aldehyde **44**, malononitrile **45** and guanidine hydrochloride **46** are reacted in water in the presence of potassium carbonate and the phase transfer catalyst tetrabutylammonium bromide (TBAB) to form the 6-substituted-2,4-diaminopyrimidine-5-carbonitriles **47**.

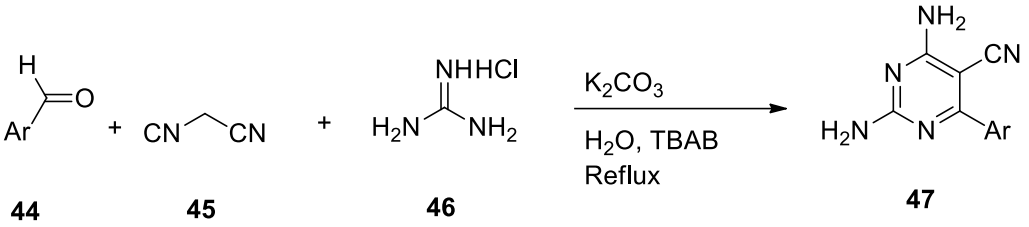

44 **45** **46** **47**

Ar = C_6H_5
Ar = 4-OH-C_6H_4
Ar = 3,4-(OCH_3)
Ar = 3-Cl-C_6H_4

Scheme 7: Synthesis of 6-substituted-2,4-diaminopyrimidine-5-carbonitriles.[50]

Scheme 8 illustrates the proposed mechanism of this reaction in relation to our compounds.

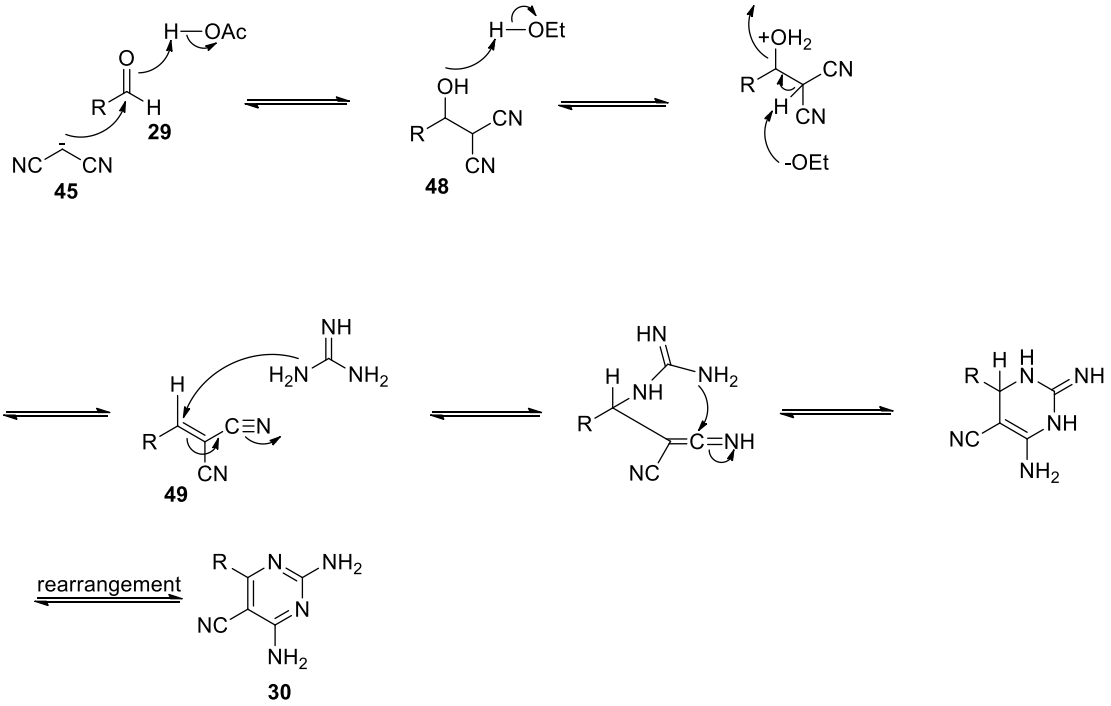

Scheme 8: Proposed mechanism for formation of 6-substituted-2,4-diaminopyrimidine-5-carbonitrile, and analogues.

In the proposed mechanism, the malononitrile is deprotonated by the NaOAc base to generate a nucleophilic malononitrile **45** which subsequently attacks the substituted aldehyde to form a substituted 2-(hydroxymethyl)malononitrile **48**. Compound **48** then undergoes a dehydration which generates the alkene intermediate **49**. The intermediate **49** serves as a good precursor for the 1,4-Michael addition that follows when reacting with the guanidine. Proceeding steps in the mechanism include an intramolecular cyclization and rearrangement and aromatisation which results in the formation of the desired compound **30**.

We attempted this approach (**Scheme 7**) for our compounds using benzaldehyde as the starting material, however this yielded unsatisfactory results. Multiple side products were generated as illustrated by multiple spots observed on the TLC plate, making purification challenging. This outcome was surprising because the same compound **47** (where Ar = C_6H_5) using the same reaction conditions gave yields of 64 % in literature.[50] We were unsure as to why this reaction did not work favourably for our synthesis. These results discouraged us from exploring this method further using non-aromatic aldehydes. Methods more suited to our compounds were sought.

Upon further investigation, a method reported by Raghuvanshi *et al*. (**Scheme 9** step *a*) and Sheibani *et al*. (**Scheme 9** step *b*) described a microwave-assisted, one-pot synthesis of 6-substituted-2,4-diaminopyrimidine-5-carbonitriles using ionic liquids and toluene respectively (**Scheme 9**).[51,52]

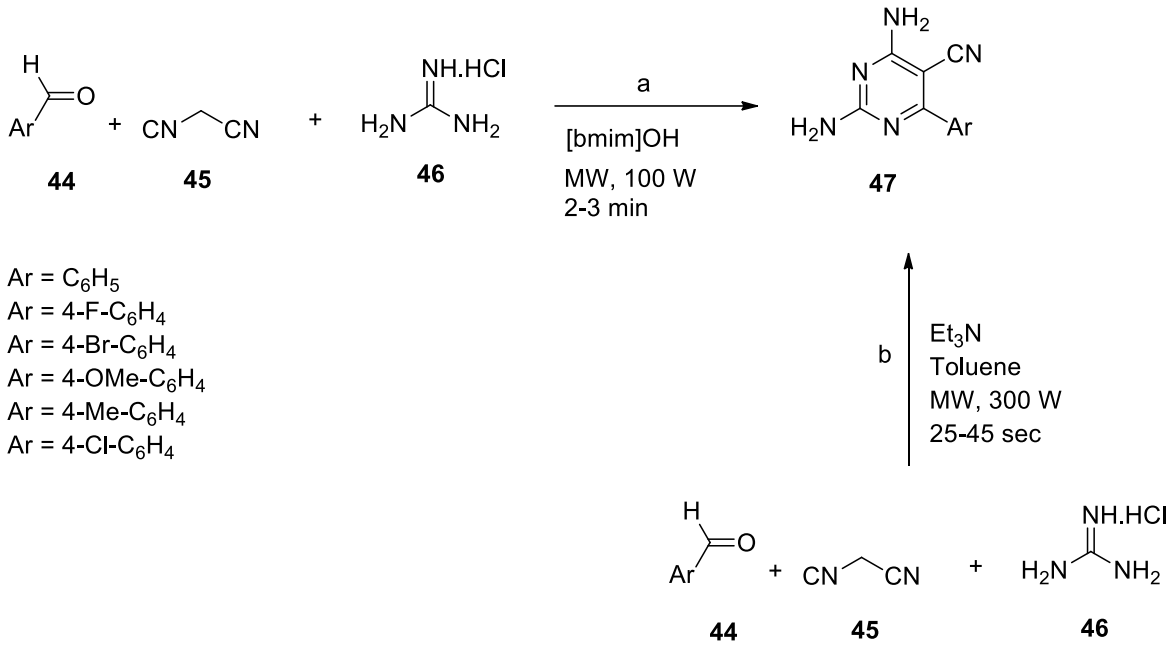

Scheme 9: Microwave-assisted one-pot synthesis of 6-substituted-2,4-diaminopyrimidine-5-carbonitriles.

We attempted the microwave-assisted one-pot synthesis following the reaction seen in **Scheme 9** *step b*, where benzaldehyde, malononitrile and gunadine hydrochloride were dissolved in toluene and treated with Et_3N base. When reacted for a time of 25-45 seconds, no reaction occurred as only starting material was observed on TLC. Reactions were also run for longer times, from 5 minutes up to 1 hour and unfortunately, in our hands the microwave assisted method was not successful as mostly the alkene intermediate **49** (where R = Ph) was isolated. We were unable to convert the intermediate **49** (where R = Ph) to the pyrimidine **30** under various conditions, which included exploring the use of different solvents, acetonitrile and THF, however the intermediate **49** (where R = Ph) persisted. The molar equivalents of the guanidine hydrochloride was also increased in an attempt to improve the reaction, however, this led to an increase in by-products, which were observed on TLC. The reaction in **Scheme 9** *step a* could not be explored because at the time of the experiment ionic liquid was not available.

Fortunately, an alternative method using conventional heating reported by Sheibani *et al.*[52], **Scheme 10**, was successful in synthesising the desired 6-substituted-2,4-diamino-5-carbonitrile-pyrimidines **30**.

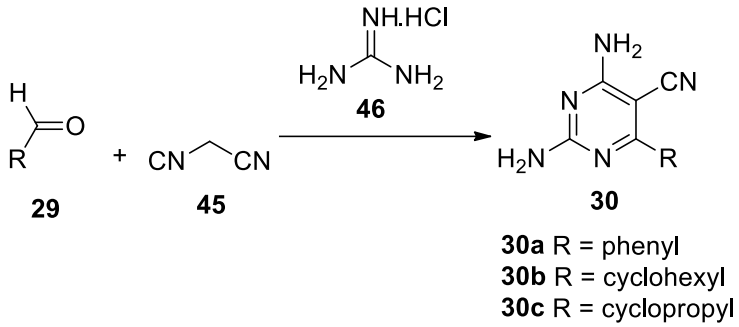

Scheme 10: Multicomponent reaction forming 6-substituted-2,4-diaminopyrimidine-5-carbonitriles (30). Reagents and conditions: NaOAc, H_2O/EtOH, reflux, N_2, 2.5-3h.

A suitably substituted aldehyde, malononitrile and guanidine hydrochloride were reacted in a one-pot synthesis in the presence of aqueous ethanol in a round bottomed flask and subjected to conventional heating to afford the desired functionalised pyrimidine core.

2.4.1. Synthesis of 2,4-diamino-6-phenylpyrimidine-5-carbonitrile (30a)[52]

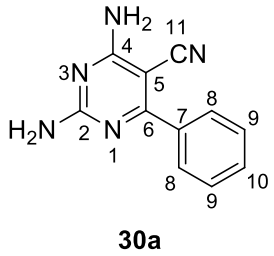

Figure 26: Structure of 2,4-diamino-6-phenylpyrimidine-5-carbonitrile (30a).

The first compound to be synthesised was compound **30a** which possesses a 6-phenyl substituent. It was fitting to start with this compound as most MCR reactions reported, afford products bearing aromatic substituents in the 6-position. Furthermore, we wish to determine whether the 6-phenyl substituent in our final compounds **28** will have an impact on the antiplasmodial activity when compared to the previously synthesised analogues **32**, (**Figure 21**). As shown in **Scheme 10**, a multicomponent reaction for the synthesis of compound **31a** (**Figure 26**) was achieved by reacting malononitrile and benzaldehyde under basic conditions, in a mixture of EtOH and H_2O. This reaction mixture was stirred at room temperature under a nitrogen atmosphere for 10 minutes to give the alkene intermediate **49**, (**Scheme 8**), which was monitored by the formation of a thick white mixture or by thin layer chromatography (TLC). Guanidine hydrochloride was then added, and the reaction mixture was heated to reflux under a nitrogen atmosphere for 2.5-3 hours. Purification of the crude product was achieved by silica

gel column chromatography, affording a yellow solid in a low yield of 11 %. A similar reaction in literature also afforded a yellow solid, however in much higher yields of 81 %.[52]

Initially, we discovered that this reaction is sensitive to the purity of the starting materials. Early attempts to form the alkene intermediate **49** resulted in a black solution, producing multiple spots on the TLC plate. With this observed, the purity of malononitrile was confirmed using ^{1}H NMR spectroscopy and the benzaldehyde was distilled prior to use using vacuum distillation. Following this optimisation, the reaction forming the alkene intermediate **49** was repeated and worked desirably.

It was also observed that reaction of malononitrile, benzaldehyde and guanidine hydrochloride resulted in consistently lower yields of product, producing a dark brown/black coloured reaction mixture. TLC suggested that the alkene intermediate was not being fully converted to product. Additional spots observed on the TLC also confirmed the presence of possible side reactions occurring. In an attempt to resolve these challenges, the more basic guanidine carbonate was used. This worked well, as the TLC confirmed a better conversion of the intermediate **49** to the desired product **30a** at an improved yield of 65 % from the previous 11 % yield reported. The use of guanidine carbonate resulted in the crude product precipitating and as a result of this, the product was purified by recrystallisation from EtOH/hexane.

It was also observed that the reaction is time sensitive when using either guanidine hydrochloride or guanidine carbonate. Reactions run overnight resulted in much lower yields and product decomposition.

Characterisation of the purified product **30a** was performed using ^{1}H and ^{13}C NMR spectroscopy, IR spectroscopy, HRMS and melting point.

The ^{1}H NMR spectrum for the product **30a** gave rise to 5 signals as expected. The signal at δ 7.75 ppm, which is a doublet of doublets, was assigned to the two equivalent aromatic protons at H-8. Three aromatic protons H-9 and H-10 gave rise to a multiplet signal at δ 7.55 – 7.43 ppm. The signal at 7.06 ppm was an overlapping singlet integrating for four protons, due to the two NH_2 groups. For further confirmation, the ^{13}C NMR spectrum was analysed, and the expected nine carbon signals were observed which matched the structure. Pyrimidine ring carbons C-6, C-4, C-2 and C-5 were observed at δ 169.4, 165.0, 163.0 and 75.9 ppm respectively, confirming formation of the aromatic ring in our MCR. Equivalent ^{13}C NMR spectroscopic signals for C-8 and C-9 were observed at δ 128.1 and 128.2 ppm respectively and the nitrile C-11 signal was observed at δ 117.9 ppm. The IR spectrum also showed the

presence of the NH_2, aromatic CH, and CN groups with bands at 3375, 3159 and 2206 cm^{-1} respectively. A melting point of 214-216 °C (lit. melting point 228 – 300°C)[52] was obtained and HRMS gave the desired mass of 212.0929 $[M+H]^+$ (theoretical value 212.0931).

With the success of this reaction, pyrimidine analogues containing an sp^3 hybridised cyclohexyl group and a smaller cyclopropyl group were explored. To the best of our knowledge, compound **30b** and **30c** are novel compounds.

2.4.2. Synthesis of 2,4-diamino-6-cyclohexylpyrimidine-5-carbonitrile (30b)

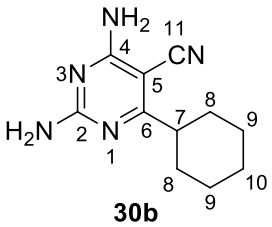

30b

Figure 27: Structure of 2,4-diamino-6-cyclohexylpyrimidine-5-carbonitrile(30b).

The synthesis of the compound **30b** was achieved using cyclohexanecarboxyaldehyde and followed the same optimised conditions for the synthesis of **30a**. The desired product **30b** was successfully synthesised and purified by recrystallisation using EtOH/hexane, giving a pale-yellow solid with a melting point of 223-224 °C in a yield of 67%.

The ^1H NMR spectrum confirmed the formation of the desired product **30b**. The two NH_2 groups gave rise to two singlet signals integrating for two protons each that were observed at δ 6.90 and 6.77 ppm, respectively. Proton H-7 gave rise to a triplet of triplets signal at δ 2.66 ppm. Multiplet signals in the aliphatic region, δ 1.73-1.09 ppm integrating for 10 protons confirmed the presence of the cyclohexyl axial and equatorial protons H-8 to H-10. The ^{13}C NMR spectrum gave rise to nine carbon signals as expected. Pyrimidine ring carbons C-6, C-4, C-2 and C-5 gave rise to signals at δ 177.4, 163.9, 162.7 and 75.7 ppm respectively. The nitrile C-11 signal was observed at δ 116.8 ppm and equivalent ^{13}C NMR spectroscopic signals for C-8 and C-9 were observed at δ 30.06 and 25.2 ppm respectively. IR spectroscopy also confirmed the presence of key functional groups; NH_2, CN and alkane CH with bands visible at 3390, 2197 and 1447cm^{-1} respectively in the IR spectrum. HRMS gave the desired mass of 218.1671 $[M+H]^+$ (theoretical value 218.1400).

2.4.3. Synthesis of 2,4-diamino-6-cyclopropylpyrimidine-5-carbonitrile (30c)

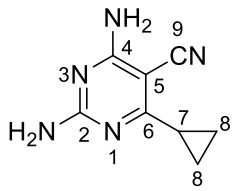

30c

Figure 28: Structure of 2,4-diamino-6-cyclopropylpyrimidine-5-carbonitrile (30c)

The synthesis of the compound **30c** was achieved using cyclopropanecarbaldehyde as the aldehyde in our optimised MCR. The desired product **30c** was successfully synthesised and purified by recrystallisation using EtOH/hexane. The product **30c** was isolated as a yellow solid in a yield of 26 %, and a mass of 176.1162 was observed by HRMS $[M+H]^+$ which corresponded to the expected mass for $C_8H_9N_5$.

Compound **30c** was the lowest yielding of this series. Attempts to increase the yield using longer reaction times and a stronger base KO^tBu were not successful as TLC confirmed the formation of by-products. The yield obtained however was enough to continue to the next step.

The ^1H NMR spectrum for product **30c** showed two NH_2 singlet signals at δ 6.91 and 6.67 ppm, respectively. Proton H-7 gave rise to a multiplet signal at δ 2.08 – 1.97 ppm. Multiplet signals observed in the aliphatic region, δ 1.01 – 0.92 ppm and integrating for four protons confirmed the presence of the cyclopropyl ring. The ^{13}C NMR spectrum showed seven carbon signals as expected. Pyrimidine ring carbons C-6, C-4, C-2 and C-5 were observed as signals at δ 174.5, 163.7, 162.9 and 76.9 ppm respectively. The nitrile C-9 signal was observed at δ 117.5 ppm and the signal for C-8 was observed at δ 9.4 ppm. Key functional groups; NH_2, CN and alkane CH were confirmed by IR spectroscopy with bands at 3426, 2204 and 1455 cm^{-1} respectively.

2.5. Synthesis of 6-substituted-2,4-diaminopyrimidine-5-carbaldehydes (31)

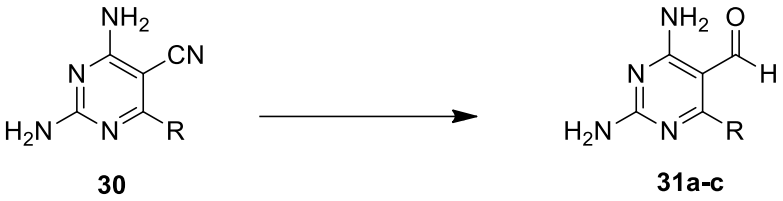

30a R = phenyl
30b R = cyclohexyl
30c R = cyclopropyl

Scheme 11: Reduction to afford 6-substituted-2,4-diaminopyrimidine-5-carbaldehyde and analogues (31)

With the carbonitrile pyrimidines **30** in hand, we were now able to convert the nitrile functional group into an aldehyde, as outlined in **Scheme 2**. The aldehyde functional group is utilised to introduce the flexible side chain via a reductive amination in a later step of the synthesis. This step involves reducing the 6-substituted-2,4-diaminopyrimidine-5-carbonitrile **30** to an imine which is hydrolysed under acidic conditions to afford 6-substituted-2,4-diaminopyrimidine-5-carbaldehydes **31**, **Scheme 11**.

Once again, we tested the reduction reaction on our 6-phenyl substituted pyrimidine first as it was readily available and the easiest to characterise. Initially, the method used to convert the nitrile to the aldehyde employed aqueous sulfuric acid (2.0 M) and 10 % Pd/C (0.1 mol eq)[53] under a hydrogen atmosphere and gave yields of 51 % of the desired product. Although this reaction gave moderate yields of product; the challenge was that the aldehyde produced could be reduced further to the alcohol, therefore resulting in a reaction mixture having both aldehyde and alcohol products in a 25 % yield. Although these products could be separated, a more selective method was desired. We therefore explored the use of Raney nickel in the reduction of our pyrimidine carbonitrile.

Raney nickel was developed by an American engineer, Murray Raney in 1926. It was used as an alternative catalyst for the hydrogenation of vegetable oils in industrial processes.[54] More recently it is used in organic synthesis as a heterogeneous catalyst and commonly for hydrogenation reactions. The proposed mechanism of this reaction in relation to our compounds is shown in **Scheme 12**.

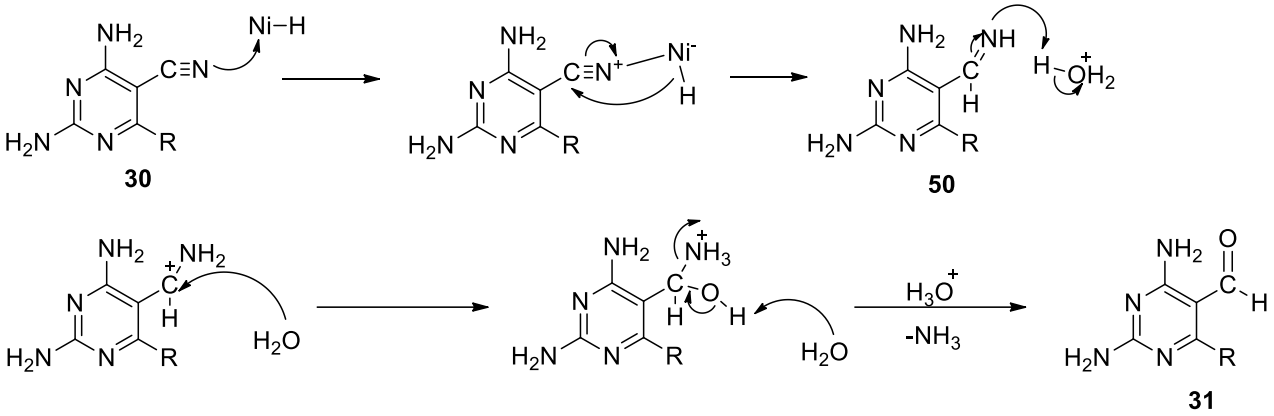

Scheme 12: Proposed mechanism for Raney nickel reduction.

As illustrated in **Scheme 12**, the nitrogen of the pyrimidine carbonitrile **30** coordinates to the nickel catalyst, which subsequently forms an imine intermediate **50**. Compound **50** then gets hydrolysed under acidic conditions to afford the desired aldehyde **31**.

Similarly, compound **31a-c**, to the best of our knowledge have not been reported in literature and therefore are novel.

2.5.1. Synthesis of 2,4-diaminopyrimidine-6-phenylpyrimidine-5-carbaldehyde (31a)

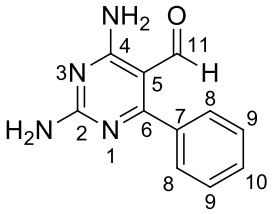

31a

Figure 29: Structure of 2,4-diaminopyrimidine-6-phenylpyrimidine-5-carbaldehyde (31a).

A Raney nickel reduction methodology converting nitriles to aldehydes was reported by Staskun *et al.* [55] The reported method was used for complex substituted heteroaromatic compounds. Initially the Raney nickel reduction method was performed using 90 % aq. formic acid. Unfortunately this reaction did not work well on our substrate as it did not fully convert the 2,4-diamino-6-phenylpyrimidine-5-carbonitrile **30a** to the desired product, making purification difficult as compound **30a** and the desired aldehyde product **31a** have a similar polarity and R*f* values, as observed on the TLC using different solvent systems. The isolated product was contaminated with starting material which was observed by a characteristic ^{13}C NMR spectroscopic peak in the region of 117 ppm and was only isolated in yields of 20 - 25

%. To try to optimise this reaction, a similar method reported by Staskun *et al*. utilising 75 % aq. formic acid as the solvent and freshly prepared Raney nickel was attempted.[55] For our compounds however, this method was not successful as only the starting material **30a** was recovered. To try and improve the conversion of compound **30a** using this method, longer reaction times were explored (1 up to 16 hours), however these attempts were also unsuccessful. These results did not discourage us however as literature suggested that various percentages of formic acid (75 – 99 %) and amounts of Raney nickel afforded significantly different results for different compounds.[55] These findings prompted us to manipulate the aqueous acid solvent systems until we found the optimum solvent system, 81 % aq. formic acid, which fully converted compound **30a** to compound **31a**, therefore making the purification easier. It is however, still unclear why a minimal change in the percentage of the acid could have such a significant effect on the reaction. The reaction was also sensitive to the quality of Raney nickel, as it was observed that freshly prepared Raney nickel gave better results than older previously prepared batches.

The optimised reduction of compound **30a** to form compound **31a** was achieved by dissolving compound **30a** in 81 % aq. formic acid. This was followed by the addition of Raney nickel (3-6 eq. by mass) to the reaction mixture. The reaction was heated at reflux under a nitrogen atmosphere for 1 hour. The resulting crude product was filtered through celite, to separate the nickel from the product (taking care not to filter to dryness) and the filtrate was collected, neutralised to pH 7 with solid $NaHCO_3$ and the organic component extracted using ethyl acetate. The organic extract was concentrated in *vacuo* and further purified by silica gel column chromatography, affording product **31a** as a white solid in a 56 % yield. IR spectroscopy confirmed the presence of the NH_2, aromatic CH, and C=O groups as bands visible at 3118, 2869 and 1536 cm^{-1} respectively.

The ^1H NMR spectrum for the product **31a** gave rise to 5 signals. The significant signal expected in this spectrum was that of the aldehyde proton as this would confirm the functional group conversion of the nitrile in compound **30a** to the aldehyde in compound **31a**. The singlet signal observed at δ 9.68 ppm was characteristic of the aldehyde proton H-11. A singlet signal at δ 8.76 ppm belonged to one of the protons of 4-NH_2 and the singlet signal of the other 4-NH_2 proton was observed at δ 5.56 ppm. This was significant as this suggested intramolecular hydrogen bonding between the one hydrogen of the NH_2 group and the oxygen of the carbonyl group, as shown in **Figure 30**. The phenyl protons H-8 to H-10 gave rise to a multiplet signal integrating for five protons at δ 7.56 – 7.44 ppm. A singlet at δ 5.36 ppm belonging to 2-NH_2

was also observed. The ^{13}C NMR spectrum confirmed the structure and purity of compound **31a**, as the nitrile signal of the starting material **30a** observed previously at 117.9 ppm was not present and a new signal due to aldehyde carbonyl C-11, was observed at δ 190.6 ppm. Equivalent ^{13}C NMR spectroscopic signals for C-8 and C-9 were observed at δ 128.6 and δ 129.6 ppm respectively. The pyrimidine ring carbons signals were observed at similar regions as compound **30a**, as expected, except for C-5 which shifted to δ 104.7 ppm, confirming the presence of the aldehyde functional group. A molecular ion of mass 215.0932 $[M+H]^+$ was observed by HRMS (theoretical value 215.0927).

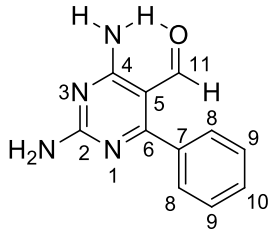

31a

Figure 30: Structure of intramolecular hydrogen bond possible in 2,4-diaminopyrimidine-6-phenylpyrimidine-5-carbaldehyde (31a)

The success of this reaction enabled us to apply this method to the synthesis of aldehydes **31b** and **31c**.

2.5.2. Synthesis of 2,4-diaminopyrimidine-6-cyclohexylpyrimidine-5-carbaldehyde (31b)

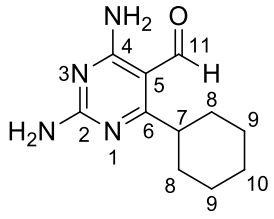

31b

Figure 31: Structure of 2,4-diaminopyrimidine-6-cyclohexylpyrimidine-5-carbaldehyde (31b)

The synthesis of the compound **31b** was achieved by a functional group conversion of the nitrile group to an aldehyde group following the optimised conditions described for the preparation of **31a**. The desired product **31b** was successfully synthesised and purified by silica gel column chromatography, giving a white solid in a yield of 59 %, with a melting point of

211-214 ºC and a molecular ion of mass 221.1398 obtained by HRMS (theoretical value 221.1397).

Evidence for the formation of the desired product was found on the ^{1}H NMR spectrum for **31b**, where a singlet signal at δ 10.15 ppm belonging to the aldehyde proton H-11 was observed. Two singlet signals at δ 8.83 and δ 5.62 ppm integrating for one proton each were observed and were assigned to the two protons of the hydrogen bonded 4-NH_2 group, similar to what was observed for compound **31a**. A triplet of triplets signal was observed for H-7 at δ 3.16 ppm as expected. The cyclohexyl protons H-8 to H-10, gave rise to multiplet signals integrating for ten protons in the range of δ 1.89 – 1.22 ppm. The ^{13}C NMR spectrum showed nine carbon signals as expected, with the characteristic pyrimidine ring carbon signals observed at similar regions to compound **31a**. The nitrile C-11 signal previously observed at δ 116.8 ppm was not present and a new carbonyl C-11 peak was observed at δ 188.0 ppm as expected. C-8 and C-9 gave rise to signals observed at 31.9 and 26.4 ppm respectively. The presence of the NH_2, C=O and alkane CH groups was confirmed by IR spectroscopy with bands visible at 3370, 1551 and 1470 cm^{-1} respectively.

2.5.3. Synthesis of 2,4-diaminopyrimidine-6-cyclopropylpyrimidine-5-carbaldehyde(31c)

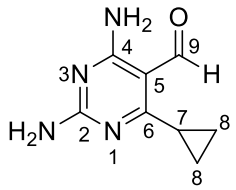

31c

Figure 32: Structure of 2,4-diaminopyrimidine-6-cyclopropylpyrimidine-5-carbaldehyde(31c)

In a similar fashion, **31c** was synthesised by Raney nickel reduction of **30c** using the same optimised conditions for the preparation of **31a** and **31b**. The desired product **31c** was isolated as a white solid with a melting point of 235-236 °C, in a yield of 50%.

The ^{1}H NMR spectrum for product **31c** showed a singlet signal at δ 10.24 ppm indicating the presence of the aldehyde proton H-9. NH_2 signals were not observed due to hydrogen-deuterium exchange with the solvent MeOD. Proton H-7 gave rise to a triplet of triplets signal at δ 2.50 ppm. Multiplet signals integrating for four protons belonging to cyclopropyl H-8 protons were observed in the range of δ 1.22 – 0.96 ppm. The ^{13}C NMR spectrum showed no nitrile C-9 signal previously observed at δ 117.5 ppm, and the desired aldehyde signal, was

observed at δ 189.3 ppm, as expected. The signal for the two C-8 carbons was observed at δ 10.5 ppm. The pyrimidine ring carbon signals were observed at similar regions to compound **31a**, as expected. The IR spectrum also showed the presence of the NH_2, C=O and alkane CH functional groups with bands visible at 3353, 1632 and 1440 cm^{-1} respectively. HRMS confirmed product formation by generating a molecular ion of mass 179.0924 $[M+H]^+$ (theoretical value 179.0927).

2.6. Attempted synthesis of 6-substituted-2,4-diaminopyrimidine-5-phenethylamines (28) using reductive amination methodology

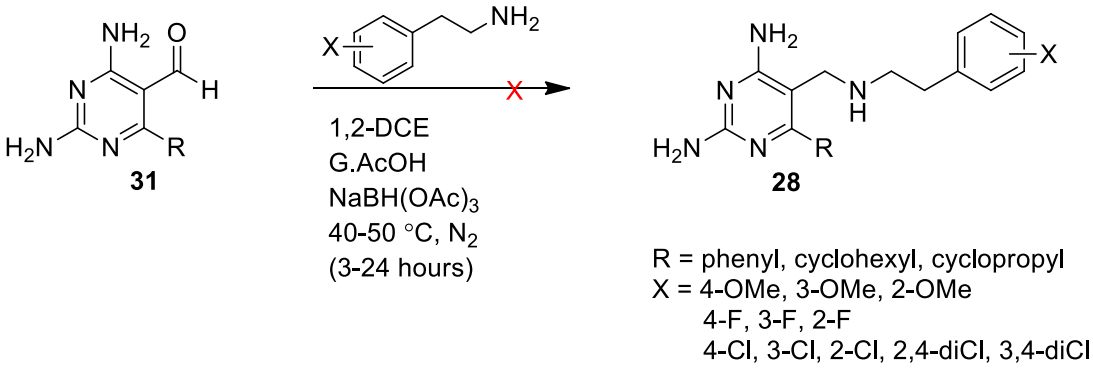

Scheme 13: Attempted one-pot reductive amination reaction.

A successful synthesis of the pyrimidine carbaldehydes **31** meant that we could now attempt the final step of our synthesis to get the desired final product **28**. A one-pot reductive amination reaction using a method reported by Abdel-Magid *et al*. was explored, as shown in **Scheme 13**.[56] To test the reaction the carbaldehyde **31a** was dissolved in 1,2-DCE in the presence of glacial acetic acid. Subsequently, a substituted phenethylamine was added to the solution and left to stir for 30 minutes. Upon dissolution, $NaBH(OAc)_3$ was added, and the reaction was left to stir under a nitrogen atmosphere. The crude product isolated from the reaction was purified using silica gel column chromatography. Unfortunately, this reaction was not ideal as the desired amine product **28** was isolated in a low yield and by-products were observed by TLC. Purification therefore proved challenging as the R*f* values of the product **28** and the other impurities were similar. Other reducing agents such as $NaCNBH_4$ and $NaBH_4$ were used to try to optimise the reaction, however these did not yield much success. Interestingly, we observed that the major product produced in this reaction was a stable imine intermediate of general structure **51** (**Figure 33**). Upon further investigation using ^1H NMR spectroscopy, it was observed that intramolecular hydrogen bonding existed between the lone pairs of the imine

nitrogen atom and a hydrogen atom of the NH_2 functional group. A crystal structure of the analogue where X = 3-OMe confirming these findings was also obtained, **Figure 33**. The presence of the intramolecular hydrogen bond also made these imines favour the (*E*) geometric isomer. Going forward however, these structures will be represented in a linear conformation to save space.

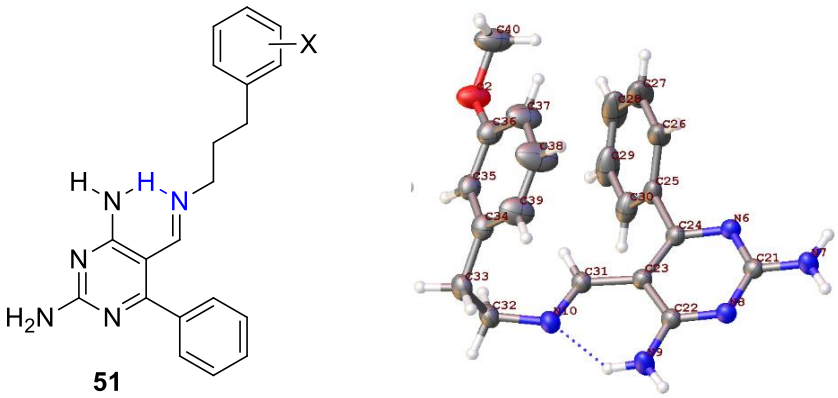

Figure 33: (Left) General structure illustrating intramolecular hydrogen bonding of stabilised imine 51 (Right) Crystal structure of stabilised imine 51b, X = 3-OMe.

Following the isolation of the imine intermediate in the one-pot reductive amination reaction, we decided to decouple the two reactions by forming the imine **51** first, and then reducing the imine to the desired amine **28** in the final step. The imine intermediate appeared to be particularly stable, which is not characteristic of conventional imines, but allowed for isolation and purification of the intermediate. This was demonstrated during the EtOAc/water extraction where normally one would expect some of the imine to hydrolyse back to the respective aldehyde. This however was not the case for our imines and we were able to purify the imine using column chromatography. This provided us with an advantage as now we could directly convert the pure imine intermediate to the desired product and have a more favourable purification of the final product. The highly polar pyrimidine analogues are notoriously difficult to purify.

2.7. Synthesis of 6-substituted-2,4-diaminopyrimidine-5-phenethylimines (51)

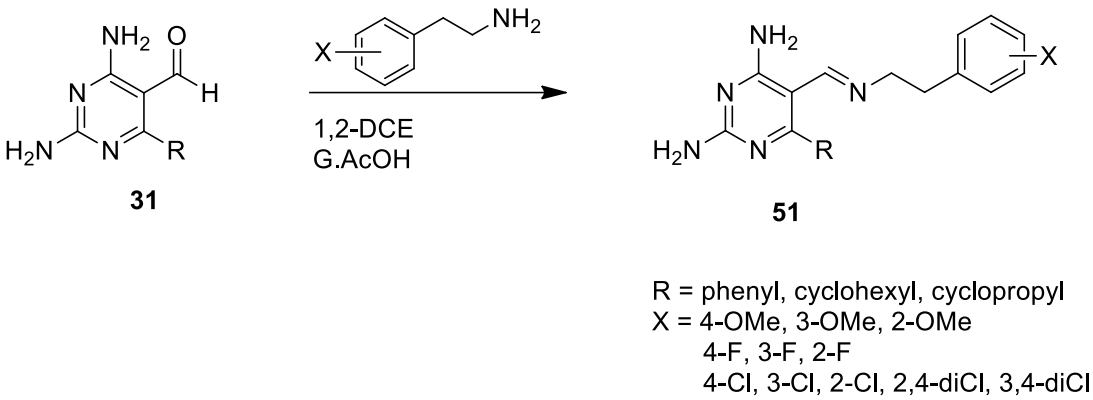

Scheme 14: **Imination reaction and conditions forming 6-substituted-2,4-diaminopyrimidine-5-phenethylimine (51) and analogues.**

The imination step involved reacting a substituted phenethylamine with 6-substituted-2,4-diaminopyrimidine-5-carbaldehydes **31**, to make 6-substituted-2,4-diaminopyrimidine-5-phenethylimines **51**, **Scheme 14**. The proposed mechanism of conversion of the aldehyde to the imine is shown in **Scheme 15**.

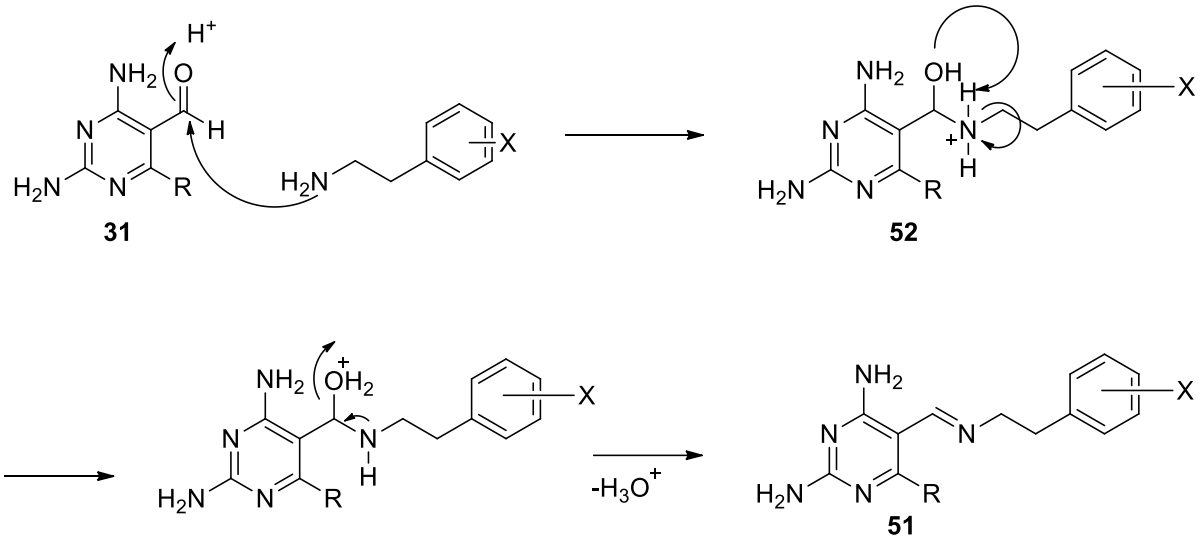

Scheme 15: Proposed mechanism for the synthesis of 6-substituted-2,4-diaminopyrimidine-5-phenethylimines (51).

In **Scheme 15** a nucleophilic addition of the phenethylamine to the carbonyl of the carbaldehyde **31** under acidic conditions initiates the reaction to form a hydroxy ethanaminium intermediate **52**. The intermediate **52** undergoes proton transfer which subsequently results in water leaving to generate the product **51**.

2.7.1. Synthesis of (*E*)-6-phenyl-5-{[(2-methoxyphenethyl)imino]methyl}pyrimidine-2,4 diamine (51a)

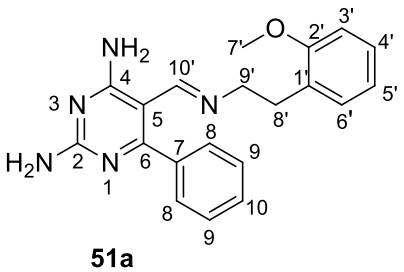

51a

Figure 34: Structure of (*E*)-6-phenyl-5-{[(2-methoxyphenethyl)imino]-methyl}-pyrimidine-2,4 diamine (51a)

To test the imination reaction, (*E*)-6-phenyl-5-{[(2-methoxyphenethyl)imino]methyl}-pyrimidine-2,4 diamine **51a**, (**Figure 34**) was synthesised. The pyrimidine carbaldehyde **31a** was dissolved in 1,2-DCE in the presence of glacial acetic acid. Following this, 2-methoxyphenethylamine was added to the reaction mixture with constant stirring. The solution was heated at reflux and left to stir for 3 hours under a nitrogen atmosphere. The reaction progress was monitored by TLC and upon completion of the reaction, the crude product was isolated and then purified using column chromatography on neutral alumina. The imine product **51a**, was isolated as a white solid in 85 % yield and had melting point of 154-156 °C.

Some conventional methods of imine formation do not require the use of an acid catalyst, that is, acetic acid in our case. However, since the substituted phenethylamines we used were poor nucleophiles, the acetic acid was required to catalyse the reaction. The role of the acid is to protonate the carbonyl oxygen of the carbaldehyde **31a,** which in turn makes the carbonyl carbon of the carbaldehyde **31a** more electrophilic, hence more susceptible to nucleophilic attack by the 2-methoxyphenethylamine.

Although the unreacted carbaldehyde **31a** and imine product **51a** had slightly differing R*f* values, it was difficult to separate the two compounds using silica gel column chromatography

or flash column chromatography on silica with different solvent systems explored. Fortunately, the use of neutral alumina in column chromatography showed optimum separation.

Characterisation using IR spectroscopy confirmed the key NH_2, aromatic CH, C=N and C-O groups with bands observed at 3267, 2922, 1647 and 1245 cm^{-1} respectively. Interestingly, a sharp NH signal in the IR spectrum was observed due to the presence of hydrogen bonding. A molecular ion of mass 348.1829 $[M+H]^+$ was obtained using HRMS which corresponded to $C_{20}H_{22}N_5O$.

The ^1H NMR spectrum for the product **51a** integrated for 21 protons as expected. As before, the signal due to the protons of the 4-NH_2 group appeared as two signals at δ 5.79 ppm and δ 9.86 ppm, each integrating for one proton. This again demonstrated intramolecular hydrogen bonding between the lone pairs of the imine nitrogen atom N-8, and a hydrogen atom of 4-NH_2, **Figure 33**. The singlet signal observed at δ 7.97 ppm was due to the imine proton H-10'. This was significant as this indicated a successful conversion of the carbaldehyde **31a** to the desired imine **51a**. The aromatic proton H-3' gave rise to a doublet signal at δ 7.06 ppm and the rest of the aromatic protons showed multiplet signals in the range of δ 7.42 – 6.77 ppm. The singlet signal at δ 3.75 ppm was characteristic of the methoxy protons H-7'. The triplet signals each integrating for two protons at δ 3.61 and 2.90 ppm arose due to H-8' and H-9' respectively. The ^{13}C NMR spectrum was also analysed for further confirmation. The pyrimidine ring C-6, C-4, C-2 and C-5 signals were observed at δ 169.5, 163.8, 161.7 and 101.3 ppm as expected. The imine C-10' signal was observed at δ 159.7 ppm, confirming product formation. Ten aromatic carbons belonging to the phenyl rings were also observed in the aromatic region of δ 157.7 to 110.3 ppm. The aliphatic region of the spectrum showed carbon signals belonging to the two CH_2 carbons, C-8' and C-9' and one CH_3 carbon, C-7' at δ 32.4, 61.1 and 55.3 ppm respectively.

The success of this reaction enabled us to apply this method to synthesise a library of analogues **51b-51g', Figure 35**. The same reaction conditions proposed in **Scheme 14** were used. All the imine analogues were isolated in relatively high yields ranging from 61-100 %, with the cyclohexyl derivatives **51l-v** generally giving the best yields (71-100 %), **Figure 35**. The imine intermediates **51a-g'** also serve as novel compounds as these compounds have not been reported in literature.

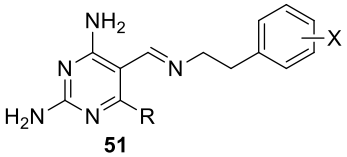

51

51a R = phenyl, X = 2-OMe, 85 %	51l R = cyclohexyl, X = 2-OMe, 88 %	51w R = cyclopropyl, X = 2-OMe, 82 %
51b R = phenyl, X = 3-OMe, 84 %	51m R = cyclohexyl, X = 3-OMe, 88 %	51x R = cyclopropyl, X = 3-OMe, 92 %
51c R = phenyl, X = 4-OMe, 95 %	51n R = cyclohexyl, X = 4-OMe, 99 %	51y R = cyclopropyl, X = 4-OMe, 88 %
51d R = phenyl, X = 2-F, 99 %	51o R = cyclohexyl, X = 2-F, 80 %	51z R = cyclopropyl, X = 2-F, 69 %
51e R = phenyl, X = 3-F, 79 %	51p R = cyclohexyl, X = 3-F, 88 %	51a' R = cyclopropyl, X = 3-F, 66 %
51f R = phenyl, X = 4-F, 86 %	51q R = cyclohexyl, X = 4-F, 87 %	51b' R = cyclopropyl, X = 4-F, 74 %
51g R = phenyl, X = 2-Cl, 98 %	51r R = cyclohexyl, X = 2-Cl, 71 %	51c' R = cyclopropyl, X = 2-Cl, 66 %
51h R = phenyl, X = 3-Cl, 61 %	51s R = cyclohexyl, X = 3-Cl, 95 %	51d' R = cyclopropyl, X = 3-Cl, 90 %
51i R = phenyl, X = 4-Cl, 97 %	51t R = cyclohexyl, X = 4-Cl, 83 %	51e' R = cyclopropyl, X = 4-Cl, 97 %
51j R = phenyl, X = 2,4-diCl, 97 %	51u R = cyclohexyl, X = 2,4-diCl, 92 %	51f' R = cyclopropyl, X = 2,4-diCl, 96 %
51k R = phenyl, X = 3,4-diCl, 94 %	51v R = cyclohexyl, X = 3,4-diCl, 100 %	51g' R = cyclopropyl, X = 3,4-diCl, 86 %

Figure 35: General structure of (*E*)-6-substituted-2,4-diaminopyrimidine-5-phenethylimines (51a-g') and isolated yields of products.

Table 4 below shows the key ^{1}H NMR and ^{13}C NMR spectroscopic signals for products **51b-g'**. Additional characterisation data can be found in the experimental section, Chapter 4.

All compounds **51b-g'** were fully characterised using ^{1}H and ^{13}C NMR spectroscopy, IR spectroscopy, HRMS and melting point. In each case, the 4-NH_2 protons split confirming intramolecular H-bonding. The singlet signal due to the imine proton (*H*-C=N) was observed for all compounds in the region of δ 7.9-8.3 ppm in the ^{1}H NMR spectra, as expected. The presence of the imine carbon (*C*=N) was further confirmed for all compounds in the ^{13}C NMR spectra by the characteristic signal being observed in the region of δ 157.9-160.6 ppm. Most of the compounds were isolated as solids (except for some 6-cyclohexyl and 6-cyclopropyl analogues isolated as gels) with relatively high melting points in the range of 115-226 °C. The 6-phenyl analogues generally displayed the highest melting points (154-226°C), followed by the 6-cyclohexyl (126-167 °C) and then the 6-cyclopropyl analogues (115-171°C). These relatively high melting points can be attributed to the intramolecular hydrogen bonding present in all the compounds.

Table 4: Key ^{1}H NMR and ^{13}C NMR spectroscopic signals for (*E*)-6-substituted-2,4-diaminopyrimidine-5-phenethylimines (51b-g').

Entry	4-NH_2 (ppm)	*H*-C=N (ppm)	*C*=N (ppm)	Entry	4-NH_2 (ppm)	*H*-C=N (ppm)	*C*=N (ppm)
51b	9.82, 5.61 (s)	7.99 (s)	160.1	**51r**	9.77, 5.44 (s)	8.38 (s)	158.4
51c	9.85, 5.48 (s)	7.96 (s)	160.1	**51s**	9.72, 5.33 (s)	8.39 (s)	158.4
51d	9.79, 5.49 (s)	8.01 (s)	160.3	**51t**	9.74, 5.35 (s)	8.33 (s)	158.4
51e	9.75, 5.48 (s)	8.00 (s)	160.4	**51u**	9.70, 5.47 (s)	8.35 (s)	158.6
51f	9.79, 5.46 (s)	7.96 (s)	160.3	**51v**	9.68, 5.37 (s)	8.37 (s)	158.6
51g	9.78, 5.64 (s)	8.00 (s)	160.3	**51w**	9.83, 5.53 (s)	8.66 (s)	157.9
51h	9.75, 5.48 (s)	8.00 (s)	160.4	**51x**	9.78, 5.58 (s)	8.65 (s)	158.3
51i	9.77, 5.46 (s)	7.93 (s)	160.4	**51y**	9.80, 5.69 (s)	8.62 (s)	158.2
51j	9.79, 5.56 (s)	7.96 (s)	160.5	**51z**	9.72, 5.56 (s)	8.65 (s)	158.5
51k	9.72, 5.58 (s)	7.95 (s)	160.6	**51a'**	9.70, 5.54 (s)	8.66 (s)	158.6
51l	9.86, 5.32 (s)	8.37 (s)	157.9	**51b'**	9.72, 5.35 (s)	8.62 (s)	158.5
51m	9.80, 5.51 (s)	8.38 (s)	158.2	**51c'**	9.74, 5.54 (s)	8.65 (s)	158.5
51n	9.85, 5.51 (s)	8.33 (s)	158.06	**51d'**	9.68, 5.67 (s)	8.67 (s)	158.6
51o	9.76, 5.43 (s)	8.38 (s)	158.3	**51e'**	9.70, 5.44 (s)	8.61 (s)	158.6
51p	9.73, 5.44 (s)	8.39 (s)	158.3	**51f'**	9.66, 5.68 (s)	8.62 (s)	158.7
51q	9.75, 5.33 (s)	8.34 (s)	158.3	**51g'**	9.64, 5.59 (s)	8.66 (s)	158.8

2.8. Synthesis of 6-substituted-2,4-diaminopyrimidine-5-phenethylamines (28)

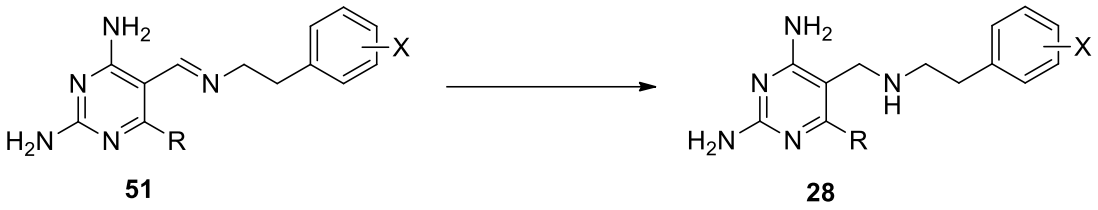

R = phenyl, cyclohexyl, cyclopropyl
X = 4-OMe, 3-OMe, 2-OMe
4-F, 3-F, 2-F
4-Cl, 3-Cl, 2-Cl, 2,4-diCl, 3,4-diCl

Scheme 16: Reduction of imines (51) for the synthesis of 6-substituted-2,4-diaminopyrimidine-5-phenethylamine and analogues (28).

The success of the imination reaction meant that we could now proceed to the final step and synthesise the desired 6-substituted-2,4-diaminopyrimidine-5-phenethylamines **28**. The final step of the synthesis involved a reduction of the imine functional group of compounds **51** to the amine functional group of compounds **28**, as shown in **Scheme 16** (attempted reactions conditions shown in **Table 5**). **Scheme 17** illustrates the proposed mechanism of the reduction of imine **51** to amine **28**.

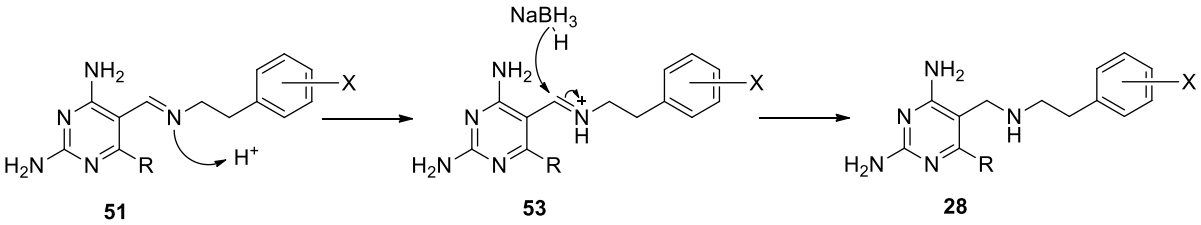

Scheme 17: Proposed mechanism for the synthesis of 6-substituted-2,4-diaminopyrimidine-5-phenethylamine and analogues (28).

The reaction proceeds with the protonation of the nitrogen of the imine functional group to form the iminium ion **53**, which undergoes a nucleophilic addition by the hydride ion of $NaBH_4$ to generate the desired product **28**.

2.8.1. Synthesis of 6-phenyl-5-{[(2-methoxyphenethyl)amino]methyl}pyrimidine-2,4-diamine (28a)

For the 6-phenyl series of compounds, although the molecular modelling results were promising, we were still sceptical about how these compounds would perform when subjected

to biological assays, based on results obtained from similar analogues (**Figure 21**, compounds **32**). Due to time constraints, we therefore decided that for this series only the analogues where X = OMe will be synthesised as these gave the best IFD docking scores. If these compounds perform well in the biological assays, the remaining 6-phenyl analogues could then also be synthesised and assessed for biological activity at a later stage.

Initial attempts to convert the imine **51** to amine **28** explored the use of hydrogenation reactions and hydride reduction reactions. **Table 5** summarises some of the reaction conditions explored, and the outcomes observed.

Table 5: Hydrogenation and hydride reduction reactions tested on 28a

Entry	Reaction Conditions	% Product 28a
i	H_2 (balloon), Pd/C (10-25 % by mass), EtOH, room temp. (16 hours)	0 %[a]
ii	H_2 (3 bar), Pd/C (25 % by mass), EtOH, (16 hours)	35 %
iii	H_2 (4 bar), Pd/C (25 % by mass), EtOH, (16 hours)	11 %
iv	H_2 (4 bar), Pd/C (25 % by mass), MeOH, (16 hours)	20 %
v	$NaBH_4$ (3 eq), DCE/THF, room temp. N_2 (16 hours)	20 %
vi	$NaBH_4$ (6.5 eq), DCE/THF, G. AcOH (10 eq), room temp. N_2 (2 hours)	30 %
vii	$NaBH_4$ (6.5 eq), DCE/THF, G. AcOH (10 eq), reflux. N_2 (16 hours)	0 %[a]
viii	LAH (1 eq), THF, room temp. N_2 (2 hours)	10 %

[a] Starting material recovered.

As shown in **Table 5**, the conventional method of hydrogenation (i) using a balloon filled with hydrogen gas and running the reaction at room temperature in a round bottomed flask was attempted, without much success, as no conversion to the product was observed. We then moved to more vigorous hydrogenation methods using a hydrogenator with pressures varying from 3-4 bars and percentage Pd/C increased from 10-25 %, and EtOH or MeOH tested as solvents (ii-iv). These attempts did not work as well as anticipated as most of the imine **51** would be recovered, hence producing low yields for the amine **28** as seen in **Table 5**. At this point it was evident that the hydrogen bonding in the imine contributes to its increased stability

hence making it relatively non-reactive. Hydride reductions using $NaBH_4$ (v-vii) were also attempted while varying temperatures and reaction times and exploring the use of an acid catalyst. The results for these were promising however, the yields needed improving. Another hydride explored was LAH (viii). This reaction was unsuccessful however, as it afforded the product in a low yield with many by-products, which made purification challenging. We avoided the conventional use of MeOH with $NaBH_4$ to avoid side reactions of MeOH acting as a nucleophile.

With this in mind, we then considered using the $NaBH_4$ hydride reducing agents at a lower pH. Some conventional methods used to reduce imines to amines do not require the reaction to be done in an acidic medium. However, since our imines **51** possess intramolecular hydrogen bonding between the lone pairs of the imine nitrogen atom and a hydrogen atom of the NH_2 functional group, **Figure 33**, this enables them to have an increased stability and as a result a lack of reactivity. The role of the acidic medium in this reaction is to disrupt the hydrogen bonding by forming an iminium ion of general structure **53**, **Scheme 17** which enables the nucleophilic attack of the hydride from $NaBH_4$ to occur more favourably.

To test the reduction reaction at a lower pH, 6-phenyl-5-{[(2-methoxyphenethyl)amino]-methyl}pyrimidine-2,4-diamine **28a** was synthesised. The imine **51a** was dissolved in a 1:2 mixture of 1,2-DCE and THF. This was followed by the addition of acetic acid to the reaction mixture until a pH of between 4 and 5 was reached. Once the desired pH was reached, $NaBH_4$ was added and the reaction was allowed to stir at room temperature, under a nitrogen atmosphere. The reaction progress was monitored by TLC and upon completion the crude product was isolated and purified using silica gel column chromatography. The amine product **28a**, **Figure 36**, was isolated as a colourless gel in a 45 % yield. It must be noted however that the reaction is time sensitive. The ideal time to run the reaction was found to be 30 minutes. When monitoring the reaction by TLC an intense product spot was observed within 10 minutes of the reaction, however, after isolation and purification it was observed that there is still unconverted imine present. This resulted in the lower yield observed in **28a**. It was also observed on TLC that when running the reaction for longer than 30 minutes (1 hour in our case), by-products formed and hence this resulted in lower yields.

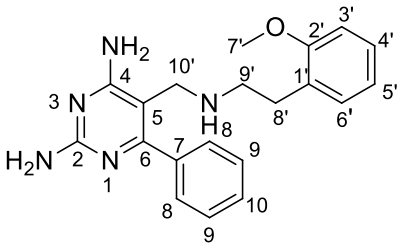

28a

Figure 36: Structure of 6-substituted-2,4-diaminopyrimidine-5-phenethylamine (28a)

The ^{1}H NMR spectrum for the product **28a** integrated for 22 protons as expected. Multiplet signals ranging from δ 7.44 – 7.34 ppm were characteristic of the phenyl protons H-8 to H-10. Signals at δ 7.19 ppm of H-4' and δ 7.01 ppm of H-5', appeared as a doublet of doublet of doublets and a triplet of doublets respectively. A multiplet peak at δ 6.90 – 6.82 ppm was characteristic of protons H-3' and H-6'. Two NH_2 singlet signals each integrating for two protons were observed at δ 6.37 ppm and δ 5.30 ppm. This was significant as the intramolecular hydrogen bonding seen in the carbaldehyde **31a** and imine **51a** was no longer present. The singlet signal observed at δ 3.77 ppm was characteristic of the methoxy protons H-7'. A singlet signal observed at δ 3.62 ppm belonged to the CH_2 protons H-10'. This was significant as this indicated a successful conversion of the imine **51a** to the desired amine **28a**. The multiplet produced at signal δ 2.80 – 2.70 ppm belonged to the two CH_2 protons, H-8' and H-9'. The ^{13}C NMR spectrum provided further confirmation of the formation of product **28a**. The pyrimidine ring C-6, C-4, C-2 and C-5 signals were observed at δ 165.3, 164.4, 160.7 and 102.8 ppm as expected. The signal at δ 157.6 was characteristic of the aromatic C-O carbon, C-2'. The remaining eight aromatic carbons belonging to the phenyl rings were also observed in the aromatic region of δ 138.3 to 110.5 ppm. DEPT NMR spectroscopy showed carbon signals belonging to the three CH_2 carbons, C-10', C-9' and C-8' and one methoxy CH_3 carbon, C-7' at δ 46.5, 48.2, 30.5, and 55.4 ppm respectively. The NH_2, aromatic CH, N-H and C-O functional groups gave rise to bands at 3174, 2939, 1613 and 1242 cm^{-1} respectively in the IR spectrum and a mass of 350.1963 $[M+H]^+$ was observed on the HRMS (theoretical value 350.1975).

The success of this reaction enabled us to apply this method to the synthesis of a library of analogues **28b-g'**, **Figure 37**. The same reaction conditions for the synthesis of **28a** was used with the reaction run for 30 minutes. All the amine analogues **28b-g'** were isolated in moderate to high yields ranging from 33-96 %, with the cyclohexyl derivatives **28l-v** generally giving

the best yields (60-96 %). To the best of our knowledge, the synthesised compounds **28** are novel compounds.

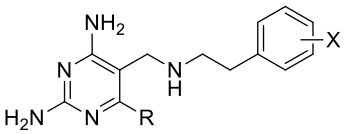

28

28a R = phenyl, X = 2-OMe, 45 %
28b R = phenyl, X = 3-OMe, 33 %
28c R = phenyl, X = 4-OMe, 63 %
28e R = phenyl, X = 3-F, 68 %
28h R = phenyl, X = 3-Cl, 63 %

28l R = cyclohexyl, X = 2-OMe, 93 %
28m R = cyclohexyl, X = 3-OMe, 91 %
28n R = cyclohexyl, X = 4-OMe, 84 %
28o R = cyclohexyl, X = 2-F, 86 %
28p R = cyclohexyl, X = 3-F, 89 %
28q R = cyclohexyl, X = 4-F, 92 %
28r R = cyclohexyl, X = 2-Cl, 96 %
28s R = cyclohexyl, X = 3-Cl, 84 %
28t R = cyclohexyl, X = 4-Cl, 87 %
28u R = cyclohexyl, X = 2,4-diCl, 60 %
28v R = cyclohexyl, X = 3,4-diCl, 71 %

28w R = cyclopropyl, X = 2-OMe, 83 %
28x R = cyclopropyl, X = 3-OMe, 78 %
28y R = cyclopropyl, X = 4-OMe, 82 %
28z R = cyclopropyl, X = 2-F, 68 %
28a' R = cyclopropyl, X = 3-F, 75 %
28b' R = cyclopropyl, X = 4-F, 74 %
28c' R = cyclopropyl, X = 2-Cl, 75 %
28d' R = cyclopropyl, X = 3-Cl, 79 %
28e' R = cyclopropyl, X = 4-Cl, 70 %
28f' R = cyclopropyl, X = 2,4-diCl, 73 %
28g' R = cyclopropyl, X = 3,4-diCl, 84 %

Figure 37: General structure of 6-substituted-2,4-diaminopyrimidine-5-phenethylamine analogues (28a-g') and isolated yields of products.

Table 6 below shows the key ^{1}H NMR and ^{13}C NMR spectroscopic signals for products **28b-g'**. Additional characterisation data can be found in the experimental section, Chapter 4.

All compounds **28b-g'** were isolated as gels. ^{1}H NMR, ^{13}C NMR and IR spectroscopy and HRMS were used as techniques to characterise the purified products **28b-g'**. As seen in **Table 6**, each compound produced two NH_2 singlet signals in the ^{1}H NMR spectrum thus confirming an absence of the hydrogen bonding seen in the carbaldehydes **31** and imines **51**. In each case a singlet signal integrating for two protons in the regions of δ 3.59-3.70 ppm confirmed product formation and the presence of the C$\underline{H_2}$-NH group. The previously observed imine proton ($\underline{H}$-C=N) in the region of δ 7.9-8.3 ppm was no longer observed. In the ^{13}C NMR spectra the imine carbon ($\underline{C}$=N) previously observed in the region of δ 157.9-160.6 ppm was now absent and instead an amine carbon ($\underline{C}H_2$-NH) was now seen in the region of δ 46.4-50.1 ppm. These key signals therefore confirmed product formation.

Table 6: Key ^{1}H NMR and ^{13}C NMR spectroscopic signals for 6-substituted-2,4-diaminopyrimidine-5-phenethylamines (28b-g').

Entry	2 x NH_2 (ppm)	C$\underline{H_2}$-NH (ppm)	$\underline{C}H_2$-NH (ppm)	Entry	2 x NH_2 (ppm)	C$\underline{H_2}$-NH (ppm)	$\underline{C}H_2$-NH (ppm)
28b	6.02, 5.64 (s)	3.59 (s)	46.4	**28u**	6.51, 5.79 (s)	3.70 (s)	48.1
28c	6.09, 4.92 (s)	3.59 (s)	46.7	**28v**	6.41, 5.65 (s)	3.69 (s)	49.5
28e	6.07, 4.92 (s)	3.62 (s)	46.7	**28w**	6.24, 5.16 (s)	3.88 (s)	48.1
28h	6.01, 4.89 (s)	3.61 (s)	46.7	**28x**	6.17, 5.25 (s)	3.86 (s)	49.7
28l	6.37, 5.61 (s)	3.69 (s)	48.3	**28y**	5.99, 4.94 (s)	3.84 (s)	50.1
28m	6.36, 5.56 (s)	3.66 (s)	49.6	**28z**	6.04, 5.04 (s)	3.85 (s)	48.7
28n	6.51, 5.74 (s)	3.66 (s)	49.9	**28a'**	6.09, 5.07 (s)	3.84 (s)	49.5
28o	6.25, 5.56 (s)	3.69 (s)	48.6	**28b'**	5.96, 4.89 (s)	3.83 (s)	49.9
28p	6.29, 5.59 (s)	3.68 (s)	49.5	**28c'**	6.02, 4.92 (s)	3.85 (s)	48.3
28q	6.23, 5.49 (s)	3.67 (s)	49.8	**28d'**	5.80, 4.77 (s)	3.83 (s)	49.6
28r	6.27, 5.55 (s)	3.70 (s)	48.2	**28e'**	5.91, 4.90 (s)	3.82 (s)	49.8
28s	6.51, 5.80 (s)	3.66 (s)	49.5	**28f'**	5.95, 4.98 (s)	3.86 (s)	48.2
28t	6.54, 5.85 (s)	3.67 (s)	49.7	**28g'**	5.79, 4.76 (s)	3.83 (s)	49.6

As seen in **Figure 37**, only five of the 6-phenyl substituted amines, **28a-c**, and compounds **28e** and **28h** (as we had sizeable quantities of the corresponding imines of these analogues) were synthesised, of which only **28a-c** were sent for biological assays. As described, previous work on similar compounds **32**, indicated that the 6-phenyl substituted analogues may be poor inhibitors of *Pf*DHFR. Compounds **32** that were tested for antiplasmodial activity in an *in vitro P.falciparum* screen on a Gambian FCR-3 mutant strain demonstrated only moderate activity (IC_{50}, 4.0 - 27 µM).[45] We therefore anticipated similar outcomes against the multidrug resistant strain (V1S). An IFD study was also performed on these analogues and suprisingly the 6-phenyl series **28a-k** showed good IFD scores (IFD score average of -2468.89 cal.mol^{-1}). As the 6-

phenyl analogues bearing methoxy substituents **28a-c** displayed the best IFD scores, we decided to test their activity first before commiting to synthesising the rest of these analogues.

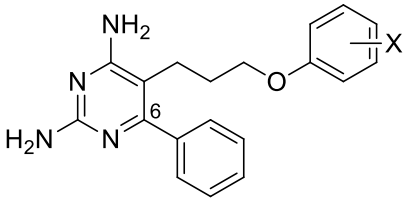

32

	(*Pf* FCR-3)
X = 4-Cl,	IC_{50} 4.0 μM
X = 3,4-diCl,	IC_{50} 15 μM
X = 3,5-diCl,	IC_{50} 0.9 μM
X = 3-F,	IC_{50} 27 μM

Figure 38: Selected general structures and IC_{50} values of previously prepared 2,4-diaminopyrimidines (32).

The percentage purity of the analogues that were submitted for biological assays was also assessed using HPLC. Generally all analogues showed a purity > 90 %, with the exception of compound **28v** and compound **28f'** which had purities of 85.44 % and 87.66 % respectively. Unfortunately, due to lack of sample and time constraints, the % purity for compounds **28p** and **28c'** could not be determined. The percentage purity for each individual analogue that was submitted for biological testing can be found in the experimental section in chapter 4.

2.9. Biological assessment of pyrimidine analogues (28)

The pyrimidine analogues **28**, **Figure 37**, were subjected to *Pf*DHFR enzyme inhibition assays against both the wild type (*Pf*DHFR-WT) and quadruple mutant (*Pf*DHFR-QM) enzymes as well as human DHFR (*Hs*DHFR) to test for inhibitory activity. The analogues that yielded promising inhibitory results were then subjected to whole cell *P. falciparum* assays *in vitro* against parasite strains bearing either wild type or quadruple mutant *Pf*DHFR to assess the antiplasmodial activity. The cytotoxicity of each compound was also assessed for two mammalian derived cell lines, Vero (African green monkey kidney epithelial cells) and KB (human epithelial carcinoma cells).

The biological assays were performed by collaborators at BIOTEC in Thailand by a team led by Dr S. Kamchonwongpaisan.

2.9.1. Enzyme inhibition and whole cell *P. falciparum* antiplasmodial studies.

The results for the *Pf*DHFR enzyme inhibition assays and whole cell *P.falciparum in vitro* assays are reported in **Table 7** and **Table 8** respectively.

Compounds **28a-c/l-g'** were assessed for enzyme inhibition activity against *Pf*DHFR-WT, *Pf*DHFR-QM and *Hs*DHFR, **Table 7**. All compounds demonstrated good selectivity with a much higher enzyme inhibition for *Pf*DHFR-WT and *Pf*DHFR-QM than *Hs*DHFR. This was desirable as this could potentially make for a good therapeutic index of the compounds in future clinical studies. All compounds showed enzyme inhibition activities in the nanomolar range, which was promising. None of the compounds inhibited the wild-type enzyme as effectively as the known inhibitor, pyrimethamine (**7**, PYR), (K_i 0.34 nM), however some compounds in the series inhibited the quadruple mutant enzyme to a similar extent as PYR **7** (K_i 29.34 nM).

Table 7: Results of DHFR enzyme inhibition studies of compounds 28a-c/l-g'.

Entry	K_i (nM) *Pf*DHFR-WT[a]	K_i (nM) *Pf*DHFR-QM[b]	K_i (nM) *Hs*DHFR[c]	Entry	K_i (nM) *Pf*DHFR-WT[a]	K_i (nM) *Pf*DHFR-QM[b]	K_i (nM) *Hs*DHFR[c]
28a	242.72 ± 20.72	208.23 ± 2.93	>500 000	**28v**	9.2 ± 0.7	28.21 ± 2.71	>250 000
28b	106.69 ± 3.23	74.06 ± 1.08	>500 000	**28w**	14.92 ± 1.06	31.32 ± 1.76	1590 ± 28.67
28c	85.99 ± 12.67	68.91 ± 5.28	>500 000	**28x**	4.4 ± 0.2	26.07 ± 0.45	1040.4 ± 34.4
28l	127.69 ± 9.09	126.34 ± 8.47	>500 000	**28y**	3.5 ± 0.4	28.84 ± 0.58	647.07 ± 6.11
28m	30.82 ± 5.07	56.12 ± 2.18	>500 000	**28z**	8.2 ± 0.3	31.5 ± 2.4	205.11 ± 1.13
28n	32.09 ± 1.08	55.05 ± 1.55	>500 000	**28a'**	10.37 ± 0.33	25.64 ± 1.75	457.95 ± 31.04
28o	60.77 ± 1.47	82.51 ± 0.77	>500 000	**28b'**	5.68 ± 0.46	34.52 ± 1.87	211.53 ± 12
28p	76.01 ± 4.96	73.60 ± 2.25	>500 000	**28c'**	9.29 ± 0.51	22.84 ± 0.59	304.04 ± 15.49
28q	79.77 ± 8.95	136.14 ± 6.84	>250 000	**28d'**	2.51 ± 0.09	19.51 ± 0.85	344.73 ± 7.41
28r	22.27 ± 2.33	37.71 ± 0.86	>250 000	**28e'**	2.48 ± 0.19	26.63 ± 0.13	141.6 ± 6.11
28s	24.61 ± 1.12	36.03 ± 4.15	>250 000	**28f'**	1.98 ± 0.03	22.09 ± 1.55	131.03 ± 5.44
28t	22.28 ± 0.45	60.01 ± 1.24	>500 000	**28g'**	1.27 ± 0.06	13.01 ± 0.04	201.65 ± 5.7
28u	7.15 ± 0.30	122.88 ± 8.37	>250 000	**PYR**	0.34 ±0.02	29.34 ± 1.47	40.96 ± 1.33

[a] wild type (WT) *Pf* DHFR. [b] quadruple mutant (QM) *Pf* DHFR. [c] human (Hs) DHFR.

Compounds in the cyclopropyl series **28w-g'** showed the best inhibition against both the wild-type *Pf*DHFR (*K*i, 1.27 – 14.92 nM) and quadruple mutant *Pf*DHFR (K_i 13.01 – 31.48 nM). This was followed by the cyclohexyl series **28l-v**, with the following activities demonstrated; *Pf*DHFR-WT (*K*i, 7.15 – 127.69 nM) and *Pf*DHFR-QM (K_i 28.27 – 136.34 nM). The phenyl series **28a-c** showed the weakest inhibition, with *K*i values ranging between, 85.99 – 242.72 nM against wild-type *Pf*DHFR; and K_i values of 68.91 – 208.23 nM against quadruple mutant *Pf*DHFR. This confirmed what we had anticipated about the 6-phenyl analogues, and this also suggests that the 6-phenyl substituent compounds **28a-c** display weak binding in the active site. Interestingly, in the IFD study performed these compounds were top scoring with -2470.36, -2471.58 and -2469.31cal.mol^{-1} for **28a**, **28b** and **28c** respectively. Possible reasons for the weak inhibition of compounds **28a-c** could be due to the size and rigid nature of the 6-phenyl ring, which as discussed earlier in the chapter may be causing the offset binding position with slightly different binding interactions, **Figure 25B**. Its size and lack of flexibility does not enable the ring to change conformation to better bind to residues in the active site or avoid unfavourable steric clashes. Compounds in the cyclopropyl series **28w-g'** showed the best inhibition against both the wild-type *Pf*DHFR and quadruple mutant *Pf*DHFR and this was expected as generally these compounds had the best IFD scores (IFD score average of -2468.97 cal.mol^{-1}), **Table 1**. Unfortunately, these compounds also showed the most potent inhibition of human DHFR (*K*i 131 – 1590 nM), while the phenyl and cyclohexyl analogues did not inhibit human DHFR at all. A weak correlation was observed between the calculated prime energy and the experimentally obtained binding constants. In a scatter plot showing each compounds' predicted energy vs its experimentally obtained activity an R^2 value of 0.3404 indicating a weak correlation was obtained. 23 of the 25 compounds assessed for activity were included in the plot, and two outliers were removed.[40]

When comparing the *K*i for the compounds within each series, for the 6-phenyl series **28a-c**, we observed that the *K*i values vary. However, **28c** with a 4-OMe substituent, displayed the best activities against both wild-type and the quadruple mutant enzyme. This data does not agree with the IFD study since **28b** (-2471.58 cal.mol^{-1}) was predicted to have the best binding ability followed by **28a** (-2470.36 cal.mol^{-1}) then **28c** (2469.31cal.mol^{-1}). Interestingly, for this series, better activities were observed for *Pf*DHFR-QM rather than *Pf*DHFR-WT, **Table 7**. For the cyclohexyl series **28l-v**, generally the best activities against the wild-type and quadruple mutant enzymes were observed for compounds bearing chloro-substituents (*K*i-WT, 7.15 - 24.61 nM and *K*i-QM, 28.21 - 60.01 nM), followed by those substituted with methoxy-

substituents (*K*i-WT, 30.82 - 127.69 nM and *K*i-QM, 55.05 – 126.34 nM) and fluoro-substituents (*K*i-WT, 60.77 - 79.77 nM and *K*i-QM, 73.60 - 136.14 nM), **Table 7**. This was also found to be the case for the cyclopropyl series **28w-g'**, with the chloro-substituted compounds displaying the best activities against the wild-type (*K*i 1.27 - 9.29 nM) and quadruple mutant (*K*i, 13.01 - 26.63 nM) enzymes. Furthermore, of all the compounds, compound **28g'**, **Figure 39**, showed the best activities against both the wild-type *Pf*DHFR and quadruple mutant *Pf*DHFR. IFD studies however for the cyclohexyl series predicted methoxy-substituents (IFD average, -2469.05 cal.mol^{-1}) to have better binding followed by fluoro-substituents (IFD average, -2468.50 cal.mol^{-1}) then chloro-substituents with average IFD score of 2468.44 cal.mol^{-1}. For the cyclopropyl series, the order of best IFD scores average is the methoxy followed by the chloro then the fluoro substituents with IFD averages of -2469.19 cal.mol^{-1}, -2469.16 cal.mol^{-1} and -2468.44 cal.mol^{-1} respectively, **Table 1**.

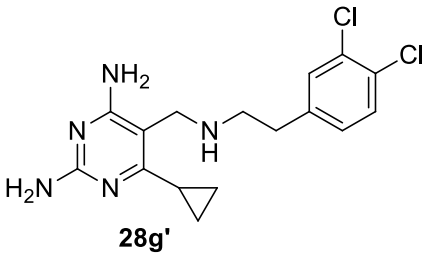

28g'

*Pf*DHFR-WT (*K*i, 1.27 nM)
*Pf*DHFR-QM (*K*i, 13.01 nM)

Figure 39: Structure of 6-cyclopropyl-5-{[(3,4-dichlorophenethyl)amino]-methyl}-pyrimidine-2,4-diamine (28g') and *K*i values.

As compounds **28a-c/l-g'** displayed promising inhibitory activity against both wild-type and mutant forms of *Pf*DHFR, we assessed them for antiplasmodial activity *in vitro* in a whole cell *P. falciparum* assay. Compounds were assayed against both a drug sensitive strain carrying WT *Pf*DHFR (TM4/8.2) and a multidrug resistant strain carrying QM *Pf*DHFR (V1S) of the parasite using a ^{3}H hypoxanthine incorporation assay. Compounds were also assessed for cytotoxicity against both normal (Vero) and cancer (KB) cell lines, **Table 8**.

A significant drop in activity was observed for the compounds **28a-c/l-g'** in the whole cell assay. All compounds displayed only moderate antiplasmodial activity *in vitro*, with IC_{50} values against drug sensitive strains ranging between 0.42 – 28.0 µM and IC_{50} values against the drug resistant strain ranging between 3.72 – 53.7 µM. None of the compounds **28a-c/l-g'** were as potent against the drug sensitive strain as the known inhibitor pyrimethamine (IC_{50}

0.053 µM), this is consistent with what was observed in the enzyme inhibition assay. We did observe however that all compounds were significantly more potent than pyrimethamine against the multidrug resistant strain (PYR, IC_{50} >100 µM), **Table 8**. This confirmed the advantage of having the flexible linker (present in compounds **28a-c/l-g'**), over a more rigid biaryl linker (present in PYR) in the compounds' activity against the multidrug resistant strain.

Interestingly, the results showed that compounds in the cyclohexyl series **(28l-v)** generally displayed the highest potencies in the whole cell assay against both drug sensitive (TM4/8.2, IC_{50} 1.76 – 4.07 µM) and drug resistant (V1S, IC_{50} 3.72 – 16.0 µM), strains. This was followed by the cyclopropyl compounds **28w-g'**, with IC_{50} values of 0.42 – 24.5 µM against the TM4/8.2 (drug sensitive) strain and IC_{50} values of 4.42 – 47.5 µM against the V1S (drug resistant) strain. The phenyl series **28a-c** once again showed the lowest potency of the compounds, with IC_{50} values against the drug sensitive strain (TM4/8.2) in the range 26.9 – 28.0 µM and against the multidrug resistant strain (V1S) in the range 33.8 – 53.7 µM. This further confirmed what we had anticipated about the 6-phenyl analogues **28a-c**.

For the 6-phenyl series **28a-c**, the IC_{50} values against drug sensitive strain (TM4/8.2) were similar for all methoxy-substituents. However, **28c** with substituent X = 4-OMe, once again displayed the best activity in the phenyl series against the multidrug resistant strain (V1S), **Table 8**.

For the cyclopropyl series **28w-g'**, generally, the best activities against both drug sensitive and multidrug resistant strains were observed for compounds bearing chloro-substituents (IC_{50}-TM4/8.2; 0.42 - 4.96 µM and IC_{50}-V1S; 4.42 - 16.8 µM), followed by those bearing methoxy-substituents (IC_{50}-TM4/8.2; 3.48 - 24.5 µM and IC_{50}-V1S; 12.7 - 34.9 µM) and fluoro-substituents (IC_{50}-TM4/8.2; 4.21 - 23.2 µM and IC_{50}-V1S; 20.2 - 47.5 µM), **Table 8**. Furthermore, of all the compounds, compound **28c'**, (**Figure 40**), showed the best activity against the drug sensitive strain (TM4/8.2) with an IC_{50} value of 0.42 µM.

Table 8: Results of *in vitro* antiplasmodial activity and *in vitro* cytotoxicity of compounds 28a-c/l-g'.

Entry	IC_{50} (µM) *Pf*TM4/8.2[a]	IC_{50} (µM) *Pf*V1S[b]	IC_{50} (µM) Vero[c]	IC_{50} (µM) KB[d]	Entry	IC_{50} (µM) *Pf*TM4/8.2[a]	IC_{50} (µM) *Pf*V1S[b]	IC_{50} (µM) Vero[c]	IC_{50} (µM) KB[d]
28a	26.9 ± 2.5	53.7 ± 2.1	>100	>100	**28v**	3.53 ± 0.25	3.99 ± 0.25	21.0 ± 0.9	22.4 ± 0.1
28b	27.4 ± 4.0	47.9 ± 1.0	>100	>100	**28w**	24.5 ± 0.7	34.9 ± 4.2	>100	>100
28c	28.0 ± 4.74	33.8 ± 1.52	>100	>100	**28x**	4.22 ± 0.22	12.7 ± 0.8	71.8 ± 1.96	74.3 ± 4.4
28l	3.67 ± 0.31	9.43 ± 1.85	21.1 ± 1.34	22.4 ± 0.3	**28y**	3.48 ± 0.16	14.6 ± 2.9	71.0 ± 6.7	71.8 ± 1.2
28m	3.47 ± 0.20	4.08 ± 0.30	22.8 ± 2.30	22.9 ± 0.3	**28z**	11.8 ± 5.2	24.5 ± 1.6	>100	>100
28n	1.76 ± 0.11	3.72 ± 0.21	21.2 ± 2.0	22.7 ± 0.2	**28a'**	4.21 ± 0.31	20.2 ± 1.77	>100	>100
28o	4.07 ± 0.64	16.0 ± 1.5	22.4 ± 1.4	47.5 ± 13.9	**28b'**	23.2 ± 2.94	47.5 ± 4.7	>100	>100
28p	3.03 ± 0.40	11.2 ± 1.8	24.5 ± 3.1	62.2 ± 2.9	**28c'**	0.42 ± 0.01	16.8 ± 2.7	66.7 ± 2.2	82.9 ± 6.6
28q	2.23 ± 0.14	6.93 ± 1.77	22.4 ± 0.64	56.3 ± 4.9	**28d'**	4.20 ± 0.86	13.5 ± 3.7	76.3 ± 3.6	81.6 ± 13.0
28r	3.30 ± 0.28	15.5 ± 1.1	20.8 ± 0.8	22.1 ± 0.1	**28e'**	4.96 ± 0.56	17.6 ± 2.6	69.5 ± 1.7	70.4 ± 0.5
28s	3.08 ± 0.40	3.99 ± 0.15	22.9 ± 1.7	22.8 ± 0.2	**28f'**	3.56 ± 0.16	6.27 ± 1.18	30.7 ± 6.97	65.7 ± 2.4
28t	3.09 ± 0.23	4.51 ± 0.28	22.9 ± 1.9	22.9 ± 0.2	**28g'**	3.28 ± 0.08	4.42 ± 0.14	21.3 ± 0.7	22.5 ± 0.5
28u	2.45 ± 0.37	4.87 ± 0.30	16.3 ± 2.1	62.2 ± 2.9	**PYR**	0.053 ± 0.007	>100	26.9 ± 2.1	60.4 ± 25.5

[a] WT *P. falciparum*. [b] *P. falciparum* with QM DHFR [c] African green monkey kidney epithelial cells. [d] human epithelial carcinoma cells.

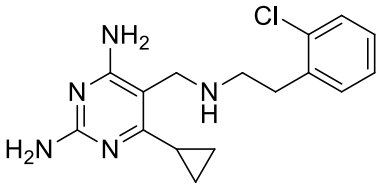

28c'

TM4/8.2 (IC_{50} 0.42 µM)

Figure 40: Structure of 6-cyclopropyl-5-{[(2-chlorophenethyl)amino]-methyl}-pyrimidine-2,4-diamine (28c') and IC_{50} value.

As noted before, this was also observed for the cyclohexyl series **28l-v**, with the best activities against the drug sensitive and multidrug resistant strains displayed by compounds bearing chloro-substituents (IC_{50}-TM4/8.2; 2.45 – 3.53 µM and IC_{50}-V1S; 3.99 – 15.5 µM), followed by the methoxy-substituted products (IC_{50}-TM4/8.2; 1.76 – 3.67 µM and IC_{50}-V1S; 3.72 – 9.43 µM) then the fluoro-substituted products (IC_{50}-TM4/8.2; 2.23 - 4.07 µM and IC_{50}-V1S; 6.93 - 16.0 µM), **Table 8**. Furthermore, of all the compounds, compound **28n**, **Figure 41**, showed the best activity against the multidrug resistant strain (V1S) with an IC_{50} value of 3.72 µM. Additionally, the cyclohexyl series of compounds (**28l-v**) generally displayed higher levels of cytotoxicity in the *in vitro* assays performed (IC_{50} Vero; 16.3 - 24.5 µM and IC_{50} KB; 22.1 - 62.2 µM), than compounds from either the cyclopropyl (IC_{50}Vero; 21.3 - > 100 µM and IC_{50} KB; 22.5 - > 100 µM) or phenyl series (IC_{50} Vero; > 100 µM and IC_{50} KB; > 100 µM). Although no cell lysis was observed in the *P. falciparum* assay, some compounds in this series proved to be relatively toxic with less than a two-fold difference between the IC_{50} value against Vero or KB cells and the *Pf* V1S IC50 value (e.g. **28o** and **28r**). However, for the majority of compounds there was a five-fold difference in IC_{50} values.

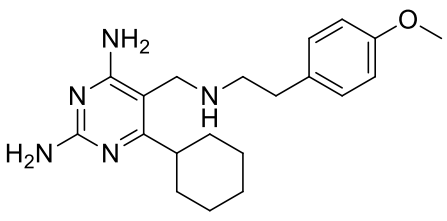

28n

V1S (IC_{50} 3.72 µM)

Figure 41: Structure of 6-cyclohexyl-5-{[(4-methoxyphenethyl)amino]-methyl}-pyrimidine-2,4-diamine (28n) and IC_{50} value.

As discussed previously, we observed a significant decrease in activity when comparing the enzyme inhibition data and the antiplasmodial whole cell assay data. To better understand the biological assay data obtained, further investigation of the pharmacokinetic properties of compounds **28a-c/l-g'** is necessary. This is essential to determine whether membrane permeability, solubility or binding to plasma proteins could possibly have influenced the compounds' activity in the whole cell *P. falciparum* assay. When analysing the qikprop pharmacokinetics predictions, it is observed that the cyclohexyl series is predicted to generally have better Caco-2 cell membrane permeability (QPPCaco) values ranging from 100.075 - 215.902 nm/s followed by the cyclopropyl series (94.967 - 210.630 nm/s) and finally the phenyl series (75.682 - 187.489 nm/s). The order of this data is consistent with the order of the antiplasmodial activity obtained from the *in vitro* studies (**Table 8**), which suggests that cell membrane permeability could potentially be a factor that could be improved to increase the activity of our series of compounds. Further investigations into the synthesis of analogues with potentially improved pharmacokinetic properties is currently underway.

CHAPTER 3: SUMMARY OF RESULTS, FUTURE DIRECTIONS AND PRELIMINARY MODELLING STUDIES

3.1. Summary of results

The aim of the first part of the research project was to synthesise antifolate analogues with the potential to disrupt folate metabolism in the parasite by inhibiting the *Pf*DHFR enzyme. Pyrimidine-based antifolates with this potential were synthesised. *In silico* molecular modelling was performed on this series of compounds and the studies showed a high binding affinity of our series of compounds **28** with IFD scores ranging from -2471.36 to -2464.66 cal.mol^{-1}; comparing well with known binders pyrimethamine (PYR) **7**, WR99210 **25** and the natural substrate DHF **19** with IFD scores of -2466.26, -2462.52 and -2470.90 cal.mol^{-1} respectively. Notably, the IFD scores from our series of compounds were better than WR99210 **25** which was reported to be active against quadruple mutant *P. falciparum*. Qikprop predictions also predicted compounds **28** to have good pharmacokinetic properties since all compounds generated values that fall within the acceptable range of each descriptor.

The synthetic route that was developed for the synthesis of compounds **28** comprised of a four-step synthetic route which afforded 6-substituted-2,4-diaminopyrimidine-5-phenethylamines as the desired final product, **Scheme 18**.

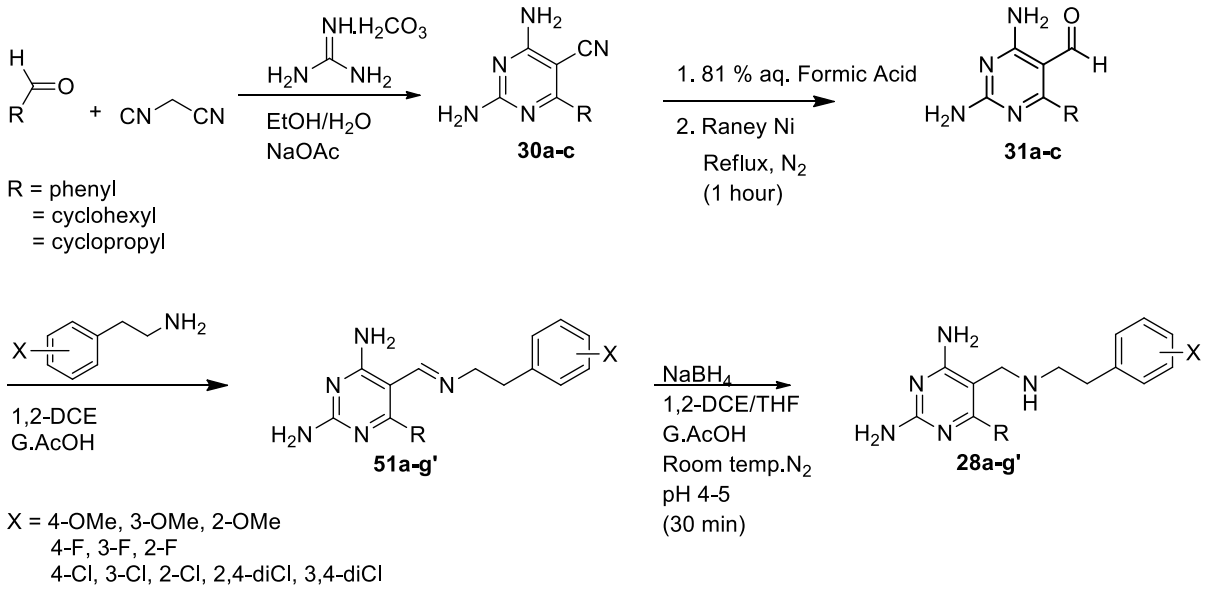

Scheme 18: Complete synthesis of 6-substituted-2,4-diaminopyrimidine-5-phenethylamines (28).

The first step involved the synthesis of 6-substituted-2,4-diamino-5-carbonitrile-pyrimidines **30a-c** by a multicomponent reaction using commercially available malononitrile and a suitably substituted aldehyde being dissolved in an ethanol/water mixture in the presence of NaOAc. Alkene intermediate **49** which forms was reacted *in situ* with guanidine carbonate to afford the products in moderate yields of 26-65 %. The second step involved a functional group interconversion of the nitrile group in compounds **30a-c** to an aldehyde using a Raney nickel reduction in 81 % aqueous formic acid from freshly prepared Raney nickel. The synthesis was successful affording 6-substituted-2,4-diaminopyrimidine-5-carbaldehydes **31a-c** in moderate yields in the range of 50-56 %. The aldehydes **31a-c** were used in the third step, involving an imination reaction to form 6-substituted-2,4-diaminopyrimidine-5-phenethylimines, where aldehydes **31a-c** were reacted with commercially available substituted phenethylamines containing OMe, F or Cl variations. Eleven compounds in each series were synthesised in relatively high yields. The 6-phenyl imines **51a-k** were isolated in yields in the range of 61-99 %, the 6-cylohexyl imines **51l-v**, were isolated in yields in the range 71-100 % and finally, the 6-cyclopropyl imines **51w-g'**, were afforded in yields in the range of 66-97 %. The success of the imination step meant that we could proceed to form the final products, 6-substituted-2,4-diaminopyrimidine-5-phenethylamine**s 28a-g'**. This was achieved using a reduction reaction, where imines **51** were dissolved in a mixture of 1,2-DCE/THF and treated with $NaBH_4$ under acidic conditions. Five compounds for the 6-phenyl amines **28a-c**, **28e** and **28h**, were synthesised in yields in the range of 33-68 %. Eleven compounds in each of the cyclohexyl (**28l-v**) and cyclopropyl (**28w-g'**) series were synthesised and isolated in yields in the range of 60-96 % for amines **28l-v** and 68-84 % for amines **28w-g'**.

A successful synthesis of the 6-substituted-2,4-diaminopyrimidine-5-phenethylamines **28** meant that we could assess these compounds for inhibitory activity against both wild type and quadruple mutant *Pf*DHFR *in vitro* and assess antiplasmodial activity in a whole cell *P. falciparum* assay. All compounds assessed showed enzyme inhibition activities in the nanomolar range, with the 6-cyclopropyl series **28w-g'** generally displaying the best inhibition against both wild type (*K*i, 1.27 – 14.92 nM) and quadruple mutant (K_i 13.01 – 31.48 nM) *Pf*DHFR, followed by the 6-cyclohexyl **28l-v** (*K*i-WT; 7.15 – 127.69 nM and K_i-QM; 28.27 – 136.34 nM) then 6-phenyl analogues **28a-c** (K_i-WT; 85.99 – 242.72 nM and K_i-QM; 68.91 – 208.23 nM). None of the compounds inhibited the wild-type enzyme as well as the known inhibitor, pyrimethamine (**7**, PYR), (K_i 0.34 nM), however some compounds in the series inhibited the quadruple mutant enzyme to a similar extent as PYR **7** (K_i 29.34 nM).

All compounds assessed displayed a moderate antiplasmodial activity *in vitro*, IC_{50}(TM4/8.2) 0.42 – 28.0 µM and IC_{50}(V1S) 3.72 – 53.7 µM. Interestingly, the 6-cyclohexyl series generally displayed the best potency of the compounds (IC_{50} TM4/8.2; 1.76 – 4.07 µM) and IC_{50} V1S; 3.72 – 16.0 µM), followed by the 6-cyclopropyl series (IC_{50} TM4/8.2; 0.42 – 24.5 µM and IC_{50} V1S; 4.42 – 47.5 µM) and then the 6-phenyl series (IC_{50} TM4/8.2; 26.9 – 28.0 µM and IC_{50} V1S; 33.8 – 53.7 µM). None of the compounds **28** were as potent against the drug sensitive strain as the known inhibitor pyrimethamine (IC_{50} 0.053 µM), however all the compounds **28a-c/l-g'** were significantly more potent than pyrimethamine against the multidrug resistant strain (PYR, IC_{50} >100 µM).

Further investigation of the pharmacokinetic properties of compounds **28** is warranted to better understand what could have possibly influenced the significant drop in activity in the whole cell *P. falciparum* assay. We anticipate that either membrane permeability, solubility or binding to plasma proteins could possibly have influenced the compounds' activity. The design and synthesis of analogues with potentially improved pharmacokinetic properties is necessary.

3.2. Future directions

As mentioned previously, the design and synthesis of analogues that could potentially display better activity in the whole cell *P. falciparum* assay is being investigated. To this end, structural modifications of amine compounds **28**, to potentially improve the pharmacokinetic properties will be explored. Variations will primarily be introduced in the 6-cyclohexyl and 6-cyclopropyl series as these showed the most promising biological assay data. These variations will include replacing the substituted phenethylamines with pyridylethanamines, of general structure **54**, **Figure 42**. Pyridine groups have important properties in medicinal chemistry, which include weak basicity, water solubility, *in vivo* /chemical stability, hydrogen bond-forming ability, and small molecular size.[57] Other structural variations will include adding an amide linker in the place of the amine linker, compounds **55** and **56**, **Figure 42**, to potentially increase the solubility and cell membrane permeability of the analogues. These variations could be important in improving the pharmacokinetic properties of our compounds. Qikprop pharmacokinetic predictions of these compounds **54-56** will be discussed below.

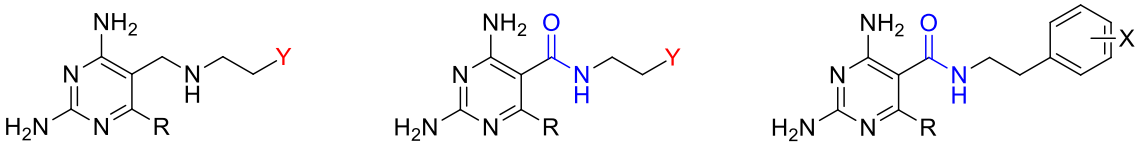

54 **55** **56**

R = cyclohexyl, cyclopropyl
X = 4-OMe, 3-OMe, 2-OMe, 4-F, 3-F, 2-F, 4-Cl, 3-Cl, 2-Cl, 2,4-diCl, 3,4-diCl
Y = 2-pyridyl, 3-pyridyl, 4-pyridyl

Figure 42: Structures of modified analogues

3.2.1. *In silico* molecular modelling – ligand docking studies of modified analogues 54-56

A less extensive ligand docking study was performed on compounds **54 - 56** to assess whether the modifications in the structure maintain comparable binding results to the original compounds **28**. The study only included the XP GScore (calculated for the final glide XP docking step) **Figure 43** shows the compounds that underwent ligand docking studies using Schrodinger.

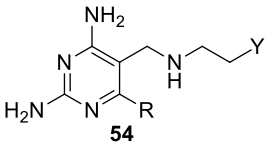

54

54a R = cyclohexyl, X = 2-pyr
54b R = cyclohexyl, X = 3-pyr
54c R = cyclohexyl, X = 4-pyr
54d R = cyclopropyl, X = 2-pyr
54e R = cyclopropyl, X = 3-pyr
54f R = cyclopropyl, X = 4-pyr

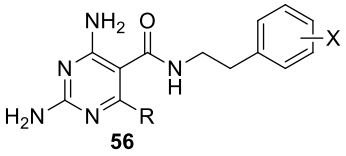

56

56a R = cyclohexyl, X = 2-OMe
56b R = cyclohexyl, X = 3-OMe
56c R = cyclohexyl, X = 4-OMe
56d R = cyclohexyl, X = 2-F
56e R = cyclohexyl, X = 3-F
56f R = cyclohexyl, X = 4-F
56g R = cyclohexyl, X = 2-Cl
56h R = cyclohexyl, X = 3-Cl
56i R = cyclohexyl, X = 4-Cl
56j R = cyclohexyl, X = 2,4-diCl
56k R = cyclohexyl, X = 3,4-diCl

56l R = cyclopropyl, X = 2-OMe
56m R = cyclopropyl, X = 3-OMe
56n R = cyclopropyl, X = 4-OMe
56o R = cyclopropyl, X = 2-F
56p R = cyclopropyl, X = 3-F
56q R = cyclopropyl, X = 4-F
56r R = cyclopropyl, X = 2-Cl
56s R = cyclopropyl, X = 3-Cl
56t R = cyclopropyl, X = 4-Cl
56u R = cyclopropyl, X = 2,4-diCl
56v R = cyclopropyl, X = 3,4-diCl

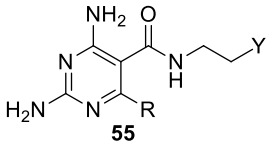

55

55a R = cyclohexyl, X = 2-pyr
55b R = cyclohexyl, X = 3-pyr
55c R = cyclohexyl, X = 4-pyr
55d R = cyclopropyl, X = 2-pyr
55e R = cyclopropyl, X = 3-pyr
55f R = cyclopropyl, X = 4-pyr

Figure 43: Compounds submitted for IFD studies.

A ligand docking study was performed on the structurally modified compounds **54 - 56** bearing 6-cyclohexyl and 6-cyclopropyl substituents respectively, with X = OMe, F, Cl and Y = 2-pyridyl, 3-pyridyl and 4-pyridyl. The binding ability of compounds **54 - 56** was also assessed to see if the modified compounds' binding compares well with the original compounds **28l-g'**. As before, the binding ability of the compounds **54 - 56** was assessed against the quadruple mutant *Pf*DHFR (PDB structure 1J3K). To keep the conditions consistent, the same docking constraints and setting used for IFD for the compounds **28** were used in this study. **Table 9** shows the XP G docking scores generated by the study.

The XPGScore calculated for compounds **54 - 56** (**Table 9**) yielded results in the ranges of -9.657 to -11.860 cal.mol^{-1} this was comparable to the XPGScores of compounds **28l-g'** (-8.926 to -11.692 cal.mol^{-1}) observed for the IFD study in **Table 1**. This was promising as this suggests that the good binding ability observed for the enzyme inhibition studies against quadruple mutant *Pf*DHFR for compounds **28l-g'** (K_i 13.01 – 136.34 nM) may still be maintained for compounds **54 - 56**.

Table 9: Results of docking studies of proposed compounds 54 - 56.

Entry	XP GScore[a]	Entry	XP Gscore[a]
54a	-9.964	**56f**	-10.827
54b	-11.307	**56g**	-10.769
54c	-9.830	**56h**	-11.860
54d	-9.855	**56i**	-11.709
54e	-9.659	**56j**	-11.825
54f	-9.616	**56k**	-11.722
55a	-10.073	**56l**	-11.167
55b	-9.974	**56m**	-11.398
55c	-10.325	**56n**	-9.657
55d	-9.391	**56o**	-11.078
55e	-11.249	**56p**	-10.778
55f	-10.165	**56q**	-10.788
56a	-10.779	**56r**	-10.710
56b	-11.607	**56s**	-10.433
56c	-10.122	**56t**	-10.441
56d	-9.486	**56u**	-11.274
56e	-10.975	**56v**	-11.944

[a] All docking scores given in units cal.mol^{-1}.

The binding interactions of compounds **54 - 56** were also investigated. **Figure 44** below provides a graphical illustration of our findings. Conserved binding interactions in the form of hydrogen bonds of the pyrimidine core to residues Ile14 and mutant Leu164 were still maintained, **Figure 44**. Strong pi-cation and pi-pi interactions with Phe58 were still observed. Hydrogen bond interactions with Cys15 and mutant Asn108, with Asn108 behaving still as both a hydrogen bond donor and acceptor from the secondary amine present in the linker chain as well as the nitrogen of the terminal pyridyl ring, in this instance, **Figure 44A**. N-1 of the pyrimidine ring was still protonated at physiological pH and had electrostatic interactions with nearby residues, with the significant salt-bridge interaction to the charged residue Asp54 being maintained for compounds **54 - 56**, **Figure 44**. The binding modes of compounds **54 - 56** still maintained the key binding interactions observed for compounds **28**. This was encouraging as it suggested that these compounds **54 - 56** may still maintain the inhibitory activity observed for compounds **28l-g'**.

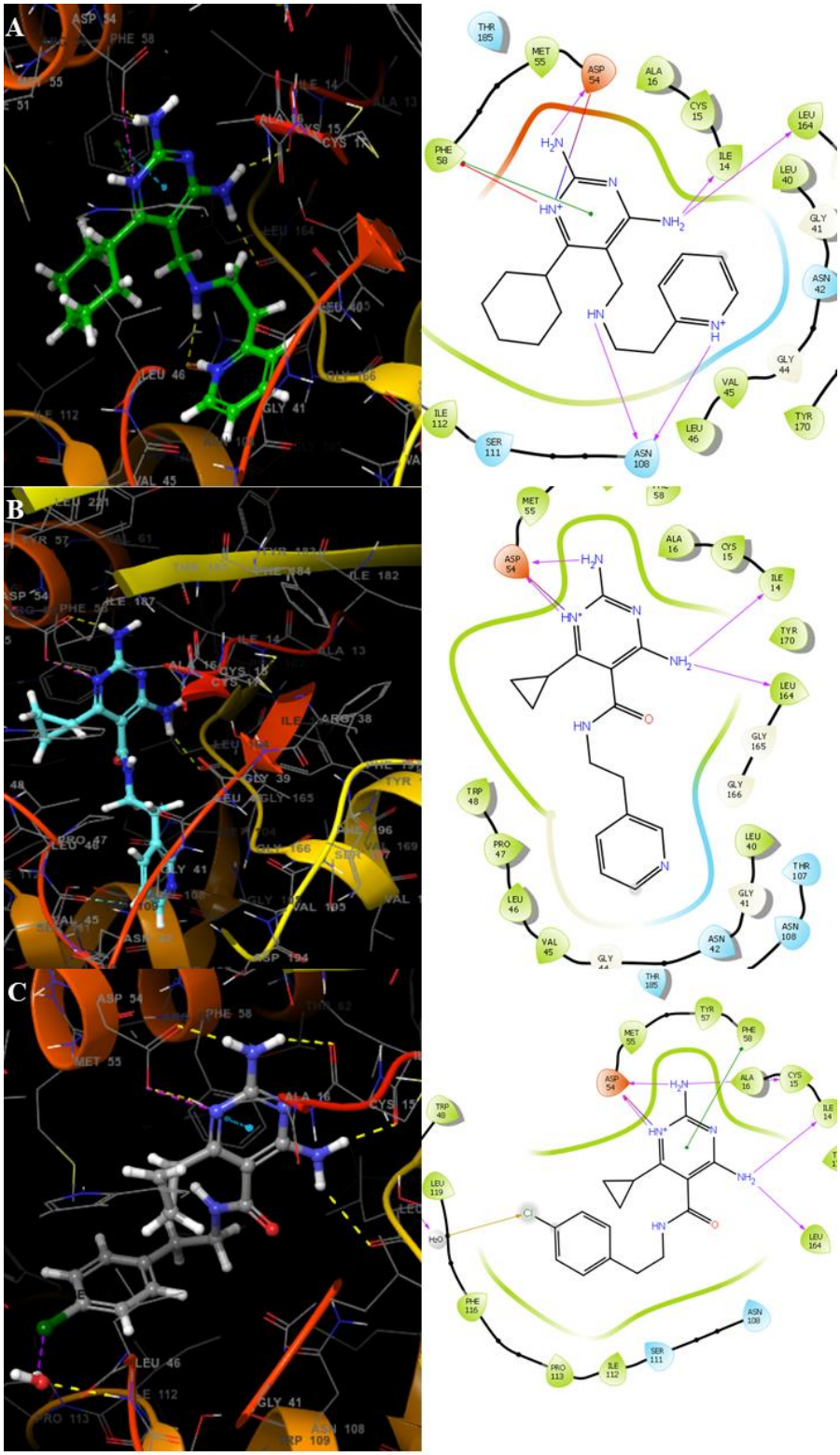

Figure 44: An illustration of (A) 54a; (B) 55e, and (C) 56t; bound in the active site of *Pf*DHFR (PDB: 1J3K) and the corresponding 2D interaction diagram for each compound.

3.2.2. *In silico* molecular modelling – qikprop pharmacokinetics property predictions of modified analogues 54-56

The predicted pharmacokinetic properties of compounds **54 - 56** was also assessed using qikprop in Schrodinger. The results produced by this study will be assessed and compared to those generated by the previous study of compounds **28** (**Table 10**). **Table 10** below summarises the predicted pharmacokinetic properties for compounds **54 - 56**.

Compounds **54 - 56** generally produced good predicted pharmacokinetic properties. The #Stars descriptor value was predicted to be 0 for all the compounds. This means that none of the modified compounds have properties that fall outside the 95 % range of similar values for known drugs. This compares well with the original analogues **28**, since three compounds (**28p**, **28s** and **28y**) showed 1 star. Like the original compounds **28**, compounds **54 - 56** obeyed both Lipinski's rule of 5 and Jorgensen's rule of 3 meaning they are predicted to be drug-like and more likely to be orally available. None of the structurally modified series of compounds **54 - 56** were predicted to display central nervous system activity (CNS) which matched what was observed for the original analogues **28**. Similar to compounds **28**, compounds **54 - 56** obey the recommended range -1.5 – 1.5 for the QPlogKhsa descriptor which predicts binding to the human serum albumin. As stated previously, we primarily aimed for improved solubility and cell permeability by adding pyridine and amide functional groups to our modified compounds **54 - 56**. Compounds **54** incorporated the pyridyl function group, while maintaining the amine linker and compounds **55** incorporated the pyridyl group with the amide linker, **Figure 43** to potentially improve the water solubility of the compounds. The predicted values observed for compounds **54** and **55** obeyed the recommended range of values for QPlogS which measures water solubility ranging from -2.949 to -1.524 with compound **54d** having the best predicted solubility of -1.524 and compounds **55** ranging from -4.460 to -2.819 with compound **55d** having the best predicted solubility of -2.819. These results produced similar values to the original compounds **28l-g'** with values ranging from -3.986 to -0.956 with compound **28w** predicted to have the best logS of -0.956. Although the modified compounds containing pyridyl and amide functional groups **54** and **55** did not significantly improve the solubility (logS), it will be essential to compare this to the experimental values that will be obtained in the future.

Table 10: Predicted pharmacokinetic properties for compounds **54 -56**.

Entry	#stars[a]	CNS[b]	MW[c]	dipole[d]	donor HB[e]	accept HB[f]	QPlogPo/w[g]	QPlogS[h]	QPPCaco[i]	QPlogBB[j]	#metab[k]	QPlogKhsa[l]	HOA[m]	%HOA[n]	PSA[o]	RO5[p]	RO3[q]
54a	0	-2	326.444	3.411	5.000	5.500	1.911	-2.949	80.400	-1.008	5	0.024	3	72.235	95.493	0	0
54b	0	-2	326.444	3.819	5.000	6.000	1.558	-2.537	62.954	-1.043	6	-0.052	3	68.268	96.276	0	0
54c	0	-2	326.444	1.928	5.000	6.000	1.721	-2.838	75.179	-1.025	6	-0.023	3	70.601	96.494	0	0
54d	0	-1	284.363	1.650	5.000	5.500	0.942	-1.524	75.382	-0.882	4	-0.311	3	66.063	95.128	0	0
54e	0	-2	284.363	4.760	5.000	6.000	0.887	-2.253	49.603	-1.260	5	-0.314	3	62.484	98.666	0	0
54f	0	-2	284.363	2.506	5.000	6.000	0.925	-2.029	63.552	-1.080	5	-0.312	3	64.636	97.364	0	0
55a	0	-2	340.427	6.335	4.000	5.500	2.428	-4.550	160.119	-1.672	3	0.159	3	80.620	114.536	0	0
55b	0	-2	340.427	3.470	4.000	6.000	2.249	-4.460	156.665	-1.680	4	0.101	3	79.397	115.766	0	0
55c	0	-2	340.427	5.504	4.000	6.000	2.231	-3.924	261.117	-1.332	4	0.060	3	83.268	113.759	0	0
55d	0	-2	298.347	4.709	4.000	5.500	1.420	-2.819	184.808	-1.358	2	-0.206	3	75.831	114.344	0	0
55e	0	-2	298.347	5.097	4.000	6.000	1.342	-3.463	109.588	-1.767	3	-0.205	3	71.310	118.939	0	0
55f	0	-2	298.347	6.866	4.000	6.000	1.359	-3.483	113.007	-1.760	3	-0.204	3	71.651	117.994	0	0
56a	0	-2	369.466	3.678	4.000	5.250	3.284	-5.230	283.578	-1.520	3	0.394	3	90.071	111.012	0	0
56b	0	-2	369.466	5.019	4.000	5.250	3.193	-5.253	247.223	-1.599	3	0.380	3	88.476	112.724	0	0
56c	0	-2	369.466	3.435	4.000	5.250	3.087	-5.090	222.607	-1.623	3	0.352	3	87.037	111.017	0	0
56d	0	-2	357.430	6.332	4.000	4.500	3.126	-4.978	232.977	-1.417	2	0.340	3	87.618	102.985	0	0
56e	0	-2	357.430	6.815	4.000	4.500	3.197	-5.149	225.693	-1.409	2	0.353	3	87.791	103.073	0	0
56f	0	-2	357.430	3.053	4.000	4.500	3.236	-4.753	394.102	-1.080	2	0.321	3	92.351	99.802	0	0
56g	0	-2	373.884	6.213	4.000	4.500	3.368	-5.086	277.633	-1.228	2	0.392	3	90.397	100.690	0	0
56h	0	-2	373.884	6.773	4.000	4.500	3.451	-5.520	224.755	-1.376	2	0.422	3	89.241	103.073	0	0
56i	0	-2	373.884	3.837	4.000	4.500	3.422	-5.081	289.190	-1.159	2	0.403	3	91.032	101.165	0	0
56j	0	-2	408.330	4.808	4.000	4.500	3.851	-5.794	279.658	-1.085	2	0.497	3	93.282	100.149	0	1
56k	0	-1	408.330	4.019	4.000	4.500	3.862	-5.424	473.131	-0.836	2	0.465	3	100.000	98.798	0	0
56l	0	-2	327.385	5.150	4.000	5.250	2.380	-4.338	220.004	-1.625	2	0.057	3	82.806	112.113	0	0
56m	0	-2	327.385	5.199	4.000	5.250	2.288	-3.326	491.965	-1.074	2	-0.033	3	88.522	108.438	0	0
56n	0	-2	327.385	5.310	4.000	5.250	2.274	-4.143	199.452	-1.626	2	0.039	3	81.426	114.342	0	0
56o	0	-2	315.349	4.251	4.000	4.500	2.404	-4.253	230.200	-1.421	1	0.039	3	83.300	105.685	0	0

Table 10: Predicted pharmacokinetic properties for compounds **54 - 56**.

Entry	#stars[a]	CNS[b]	MW[c]	dipole[d]	donor HB[e]	accept HB[f]	QPlogPo/w[g]	QPlogS[h]	QPPCaco[i]	QPlogBB[j]	#metab[k]	QPlogKhsa[l]	HOA[m]	%HOA[n]	PSA[o]	RO5[p]	RO3[q]
56p	0	-2	315.349	4.970	4.000	4.500	2.379	-4.186	202.328	-1.411	1	0.035	3	82.148	105.983	0	0
56q	0	-2	315.349	5.023	4.000	4.500	2.432	-4.325	212.948	-1.422	1	0.046	3	82.859	106.094	0	0
56r	0	-2	331.804	5.189	4.000	4.500	2.460	-4.157	198.816	-1.375	1	0.065	3	82.485	106.049	0	0
56s	0	-2	331.804	4.934	4.000	4.500	2.628	-4.541	202.207	-1.375	1	0.100	3	83.601	105.985	0	0
56t	0	-2	331.804	4.983	4.000	4.500	2.684	-4.683	213.552	-1.384	1	0.112	3	84.354	106.045	0	0
56u	0	-2	366.249	5.681	4.000	4.500	2.939	-4.869	197.967	-1.243	1	0.167	3	85.256	106.035	0	0
56v	0	-2	366.249	8.647	4.000	4.500	3.053	-5.145	202.482	-1.262	1	0.197	3	86.099	105.950	0	0

Key for **Table 10**: [a] Number of parameters falling outside of a 95% similarity range for known drugs, [b] Central nervous system activity [c] Molecular weight [d] Calculated dipole moment, [e] Number of H-bond donors, [f] Number of H-bond acceptors, [g] Octanol/water partition coefficient, [h] Water solubility, [i] Caco-2 cell permeability in nm/s (model for gut-blood barrier, only non-active transport is considered), [j] Blood – brain barrier permeability, [k] Number of likely metabolites, [l] Human serum albumin binding coefficient, [m] Human oral absorption: Measure of human oral absorption combing serval factors, [n] Percentage Human oral absorption: Predicted human oral absorptivity percentage scale, value is used in the calculation of HOA, [o] Polar surface area, [p] Number of violations of Lipinski's rule of 5, [q] Number of violations of Jorgensen's rule of 3.

Cell permeability was also of interest to us in the modified compounds. A significant increase in the predicted cell permeability (QPPCaco) was observed with compounds **56** bearing an amide linker with values ranging between 197.967 – 491.965 nm/s. These predictions showed much better values in comparison to compounds **28l-g'** where values ranged from 94.967 – 215.902 nm/s. The cyclohexyl series **28l-v** of the original compounds generally had better Caco-2 cell membrane permeability with (QPPCaco) values ranging from 100.075 - 215.902 nm/s, followed by the cyclopropyl series **28w-g'** (94.967 - 210.630 nm/s). A similar trend was observed in the order of the antiplasmodial activity obtained from the *in vitro* studies (**Table 8**), which suggested that cell membrane permeability is a possible factor that could be improved to increase the activity of our series of compounds. The modified compounds **56** also show a similar trend with much improved cell permeability values with the cyclohexyl series **56a-k** having predicted values ranging from 222.607 to 473.131 nm/s and the cyclopropyl series **56l-v** having predicted values in the range of 197.967 – 491.965 nm/s. The predicted percentage human absorption (%HOA) for compounds **54 - 56** was found to be in the recommended range (<25 % poor; >80 % high). Compounds **54** had predicted values of 62.5 – 72.2 %, which did not perform better than the original compounds **28l-g'** with predicted %HOA values of 72.8 – 82.9 %. The amide-linker containing compounds **55 -56** however showed similar or better %HOA values than the original compounds **28** with compounds **55** having values in the range of 71.3 – 83.3 %. The cyclopropyl series **56l-v** had values from 81.4 – 88.5 % and the cyclohexyl series **56a-k** once again showed the best values of 87.0 – 100 %. Compound **56k** displayed the best %HOA of 100 % which also far exceeds that of the known inhibitor WR99210 (91.180 %). These modified compounds **54 - 56** therefore show several advantages in the predicted pharmacokinetic properties when compared to the original compounds **28l-g'**, which may potentially translate into better antiplasmodial *in vitro* assay results in the future.

3.2.3. Proposed synthetic route to modified analogues

In conclusion, the proposed synthetic route for the modified compounds **54 - 56**, is shown in **Scheme 19** and **Scheme 20**. **Scheme 19** will incorporate the first two steps of the methodology developed in this project, as shown in **Scheme 18**, to form the 6-substituted-2,4-diaminopyrimidine-5-carbaldehydes **31**, which will be converted to the desired modified pyridyl containing analogues **54**. **Scheme 20** will incorporate the first step of the methodology developed in this project, to form the 6-substituted-2,4-diaminopyrimidine-5-carbonitrile analogues **30** which will be converted to the desired modified analogues **55** and **56**. In **Scheme 20** *step ii*, although there might be likelihood of the acid chloride polymerising, fortunately

because the amino groups in the 2 and 4 position on the pyrimidine are not nucleophilic, there is not much chance of polymerisation.

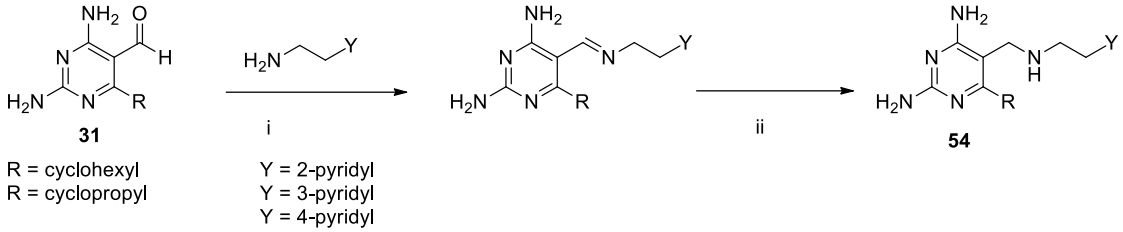

Scheme 19: Reagents and conditions: i) 1,2-DCE, G.AcOH; ii) 1,2-DCE/THF, G.AcOH (pH 4-5), $NaBH_4$.

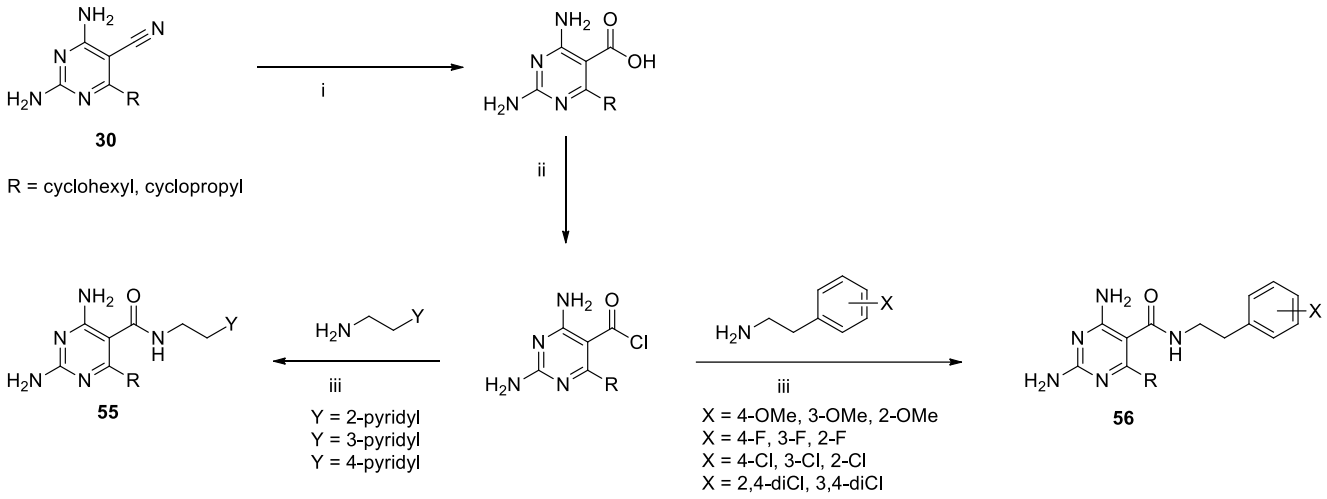

Scheme 20: Reagents and conditions: i) H^+/H_2O (ii) $SOCl_2$; iii) n-BuLi -10 °C, THF.

CHAPTER 4: EXPERIMENTAL-PART 1

4.1. Modelling

Maestro version 12.7.161, 2021-1 release by Schrödinger[43] was used for all computational experiments. The protein crystal structure 1J3K[47] of quadruple mutant *Pf*DHFR with resolution 2.10 Å, was downloaded from the protein data bank. This structure consists of four subunits, with the ligand WR99210 bound in the active site present in subunit A and was prepared using the protein preparation wizard. In this workflow non-explicit hydrogens were added, missing side chains and loops were incorporated using Prime, internal hydrogen bonds were optimized at a pH of 7.4, and the waters of crystallization were removed. The ligands selected for analysis consist of the natural substrate DHF **19**, known binders including pyrimethamine (PYR) **7** and WR99210 **25**, and 33 relevant synthetic structures **28a-g'**. Ligands were prepared using the LigPrep tool from Schrödinger; OPLS4 was selected as the force field for the energy minimization step, and Epik was used to generate possible states for the ligands under physiological conditions (pH 7.4 ±2). This study incorporated docking constraints in the form of forced hydrogen bonds to the backbone of residues Ile14 and mutant Ile164 and to the Asp54 side chain. This was done to ensure the ligands adhered to the known conserved binding mode. For the initial Glide docking and Prime refinement steps, the default settings were used, while for the redocking step, the more rigorous Glide XP algorithm was used for the glide redocking step. Prediction of pharmacokinetic properties for compound **28a-g'** was done using QikProp.

4.2. General Procedures

Reagents purchased from Sigma-Aldrich (Steinheim, Germany) Merck KGaA (South Africa) and MK Chemicals (South Africa) were of reagent grade and were used without any further purification unless specified. Ethyl acetate (EtOAc) and hexane used for chromatography or extractions were distilled prior to use. Tetrahydrofuran (THF) was distilled from sodium prior to use.

Reactions were monitored by thin-layer chromatography (TLC) using precoated aluminium-backed plates (Merck silica gel 60 F254) visualised under UV light ($\lambda = 254$ nm). Intermediates and final compounds were purified by column chromatography on Macherey-Nagel silica gel 60 (particle size 0.063 mm to 0.200 mm) as well as aluminium oxide-neutral (0.063-0.200 mm).

NMR spectra were acquired on a Bruker 300, 400 or 500 MHz spectrometer at room temperature, using the specified deuterated solvent. For those compounds soluble in deuterated chloroform ($CDCl_3$), the solvent contained tetramethylsilane (TMS, 0.05% v/v) as internal standard. For others, the residual solvent signal was used for referencing. Data processing was done using MestreNova Software under license from Mestrelab Research, CA, USA.

Infra-red spectra were recorded on a Bruker Tensor-27 Fourier Transform spectrometer. Mass Spectra (High Resolution) were recorded on a Bruker Compact mass spectrometer. Melting points were determined on a Stuart SMP10 melting point apparatus and are uncorrected.

The following abbreviations are used to designate multiplicity: s =singlet, d = doublet, t = triplet, q = quartet, p = pentet, m = multiplet, dd = doublet of doublets.

For the mass spectrometry data, all calculations for the compounds below are for the MH+ ion.

4.3. General procedure for synthesis of 6-substituted-2,4-diaminopyrimidine-5-carbonitrile and analogues (30)

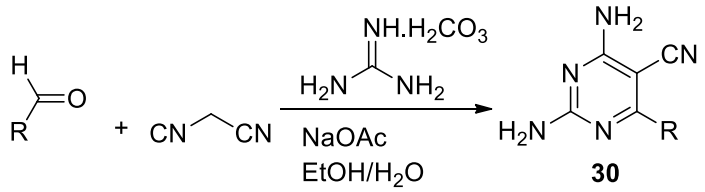

R = phenyl
R = cyclohexyl
R = cyclopropyl

Malononitrile (1.50 g, 1.0 eq) was dissolved in ethanol (15 mL) in a round bottomed flask in the presence of a magnetic stirrer bar. Upon dissolving, the aldehyde (1.0 eq) was added to the mixture while stirring. When mixed well, water (30 mL) was added followed by the addition of sodium acetate (1.0 eq) and the resulting solution was stirred for 10 minutes at room temperature. The mixture was then treated with guanidine carbonate (1.0 eq) and the reaction was heated at reflux temperature for 2.5-3 hours (monitored by TLC), under nitrogen atmosphere. The reaction was then allowed to cooled to room temperature. Where a precipitate formed, this was filtered, or alternatively, the mixture was extracted with EtOAc (3 × 150 mL). The extracts were dried using $MgSO_4$ or Na_2SO_4, filtered through celite and concentrated *in vacuo*. The crude product was purified by recrystallisation from ethanol. The following compounds were prepared by this method:

4.3.1. Synthesis of 2,4-diamino-6-phenylpyrimidine-5-carbonitrile (30a)[52]

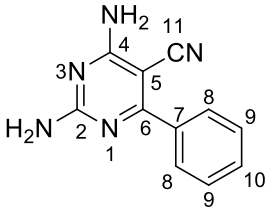

Prepared from benzaldehyde (2.32 mL, 22.7 mmol), malononitrile (1.50 g, 22.7 mmol), sodium acetate (1.87 g, 22.7 mmol) and guanidine carbonate (2.05 g, 22.7 mmol). Isolated as a yellow solid (3.14 g, 65.4 %). m.p. 214-216 °C; **^{1}H NMR (400 MHz, DMSO)** δ 7.75 (H-8, dd, *J* = 7.3, 1.9 Hz, 2H), 7.55 – 7.43 (H-9 and H-10, m, 3H), 7.06 (2 NH_2, s, overlapping 4H); **^{13}C NMR (101 MHz, DMSO)** δ 169.4 (C-6), 165.0 (C-4), 163.0 (C-2), 137.2 (C-7), 130.2 (C-10), 128.2 (C-9), 128.1 (C-8), 117.9 (C-11), 75.9 (C-5); **IR (ν_{max}/cm^{-1})** 3375 (N-H); 3159 (=C-H); 2206 (CN); 1610 (Ar-C=C), **HRMS** *m/z*: calculated for : $C_{11}H_{10}N_5$, 212.0931 found: $[M+H]^+$ 212.0929

4.3.2. Synthesis of 2,4-diamino-6-cyclohexylpyrimidine-5-carbonitrile (30b)

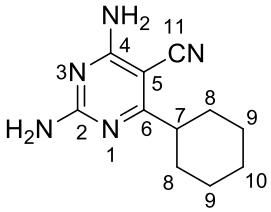

Prepared from cyclohexanecarboxyaldehyde (2.30 mL, 18.9 mmol), malononitrile (1.25 g, 18.9 mmol), sodium acetate (1.55 g, 18.9 mmol) and guanidine carbonate (1.70 g, 18.9 mmol). Isolated as a pale-yellow solid (2.75 g, 66.9 %). m.p. 223-224 °C; **^{1}H NMR (400 MHz, DMSO)** δ 6.90 (NH_2, s, 2H), 6.77 (NH_2, s, 2H), 2.66 (H-7, tt, *J* = 11.7, 3.5 Hz, 1H), 1.77 (cyclohexyl, dt, *J* = 12.9, 3.2 Hz, 2H), 1.73 – 1.64 (cyclohexyl, m, 3H), 1.59 – 1.45 (cyclohexyl, m, 2H), 1.30 (cyclohexyl, qt, *J* = 12.9, 3.2 Hz, 2H); 1.23 – 1.09 (cyclohexyl, m, 1H) **^{13}C NMR (101 MHz, DMSO)** δ 177.4 (C-6), 163.9 (C-4), 162.7 (C-2), 116.8, (C-11) 75.7 (C-5), 43.5 (C-7), 30.06 (C-8), 25.2 (C-9), 25.1 (C-10);); **IR (ν_{max}/cm^{-1}):** 3390 (N-H); 2197 (CN); 2918, 1447, 890 (C-H); **HRMS** *m/z*: calculated for : $C_{11}H_{16}N_5$, 218.1400 found: $[M+H]^+$ 218.1671.

4.3.3. Synthesis of 2,4-diamino-6-cyclopropylpyrimidine-5-carbonitrile (30c)

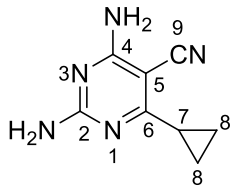

Prepared from cyclopropanecarboxyaldehyde (1.70 mL, 22.7 mmol), malononitrile (1.50 g, 22.7 mmol), sodium acetate (1.87 g, 22.7 mmol) and guanidine carbonate (2.04 g, 22.7 mmol). Isolated as a yellow solid (1.02 g, 25.6 %). m.p. 255-256 °C; **^{1}H NMR (400 MHz, DMSO)** δ 6.91 (2-NH_2, s, 2H), 6.67 (4-NH_2, s, 2H), 2.08 – 1.97 (H-7, m, 1H), 1.01 – 0.92 (H-8, m, 4H); **^{13}C NMR (101 MHz, DMSO)** δ 174.5 (C-6), 163.7 (C-4), 162.9 (C-2), 117.5 (C-9), 76.9 (C-5), 14.8 (C-7), 9.4 (C-8); **IR (ν_{max}/cm^{-1}):** 3498, 3426 (N-H); 2204 (CN); 3092, 1455, 1282 (C-H); **HRMS** *m/z*: calculated for : $C_8H_{10}N_5$, 176.0931 found: $[M+H]^+$ 176.1162.

4.4. Preparation of Raney Nickel

Sodium hydroxide pellets (90 g) were dissolved in water (180 mL) and stirred in a 500 mL beaker. The aqueous solution was allowed to cool to room temperature. In a separate 2 litre beaker, nickel aluminium alloy (30 g) was suspended in water (80 mL) and stirred to form a slurry. Aqueous sodium hydroxide (de-oxygenated with nitrogen gas) was added dropwise to the nickel aluminium aqueous suspension. Reaction warmed up and hydrogen gas was given off. After adding about 15 mL aqueous sodium hydroxide, 200 mL of water was added, and the mixture left to stir for 5 minutes. The remaining aqueous sodium hydroxide solution was left to stir for 15 min. The solution was then heated at 80 ºC on a hot plate for a further 2 hours with stirring. The resulting mixture was filtered and washed with water (taking care not to filter to dryness). Filter cake was washed until filtrate was at pH 7. Filter cake was then transferred to Schott bottle and the water was replaced with ethanol. Reaction yielded approximately 20 g of activated nickel.

4.5. General procedure for synthesis of 6-substituted-2,4-diaminopyrimidine-5-carbaldehydes (31)

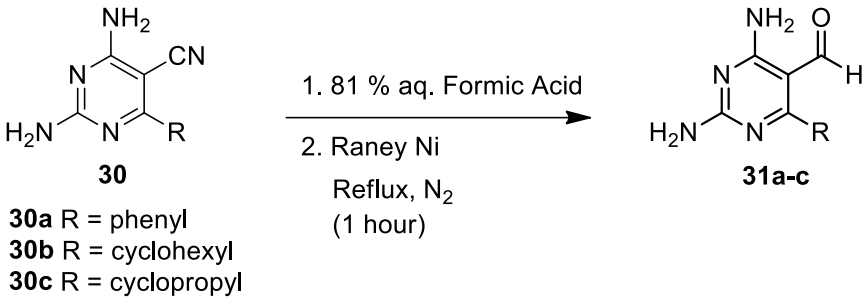

30a R = phenyl
30b R = cyclohexyl
30c R = cyclopropyl

A 6-substituted 2,4-diamino-5-carbonitrile **30** was dissolved in 81 % aq. formic acid. This was followed by the addition of Raney Nickel (3-6 eq. by mass) to the reaction mixture. The reaction was heated at reflux under a nitrogen atmosphere for 1 hour. Upon complete consumption of starting material, the reaction mixture was filtered through celite (taking care not to filter to dryness) and the filtrate was collected, neutralised to pH 7 with solid $NaHCO_3$. The aqueous solution was then extracted with EtOAc (3 × 100 mL), and the combined organic layers were dried using $MgSO_4$ or Na_2SO_4, filtered through celite and concentrated *in vacuo*. The crude product was purified by column chromatography (50% EtOAc/hexane). The following compounds were prepared by this method:

4.5.1. Synthesis of 2,4-diaminopyrimidine-6-phenylpyrimidine-5-carbaldehyde (31a)

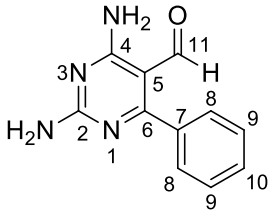

Prepared from 2,4-diamino-6-phenylpyrimidine-5-carbonitrile **30a** (0.150 g, 0.710 mmol), 81 % aq. formic acid (4 mL), Raney Nickel (0.600 g). Pure product isolated as white solid (0.085 g, 56 %) m.p. 237-238 °C; **^{1}H NMR (400 MHz, $CDCl_3$)** δ 9.68 (H-11, s, 1H), 8.76 (one of 4-NH_2, s, 1H), 7.56 – 7.44 (phenyl, m, 5H), 5.56 (one of 4-NH_2, s, 1H), 5.36 (2-NH_2, s, 2H); **^{13}C NMR (101 MHz, $CDCl_3$)** δ 190.6 (C-11), 175.2 (C-6), 164.2 (C-4), 163.1 (C-2), 136.5 (C-7), 130.2 (C-10), 129.6 (C-9), 128.6 (C-8), 104.7 (C-5); **IR (ν_{max}/cm^{-1}):** 3118, 3059 (N-H); 2869, 2777 (=C-H); 1536 (C=O); 1578 (C=C); **HRMS** *m/z*: calculated for : $C_{11}H_{11}N_4$, 215.0927 found: $[M+H]^+$ 215.0932.

4.5.2. Synthesis of 2,4-diaminopyrimidine-6-cyclohexylpyrimidine-5-carbaldehyde (31b)

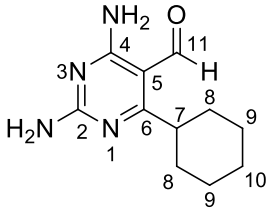

Prepared from 2,4-diamino-6-cyclohexylpyrimidine-5-carbonitrile **30b** (0.200 g, 0.92 mmol), 81 % aq. formic acid (4 mL), Raney Nickel (0.600 g). Pure product isolated as white solid (0.12 g, 59 %) m.p. 211-214 ºC; **^{1}H NMR (400 MHz, $CDCl_3$)** δ 10.15 (H-11, s, 1H), 8.83 (one of 4-NH_2, s, 1H), 5.62 (one of 4-NH_2, s, 1H), 5.36 (2-NH_2, s, 2H), 3.16 (H-7 tt, *J* = 11.4, 3.7 Hz, 1H), 1.89 – 1.80 (cyclohexyl, m, 2H), 1.80 – 1.62 (cyclohexyl, m, 5H), 1.42 – 1.22 (cyclohexyl, m, 3H); **^{13}C NMR (101 MHz, $CDCl_3$)** δ 188.0 (C-11), 181.5 (C-6), 164.0 (C-4), 163.5 (C-2), 103.1 (C-5), 40.4 (C-7), 31.9 (C-8), 26.4 (C-9), 26.0 (C-10); **IR (ν_{max}/cm^{-1}):** 3462, 3370 (N-H); 1551 (C=O); 2928, 1470 (C-H); **HRMS** *m/z*: calculated for : $C_{11}H_{17}N_4O$, 221.1397 found: $[M+H]^+$ 221.1398.

4.5.3. Synthesis of 2,4-diaminopyrimidine-6-cyclopropylpyrimidine-5-carbaldehyde(31c)

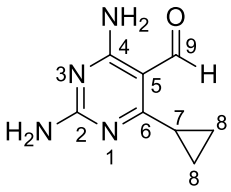

Prepared from 2,4-diamino-6-cyclopropylpyrimidine-5-carbonitrile **30c** (0.150 g, 0.856 mmol), 81 % aq. formic acid (4 mL), Raney Nickel (0.600 g). Pure product isolated as white solid (0.077 g, 50 %) m.p. 235-236 °C; **1H NMR (500 MHz, MeOD)** δ 10.24 (H-9, s, 1H), 2.50 (H-7, tt, *J* = 8.4, 4.6 Hz, 1H), 1.22 – 1.16 (H-8, m, 2H), 1.02 – 0.96 (H-8, m, 2H); **13C NMR (126 MHz, MeOD)** δ 189.3 (C-9), 179.4 (C-6), 165.1 (C-4, C-2 overlapping), 105.3 (C-5), 12.4 (C-7), 10.5 (C-8); **IR (ν_{max}/cm^{-1}):** 3353 (N-H); 1632 (C=O); 2798, 1440 (C-H); **HRMS** *m/z*: calculated for : $C_8H_{11}N_4O$, 179.0927 found: $[M+H]^+$ 179.0924.

4.6. General procedure for the synthesis of 2,4-diaminopyrimidine-5-phenethylimines (51)

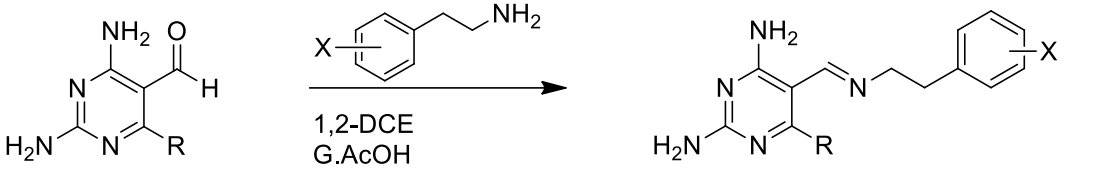

R = phenyl, cyclohexyl, cyclopropyl
X = 4-OMe, 3-OMe, 2-OMe
4-F, 3-F, 2-F
4-Cl, 3-Cl, 2-Cl, 2,4-diCl, 3,4-diCl

In a round bottomed flask, the carbaldehyde **31** was dissolved in 1,2-DCE in the presence of G.AcOH (2 eq.). When fully dissolved, the substituted phenethylamine (1.3 eq.) was added with constant stirring. The solution was heated at reflux temperature and left to stir for 3 hours under a nitrogen atmosphere. Upon completion, the solution was cooled to room temperature, diluted with water, and extracted with EtOAc (3 x 100 mL). The organic layer was dried with $MgSO_4$ or Na_2SO_4 and filtered through celite/cotton wool. The solvent was removed in *vacuo* and the crude product was purified using aluminium oxide (neutral) column chromatography, using 50% EtOAc/hexane as eluent. The following compounds were prepared by this method:

4.6.1. Synthesis of (*E*)-6-phenyl-5-{[(2-methoxyphenethyl)imino]methyl}pyrimidine-2,4 diamine (51a)

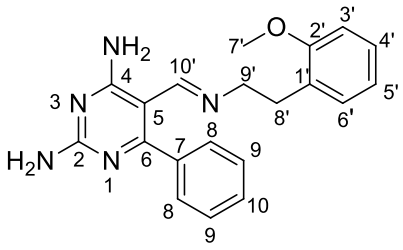

Prepared from 2,4-diamino-6-phenylpyrimidine-5-carbaldehyde **31a** (0.080 g, 0.37 mmol), 2-methoxyphenethylamine (0.071 mL, 0.48 mmol), 1,2-dichloroethane (4 mL), glacial acetic acid (0.043 mL, 0.75 mmol). Pure product isolated as a white solid (0.111 g, 85.3 %). m.p. 154-156 °C. **^{1}H NMR (400 MHz, $CDCl_3$)** δ 9.86 (one of 4-NH_2, s, 1H), 7.97 (H-10', s, 1H), 7.42 – 7.28 (H-8 and H-10, m, 3H), 7.28 – 7.15 (H-9 and H-6', m, 3H), 7.06 (H-3', d, *J* = 7.4 Hz, 1H), 6.90 – 6.77 (H-4, and H-5', m, 2H), 5.79 (one of 4-NH_2, s, 1H), 5.52 (2-NH_2, s, 2H), 3.75 (H-7', s, 3H), 3.61 (H-8', t, *J* = 6.9 Hz, 2H), 2.90 (H-9', t, *J* = 6.8 Hz, 2H);

^{13}C NMR (101 MHz, $CDCl_3$) δ 169.5 (C-6), 163.8 (C-4), 161.7 (C-2), 159.7 (C-10'), 157.7 (C-2'), 137.8 (C-7), 130.9 (C-6'), 129.3 (C-9), 128.9 (C-10) 128.3 (C-8), 128.2 (C-4'), 127.5 (C-1'), 120.4 (C-5'), 110.3 (C-3'), 101.3 (C-5), 61.1 (C-9'), 55.3 (C-7'), 32.4 (C-8'); **IR (ν_{max}/cm^{-1}):** 3267, 3105 (N-H); 2922, 2882 (=C-H); 1647 (C=N); 1245 (C-O); **HRMS** *m/z*: calculated for : $C_{20}H_{22}N_5O$, 348.1819 found: $[M+H]^+$ 348.1829.

4.6.2. Synthesis of (*E*)-6-phenyl-5-{[(3-methoxyphenethyl)imino]methyl}pyrimidine-2,4 diamine (51b)

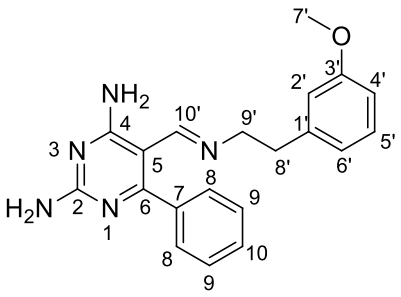

Prepared from 2,4-diamino-6-phenylpyrimidine-5-carbaldehyde **31a** (0.075 g, 0.35 mmol), 3-methoxyphenethylamine (0.066 mL, 0.46 mmol), 1,2-dichloroethane (4 mL), glacial acetic acid (0.040 mL, 0.70 mmol). Pure product isolated as white solid (0.103 g, 84.4 %). m.p. 156-157 °C. **^{1}H NMR (400 MHz, $CDCl_3$)** δ 9.82 (one of 4-NH_2, s, 1H), 7.99 (H-10', s, 1H), 7.44 – 7.32 (H-8 and H-10, m, 3H), 7.30 – 7.23 (H-9, m, 2H), 7.19 (H-5', t, *J* = 7.8 Hz, 1H), 6.80 – 6.68 (H-2', H-4' and H-6', m, 3H), 5.61 (one of 4-NH_2, s, 1H), 5.27 (2-NH_2, s, 2H), 3.77 (H-7', s, 3H), 3.64 (H-8', t, *J* = 6.9 Hz, 2H), 2.87 (H-9', t, *J* = 6.9 Hz, 2H); **^{13}C NMR (101 MHz, $CDCl_3$)** δ 169.7 (C-6), 163.9 (C-4), 161.7 (C-2), 160.1 (C-10'), 159.7 (C-3'), 141.7 (C-1'), 137.8 (C-7), 129.4 (C-5'), 129.3 (C-9), 129.2 (C-10), 128.3 (C-8), 121.6 (C-6'), 114.8 (C-2'), 111.6 (C-4'), 101.4 (C-5), 62.7 (C-9'), 55.3 (C-7'), 37.9 (C-8'); **IR (ν_{max}/cm^{-1}):** 3168, 3073 (N-H); 2924, 2863 (=C-H); 1645 (C=N); 1256 (C-O); **HRMS** *m/z*: calculated for : $C_{20}H_{22}N_5O$, 348.1819 found: $[M+H]^+$ 348.1768.

4.6.3. Synthesis of (*E*)-6-phenyl-5-{[(4-methoxyphenethyl)imino]methyl}pyrimidine-2,4 diamine (51c)

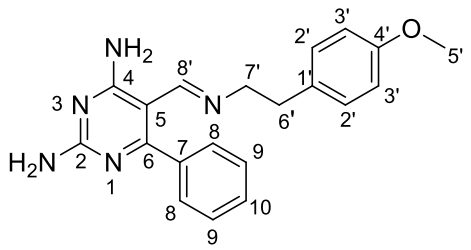

Prepared from 2,4-diamino-6-phenylpyrimidine-5-carbaldehyde **31a** (0.070 g, 0.33 mmol), 4-methoxyphenethylamine (0.062 mL, 0.43 mmol), 1,2-dichloroethane (4 mL), glacial acetic acid (0.037 mL, 0.66 mmol). Pure product isolated as white solid (0.108 g, 94.7 %). m.p. 202-204 °C. **^{1}H NMR (400 MHz, $CDCl_3$)** δ 9.85 (one of 4-NH_2, s, 1H), 7.96 (H-8', s, 1H), 7.42 – 7.32 (H-8 and H-10, m, 3H), 7.25 (H-9, d, *J* = 6.9 Hz, 2H), 7.05 (H-2', d, *J* = 8.2 Hz, 2H), 6.83 (H-3', d, *J* = 8.3 Hz, 2H), 5.48 (one of 4-NH_2, s, 1H), 5.03 (2-NH_2, s, 2H), 3.79 (H-5', s, 3H), 3.61 (H-6', t, *J* = 6.8 Hz, 2H), 2.84 (H-7', t, *J* = 6.8 Hz, 2H);
^{13}C NMR (101 MHz, $CDCl_3$) δ 169.8 (C-6), 163.9 (C-4), 161.7 (C-2), 160.1 (C-8'), 158.2 (C-4'), 137.9 (C-7), 132.2 (C-1'), 130.2 (C-2'), 129.3 (C-9), 129.2 (C-10), 128.3 (C-8) , 113.9 (C-3'), 101.5 (C-5), 63.1 (C-7'), 55.4 (C-5'), 37.0 (C-8'); **IR (ν_{max}/cm^{-1}):** 3269, 3103 (N-H); 2920, 2883 (=C-H); 1617 (C=N); 1240 (C-O); **HRMS** *m/z*: calculated for : $C_{20}H_{22}N_5O$, 348.1819 found: $[M+H]^+$ 348.1819.

4.6.4. Synthesis of (*E*)-6-phenyl-5-{[(2-fluorophenethyl)imino]methyl}pyrimidine-2,4 diamine (51d)

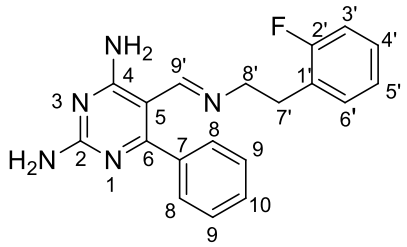

(Prepared from 2,4-diamino-6-phenylpyrimidine-5-carbaldehyde **31a** (0.082 g, 0.38 mmol), 2-fluorophenethylamine (0.065 mL, 0.50 mmol), 1,2-dichloroethane (4 mL), glacial acetic acid (0.044 mL, 0.77 mmol). Pure product isolated as white solid (0.127 g, 99.2 %). m.p. 197-199 °C. **^{1}H NMR (400 MHz, $CDCl_3$)** δ 9.79 (one of 4-NH_2, s, 1H), 8.01 (H-9', s, 1H), 7.53 – 7.32 (H-8 and H-4', m, 3H), 7.28 – 7.10 (H-9, H-10 and H-3', m, 4H), 7.08 – 6.98 (H-5' and H-6', m, 2H), 5.49 (one of 4-NH_2, s, 1H), 5.07 (2-NH_2, s, 2H), 3.64 (H-7', t, *J* = 6.8 Hz, 2H), 2.95

(H-8', t, *J* = 6.8 Hz, 2H); **^{13}C NMR (101 MHz, $CDCl_3$)** δ 169.8 (C-6), 163.9 (C-4), 161.7 (C-2), 161.42 (C-2', d, *J* = 245.0 Hz), 160.3 (C-9'), 137.9 (C-7), 131.6 (C-6', d, *J* = 5.1 Hz), 129.3 (C-9), 129.2 (C-10), 128.4 (C-8), 128.0 (C-1', d, *J* = 8.1 Hz), 126.9 (C-4', d, *J* = 15.8 Hz), 124.0 (C-5', d, *J* = 3.7 Hz), 115.4 (C-3', d, *J* = 22.0 Hz), 101.5 (C-5), 61.3 (C-8'), 31.2 (C-7'); **IR (ν_{max}/cm^{-1}):** 3265, 3099 (N-H); 2935, 2882 (=C-H); 1646 (C=N); 1489 (C-F); **HRMS** *m/z*: calculated for : $C_{19}H_{19}N_5F$, 336.1619 found: $[M+H]^+$ 336.1650.

4.6.5. Synthesis of (*E*)-6-phenyl-5-{[(3-fluorophenethyl)imino]methyl}pyrimidine-2,4 diamine (51e)

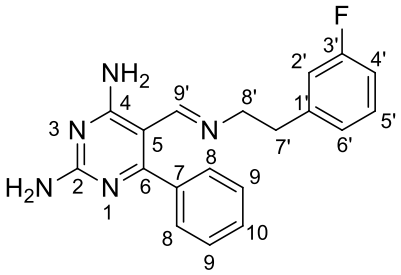

Prepared from 2,4-diamino-6-phenylpyrimidine-5-carbaldehyde **31a** (0.070 g, 0.33 mmol), 3-fluorophenethylamine (0.055 mL, 0.42 mmol), 1,2-dichloroethane (4 mL), glacial acetic acid (0.044 mL, 0.66 mmol). Pure product isolated as white solid (0.087 g, 79.1 %). m.p. 201-202 °C. **^{1}H NMR (400 MHz, $CDCl_3$)** δ 9.75 (one of 4-NH_2, s, 1H), 8.00 (H-9', s, 1H), 7.45 – 7.33 (H-8 and H-10, m, 3H), 7.30 – 7.18 (H-9 and H-5', m, 3H), 6.95 – 6.84 (H-2', H-4' and H-6', m, 3H), 5.48 (one of 4-NH_2, s, 1H), 5.05 (2-NH_2, s, 2H), 3.65 (H-7', t, *J* = 6.8 Hz, 2H), 2.90 (H-8', t, *J* = 6.8 Hz, 2H); **^{13}C NMR (101 MHz, $CDCl_3$)** δ 169.9 (C-6), 163.8 (C-4), 163.0 (C-3', d, *J* = 244.9 Hz), 161.7 (C-2), 160.4 (C-9'), 142.7 (C-1', d, *J* = 7.3 Hz), 137.9 (C-5', d, *J* = 3.2 Hz), 129.8 (C-6', d, *J* = 8.4 Hz), 129.24 (C-9), 129.20 (C-7), 128.37 (C-8), 124.9 (C-10), 115.9 (C-2', d, *J* = 20.5 Hz), 113.1 (C-4', d, *J* = 20.9 Hz), 101.4 (C-5), 62.4 (C-8'), 37.6 (C-7'); **IR (ν_{max}/cm^{-1}):** 3268, 3090 (N-H); 2936, 2885 (=C-H); 1619 (C=N); 1488 (C-F); **HRMS** *m/z*: calculated for : $C_{19}H_{19}N_5F$, 336.1619 found: $[M+H]^+$ 336.1148.

4.6.6. Synthesis of (*E*)-6-phenyl-5-{[(4-fluorophenethyl)imino]methyl}pyrimidine-2,4 diamine (51f)

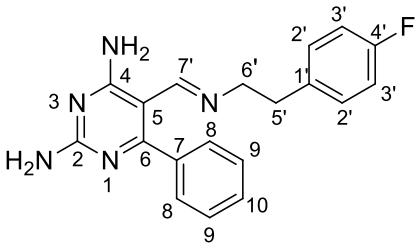

Prepared from 2,4-diamino-6-phenylpyrimidine-5-carbaldehyde **31a** (0.085 g, 0.40 mmol), 4-fluorophenethylamine (0.068 mL, 0.52 mmol), 1,2-dichloroethane (4 mL), glacial acetic acid (0.045 mL, 0.80 mmol). Pure product isolated as white solid (0.113 g, 85.6 %). m.p. 214-215 °C. **^{1}H NMR (400 MHz, $CDCl_3$)** δ 9.79 (one of 4-NH_2, s, 1H), 7.96 (H-7', s, 1H), 7.43 – 7.33 (H-8, m, 2H), 7.29 – 7.23 (H-9 and H-10, m, 3H), 7.13 – 7.05 (H-2', m, 2H), 6.97 (H-3', t, *J* = 8.6 Hz, 2H), 5.46 (one of 4-NH_2, s, 1H), 5.02 (2-NH_2, s, 2H), 3.62 (H-5', t, *J* = 6.5 Hz, 2H), 2.87 (H-6', t, *J* = 6.8 Hz, 2H); **^{13}C NMR (101 MHz, $CDCl_3$)** δ 169.9 (C-6), 163.9 (C-4), 161.6 (C-4', d, *J* = 243.6 Hz), 161.7 (C-2), 160.3 (C-7'), 137.9 (C-7), 135.74 (C-1', d, *J* = 3.3 Hz), 130.6 (C-2', d, *J* = 8.1 Hz), 129.2 (C-9), 129.2 (C-10), 128.4 (C-8), 115.22 (C-3', d, *J* = 20.9 Hz), 101.5 (C-5), 62.8 (C-6'), 37.1 (C-5'); **IR (ν_{max}/cm^{-1}):** 3279, 3096 (N-H); 2923, 2882 (=C-H); 1646 (C=N); 1497 (C-F); **HRMS** *m/z*: calculated for : $C_{19}H_{19}N_5F$, 336.1619 found: $[M+H]^+$ 336.1613.

4.6.7. Synthesis of (*E*)-6-phenyl-5-{[(2-chlorophenethyl)imino]methyl}pyrimidine-2,4 diamine (51g)

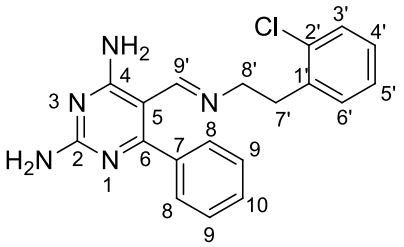

Prepared from 2,4-diamino-6-phenylpyrimidine-5-carbaldehyde **31a** (0.068 g, 0.32 mmol), 2-chlorophenethylamine (0.058 mL, 0.41 mmol), 1,2-dichloroethane (4 mL), glacial acetic acid (0.036 mL, 0.63 mmol). Pure product isolated as a white solid (0.113 g, 98.2 %). m.p. 172-173 °C. **^{1}H NMR (400 MHz, $CDCl_3$)** δ 9.78 (one of 4-NH_2, s, 1H), 8.00 (H-9', s, 1H), 7.43 – 7.32 (H-9, H-10 and H-3', m, 4H), 7.29 – 7.22 (H-4', H-5' and H-6', m, 3H), 7.16 (H-8, d, *J* = 2.9 Hz, 2H), 5.64 (one of 4-NH_2, s, 1H), 5.32 (2-NH_2, s, 2H), 3.66 (H-7', t, *J* = 6.8 Hz, 2H), 3.04

(H-8', t, *J* = 6.9 Hz, 2H); **^{13}C NMR (101 MHz, $CDCl_3$)** δ 169.7 (C-6), 163.8 (C-4), 161.7 (C-2), 160.3 (C-9'), 137.8 (C-1'), 137.6 (C-2'), 134.3 (C-7), 131.5 (C-3'), 129.6 (C-10), 129.3 (C-9), 129.2 (C-4'), 128.3 (C-8), 127.8 (C-5'), 126.7 (C-6'), 101.3 (C-5), 60.7 (C-8'), 35.6 (C-7'); **IR (ν_{max}/cm^{-1}):** 3274, 3089 (N-H); 2937, 2883 (=C-H); 1648 (C=N); 753 (C-Cl); **HRMS** *m/z*: calculated for : $C_{19}H_{19}N_5{}^{35}Cl$, 352.1323 found: $[M+H]^+$ 352.1325.

4.6.8. Synthesis of (*E*)-6-phenyl-5-{[(3-chlorophenethyl)imino]methyl}pyrimidine-2,4 diamine (51h)

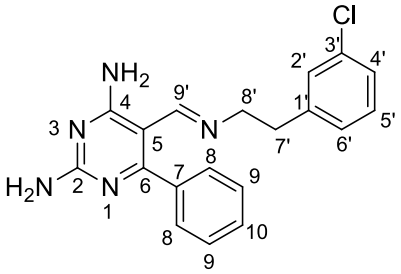

Prepared from 2,4-diamino-6-phenylpyrimidine-5-carbaldehyde **31a** (0.060 g, 0.28 mmol), 2-chlorophenethylamine (0.051 mL, 0.36 mmol), 1,2-dichloroethane (4 mL), glacial acetic acid (0.036 mL, 0.56 mmol). Pure product isolated as a white solid (0.060 g, 61 %). m.p. 175-176 °C. **^{1}H NMR (400 MHz, $CDCl_3$)** δ 9.75 (one of 4-NH_2, s, 1H), 8.00 (H-9', t, *J* = 1.3 Hz, 1H), 7.42 – 7.35 (H-8 and H-2', m, 3H), 7.27 (H-9, dt, *J* = 7.8, 1.6 Hz, 2H), 7.22 – 7.17 (H-10 and H-5', m, 2H), 7.17 – 7.14 (H-4', m, 1H), 7.02 (H-6', ddd, *J* = 5.5, 3.6, 1.7 Hz, 1H), 5.48 (one of 4-NH_2s, 1H), 5.06 (2-NH_2, s, 2H), 3.64 (H-7', td, *J* = 6.8, 1.3 Hz, 2H), 2.88 (H-8't, *J* = 6.8 Hz, 2H); **^{13}C NMR (101 MHz, $CDCl_3$)** δ 169.9 (C-6), 163.9 (C-4), 161.7 (C-2), 160.4 (C-9'), 142.2 (C-1'), 137.9 (C-3'), 134.3 (C-7), 129.7 (C-5'), 129.3 (C-9 and C-2', overlapping), 129.2 (C-10), 128.4 (C-8), 127.5 (C-4'), 126.4 (C-6'), 101.4 (C-5), 62.4 (C-8'), 37.56 (C-7'); **IR (ν_{max}/cm^{-1}):** 3269, 3094 (N-H); 2927, 2882 (=C-H); 1620 (C=N); 753 (C-Cl); **HRMS** *m/z*: calculated for : $C_{19}H_{19}N_5{}^{35}Cl$, 352.1323 found: $[M+H]^+$ 352.1128.

4.6.9. Synthesis of (*E*)-6-phenyl-5-{[(4-chlorophenethyl)imino]methyl}pyrimidine-2,4 diamine (51i)

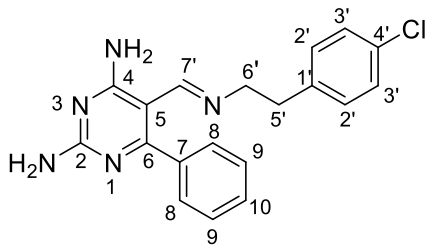

Prepared from 2,4-diamino-6-phenylpyrimidine-5-carbaldehyde **31a** (0.055 g, 0.26 mmol), 4-chlorophenethylamine (0.047 mL, 0.33 mmol), 1,2-dichloroethane (4 mL), glacial acetic acid (0.029 mL, 0.52 mmol). Pure product isolated as a white solid (0.088 g, 97 %). m.p. 225-226 °C. **^{1}H NMR (400 MHz, $CDCl_3$)** δ 9.77 (one of 4-NH_2, s, 1H), 7.93 (H-7', s, 1H), 7.41 – 7.34 (H-8 and H-10, m, 3H), 7.28 – 7.21 (H-9 and H-3', m, 4H), 7.07 (H-2', d, *J* = 8.1 Hz, 2H), 5.46 (one of 4-NH_2, s, 1H), 5.01 (2-NH_2, s, 2H), 3.62 (H-5', t, *J* = 6.7 Hz, 2H), 2.87 (H-6', t, *J* = 6.7 Hz, 2H); **^{13}C NMR (101 MHz, $CDCl_3$)** δ 169.9 (C-6), 163.8 (C-4), 161.7 (C-2), 160.4 (C-7'), 138.6 (C-1'), 137.9 (C-7), 132.1 (C-4'), 130.6 (C-9), 129.2 (C-10 and C-3', overlapping), 128.6 (C-2'), 128.4 (C-8), 101.4 (C-5), 62.6 (C-6'), 37.2 (C-5'); **IR (ν_{max}/cm^{-1}):** 3269, 3091 (N-H); 2929, 2881 (=C-H); 1647 (C=N); 742 (C-Cl); **HRMS** *m/z*: calculated for : $C_{19}H_{19}N_5{}^{35}Cl$, 352.1323 found: $[M+H]^+$ 352.1260.

4.6.10. Synthesis of (*E*)-6-phenyl-5-{[(2,4-dichlorophenethyl)imino]methyl}pyrimidine-2,4 diamine (51j)

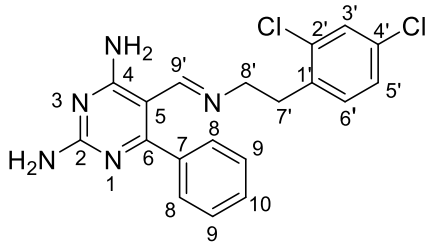

Prepared from 2,4-diamino-6-phenylpyrimidine-5-carbaldehyde **31a** (0.061 g, 0.29 mmol), 2,4-chlorophenethylamine (0.063 mL, 0.37 mmol), 1,2-dichloroethane (4 mL), glacial acetic acid (0.033 mL, 0.57 mmol). Pure product isolated as a white solid (0.107 g, 97.2 %). m.p. 182-184 °C. **^{1}H NMR (400 MHz, $CDCl_3$)** δ 9.79 (one of 4-NH_2, s, 1H), 7.96 (H-9', s, 1H), 7.43 – 7.35 (H-8 and H-9, m, 4H), 7.29 – 7.22 (H-10 and H-3', m, 2H), 7.17 (H-5', dd, *J* = 8.2, 2.1 Hz, 1H), 7.09 (H-6', d, *J* = 8.2 Hz, 1H), 5.56 (one of 4-NH_2, s, 1H), 5.17 (2-NH_2, s, 2H), 3.64 (H-7', td, *J* = 6.7, 1.2 Hz, 2H), 3.01 (H-8', t, *J* = 6.7 Hz, 2H); **^{13}C NMR (101 MHz,**

$CDCl_3$) δ 169.7 (C-6), 163.8 (C-4), 161.5 (C-2), 160.5 (C-9'), 137.6 (C-1'), 136.2 (C-2'), 134.9 (C-4'), 132.8 (C-7), 132.3 (C-6'), 129.4 (C-3'), 129.2 (C-9), 128.4 (C-8), 127.0 (C-10), 101.4 (C-5), 60.5 C-8'), 34.9 (C-7'); **IR (ν_{max}/cm^{-1}):** 3303, 3090 (N-H); 2940, 2860 (=C-H); 1615 (C=N); 742 (C-Cl); **HRMS** *m/z*: calculated for : $C_{19}H_{18}N_5{}^{35}Cl_2$, 386.0934 found: $[M+H]^+$ 386.0924.

4.6.11. Synthesis of (*E*)-6-phenyl-5-{[(3,4-dichlorophenethyl)imino]methyl}pyrimidine-2,4 diamine (51k)

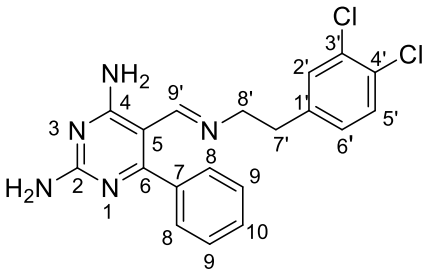

Prepared from 2,4-diamino-6-phenylpyrimidine-5-carbaldehyde **31a** (0.066 g, 0.31 mmol), 3,4-chlorophenethylamine (0.068 mL, 0.40 mmol), 1,2-dichloroethane (4 mL), glacial acetic acid (0.035 mL, 0.62 mmol). Pure product isolated as a white solid (0.112 g, 94.1 %). m.p. 174-175 °C. ^{1}H NMR (400 MHz, $CDCl_3$) δ 9.72 (one of 4-NH_2, s, 1H), 7.95 (H-9', s, 1H), 7.44 – 7.36 (H-8 and H-10, m, 3H), 7.34 (H-5', d, *J* = 8.2 Hz, 1H), 7.28 – 7.23 (H-9 and H-2', m, 3H), 6.97 (H-6', dd, *J* = 8.2, 2.1 Hz, 1H), 5.58 (one of 4-NH_2, s, 1H), 5.24 (2-NH_2, s, 2H), 3.62 (H-7', td, *J* = 6.6, 1.1 Hz, 2H), 2.85 (H-8', t, *J* = 6.6 Hz, 2H); **^{13}C NMR (101 MHz, $CDCl_3$)** δ 170.0 (C-6), 163.8 (C-4), 161.7 (C-2), 160.6 (C-9'), 140.4 (C-1'), 137.8 (C-3'), 132.3 (C-7), 131.1 (C-4'), 130.3 (C-5'), 130.2 (C-2'), 129.3 (C-10), 129.1 (C-9), 128.8 (C-6'), 128.4 (C-8), 101.3 (C-5), 62.2 (C-8'), 36.9 (C-7'); **IR (ν_{max}/cm^{-1}):** 3297, 3118 (N-H); 2931, 2854 (=C-H); 1618 (C=N); 742 (C-Cl); **HRMS** *m/z*: calculated for : $C_{19}H_{18}N_5{}^{35}Cl_2$, 386.0934 found: $[M+H]^+$ 386.0942.

4.6.12. Synthesis of (*E*)-6-cyclohexyl-5-{[(2-methoxyphenethyl)imino]methyl}pyrimidine-2,4 diamine (51l)

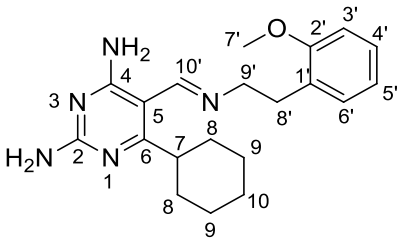

Prepared from 2,4-diamino-6-cyclohexylpyrimidine-5-carbaldehyde **31b** (0.060 g, 0.27 mmol), 2-methoxyphenethylamine (0.051mL, 0.35 mmol), 1,2-dichloroethane (4 mL), glacial acetic acid (0.031 mL, 0.54 mmol). Pure product isolate as colourless gel (0.084 g, 88 %); **^{1}H NMR (400 MHz, $CDCl_3$)** δ 9.86 (one of 4-NH_2, s, 1H), 8.37 (H-10', s, 1H), 7.22 – 7.07 (H-6'and H-5', m, 2H), 6.91 – 6.81 (H-3'and H-4', m, 2H), 5.32 (one of 4-NH_2, s, 1H), 4.82 (2-NH_2, s, 2H), 3.82 (H-7', s, 3H), 3.77 (H-9', t, *J* = 7.3 Hz, 2H), 2.96 (H-8', t, *J* = 7.1 Hz, 2H), 2.86 – 2.71 (H-7, m, 1H), 1.89 – 1.54 (H-8-10 cyclohexyl, m, 6H), 1.38 – 1.20 (H-8-10 cyclohexyl, m, 4H) **^{13}C NMR (101 MHz, $CDCl_3$)** δ 175.5 (C-6), 163.6 (C-4), 162.0 (C-2), 157.9 (C-10'), 157.8 (C-2'), 130.9 (C-6'), 128.4 (C-1'), 127.6 (C-4'), 120.5 (C-5'), 110.4 (C-3'), 100.1 (C-5), 61.5(C-9'), 55.4 (C-7'), 40.5 (C-7), 32.6 (C-8'), 31.6 (C-8), 26.6 (C-9), 26.1 (C-10); **IR (ν_{max}/cm^{-1})** 3317, 3167 (N-H); 2924, 2850 (C-H); 1610 (C=N); 1343, 1380 (C-N); 826 (C=C); 1240 (C-O); **HRMS** *m/z*: calculated for : $C_{20}H_{28}N_5O$, 354.2288 found: $[M+H]^+$ 354.2261.

4.6.13. Synthesis of (*E*)-6-cyclohexyl-5-{[(3-methoxyphenethyl)imino]methyl}pyrimidine-2,4 diamine (51m)

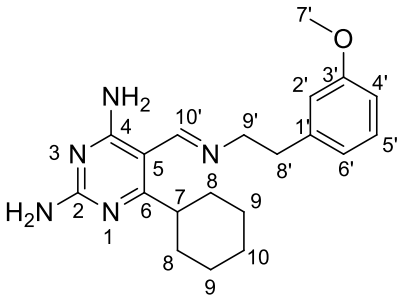

Prepared from 2,4-diamino-6-cyclohexylpyrimidine-5-carbaldehyde **31b** (0.099 g, 0.45 mmol), 3-methoxyphenethylamine (0.086 mL, 0.58 mmol), 1,2-dichloroethane (4 mL), glacial acetic acid (0.051 mL, 0.90 mmol). Pure product isolate as colourless gel (0.14 g, 88 %) **^{1}H NMR (400 MHz, $CDCl_3$)** δ 9.80 (one of 4-NH_2, s, 1H), 8.38 (H-10', s, 1H), 7.19 (H-5', t, *J* = 7.3 Hz, 1H), 6.85 – 6.65 (H-2',H-4' and H-6', m, 3H), 5.51 (one of 4-NH_2, s, 1H), 5.04 (2-

NH_2, s, 2H), 3.81 – 3.74 (H-7'and H-9', m, 5H), 2.92 (H-8', t, *J* = 6.9 Hz, 2H), 2.86 – 2.72 (H-7, m, 1H), 1.84 – 1.55 (H-8-10 cyclohexyl, m, 7H), 1.36 – 1.21 (H-8-10, cyclohexyl, m, 3H); **^{13}C NMR (101 MHz, $CDCl_3$)** δ 175.6 (C-6), 163.6 (C-4), 162.1 (C-2), 159.7 (C-3'), 158.2 (C-10'), 141.7 (C-1'), 129.4 (C-5'), 121.5 (C-6'), 114.9 (C-2'), 111.6 (C-4'), 99.9 (C-5), 63.0 (C-9'), 55.2 (C-7'), 40.5 (C-7), 38.1 (C-8') 31.6 (C-8), 26.5 (C-9), 26.0 (C-10); **IR (ν_{max}/cm^{-1})** 3324, 3187 (N-H); 2922, 2850 (C-H); 1608 (C=N); 1341, 1380 (C-N); 823 (C=C); 1227 (C-O); **HRMS** *m/z*: calculated for : $C_{20}H_{28}N_5O$, 354.2288 found: $[M+H]^+$ 354.2271.

4.6.14. Synthesis of (*E*)-6-cyclohexyl-5-{[(4-methoxyphenethyl)imino]methyl}pyrimidine-2,4 diamine (51n)

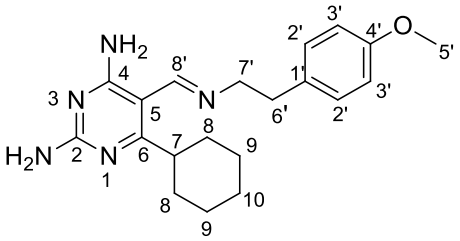

Prepared from 2,4-diamino-6-cyclohexylpyrimidine-5-carbaldehyde **31b** (0.091 g, 0.41 mmol), 4-methoxyphenethylamine (0.079 mL, 0.54 mmol), 1,2-dichloroethane (4 mL), glacial acetic acid (0.047 mL, 0.83 mmol). Pure product isolated as a white solid (0.145 g, 99.3 %). m.p. 131-133 °C; **^{1}H NMR (400 MHz, $CDCl_3$)** δ 9.85 (one of 4-NH_2, s, 1H), 8.33 (H-8', s, 1H), 7.10 (H-2', d, *J* = 8.1 Hz, 2H), 6.81 (H-3', d, *J* = 8.1 Hz, 2H), 5.51 (one of 4-NH_2, s, 1H), 5.05 (2-NH_2, s, 2H), 3.82 – 3.71 (H-5'and H-7', m, 5H), 2.88 (H-6', t, *J* = 6.9 Hz, 2H), 2.76 (H-7, tt, *J* = 10.1, 5.5 Hz, 1H), 1.84 – 1.52 (H-8-10 cyclohexyl, m, 7H), 1.37 – 1.18 (H-8-10, m, 3H); **^{13}C NMR (101 MHz, $CDCl_3$)** δ 175.6 (C-6), 163.6 (C-4), 162.0 (C-2), 158.09 (C-4'), 158.06 (C-8'), 132.1 (C-1'), 130.1 (C-3'), 113.8 (C-2'), 99.9 (C-5), 63.4 (C-7'), 55.3 (C-5'), 40.5 (C-7), 37.1 (C-6'), 31.6 (C-8), 26.5 (C-9), 26.0 (C-10); **IR (ν_{max}/cm^{-1})** 3330, 3204 (N-H); 2923, 2848 (C-H); 1613 (C=N); 1343, 1381 (C-N); 830 (C=C); 1306 (C-O) **HRMS** *m/z*: calculated for : $C_{20}H_{28}N_5O$, 354.2288 found: $[M+H]^+$ 354.2285.

4.6.15. Synthesis of (*E*)-6-cyclohexyl-5-{[(2-fluorophenethyl)imino]methyl}pyrimidine-2,4 diamine (51o)

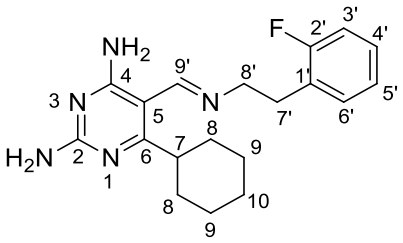

Prepared from 2,4-diamino-6-cyclohexylpyrimidine-5-carbaldehyde **31b** (0.067 g, 0.30 mmol), 2-fluorophenethylamine (0.052 mL, 0.40 mmol), 1,2-dichloroethane (4 mL), glacial acetic acid (0.035 mL, 0.60 mmol). Pure product isolate as yellow gel (solidified) (0.083 g, 80 %). m.p. 141-142 °C; **^{1}H NMR (400 MHz, $CDCl_3$)** δ 9.76 (one of 4-NH_2, s, 1H), 8.38 (H-9', s, 1H), 7.21 – 7.12 (H-3'and H-4', m, 2H), 7.07 – 6.97 (H-5' and H-6', m, 2H), 5.43 (one of, 4-NH_2, s, 1H), 4.97 (2-NH_2, s, 2H), 3.79 (H-8', t, *J* = 7.0 Hz, 2H), 3.00 (H-7', t, *J* = 7.1 Hz, 2H), 2.85 – 2.70 (H-7, m, 1H), 1.87 – 1.46 (H-8-10 cyclohexyl, m, 7H), 1.39-1.16 (H-8-10 cyclohexyl, m, 3H); **^{13}C NMR (101 MHz, $CDCl_3$)** δ 175.7 (C-6), 163.6 (C-4), 162.6 (C-2), 161.4 (C-2', d, *J* = 245.0 Hz) (C-2'), 158.3 (C-9'), 131.6 (d, *J* = 5.1 Hz) (C-6'), 128.0 (d, *J* = 8.1 Hz) (C-4') 127.0 (C-1', d, *J* = 15.7 Hz), 124.0 (C-5', d, *J* = 3.6 Hz); 115.3 (C-3', d, *J* = 22.1 Hz), 100.0 (C-5), 61.6 (C-8'), 40.5 (C-7), 31.6 (C-8), 31.4 (C-7'), 26.5 (C-9), 26.1 (C-10); **IR (ν_{max}/cm^{-1})** 3312, 3178 (N-H); 2920, 2848 (C-H); 1611 (C=N); 1362, 1385 (C-N); 1419 (C-F); **HRMS** *m/z*: calculated for : $C_{19}H_{25}N_5F$, 342.2089 found: $[M+H]^+$ 342.2069.

4.6.16. Synthesis of (*E*)-6-cyclohexyl-5-{[(3-fluorophenethyl)imino]methyl}pyrimidine-2,4 diamine (51p)

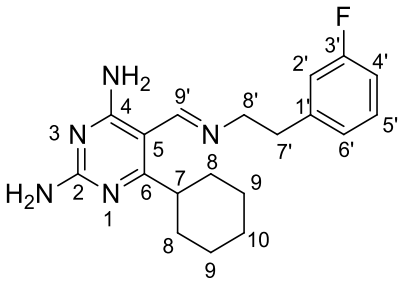

Prepared from 2,4-diamino-6-cyclohexylpyrimidine-5-carbaldehyde **31b** (0.064 g, 0.29 mmol), 3-fluorophenethylamine (0.049 mL, 0.38 mmol), 1,2-dichloroethane (2 mL), glacial acetic acid (0.033 mL, 0.58 mmol). Pure product isolate as a colourless gel (0.087 g, 88 %). **^{1}H NMR (400 MHz, $CDCl_3$)** δ 9.73 (one of 4-NH_2, s, 1H), 8.39 (H-9', s, 1H), 7.22 (H-2', q, *J* = 7.3 Hz, 1H), 6.96 (H-5', d, *J* = 7.7 Hz, 1H), 6.94 – 6.83 (H-4' and H-6', m, 2H) 5.44 (one of

4-NH_2, s, 1H), 4.97 (2-NH_2, s, 2H), 3.79 (H-8', t, *J* = 7.0 Hz, 2H), 2.95 (H-7', t, *J* = 7.0 Hz, 2H), 2.78 (H-7, tt, *J* = 10.1, 5.2 Hz, 1H), 1.87 – 1.51 (H-8-10 cyclohexyl, m, 7H), 1.39 – 1.18 (H-8-10 cyclohexyl, m, 3H) **^{13}C NMR (101 MHz, $CDCl_3$)** δ 175.8 (C-6), 163.6 (C-4), 163.00 (C-3',d, *J* = 245.4 Hz 162.2 (C-2), 158.3 (C-9'), 142.7 (C-1', d, *J* = 7.2 Hz), 129.8 (C-5', d, *J* = 8.2 Hz), 124.9 (C-6', d, *J* = 2.8 Hz), 115.9 (C-2', d, *J* = 20.9 Hz), 113.1 (C-4', d, *J* = 21.0 Hz), 99.9 (C-5), 62.8 (C-8'), 40.6 (C-7), 37.8 (C-7'), 31.6 (C-8), 26.5 (C-9), 26.0 (C-10); **IR (ν_{max}/cm^{-1})** 3312, 3178 (N-H); 2920, 2848 (C-H); 1611 (C=N); 1362, 1385 (C-N); 1419 (C-F) **HRMS** *m/z*: calculated for : $C_{19}H_{25}N_5F$, 342.2089 found: $[M+H]^+$ 342.2063.

4.6.17. Synthesis of (*E*)-6-cyclohexyl-5-{[(4-fluorophenethyl)imino]methyl}pyrimidine-2,4 diamine (51q)

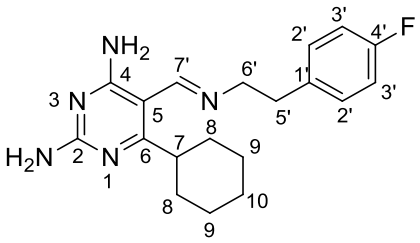

Prepared from 2,4-diamino-6-cyclohexylpyrimidine-5-carbaldehyde **31b** (0.056 g, 0.25 mmol), 4-fluorophenethylamine (0.043 mL, 0.33 mmol), 1,2-dichloroethane (4 mL), glacial acetic acid (0.029 mL, 0.50 mmol). Pure product isolated as a white solid (0.076 g, 87 %). m.p. 151-152 °C; **^{1}H NMR (400 MHz, $CDCl_3$)** δ 9.75 (one of 4-NH_2, s, 1H), 8.34 (H-7', s, 1H), 7.17 – 7.09 (H-2', m, 2H), 7.00 – 6.91 (H-3', m, 2H), 5.33 (one of 4-NH_2, s, 1H), 4.84 (2-NH_2, s, 2H), 3.77 (H-6', t, *J* = 6.9 Hz, 2H), 2.92 (H-5', t, *J* = 6.6 Hz, 2H), 2.76 (H-7, (tt, *J* = 10.3, 4.6 Hz, 1H), 1.85 – 1.52 (H-8-10 cyclohexyl, m, 7H), 1.28 (H-8-10 cyclohexyl, m, 3H) **^{13}C NMR (101 MHz, $CDCl_3$)** δ 175.8 (C-6), 163.6 (C-4), 162.1 (C-2), 161.6 (C-4', d, *J* = 243.9 Hz), 158.3 (C-7'), 135.8 (C-1', d, *J* = 3.3 Hz), 130.6 (C-2', d, *J* = 7.7 Hz), 115.2 (C-3', d, *J* = 21.3 Hz), 100.0 (C-5), 63.2 (C-6'), 40.6 (C-7), 37.2 (C-5'), 31.6 (C-8), 26.5 (C-9), 26.1 (C-10); **IR (ν_{max}/cm^{-1})** 3315, 3189 (N-H); 2921, 2846 (C-H); 1610 (C=N); 1361, 1384 (C-N); 1474 (C-F) **HRMS** *m/z*: calculated for : $C_{19}H_{25}N_5F$, 342.2089 found: $[M+H]^+$ 342.2087.

4.6.18. Synthesis of (*E*)-6-cyclohexyl-5-{[(2-chlorophenethyl)imino]methyl}pyrimidine-2,4 diamine (51r)

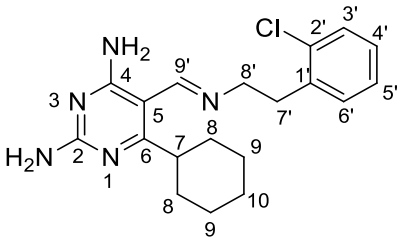

Prepared from 2,4-diamino-6-cyclohexylpyrimidine-5-carbaldehyde **31b** (0.075g, 0.34 mmol), 2-chlorophenethylamine (0.062 mL, 0.44 mmol), 1,2-dichloroethane (4 mL), glacial acetic acid (0.039 mL, 0.68 mmol). Pure product isolate as colourless gel (0.087 g, 71 %). **^{1}H NMR (400 MHz, $CDCl_3$)** δ 9.77 (one of 4-NH_2, s, 1H), 8.38 (H-9', s, 1H), 7.38 – 7.32 (H-3', m, 1H), 7.22 – 7.10 (H-4', H-5' and H-6', m, 3H), 5.44 (one of 4-NH_2, s, 1H), 4.97 (2-NH_2, s, 2H), 3.82 (H-8', t, *J* = 6.9 Hz, 2H), 3.09 (H-7', t, *J* = 6.6 Hz, 2H), 2.87 – 2.68 (H-7, m, 1H), 1.89 – 1.53 (H-8-10 cyclohexyl, m, 7H), 1.40 – 1.18 (H-8-10 cyclohexyl, m, 3H); **^{13}C NMR (101 MHz, $CDCl_3$)** δ 175.7 (C-6), 163.6 (C-4), 162.1 (C-2), 158.4 (C-9'), 137.6 (C-1'), 134.3 (C-2'), 131.5 (C-3'), 129.6 (C-4'), 127.8 (C-5'), 126.7 (C-6'), 99.9 (C-5), 61.0 (C-8'), 40.5 (C-7), 35.8 (C-7'), 31.6 (C-8), 26.5 (C-9), 26.0 (C-10); **IR (ν_{max}/cm^{-1})** 3297, 3133 (N-H); 2923,, 2851 (C-H); 1612 (C=N); 1345, 1268 (C-N); 966 (C=C); 830 (C-Cl); **HRMS** *m/z*: calculated for : $C_{19}H_{25}N_5{}^{35}Cl$, 358.1793 found: $[M+H]^+$ 358.1587.

4.6.19. Synthesis of (*E*)-6-cyclohexyl-5-{[(3-chlorophenethyl)imino]methyl}pyrimidine-2,4 diamine (51s)

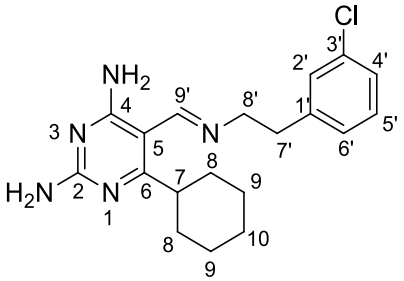

Prepared from 2,4-diamino-6-cyclohexylpyrimidine-5-carbaldehyde **31b** (0.081 g, 0.37 mmol), 4-chlorophenethylamine (0.066 mL, 0.48 mmol), 1,2-dichloroethane (4 mL), glacial acetic acid (0.042 mL, 0.74 mmol). Pure product isolated as a white solid (0.125 g, 94.6 %). m.p. 132-133 °C. **^{1}H NMR (400 MHz, $CDCl_3$)** δ 9.72 (one of 4-NH_2, s, 1H), 8.39 (H-9', s,

1H), 7.24 – 7.13 (H-2', H-4' and H-5', m, 3H), 7.12 – 7.03 (H-6', m, 1H), 5.33 (one of 4-NH_2, s, 1H), 4.84 (2-NH_2, s, 2H), 3.79 (H-8', t, *J* = 6.9 Hz, 2H), 2.93 (H-7', t, *J* = 6.1 Hz, 2H), 2.87 – 2.73 (H-7, m, 1H), 1.94 – 1.53 (H-8-10 cyclohexyl, m, 7H), 1.27 (H-8-10 cyclohexyl, d, *J* = 10.8 Hz, 3H); **^{13}C NMR (101 MHz, $CDCl_3$)** δ 175.8 (C-6), 163.6 (C-4), 162.1 (C-2), 158.4 (C-9'), 142.2 (C-1'), 134.2 (C-3'), 129.7 (C-5'), 129.3 (C-2'), 127.5 (C-6'), 126.5 (C-4'), 100.0 (C-5), 62.8 (C-8'), 40.6 (C-7), 37.7 (C-7'), 31.7 (C-8), 26.6 (C-9), 26.1 (C-10); **IR (ν_{max}/cm^{-1})** 3319, 3189 (N-H); 2921, 2850 (C-H); 1611 (C=N); 1342, 1266 (C-N); 964 (C=C); 824 (C-Cl); **HRMS** *m/z*: calculated for : $C_{19}H_{25}N_5{}^{35}Cl$, 358.1793 found: $[M+H]^+$ 358.1764.

4.6.20. Synthesis of (*E*)-6-cyclohexyl-5-{[(4-chlorophenethyl)imino]methyl}pyrimidine-2,4 diamine (51t)

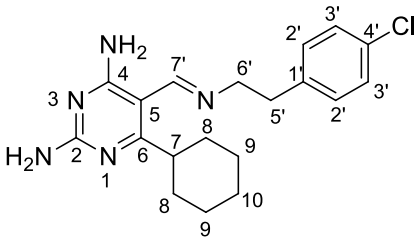

Prepared from 2,4-diamino-6-cyclohexylpyrimidine-5-carbaldehyde **31b** (0.091 g, 0.41 mmol), 4-chlorophenethylamine (0.075 mL, 0.54 mmol), 1,2-dichloroethane (4 mL), glacial acetic acid (0.047 mL, 0.83 mmol). Pure product isolated as a white solid (0.123 g, 83.1 %). m.p. 165-167 ºC. **^{1}H NMR (400 MHz, $CDCl_3$)** δ 9.74 (one of 4-NH_2, s, 1H), 8.33 (H-7', s, 1H), 7.24 (H-3', d, *J* = 7.1 Hz, 2H), 7.11 (H-2', d, *J* = 7.1 Hz, 2H), 5.35 (one of 4-NH_2, s, 1H), 4.88 (2-NH_2, s, 2H), 3.77 (H-6', t, *J* = 6.9 Hz, 2H), 2.92 (H-5', t, *J* = 6.9 Hz, 2H), 2.81 – 2.70 (H-7, m, 1H), 1.85 – 1.50 (H-8-10 cyclohexyl, m, 7H), 1.27 (H-8-10 cyclohexyl, d, *J* = 8.1 Hz, 3H); **^{13}C NMR (101 MHz, $CDCl_3$)** δ 175.8 (C-6), 163.6 (C-4), 162.1 (C-2), 158.4 (C-7'), 138.6 (C-1'), 132.1 (C-4'), 130.6 (C-3'), 128.5 (C-2'), 99.9 (C-5), 62.9 (C-6') , 40.6 (C-7), 37.4 (C-5'), 31.6 (C-8), 26.5 (C-9), 26.1 (C-10); **IR (ν_{max}/cm^{-1})** 3318, 3186 (N-H); 2921, 2851 (C-H); 1611 (C=N); 1253, 1269 (C-N); 963 (C=C); 834 (C-Cl); **HRMS** *m/z*: calculated for : $C_{19}H_{25}N_5{}^{35}Cl$, 358.1793 found: $[M+H]^+$ 358.1777.

4.6.21. Synthesis of (*E*)-6-cyclohexyl-5-{[(2,4-dichlorophenethyl)imino]-methyl}-pyrimidine-2,4 diamine (51u)

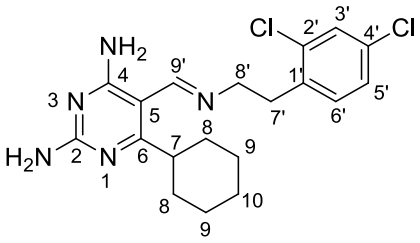

Prepared from 2,4-diamino-6-cyclohexylpyrimidine-5-carbaldehyde **31b** (0.088 g, 0.40 mmol), 2,4-dichlorophenethylamine (0.089 mL, 0.52 mmol), 1,2-dichloroethane (4 mL), glacial acetic acid (0.046 mL, 0.80 mmol). Pure product isolated as a white solid (0.145 g, 91.7 %). m.p. 151-152 °C; **^{1}H NMR (400 MHz, $CDCl_3$)** δ 9.70 (one of 4-NH_2, s, 1H), 8.35 (H-9', s, 1H), 7.37 (H-3', m, 1H), 7.17 – 7.07 (H-5'and H-6', m, 2H), 5.47 (one of 4-NH_2, s, 1H), 5.01 (2-NH_2, s, 2H), 3.79 (H-8', t, *J* = 6.8 Hz, 2H), 3.05 (H-7', t, *J* = 6.8 Hz, 2H), 2.77 (H-7, tt, *J* = 10.7, 4.5 Hz, 1H), 1.90 – 1.51 (H-8-10 cyclohexyl, m, 6H), 1.39 – 1.17 (H-8-10 cyclohexyl, m, 4H); **^{13}C NMR (101 MHz, $CDCl_3$)** δ 175.8 (C-6), 163.6 (C-4), 162.2 (C-2), 158.6 (C-9'), 136.2 (C-1'), 134.9 (C-2'), 132.8 (C-4'), 132.3 (C-6'), 129.4 (C-3'), 127.0 (C-5'), 99.8 (C-5), 60.8 (C-8'), 40.6 (C-7), 35.2 (C-7'), 31.6 (C-8), 26.5 (C-9), 26.0 (C-10); **IR (ν_{max}/cm^{-1})** 3514, 3341 (N-H); 2914, 2850 (C-H); 1645 (C=N); 1340, 1312 (C-N); 963 (C=C); 815, 853 (C-Cl) **HRMS** *m/z*: calculated for : $C_{19}H_{24}N_5{}^{35}Cl_2$, 392.1403 found: $[M+H]^+$ 392.1363.

4.6.22. Synthesis of (*E*)-6-cyclohexyl-5-{[(3,4-dichlorophenethyl)imino]-methyl}-pyrimidine-2,4 diamine (51v)

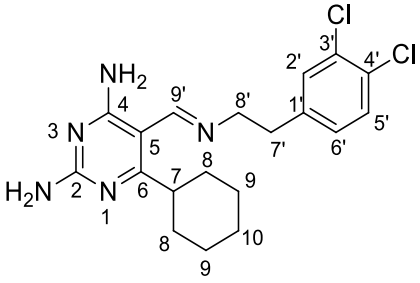

Prepared from 2,4-diamino-6-cyclohexylpyrimidine-5-carbaldehyde **31b** (0.077 g, 0.35 mmol), 3,4-dichlorophenethylamine (0.078 mL, 0.46 mmol), 1,2-dichloroethane (4 mL), glacial acetic acid (0.040 mL, 0.70 mmol). Pure product isolated as a white solid (0.137 g, 100 %). m.p. 126-127 °C; **^{1}H NMR (400 MHz, $CDCl_3$)** δ 9.68 (one of 4-NH_2, s, 1H), 8.37 (H-9', s, 1H), 7.36 – 7.27 (H-5' and H-6', m, 2H), 7.01 (H-2', d, *J* = 8.1 Hz, 1H), 5.37 (one of 4-NH_2,

s, 1H), 4.89 (2-NH_2, s, 2H), 3.77 (H-8', t, *J* = 6.9 Hz, 2H), 2.90 (H-7', t, *J* = 6.9 Hz, 2H), 2.83 – 2.72 (H-7, m, 1H), 1.90 – 1.48 (H-8-10 cyclohexyl, m, 6H), 1.39 – 1.21 (H-8-10 cyclohexyl, m, 4H); **^{13}C NMR (101 MHz, $CDCl_3$)** δ 175.9 (C-6), 163.6 (C-4), 162.2 (C-2), 158.6 (C-9'), 140.5 (C-1'), 132.3 (C-3'), 131.1 (C-4'), 130.33 (C-5'), 130.26 (C-2'), 128.7 (C-6'), 99.8 (C-5), 62.7 (C-8'), 40.6 (C-7), 37.2 (C-7'), 31.7 (C-8), 26.5 (C-9), 26.1 (C-10); **IR (ν_{max}/cm^{-1})** 3319, 3183 (N-H); 2927, 2850 (C-H); 1611 (C=N); 1344, 1266 (C-N); 964 (C=C); 806 (C-Cl) **HRMS** *m/z*: calculated for : $C_{19}H_{24}N_5{}^{35}Cl_2$, 392,1403 found: $[M+H]^+$ 392.1185.

4.6.23. Synthesis of (*E*)-6-cyclopropyl-5-{[(2-methoxyphenethyl)-imino]methyl}-pyrimidine-2,4-diamine (51w)

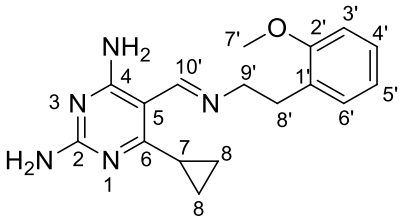

Prepared from 2,4-diamino-6-cyclopropylpyrimidine-5-carbaldehyde **31c** (0.045 g, 0.25 mmol), 2-methoxyphenethylamine (0.048 mL, 0.33 mmol), 1,2-dichloroethane (4 mL), glacial acetic acid (0.029mL, 0.50 mmol). Pure product isolate as colourless gel (0.065 g, 82 %). **^{1}H NMR (400 MHz, $CDCl_3$)** δ 9.83 (one of 4-NH_2, s, 1H), 8.66 (H-10', s, 1H), 7.23 – 7.11 (H-3' and H-6', m, 2H), 6.91 – 6.82 (H-4' and H-5', m, 2H), 5.53 (one of 4-NH_2, s, 1H), 5.00 (2-NH_2, s, 2H), 3.82 (H-7', s, 3H), 3.77 (H-9', t, *J* = 7.2 Hz, 2H), 2.96 (H-8', t, *J* = 7.2 Hz, 2H), 2.11 – 2.02 (H-7, m, 1H), 1.09 (cyclopropyl-H, m, 2H), 0.90 – 0.82 (cyclopropyl-H, m, 2H); **^{13}C NMR (101 MHz, $CDCl_3$)** δ 171.5 (C-6), 163.1 (C-4), 161.9 (C-2), 157.9 (C-10'), 157.7 (C-2'), 130.8 (C-6'), 128.4 (C-4'), 127.5 (C-1'), 120.4 (C-5'), 110.4 (C-3'), 101.8 (C-5), 61.6 (C-9'), 55.3 (C-7'), 32.7 (C-8'), 12.3 (C-7), 9.2 (C-8); **IR (ν_{max}/cm^{-1})** 3319, 3170 (N-H); 2923, 1440, 908 (C-H); 1601 (C=N), 1188 (C-O) **HRMS** *m/z*: calculated for : $C_{17}H_{22}N_5O$, 312.1819 found: $[M+H]^+$ 312.1769.

4.6.24. Synthesis of (*E*)-6-cyclopropyl-5-{[(3-methoxyphenethyl)imino]-methyl}-pyrimidine-2,4-diamine (51x)

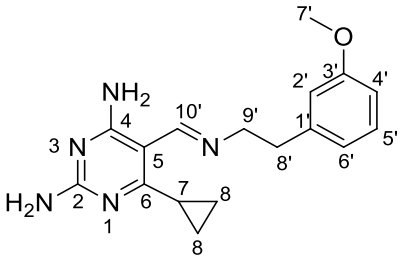

Prepared from 2,4-diamino-6-cyclopropylpyrimidine-5-carbaldehyde **31c** (0.068 g, 0.38 mmol), 3-methoxyphenethylamine (0.073 mL, 0.50 mmol), 1,2-dichloroethane (4 mL), glacial acetic acid (0.044 mL, 0.76 mmol). Pure product isolate as yellow gel (0.11 g, 92 %). **^{1}H NMR (400 MHz, $CDCl_3$)** δ 9.78 (one of 4-NH_2, s, 1H), 8.65 (H-10', s, 1H), 7.20 (H-6', t, *J* = 7.8 Hz, 1H), 6.84 – 6.71 (H-2', H-4' and H-5', m, 3H), 5.58 (one of 4-NH_2, s, 1H), 5.05 (2-NH_2, s, 2H), 3.84 – 3.73 (H-7' and H-9', m, 5H), 2.93 (H-8', t, *J* = 7.2 Hz, 2H), 2.06 (H-, tt, *J* = 8.1, 4.8 Hz, 1H), 1.14 – 1.07 (cyclopropyl-H, m, 2H), 0.91 – 0.82 (cyclopropyl-H, m, 2H); **^{13}C NMR (101 MHz, $CDCl_3$)** δ 171.6 (C-6), 163.1 (C-4), 161.9 (C-2), 159.7 (C-3'), 158.3 (C-10'), 141.8 (C-1'), 129.4 (C-5'), 121.5 (C-6'), 114.8 (C-2'), 111.6 (C-4'), 101.68 (C-5), 63.1 (C-9'), 55.3 (C-7'), 38.2 (C-8'), 12.3 (C-7), 9.2 (C-8); **IR (ν_{max}/cm^{-1})** 3325, 3192 (N-H); 2901, 2833, 964 (C-H); 1601 (C=N) 1189 (C-O) **HRMS** *m/z*: calculated for : $C_{17}H_{22}N_5O$, 312.1819 found: $[M+H]^+$ 312.1772.

4.6.25. Synthesis of (*E*)-6-cyclopropyl-5-{[(4-methoxyphenethyl)imino]-methyl}-pyrimidine-2,4-diamine (51y)

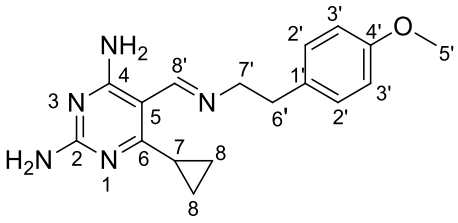

Prepared from 2,4-diamino-6-cyclopropylpyrimidine-5-carbaldehyde **31c** (0.073 g, 0.41 mmol), 4-methoxyphenethylamine (0.078 mL, 0.53 mmol), 1,2-dichloroethane (4 mL), glacial acetic acid (0.047 mL, 0.82 mmol). Pure product isolate as yellow gel (can solidify) (0.112 g, 87.5 %). m.p. 115-117 ºC. **^{1}H NMR (400 MHz, $CDCl_3$)** δ 9.80 (one of 4-NH_2, s, 1H), 8.62 (H-8', s, 1H), 7.16 – 7.07 (H-2', m, 2H), 6.88 – 6.78 (H-3', m, 2H), 5.69 (one of 4-NH_2, s, 1H), 5.17 (2-NH_2, s, 2H), 3.81 – 3.66 (H-5' and H-7', m, 5H), 2.89 (H-6', t, *J* = 7.1 Hz, 2H), 2.08 – 2.01 (H-7, m, 1H), 1.14 – 1.06 (cyclopropyl-H, m, 2H), 0.92 – 0.82 (cyclopropyl-H, m, 2H);

^{13}C NMR (101 MHz, $CDCl_3$) δ 171.4 (C-6), 163.1 (C-4), 161.8 (C-2), 158.2 (C-8') , 158.0 (C-4'), 132.2 (C-1'), 129.9 (C-2'), 113.8 (C-3'), 101.6 (C-5), 63.4 (C-7'), 55.3 (C-5'), 37.2 (C-6'), 12.2 (C-7), 9.2 (C-8); **IR (ν_{max}/cm^{-1})** 3346, 3216 (N-H); 2904, 2833, 967 (C-H); 1608 (C=N), 1241 (C-O) **HRMS** *m/z*: calculated for : $C_{17}H_{22}N_5O$, 312.1819 found: $[M+H]^+$ 312.1772.

4.6.26. Synthesis of (*E*)-6-cyclopropyl-5-{[(2-fluorophenethyl)imino]methyl}pyrimidine-2,4-diamine (51z)

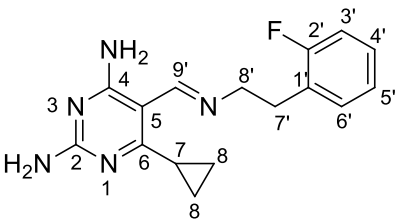

Prepared from 2,4-diamino-6-cyclopropylpyrimidine-5-carbaldehyde **31c** (0.060 g, 0.34 mmol), 2-fluorophenethylamine (0.057 mL, 0.44 mmol), 1,2-dichloroethane (4 mL), glacial acetic acid (0.039 mL, 0.68 mmol). Pure product isolate as a colourless gel (0.070 g, 69 %). **^{1}H NMR (400 MHz, $CDCl_3$)** δ 9.72 (one of 4-NH_2, s, 1H), 8.65 (H-9', s, 1H), 7.23 – 7.13 (H-3' and H-4', m, 2H), 7.08 – 6.95 (H-5' and H-6', m, 2H), 5.56 (one of 4-NH_2, s, 1H), 5.03 (2-NH_2, s, 2H), 3.79 (H-8', t, *J* = 7.1 Hz, 2H), 2.99 (H-7', t, *J* = 7.1 Hz, 2H), 2.10 – 1.99 (H-7, m, 1H), 1.13 – 1.03 (cyclopropyl-H, m, 2H), 0.90 – 0.80 (cyclopropyl-H, m, 2H); **^{13}C NMR (101 MHz, $CDCl_3$)** δ 171.7 (C-6), 163.1 (C-4), 162.6 (C-2), 161.4 (C-2', d, *J* = 244.7 Hz, 158.5 (C-9'), 131.5 (C-6', d, *J* = 5.1 Hz), 128.0 (C-1',d, *J* = 8.1 Hz), 127.0 (C-4', d, *J* = 15.8 Hz), 124.0 (C-5', d, *J* = 3.7 Hz), 115.3 (C-3', d, *J* = 22.4 Hz), 101.6 (C-5), 61.6 (C-8'), 31.5 (C-7), 12.3 (C-7'), 9.2 (C-8); **IR (ν_{max}/cm^{-1})** 3324, 3176 (N-H); 2901, 2837, 967 (C-H), 1644 (C=N), 1540 (C-F) **HRMS** *m/z*: calculated for : $C_{16}H_{19}N_5F$, 300.1619 found: $[M+H]^+$ 300.1577.

4.6.27. Synthesis of (*E*)-6-cyclopropyl-5-{[(3-fluorophenethyl)imino]methyl}pyrimidine-2,4-diamine (51a')

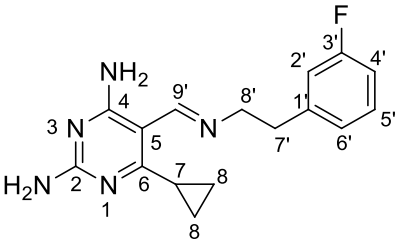

Prepared from 2,4-diamino-6-cyclopropylpyrimidine-5-carbaldehyde **31c** (0.055 g, 0.31 mmol), 3-fluorophenethylamine (0.052 mL, 0.40 mmol), 1,2-dichloroethane (4 mL), glacial

acetic acid (0.035 mL, 0.62 mmol). Pure product isolate as a colourless gel (0.061 g, 66 %). **^{1}H NMR (400 MHz, $CDCl_3$)** δ 9.70 (one of 4-NH_2, s, 1H), 8.66 (H-9', s, 1H), 7.29 – 7.18 (H-5', m, 1H), 7.03 – 6.82 (H-2', H-4', and H-6', m, 3H), 5.54 (one of 4-NH_2, s, 1H), 5.01 (2-NH_2, s, 2H), 3.79 (H-8', t, *J* = 7.1 Hz, 2H), 2.95 (H-7', t, *J* = 7.1 Hz, 2H), 2.06 (H-7, tt, *J* = 8.1, 4.7 Hz, 1H), 1.14 – 1.06 (cyclopropyl-H, m, 2H), 0.92 – 0.81 (cyclopropyl-H, m, 2H); **^{13}C NMR (101 MHz, $CDCl_3$)** δ 171.8 (C-6), 163.2 (C-4), 162.9 (C-3', d, *J* = 245.0 Hz), 162.1 (C-2), 158.6 (C-9'), 142.8 (C-1', d, *J* = 7.3 Hz), 129.8 (C-5', d, *J* = 8.4 Hz), 124.8 (C-6', d, *J* = 2.6 Hz), 115.9 (C-2', d, *J* = 20.5 Hz), 113.1 (C-4', d, *J* = 20.9 Hz), 101.6 (C-5), 62.8 (C-8'), 37.9 (C-7), 12.3 (C-7'), 9.2 (C-8); **IR (ν_{max}/cm^{-1})** 3319, 3188 (N-H); 2896, 2836, 964 (C-H), 1611 (C=N), 1535 (C-F) **HRMS** *m/z*: calculated for : $C_{16}H_{19}N_5F$, 300.1619 found: $[M+H]^+$ 300.1578.

4.6.28. Synthesis of (*E*)-6-cyclopropyl-5-{[(4-fluorophenethyl)imino]methyl}pyrimidine-2,4-diamine (51b')

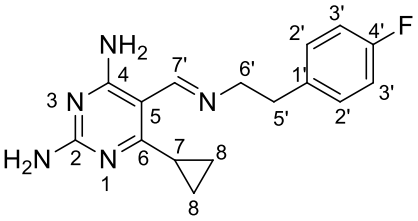

Prepared from 2,4-diamino-6-cyclopropylpyrimidine-5-carbaldehyde **31c** (0.045 g, 0.25 mmol), 4-fluorophenethylamine (0.043 mL, 0.33 mmol), 1,2-dichloroethane (4 mL), glacial acetic acid (0.029 mL, 0.50 mmol). Pure product isolated as a white solid (0.056 g, 74 %). m.p. 153-155 °C. **^{1}H NMR (400 MHz, $CDCl_3$)** δ 9.72 (one of 4-NH_2, s, 1H), 8.62 (H-7', s, 1H), 7.03 – 6.92 (H-2', m, 2H), 7.19 – 7.10 (H-3', m, 2H), 5.35 (one of 4-NH_2, s, 1H), 4.81 (2-NH_2, s, 2H), 3.77 (H-6', t, *J* = 7.1 Hz, 2H), 2.92 (H-5', t, *J* = 7.0 Hz, 2H), 2.09 – 1.98 (H-7, m, 1H), 1.09 (cyclopropyl-H, m, 2H), 0.91 – 0.80 (cyclopropyl-H, m, 2H**)**; **^{13}C NMR (101 MHz, $CDCl_3$)** δ 171.8 (C-6), 163.2 (C-4), 161.6 (C-4', d, *J* = 243.6 Hz), 162.1 (C-2), 158.5 (C-7'), 135.8 (C-1', d, *J* = 3.3 Hz), 130.5 (C-2', d, *J* = 7.7 Hz), 115.2 (C-3', d, *J* = 21.3 Hz), 101.7 (C-5), 63.3 (C-7), 37.4 (C-6'), 12.3 (C-5'), 9.3 (C-8); **IR (ν_{max}/cm^{-1})** 3319, 3274 (N-H); 2901, 2838, 966 (C-H), 1615 (C=N), 1551 (C-F) **HRMS** *m/z*: calculated for : $C_{16}H_{19}N_5F$, 300.1619 found: $[M+H]^+$ 300.1573.

4.6.29. Synthesis of (*E*)-6-cyclopropyl-5-{[(2-chlorophenethyl)imino]methyl}pyrimidine-2,4-diamine (51c')

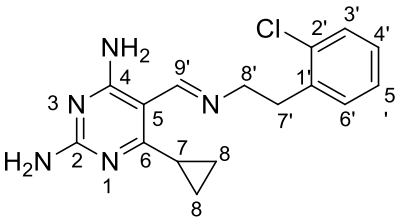

Prepared from 2,4-diamino-6-cyclopropylpyrimidine-5-carbaldehyde **31c** (0.059 g, 0.28 mmol), 2-chlorophenethylamine (0.051 mL, 0.37 mmol), 1,2-dichloroethane (4 mL), glacial acetic acid (0.032 mL, 0.56 mmol). Pure product isolate as a colourless gel (0.059 g, 66 %). **^{1}H NMR (400 MHz, $CDCl_3$)** δ 9.74 (one of 4-NH_2, s, 1H), 8.65 (H-9', s, 1H), 7.38 – 7.33 (H-3', m, 1H), 7.24 – 7.11 (H-4', H-5' and H-6', m, 3H), 5.54 (one of 4-NH_2, s, 1H), 5.01 (2-NH_2, s, 2H), 3.81 (H-8', t, *J* = 7.1 Hz, 2H), 3.08 (H-7', t, *J* = 7.1 Hz, 2H), 2.11 – 1.99 (H-7, m, 1H), 1.12 – 1.06 (cyclopropyl-H, m, 2H), 0.90 – 0.82 (cyclopropyl-H, m, 2H); **^{13}C NMR (101 MHz, $CDCl_3$)** δ 171.7 (C-6), 163.1 (C-4), 161.9 (C-2), 158.5 (C-9'), 137.7 (C-1'), 134.2 (C-2'), 131.4 (C-3'), 129.7 (C-6'), 127.8 (C-4'), 126.7 (C-5'), 101.7 (C-5), 61.1 (C-8'), 35.9 (C-7'), 12.3 (C-7), 9.2 (C-8); **IR (ν_{max}/cm^{-1})** 3319, 3201 (N-H); 2901, 2860, 966 (C-H), 1615 (C=N), 748 (C-Cl) **HRMS** *m/z*: calculated for : $C_{16}H_{19}N_5{}^{35}Cl$, 316.1323 found: $[M+H]^+$ 316.1272.

4.6.30. Synthesis of (*E*)-6-cyclopropyl-5-{[(3-chlorophenethyl)imino]methyl}pyrimidine-2,4-diamine (51d')

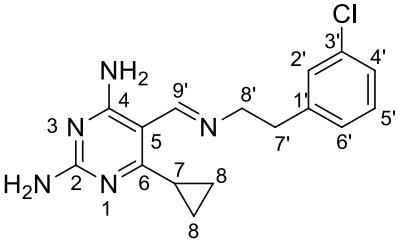

Prepared from 2,4-diamino-6-cyclopropylpyrimidine-5-carbaldehyde **31c** (0.073 g, 0.41 mmol), 4-chlorophenethylamine (0.074 mL, 0.53 mmol), 1,2-dichloroethane (4 mL), glacial acetic acid (0.047 mL, 0.82 mmol). Pure product isolate as colourless gel (0.116 g, 89.9 %). **^{1}H NMR (400 MHz, $CDCl_3$)** δ 9.68 (one of 4-NH_2, s, 1H), 8.67 (H-9', s, 1H), 7.27 – 7.13 (H-2', H-4' and H-5', m, 3H), 7.08 (H-6', dt, *J* = 7.1, 1.7 Hz, 1H), 5.67 (one of 4-NH_2, s, 1H), 5.16 (2-NH_2, s, 2H), 3.78 (H-8', t, *J* = 7.1 Hz, 2H), 2.92 (H-7', t, *J* = 7.1 Hz, 2H), 2.06 (H-7, tt, *J* = 8.1, 4.8 Hz, 1H), 1.13 – 1.06 (cyclopropyl-H, m, 2H), 0.91 – 0.84 (cyclopropyl-H, m, 2H); **^{13}C NMR (101 MHz, $CDCl_3$)** δ 171.8 (C-6), 163.1 (C-4), 162.1 (C-2), 158.6 (C-9'), 142.3 (C-1'),

134.1 (C-3'), 129.6 (C-5'), 129.1 (C-2'), 127.3 (C-4'), 126.3 (C-6'), 62.8 (C-8'), 37.8 (C-7'), 12.3 (C-7), 9.2 (C-8); **IR (ν_{max}/cm^{-1})** 3328, 3184 (N-H); 2926, 2847, 966 (C-H), 1612 (C=N), 742 (C-Cl) **HRMS** *m/z*: calculated for : $C_{16}H_{19}N_5{}^{35}Cl$, 316.1323 found: $[M+H]^+$ 316.1275.

4.6.31. Synthesis of (*E*)-6-cyclopropyl-5-{[(4-chlorophenethyl)imino]methyl}pyrimidine-2,4-diamine (51e')

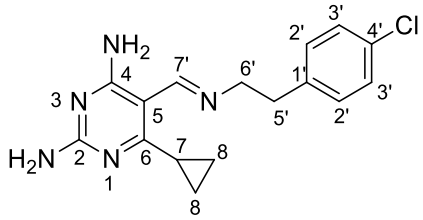

Prepared from 2,4-diamino-6-cyclopropylpyrimidine-5-carbaldehyde **31c** (0.077 g, 0.43 mmol), 4-chlorophenethylamine (0.079 mL, 0.56 mmol), 1,2-dichloroethane (4 mL), glacial acetic acid (0.049 mL, 0.86 mmol). Pure product isolated as a white solid (0.132 g, 97.1 %). m.p. 161-163 ºC. **^{1}H NMR (400 MHz, CDCl$_3$)** δ 9.70 (one of 4-NH_2, s, 1H), 8.61 (H-7', t, *J* = 1.2 Hz, 1H), 7.26 – 7.22 (H-3', m, 2H), 7.15 – 7.11 (H-2', m, 2H), 5.44 (one of 4-NH_2, s, 1H), 4.88 (2-NH_2, s, 2H), 3.77 (H-6', td, *J* = 7.0, 1.2 Hz, 2H), 2.92 (H-5', t, *J* = 7.0 Hz, 2H), 2.09 – 1.97 (H-7, m, 1H), 1.12 – 1.05 (cyclopropyl-H, m, 2H), 0.92 – 0.83 (cyclopropyl-H, m, 2H); **^{13}C NMR (101 MHz, CDCl$_3$)** δ 171.9 (C-6), 163.1 (C-4), 162.0 (C-2), 158.6 (C-7'), 138.7 (C-1'), 131.9 (C-4'), 130.5 (C-2'), 128.5 (C-3'), 101.6 (C-5), 63.0 (C-6'), 37.5 (C-5'), 12.3 (C-7), 9.3 (C-8); **IR (ν_{max}/cm^{-1})** 3208, 3090 (N-H); 2903, 2833, 968 (C-H), 1609 (C=N), 797 (C-Cl) **HRMS** *m/z*: calculated for : $C_{16}H_{19}N_5{}^{35}Cl$, 316.1323 found: $[M+H]^+$ 316.1278.

4.6.32. Synthesis of (*E*)-6-cyclopropyl-5-{[(2,4-dichlorophenethyl)imino]-methyl}-pyrimidine-2,4-diamine (51f')

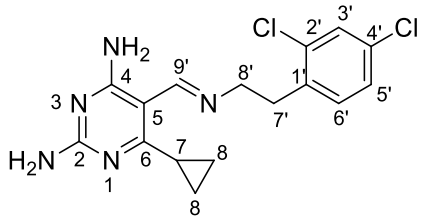

Prepared from 2,4-diamino-6-cyclopropylpyrimidine-5-carbaldehyde **31c** (0.064 g, 0.36 mmol), 2,4-chlorophenethylamine (0.080 mL, 0.47 mmol), 1,2-dichloroethane (4 mL), glacial acetic acid (0.041 mL, 0.72 mmol). Pure product isolated as a white solid (0.121 g, 96.0 %). m.p. 120-122 °C. **^{1}H NMR (400 MHz, CDCl$_3$)** δ 9.66 (one of 4-NH_2, s, 1H), 8.62 (H-9', t, *J* = 1.2 Hz, 1H), 7.35 (H-5', t, *J* = 1.3 Hz, 1H), 7.13 (H-3' and H-6', d, *J* = 1.3 Hz, 2H), 5.68

(one of 4-NH_2, s, 1H), 5.15 (2-NH_2, s, 2H), 3.77 (H-8', td, *J* = 7.0, 1.2 Hz, 2H), 3.03 (H-7', t, *J* = 7.0 Hz, 2H), 2.04 (H-7, tt, *J* = 8.2, 4.8 Hz, 1H), 1.12 – 1.05 (cyclopropyl-H, m, 2H), 0.91 – 0.81 (cyclopropyl-H, m, 2H); ^{13}C NMR (101 MHz, $CDCl_3$) δ 171.8 (C-6), 163.1 (C-4), 162.1 (C-2), 158.7 (C-9'), 136.3 (C-1'), 134.8 (C-2'), 132.6 (C-4'), 132.2 (C-6'), 129.3 (C-3'), 126.9 (C-5'), 101.5 (C-5), 60.8 (C-8'), 35.2 (C-7'), 12.3 (C-7), 9.2 (C-8); **IR (ν_{max}/cm^{-1})** 3216, 3092 (N-H); 2917, 2834, 967 (C-H), 1612 (C=N), 744 (C-Cl) **HRMS** *m/z*: calculated for : $C_{16}H_{18}N_5{}^{35}Cl_2$, 350.0934 found: $[M+H]^+$ 350.0876.

4.6.33. Synthesis of (*E*)-6-cyclopropyl-5-{[(3,4-dichlorophenethyl)imino]-methyl}-pyrimidine-2,4-diamine (51g')

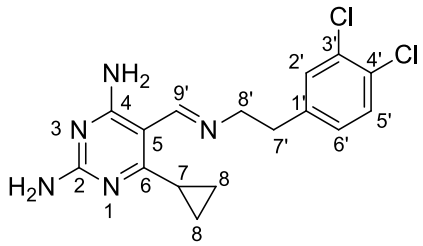

Prepared from 2,4-diamino-6-cyclopropylpyrimidine-5-carbaldehyde **31c** (0.067 g, 0.38 mmol), 3,4-chlorophenethylamine (0.084 mL, 0.49 mmol), 1,2-dichloroethane (4 mL), glacial acetic acid (0.043 mL, 0.76 mmol). Pure product isolated as a white solid (0.113 g, 85.6 %). m.p. 168-171 °C. **^{1}H NMR (400 MHz, $CDCl_3$)** δ 9.64 (one of 4-NH_2, s, 1H), 8.66 (H-9', s, 1H), 7.40 – 7.26 (H-2' and H-5', m, 2H), 7.04 (H-6', dd, *J* = 8.2, 2.1 Hz, 1H), 5.59 (one of 4-NH_2, s, 1H), 5.06 (2-NH_2, s, 2H), 3.77 (H-8', t, *J* = 6.5 Hz, 2H), 2.90 (H-7', t, *J* = 6.9 Hz, 2H), 2.11 – 2.00 (H-7, m, 1H), 1.09 (cyclopropyl-H, m, 2H), 0.94 – 0.80 (cyclopropyl-H, m, 2H); **^{13}C NMR (101 MHz, $CDCl_3$)** δ 171.9 (C-6), 163.1 (C-4), 162.1 (C-2), 158.8 (C-9'), 140.5 (C-1'), 132.2 (C-3'), 131.0 (C-5'), 130.3 (C-2'), 130.1 (C-4'), 128.6 (C-6'), 101.5 (C-5), 62.6 (C-8'), 37.2 (C-7'), 12.3 (C-7), 9.2 (C-8); **IR (ν_{max}/cm^{-1})** 3312, 3162 (N-H); 2946, 2844, 961 (C-H), 1609 (C=N), 740 (C-Cl) ***HRMS*** *m/z*: calculated for : $C_{16}H_{18}N_5{}^{35}Cl_2$, 350.0934 found: $[M+H]^+$ 350.0877.

4.7. General procedure for synthesis of 2,4-diaminopyrimidine-5-phenethylamine (28)

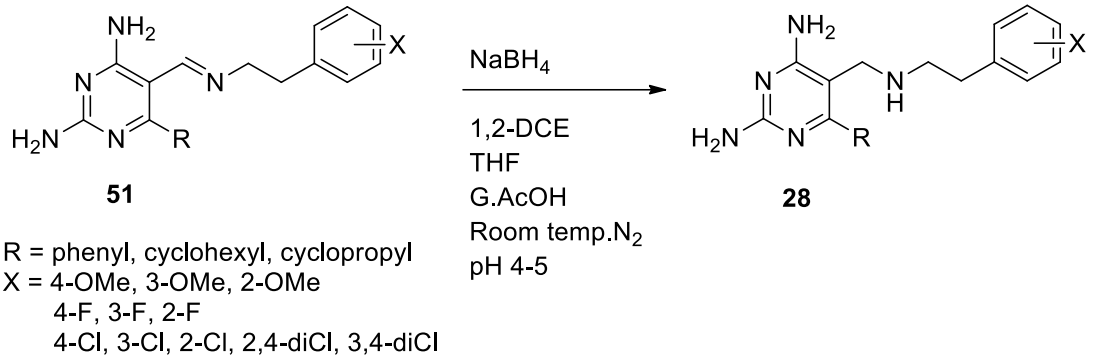

51 **28**

R = phenyl, cyclohexyl, cyclopropyl
X = 4-OMe, 3-OMe, 2-OMe
4-F, 3-F, 2-F
4-Cl, 3-Cl, 2-Cl, 2,4-diCl, 3,4-diCl

In a round bottomed flask, the imine was dissolved in a mixture of 1,2-DCE and THF (1:2). glacial acetic acid was added to the mixture until a pH of between 4 and 5. Once the desired pH was reached, $NaBH_4$ (6.5 eq) was added and the reaction was allowed to stir for 30 minutes under nitrogen atmosphere. Upon completion, the solution was diluted with water to quench $NaBH_4$ and neutralised to pH 7 using solid $NaHCO_3$. The organics were extracted with EtOAc (2 x 100 mL). The organic layer was dried with $MgSO_4$ or Na_2SO_4 and filtered through celite/cotton wool. The solvent was removed in *vacuo* and the crude product was purified using silica gel column chromatography, using gradient elution of 50% ethyl acetate/hexane to 100% ethyl acetate. The following compounds were prepared by this method:

4.7.1. Synthesis of 6-phenyl-5-{[(2-methoxyphenethyl)amino]methyl}pyrimidine-2,4-diamine (28a)

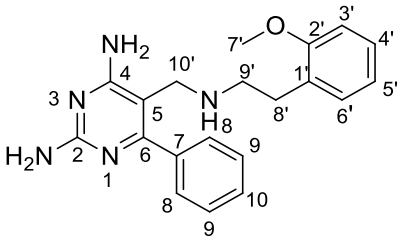

Prepared from (*E*)-6-phenyl-5-{[(2-methoxyphenethyl)imino]methyl}pyrimidine-2,4-diamine **51a** (0.098 g, 0.28 mmol), 1,2-dichloroethane (3 mL), tetrahydrofuran (6 mL), sodium borohydride (0.107 mg, 2.82 mmol). Pure product isolate as colourless gel (0.044 g, 45 %). **^{1}H NMR (400 MHz, $CDCl_3$)** δ 7.44 – 7.34 (H-8 and H-10, m, 3H), 7.35 – 7.28 (H-9, m, 2H), 7.19 (H-4', ddd, *J* = 8.1, 7.5, 1.8 Hz, 1H), 7.01 (H-5'td, *J* = 8.0, 1.8 Hz, 1H), 6.90 – 6.82 (H-3' and H-6', m, 2H), 6.37 (NH_2, s, 2H), 5.30 (NH_2, s, 2H), 3.77 (H-7', s, 3H), 3.62 (H-10', s, 2H), 2.80 – 2.70 (H-8' and H-9', m, 4H); **^{13}C NMR (101 MHz, $CDCl_3$)** δ 165.3 (C-6), 164.4 (C-4),

160.7 (C-2), 157.6 (C-2'), 138.3 (C-7), 130.5 (C-6'), 128.7 (C-1'), 128.4 (C-9), 128.4 (C-8), 128.0 (C-10), 127.7 (C-4'), 120.6 (C-5'), 110.5 (C-3'), 102.8 (C-5), 55.4 (C-7'), 48.2 (C-9'), 46.5 (C-10'), 30.5 (C-8'); **IR (ν_{max}/cm^{-1}):** 3174, 3062 (N-H); 2939, 2836 (=C-H); 1613 (N-H); 1242 (C-O); **HRMS** *m/z*: calculated for : $C_{20}H_{24}N_5O$, 350.1975 found: $[M+H]^+$ 350.1963. HPLC purity: 98.88 %.

4.7.2. Synthesis of 6-phenyl-5-{[(3-methoxyphenethyl)amino]methyl}pyrimidine-2,4-diamine (28b)

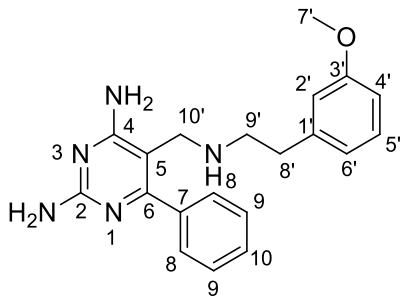

Prepared from (*E*)-6-phenyl-5-{[(3-methoxyphenethyl)imino]methyl}pyrimidine-2,4-diamine **51b** (0.090 g, 0.26 mmol), 1,2-dichloroethane (3 mL), tetrahydrofuran (6 mL), sodium borohydride (0.098 mg, 1.68 mmol). Pure product isolate as colourless gel (0.030 g, 33 %). ^{1}H NMR (400 MHz, $CDCl_3$) δ 7.46 – 7.34 (H-8 and H-10, m, 3H), 7.33 – 7.25 (H-9, m, 2H), 7.24 – 7.15 (H-5', m, 1H), 6.79 – 6.74 (H-2', m, 1H), 6.71 – 6.62 (H-4' and H-6', m, 2H), 6.02 (NH_2, s, 2H), 5.64 (NH_2, s, 2H), 3.79 (H-7', s, 3H), 3.59 (H-10', s, 2H), 2.77 (H-9', t, *J* = 6.2 Hz, 2H), 2.68 (H-8', t, *J* = 6.7 Hz, 2H); **^{13}C NMR (101 MHz, $CDCl_3$)** δ 165.0 (C-6), 164.1 (C-4), 160.4 (C-2), 159.9 (C-3'), 141.2 (C-1'), 137.7 (C-7), 129.6 (C-5'), 128.9 (C-10), 128.4 (C-9), 128.3(C-8), 121.1 (C-6'), 114.7 (C-2'), 111.6 (C-4'), 102.5 (C-5), 55.3 (C-7'), 49.4 (C-9'), 46.4 (C-10'), 35.8 (C-8'); **IR (ν_{max}/cm^{-1}):** 3182, 3057 (N-H); 2936, 2834 (=C-H); 1583 (N-H); 1257 (C-O); **HRMS** *m/z*: calculated for : $C_{20}H_{24}N_5O$, 350.1975 found: $[M+H]^+$ 350.1967. HPLC purity: 95.58 %.

4.7.3. Synthesis of 6-phenyl-5-{[(4-methoxyphenethyl)amino]methyl}pyrimidine-2,4-diamine (28c)

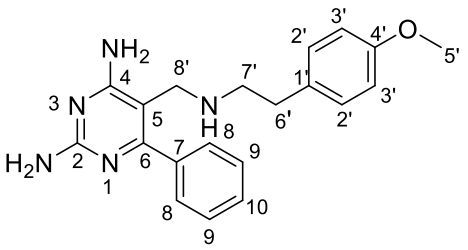

Prepared from (*E*)-6-phenyl-5-{[(4-methoxyphenethyl)imino]methyl}pyrimidine-2,4-diamine **51c** (0.088 g, 0.25 mmol), 1,2-dichloroethane (3 mL), tetrahydrofuran (6 mL), sodium borohydride (0.062 mg, 1.64 mmol). Pure product isolate as colourless gel (0.055 g, 63 %). **^{1}H NMR (400 MHz, $CDCl_3$)** δ 7.43 – 7.35 (H-8 and H-10, m, 3H), 7.35 – 7.27 (H-9, m, 2H), 7.05 – 6.98 (H-2', m, 2H), 6.85 – 6.76 (H-3', m, 2H), 6.09 (NH_2, s, 2H), 4.92 (NH_2, s, 2H), 3.78 (H-5', s, 3H), 3.59 (H-8', s, 2H), 2.75 (H-7', t, *J* = 6.9 Hz, 2H), 2.64 (H-6', t, *J* = 6.6 Hz, 2H); **^{13}C NMR (101 MHz, $CDCl_3$)** δ 165.5 (C-6), 164.9 (C-4), 161.3 (C-2), 158.2 (C-4'), 139.1 (C-7) , 131.8 (C-1'), 129.7 (C-2'), 128.5 (C-10), 128.4 (C-9), 128.3 (C-8), 113.9 (C-3'), 103.1 (C-5), 55.4 (C-5'), 49.9 (C-7'), 46.7 (C-8'), 35.1 (C-6'); **IR (ν_{max}/cm^{-1}):** 3302, 3152 (N-H); 2932, 2834 (=C-H); 1610 (N-H); 1242 (C-O); **HRMS** *m/z*: calculated for : $C_{20}H_{24}N_5O$, 350.1975 found: $[M+H]^+$ 350.1972. HPLC purity: 95.97 %.

4.7.4. Synthesis of 6-phenyl-5-{[(3-fluorophenethyl)amino]methyl}pyrimidine-2,4-diamine (28e)

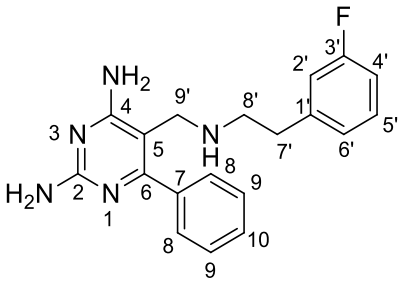

Prepared from (*E*)-6-phenyl-5-{[(3-fluorophenethyl)imino]methyl}pyrimidine-2,4-diamine **51e** (0.037 g, 0.11 mmol), 1,2-dichloroethane (2 mL), tetrahydrofuran (4 mL), sodium borohydride (0.080 mg, 2.10 mmol). Pure product isolate as colourless gel (0.025 g, 68 %). ^{1}H NMR (400 MHz, $CDCl_3$) δ 7.52 – 7.36 (H-8 and H-10, m, 3H), 7.34 – 7.28 (H-9, m, 2H), 7.25 – 7.20 (H-5', m, 1H), 6.93 – 6.86 (H-4' and H-6', m, 2H), 6.86 – 6.79 (H-2', m, 1H), 6.07

(NH_2, s, 2H), 4.92 (NH_2, s, 2H), 3.62 (H-9', s, 2H), 2.79 (H-8', td, *J* = 6.5, 1.1 Hz, 2H), 2.70 (H-7', t, *J* = 6.7 Hz, 2H);

^{13}C NMR (101 MHz, $CDCl_3$) δ 165.5 (C-6), 164.6 (C-4), 163.1 (C-3', d, *J* = 245.8 Hz), 161.1 (C-2), 142.4 (C-1', d, *J* = 7.3 Hz), 138.7 (C-7), 130.1 (C-5', d, *J* = 8.4 Hz), 128.7 (C-10), 128.4 (C-9), 128.4 (C-8), 124.5 (C-6', d, *J* = 2.9 Hz), 115.6 (C-2', d, *J* = 20.5 Hz), 113.3 (C-4', d, *J* = 21.3 Hz), 102.9 (C-5), 49.4 (C-7'), 46.7 (C-9'), 35.8 (C-8'); **IR (ν_{max}/cm^{-1})** 3309, 3167 (N-H); 2925, 2854 (=C-H); 1608 (C=N); 1426 (C-F); **HRMS** *m/z*: calculated for : $C_{19}H_{21}N_5F$, 338.1776 found: $[M+H]^+$ 338.1790.

4.7.5. Synthesis of 6-phenyl-5-{[(3-chlorophenethyl)amino]methyl}pyrimidine-2,4-diamine (28h)

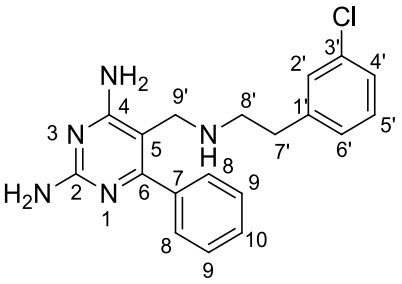

Prepared from **(***E***)**-6-phenyl-5-{[(3-chlorophenethyl)imino]methyl}pyrimidine-2,4-diamine **51h** (0.030 g, 0.09 mmol), 1,2-dichloroethane (2 mL), tetrahydrofuran (4 mL), sodium borohydride (0.021 mg, 0.55 mmol). Pure product isolate as colourless gel (0.019 g, 63 %). **^{1}H NMR (400 MHz, $CDCl_3$)** δ 7.44 – 7.35 (H-8 and H-10, m, 3H), 7.34 – 7.29 (H-9, m, 2H), 7.22 – 7.16 (H-4' and H-5', m, 2H), 7.12 (H-2', s, 1H), 6.98 (H=6', d, *J* = 6.3 Hz, 1H), 6.01 (NH_2, s, 2H), 4.89 (NH_2, s, 2H), 3.61 (H-9', s, 2H), 2.78 (H-8', t, *J* = 6.7 Hz, 2H), 2.67 (H-7', t, *J* = 6.7 Hz, 2H); **^{13}C NMR (101 MHz, $CDCl_3$)** δ 165.4 (C-6), 165.1 (C-4), 161.3 (C-2), 142.0 (C-1'), 139.1 (C-3'), 134.4 (C-7), 129.8 (C-5'), 128.9 (C-2'), 128.6 (C-10), 128.3 (C-9), 128.4 (C-8), 127.0 (C-4'), 126.6 (C-6'), 102.9 (C-5), 49.4 (C-8'), 46.7 (C-9'), 35.8 (C-7'); **IR (ν_{max}/cm^{-1})** 3303, 3157 (N-H); 2923, 2852 (=C-H); 1596 (C=N); 698 (C-Cl); **HRMS** *m/z*: calculated for : $C_{19}H_{21}N_5Cl$, 354.1480 found: $[M+H]^+$ 354.1479.

4.7.6. Synthesis of 6-cyclohexyl-5-{[(2-methoxyphenethyl)amino]methyl}pyrimidine-2,4-diamine (28l)

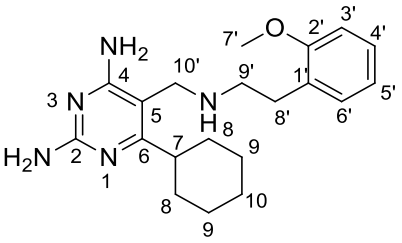

Prepared from (*E*)-6-cyclohexyl-5-{[(2-methoxyphenethyl)imino]-methyl}-pyrimidine-2,4-diamine **51l** (0.080 g, 0.23 mmol), 1,2-dichloroethane (3 mL), tetrahydrofuran (6 mL), sodium borohydride (0.056 g, 1.47 mmol). Pure product isolate as a colourless gel (0.074 g, 93 %). **^{1}H NMR (400 MHz, $CDCl_3$)** δ 7.22 – 7.15 (H-6', m, 1H), 7.10 (H-3', dd, *J* = 7.5, 1.8 Hz, 1H), 6.91 – 6.81 (H-4' and H-5', m, 2H), 6.37 (NH_2, s, 2H), 5.61 (NH_2, s, 2H), 3.79 (H-7', s, 3H), 3.69 (H-10', s, 2H), 2.89 – 2.78 (H-8' and H-9', m, 4H), 2.69 (H-7, tt, *J* = 11.7, 3.6 Hz, 1H), 2.02 (NH, s, 1H), 1.85 – 1.74 (cyclohexyl-H, m, 2H), 1.74 – 1.52 (cyclohexyl-H, m, 5H), 1.34 – 1.21 (cyclohexyl-H, m, 3H); **^{13}C NMR (101 MHz, $CDCl_3$)** δ 168.1 (C-6), 164.9 (C-4), 160.0 (C-2), 157.6 (C-2'), 130.4 (C-6'), 127.9 (C-1'), 127.7 (C-4'), 120.6 (C-5'), 110.5 (C-3'), 101.6 (C-5), 55.4 (C-7'), 48.3 (C-10'), 44.8 (C-9'), 40.8 (C-7), 31.1 (C-8), 30.6 (C-8'), 26.5 (C-9), 25.8 (C-10); **IR (ν_{max}/cm^{-1})** 3327, 3193 (N-H); 2923, 2851 (C-H); 1623 (N-H); 1241 (C-O); **HRMS** *m/z*: calculated for : $C_{20}H_{30}N_5O$, 356.2445 found: $[M+H]^+$ 356.2431. HPLC purity: 97.97 %.

4.7.7. Synthesis of 6-cyclohexyl-5-{[(3-methoxyphenethyl)amino]methyl}pyrimidine-2,4-diamine (28m)

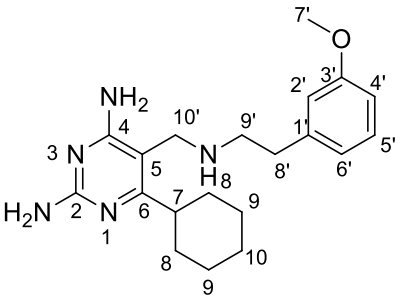

Prepared from (*E*)-6-cyclohexyl-5-{[(3-methoxyphenethyl)imino]-methyl}-pyrimidine-2,4-diamine **51m** (0.130 g, 0.37 mmol), 1,2-dichloroethane (3 mL), tetrahydrofuran (6 mL), sodium borohydride (0.090 g, 2.39 mmol). Pure product isolate as colourless gel (0.118 g, 90.8 %). **^{1}H NMR (400 MHz, $CDCl_3$)** δ 7.19 (H-5', t, *J* = 7.6 Hz, 1H), 6.81 – 6.66 (H-2', H-4' and H-6', m, 3H), 6.36 (NH_2, s, 2H), 5.56 (NH_2, s, 2H), 3.77 (H-7', s, 3H), 3.66 (H-10', s, 2H),

2.86 (H-9', t, *J* = 6.4 Hz, 2H), 2.76 (H-8', t, *J* = 6.7 Hz, 2H), 2.68 (H-7, tt, *J* = 11.7, 3.5 Hz, 1H), 2.02 (NH, s, 1H), 1.84 – 1.76 (cyclohexyl-H, m, 3H), 1.73 – 1.60 (cyclohexyl-H, m, 2H), 1.55 (cyclohexyl-H, d, *J* = 11.8 Hz, 2H), 1.34 – 1.21 (cyclohexyl-H, m, 3H); **^{13}C NMR (101 MHz, $CDCl_3$)** δ 167.4 (C-6), 165.1 (C-4), 159.9 (C-2), 159.8 (C-3'), 141.3 (C-1'), 129.6 (C-5'), 121.1 (C-6'), 114.6 (C-2'), 111.5 (C-4'), 101.8 (C-5), 55.2 (C-7'), 49.6 (C-10'), 44.9 (C-9'), 40.6 (C-8'), 36.1 (C-7), 31.2 (C-8), 26.5 (C-9), 25.7 (C-10); **IR (ν_{max}/cm^{-1})** 3321, 3184 (N-H); 2923, 2851 (C-H); 1601 (N-H); 1257 (C-O); **HRMS** *m/z*: calculated for : $C_{20}H_{30}N_5O$, 356.2445 found: $[M+H]^+$ 356.2428. HPLC purity: 96.71 %.

4.7.8. Synthesis of 6-cyclohexyl-5-{[(4-methoxyphenethyl)amino]methyl}pyrimidine-2,4-diamine (28n)

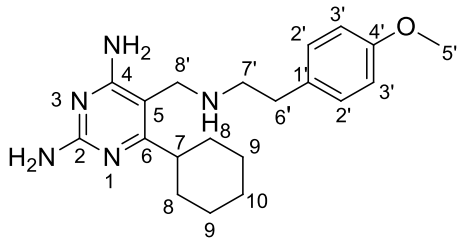

Prepared from (*E*)-6-cyclohexyl-5-{[(4-methoxyphenethyl)imino]-methyl}-pyrimidine-2,4-diamine **51n** (0.135 g, 0.38 mmol), 1,2-dichloroethane (3 mL), tetrahydrofuran (6 mL), sodium borohydride (0.094 g, 2.48 mmol). Pure product isolate as colourless gel (0.114 g, 84.4 %). **^{1}H NMR (400 MHz, $CDCl_3$)** δ 7.08 (H-2', d, *J* = 8.6 Hz, 2H), 6.81 (H-3', d, *J* = 8.6 Hz, 1H), 6.51 (NH_2, s, 2H), 5.74 (NH_2, s, 2H), 3.75 (H-5', s, 3H), 3.66 (H-8', s, 2H), 2.83 (H-7', t, *J* = 6.9 Hz, 2H), 2.76 – 2.62 (H-6' and H-7, m, 3H), 2.00 (NH, s, 1H), 1.84 – 1.75 (cyclohexyl-H, m, 1H), 1.76 – 1.60 (cyclohexyl-H, m, 4H), 1.55 (cyclohexyl-H, d, *J* = 12.9 Hz, 2H), 1.35 – 1.18 (cyclohexyl-H, m, 3H); **^{13}C NMR (101 MHz, $CDCl_3$)** δ 166.6 (C-6), 165.1 (C-4), 159.6 (C-2), 158.2 (C-4'), 131.5 (C-1'), 129.7 (C-3'), 114.0 (C-2'), 101.7 (C-5), 55.3 (C-5'), 49.9 (C-8') , 44.9 (C-7'), 40.5 (C-6'), 35.0 (C-7), 31.2 (C-8), 26.4 (C-9), 25.6 (C-10); **IR (ν_{max}/cm^{-1})** 3320, 3180 (N-H); 2923, 2850 (C-H); 1610 (N-H); 1243 (C-O); ***HRMS*** *m/z*: calculated for : $C_{20}H_{30}N_5O$, 356.2445 found: $[M+H]^+$ 356.2427. HPLC purity: 94.13 %.

4.7.9. Synthesis of 6-cyclohexyl-5-{[(2-fluorophenethyl)amino]methyl}pyrimidine-2,4-diamine (28o)

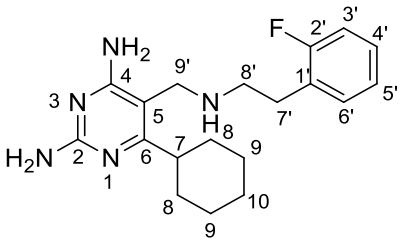

Prepared from (*E*)-6-cyclohexyl-5-{[(2-fluorophenethyl)imino]methyl}pyrimidine-2,4-diamine **51o** (0.080 g, 0.23 mmol), 1,2-dichloroethane (3 mL), tetrahydrofuran (6 mL), sodium borohydride (0.058 g, 1.52 mmol). Pure product isolate as a colourless gel (0.069 g, 86 %). **^{1}H NMR (400 MHz, $CDCl_3$)** δ 7.22 – 7.12 (H-5' and H-6', m, 2H), 7.09 – 6.98 (H-3' and H-4', m, 2H), 6.25 (NH_2, s, 2H), 5.56 (NH_2, s, 2H), 3.69 (H-9', s, 2H), 2.91 – 2.86 (H-8', m, 2H), 2.86 – 2.80 (H-7', m, 2H), 2.69 (H-7, tt, *J* = 11.7, 3.6 Hz, 1H), 2.02 (NH, s, 1H), 1.84 – 1.77 (cyclohexyl-H, m, 2H), 1.72 – 1.60 (cyclohexyl-H, m, 3H), 1.59 – 1.51 (cyclohexyl-H, m, 2H), 1.35 – 1.22 (cyclohexyl-H, m, 3H); **^{13}C NMR (101 MHz, $CDCl_3$)** δ 168.6 (C-6), 164.8 (C-4), 161.34 (C-2', d, *J* = 244.7 Hz) , 160.2 (C-2), 131.01 (C-6', d, *J* = 5.1 Hz), 128.2 (C-1', d, *J* = 8.1 Hz), 126.6 (C-4', d, *J* = 16.1 Hz), 124.2 (C-5', d, *J* = 3.7 Hz), 115.5 (C-3', d, *J* = 22.0 Hz), 101.6 (C-5), 48.6 (C-9'), 44.9 (C-8'), 40.8 (C-7), 31.2 (C-8), 29.4 (C-7') , 26.5 (C-9), 25.8 (C-10); **IR (ν_{max}/cm^{-1})** 3323, 3188 (N-H); 2923, 2851 (C-H); 1616 (N-H); 1431 (C-F); **HRMS** *m/z*: calculated for : $C_{19}H_{27}N_5F$, 344.2245 found: $[M+H]^+$ 344.2228. HPLC purity: 99.43 %.

4.7.10. Synthesis of 6-cyclohexyl-5-{[(3-fluorophenethyl)amino]methyl}pyrimidine-2,4-diamine (28p)

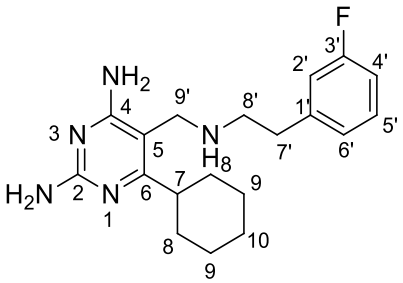

Prepared from (*E*)-6-cyclohexyl-5-{[(3-fluorophenethyl)imino]methyl}pyrimidine-2,4-diamine **51p** (0.084 g, 0.25 mmol), 1,2-dichloroethane (3 mL), tetrahydrofuran (6 mL), sodium borohydride (0.060 g, 1.60 mmol). Pure product isolate as a colourless gel (0.075 g, 89 %). **^{1}H NMR (400 MHz, $CDCl_3$)** δ 7.28 – 7.20 (H-5', m, 1H), 6.97 – 6.86 (H-2', H-4' and H-6', m, 3H), 6.29 (NH_2, s, 2H), 5.59 (NH_2, s, 2H), 3.68 (H-9', s, 2H), 2.87 (H-8', t, *J* = 6.3 Hz, 2H),

2.79 (H-7', t, *J* = 6.4 Hz, 2H), 2.68 (H-7, tt, *J* = 11.7, 3.6 Hz, 1H), 2.02 (NH, s, 1H), 1.85 – 1.74 (cyclohexyl-H, m, 2H), 1.74 – 1.61 (cyclohexyl-H, m, 3H), 1.61 – 1.50 (cyclohexyl-H, m, 2H), 1.36 – 1.20 (cyclohexyl-H, m, 3H); **^{13}C NMR (101 MHz, $CDCl_3$)** δ 168.6 (C-6), 164.8 (C-4), 163.03 (C-3', d, *J* = 246.1 Hz), 160.1 (C-2), 142.33 (C-1', d, *J* = 7.3 Hz), 130.08 (C-5', d, *J* = 8.4 Hz), 124.44 (C-6', d, *J* = 2.6 Hz), 115.59 (C-2', d, *J* = 20.9 Hz), 113.35 (C-4', d, *J* = 20.9 Hz), 101.6 (C-5), 49.5 (C-9'), 45.0 (C-8'), 40.9 (C-7'), 35.9 (C-7), 31.2 (C-8), 26.5 (C-9), 25.8 (C-10); **IR (ν_{max}/cm^{-1})** 3324, 3193 (N-H); 2924, 2852 (C-H); 1616 (N-H); 1431 (C-F); **HRMS** *m/z*: calculated for : $C_{19}H_{27}N_5F$, 344.2245 found: $[M+H]^+$ 344.2228.

4.7.11. Synthesis of 6-cyclohexyl-5-{[(4-fluorophenethyl)amino]methyl}pyrimidine-2,4-diamine (28q)

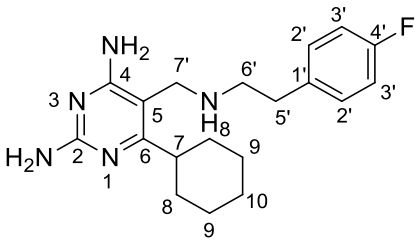

Prepared from (*E*)-6-cyclohexyl-5-{[(4-fluorophenethyl)imino]methyl}pyrimidine-2,4-diamine **51q** (0.072 g, 0.21 mmol), 1,2-dichloroethane (3 mL), tetrahydrofuran (6 mL), sodium borohydride (0.052 g, 1.37 mmol). Pure product isolate as colourless gel (0.066 g, 92 %). **^{1}H NMR (400 MHz, $CDCl_3$)** δ 7.16 – 7.09 (H-2', m, 2H), 7.00 – 6.92 (H-3', m, 2H), 6.23 (NH_2, s, 2H), 5.49 (NH_2, s, 2H), 3.67 (H-7', s, 2H), 2.85 (H-6', t, *J* = 6.4 Hz, 2H), 2.75 (H-5', t, *J* = 6.7 Hz, 2H), 2.67 (H-7, tt, *J* = 11.7, 3.6 Hz, 1H), 2.02 (NH, s, 1H), 1.85 – 1.75 (cyclohexyl-H, m, 3H), 1.74 – 1.58 (cyclohexyl-H, m, 3H), 1.54 (cyclohexyl-H, d, *J* = 13.7 Hz, 2H), 1.35 – 1.17 (cyclohexyl-H, m, 2H); **^{13}C NMR (101 MHz, $CDCl_3$)** δ 168.8 (C-6), 164.8 (C-4), 161.6 (C-4', d, *J* = 243.9 Hz), 160.3 (C-2), 135.4 (C-1', d, *J* = 3.3 Hz), 130.1 (C-2', d, *J* = 7.7 Hz), 115.39 (C-3', d, *J* = 20.9 Hz), 101.6 (C-5), 49.8 (C-7'), 45.1 (C-6'), 40.9 (C-5'), 35.4 (C-7), 31.3 (C-8), 26.5 (C-9), 25.8 (C-10); **IR (ν_{max}/cm^{-1})** 3328, 3185 (N-H); 2924, 2852 (C-H); 1622 (N-H); 1431 (C-F); **HRMS** *m/z*: calculated for : $C_{19}H_{27}N_5F$, 344.2245 found: $[M+H]^+$ 344.2230. HPLC purity: 100.00 %.

4.7.12. Synthesis of 6-cyclohexyl-5-{[(2-chlorophenethyl)amino]methyl}pyrimidine-2,4-diamine (28r)

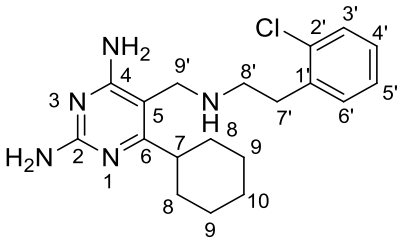

Prepared from (*E*)-6-cyclohexyl-5-{[(2-chlorophenethyl)imino]methyl}pyrimidine-2,4-diamine **51r** (0.080 g, 0.22 mmol), 1,2-dichloroethane (3 mL), tetrahydrofuran (6 mL), sodium borohydride (0.055 g, 1.46 mmol). Pure product isolate as colourless gel (0.077 g, 96 %). **^{1}H NMR (400 MHz, $CDCl_3$)** δ 7.36 – 7.31 (H-3', m, 1H), 7.22 – 7.11 (H-4', H-5' and H-6', m, 3H), 6.27 (NH_2, s, 2H), 5.55 (NH_2, s, 2H), 3.70 (H-9', s, 2H), 2.99 – 2.84 (H-7' and H-8', m, 4H), 2.70 (H-7, tt, *J* = 11.7, 3.7 Hz, 1H), 2.03 (NH, s, 1H), 1.81 (cyclohexyl-H, m, 2H), 1.66 (cyclohexyl-H, m, 2H), 1.56 (cyclohexyl-H, d, *J* = 13.8 Hz, 2H), 1.37 – 1.20 (cyclohexyl-H, m, 4H); ^{13}C NMR (101 MHz, $CDCl_3$) δ 168.5 (C-6), 164.8 (C-4), 160.1 (C-2), 137.4 (C-1'), 134.2 (C-2'), 130.9 (C-3'), 129.8 (C-4'), 127.9 (C-5'), 126.9 (C-6'), 101.7 (C-5), 48.2 (C-9'), 45.1 (C-8'), 40.8 (C-7), 33.9 (C-7'), 31.2 (C-8), 26.5 (C-9), 25.8 (C-10); **IR (ν_{max}/cm^{-1})** 3320, 3189 (N-H); 2924, 2852 (C-H); 1626 (N-H); 729 (C-Cl); **HRMS** *m/z*: calculated for : $C_{19}H_{27}N_5{}^{35}Cl$, 360.1950 found: $[M+H]^+$ 360.1944. HPLC purity: 99.99 %.

4.7.13. Synthesis of 6-cyclohexyl-5-{[(3-chlorophenethyl)amino]methyl}pyrimidine-2,4-diamine (28s)

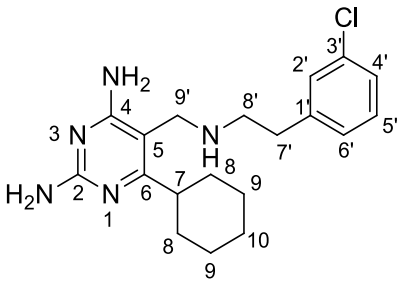

Prepared from (*E*)-6-cyclohexyl-5-{[(3-chlorophenethyl)imino]methyl}pyrimidine-2,4-diamine **51s** (0.115 g, 0.32 mmol), 1,2-dichloroethane (3 mL), tetrahydrofuran (6 mL), sodium borohydride (0.080 mg, 2.09 mmol). Pure product isolate as colourless gel (0.097 g, 84 %). **^{1}H NMR (400 MHz, $CDCl_3$)** δ 7.23 – 7.10 (H-2', H-4' and H-6', m, 3H), 7.04 (H-5', d, *J* = 7.1 Hz, 1H), 6.51 (NH_2, s, 2H), 5.80 (NH_2, s, 2H), 3.66 (H-9', s, 2H), 2.85 (H-8', t, *J* = 6.8 Hz, 2H), 2.75 (H-7', t, *J* = 6.8 Hz, 2H), 2.68 (H-7, td, *J* = 11.8, 5.9 Hz, 1H), 1.99 (NH, s, 1H), 1.82

– 1.73 (cyclohexyl-H, m, 2H), 1.74 – 1.60 (cyclohexyl-H, m, 3H), 1.55 (cyclohexyl-H, d, *J* = 12.6 Hz, 2H), 1.32 – 1.21 (cyclohexyl-H, m, 3H); **^{13}C NMR (101 MHz, CDCl$_3$)** δ 166.6 (C-6), 165.0 (C-4), 159.6 (C-2), 141.8 (C-1'), 134.3 (C-3'), 129.9 (C-5'), 128.8 (C-2'), 126.9 (C-6'), 126.6 (C-4'), 101.6 (C-5), 49.5 (C-9'), 44.9 (C-8'), 40.5 (C-7'), 35.7 (C-7), 31.2 (C-8), 26.4 (C-9), 25.6 (C-10); **IR (ν_{max}/cm^{-1})** 3316, 3182 (N-H); 2921, 2850 (C-H); 1636 (N-H); 779 (C-Cl); **HRMS** *m/z*: calculated for : $C_{19}H_{27}N_5{}^{35}Cl$, 360.1950 found: $[M+H]^+$ 360.1937. HPLC purity: 97.79 %.

4.7.14. Synthesis of 6-cyclohexyl-5-{[(4-chlorophenethyl)amino]methyl}pyrimidine-2,4-diamine (28t)

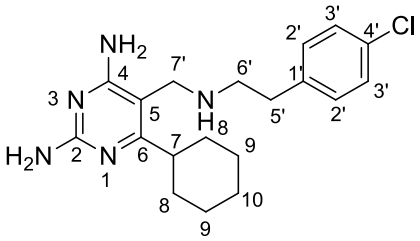

Prepared from (*E*)-6-cyclohexyl-5-{[(4-chlorophenethyl)imino]methyl}pyrimidine-2,4-diamine **51t** (0.113 g, 0.32 mmol), 1,2-dichloroethane (3 mL), tetrahydrofuran (6 mL), sodium borohydride (0.078 mg, 2.05 mmol). Pure product isolate as colourless gel (0.098 g, 87 %). **^{1}H NMR (400 MHz, CDCl$_3$)** δ 7.25 – 7.21 (H-3', m, 2H), 7.12 – 7.07 (H-2', m, 2H), 6.54 (NH_2, s, 2H), 5.85 (NH_2, s, 2H), 3.67 (H-7', s, 2H), 2.85 (H-6', t, *J* = 6.4 Hz, 2H), 2.76 (H-5', t, *J* = 7.1 Hz, 2H), 2.68 (H-7, tt, *J* = 11.9, 3.5 Hz, 1H), 2.01 (NH, s, 1H), 1.84 – 1.75 (cyclohexyl-H, m, 2H), 1.75 – 1.60 (cyclohexyl-H, m, 2H), 1.55 (cyclohexyl-H, d, *J* = 12.7 Hz, 2H), 1.33 – 1.19 (cyclohexyl-H, m, 4H); **^{13}C NMR (101 MHz, CDCl$_3$)** δ 166.5 (C-6), 165.0 (C-4), 159.4 (C-2), 138.1 (C-1'), 132.2 (C-4'), 130.1 (C-2'), 128.7 (C-3'), 101.6 (C-5), 49.7 (C-7'), 44.9 (C-6'), 40.5 (C-5'), 35.4 (C-7), 31.1 (C-8), 26.5 (C-9), 25.6 (C-10); **IR (ν_{max}/cm^{-1})** 3321, 3187 (N-H); 2924, 2850 (C-H); 1637 (N-H); 807 (C-Cl); **HRMS** *m/z*: calculated for : $C_{19}H_{27}N_5{}^{35}Cl$, 360.1950 found: $[M+H]^+$ 360.1932. HPLC purity: 95.87 %.

4.7.15. Synthesis of 6-cyclohexyl-5-{[(2,4-dichlorophenethyl)amino]methyl}pyrimidine-2,4-diamine (28u)

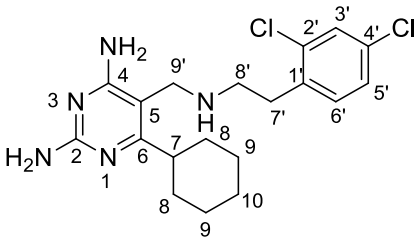

Prepared from **(***E*)-6-cyclohexyl-5-{[(2,4-dichlorophenethyl)imino]-methyl}-pyrimidine-2,4-diamine **51u** (0.135 g, 0.40 mmol), 1,2-dichloroethane (3 mL), tetrahydrofuran (6 mL), sodium borohydride (0.085 mg, 2.24 mmol). Pure product isolate as colourless gel (0.081 g, 60 %). **^{1}H NMR (400 MHz, $CDCl_3$)** δ 7.35 (H-3', d, *J* = 2.2 Hz, 1H), 7.20 – 7.12 (H-5' and H-6', m, 2H), 6.51 (NH_2, s, 2H), 5.79 (NH_2, s, 2H), 3.70 (H-9', s, 2H), 2.93 – 2.84 (H-8' and H-7', m, *J* = 3.9 Hz, 4H), 2.72 (H-7, tt, *J* = 11.7, 3.5 Hz, 1H), 2.02 (NH, s, 1H), 1.87 – 1.78 (cyclohexyl-H, m, 3H), 1.75 – 1.62 (cyclohexyl-H, m, 2H), 1.57 (cyclohexyl-H, d, *J* = 12.6 Hz, 2H), 1.37 – 1.21 (cyclohexyl-H, m, 3H); **^{13}C NMR (101 MHz, $CDCl_3$)** δ 165.1 (C-6 and C-4, overlapping), 159.3 (C-2), 135.9 (C-1'), 134.8 (C-2'), 132.9 (C-4'), 131.6 (C-6'), 129.5 (C-3'), 127.3 (C-5'), 101.7 (C-5), 48.1 (C-9'), 45.0 (C-8'), 40.5 (C-7), 33.4 (C-7'), 31.2 (C-8), 26.5 (C-9), 25.6 (C-10); **IR (ν_{max}/cm^{-1})** 3317, 3179 (N-H); 2924, 2851 (C-H); 1637 (N-H); 817 (C-Cl); **HRMS** *m/z*: calculated for : $C_{19}H_{26}N_5{}^{35}Cl_2$, 394.1560 found: $[M+H]^+$ 360.1538. HPLC purity: 98.20 %.

4.7.16. Synthesis of 6-cyclohexyl-5-{[(3,4-dichlorophenethyl)amino]methyl}pyrimidine-2,4-diamine (28v)

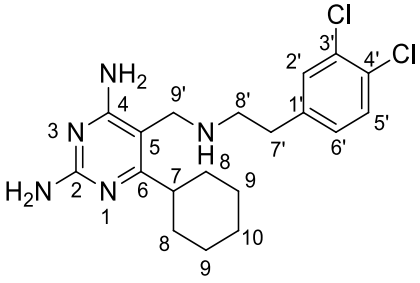

Prepared from (*E*)-6-cyclohexyl-5-{[(3,4-dichlorophenethyl)imino]methyl}pyrimidine-2,4-diamine **51v** (0.127 g, 0.32 mmol), 1,2-dichloroethane (3 mL), tetrahydrofuran (6 mL), sodium borohydride (0.080 mg, 2.10 mmol). Pure product isolate as a colourless gel (0.090 g, 71 %). **^{1}H NMR (400 MHz, $CDCl_3$)** δ 7.35 (H-5', d, *J* = 8.2 Hz, 1H), 7.31 – 7.24 (H-2', m, 1H), 7.03 (H-6', dd, *J* = 8.2, 2.1 Hz, 1H), 6.41 (NH_2, s, 2H), 5.65 (NH_2, s, 2H), 3.69 (H-9', s, 2H), 2.87

(H-8', t, *J* = 6.9 Hz, 2H), 2.80 – 2.63 (H-7' and H-7, m, 3H), 2.03 (NH, s, 1H), 1.86 – 1.78 (cyclohexyl-H, m, 2H), 1.73 – 1.61 (cyclohexyl-H, m, 2H), 1.57 (cyclohexyl-H, d, *J* = 14.2 Hz, 2H), 1.39 – 1.18 (cyclohexyl-H, m, 4H); **^{13}C NMR (101 MHz, $CDCl_3$)** δ 167.2 (C-6), 164.9 (C-4), 159.8 (C-2), 140.1 (C-1'), 132.4 (C-3'), 130.7 (C-4'), 130.5 (C-5'), 130.4 (C-2'), 128.3 (C-6'), 101.7 (C-5), 49.5 (C-9'), 45.0 (C-8'), 40.6 (C-7'), 35.3 (C-7), 31.2 (C-8), 26.5 (C-9), 25.7 (C-10); **IR (ν_{max}/cm^{-1})** 3321, 3186 (N-H); 2924, 2852 (C-H); 1629 (N-H); 784 (C-Cl); **HRMS** *m/z*: calculated for : $C_{19}H_{26}N_5{}^{35}Cl_2$, 394.1560 found: $[M+H]^+$ 360.1541. HPLC purity: 85.44 %.

4.7.17. Synthesis of 6-cyclopropyl-5-{[(2-methoxyphenethyl)amino]methyl}pyrimidine-2,4-diamine (28w)

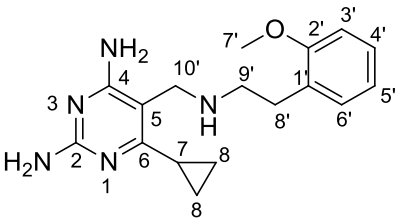

Prepared from (*E*)-6-cyclopropyl-5-{[(2-methoxyphenethyl)imino]-methyl}-pyrimidine-2,4-diamine **51w** (0.060 g, 0.19 mmol), 1,2-dichloroethane (3 mL), tetrahydrofuran (6 mL), sodium borohydride (0.047 mg, 1.25 mmol). Pure product isolate as colourless gel (0.050 g, 83 %). **^{1}H NMR (400 MHz, $CDCl_3$)** δ 7.19 (H-5', td, *J* = 8.0, 1.7 Hz, 1H), 7.12 (H-6', dd, *J* = 7.3, 1.8 Hz, 1H), 6.92 – 6.80 (H-3' and H-4', m, 2H), 6.24 (NH_2, s, 2H), 5.16 (NH_2, s, 2H), 3.88 (H-10', s, 2H), 3.79 (H-7', s, 3H), 2.95 – 2.88 (H-9', m, 2H), 2.88 – 2.81 (H-8', m, 2H), 2.01 (NH, s, 1H), 1.91 (H-7, tt, *J* = 8.2, 4.8 Hz, 1H), 1.05 – 0.98 (cyclopropyl, m, 2H), 0.87 – 0.78 (cyclopropyl-H, m, 2H); ^{13}C NMR **(101 MHz, $CDCl_3$)** δ 166.6 (C-6) , 163.8 (C-4), 160.6 (C-2), 157.6 (C-2'), 130.5 (C-6'), 127.8 (C-1'), 127.7 (C-4'), 120.6 (C-5'), 110.5 (C-3'), 102.0 (C-5), 55.3 (C-7'), 48.1 (C-10'), 44.7 (C-9'), 30.3 (C-8'), 12.7 (C-7), 8.8 (C-8); **IR (ν_{max}/cm^{-1})** 3354, 3139 (N-H); 2925, 2862 (C-H); 1601 (N-H), 1237 (C-O); **HRMS** *m/z*: calculated for : $C_{17}H_{24}N_5O$, 314.1975 found: $[M+H]^+$ 314.1962. HPLC purity: 93.94 %.

4.7.18. Synthesis of 6-cyclopropyl-5-{[(3-methoxyphenethyl)amino]methyl}pyrimidine-2,4-diamine (28x)

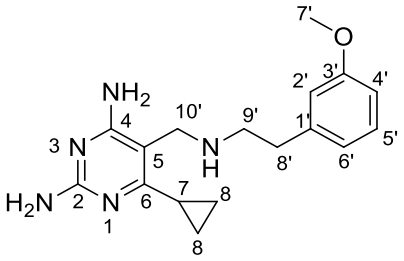

Prepared from (*E*)-6-cyclopropyl-5-{[(3-methoxyphenethyl)imino]-methyl}-pyrimidine-2,4-diamine **51x** (0.105 g, 0.34 mmol), 1,2-dichloroethane (3 mL), tetrahydrofuran (6 mL), sodium borohydride (0.083 g, 2.19 mmol). Pure product isolated as colourless gel (0.082 g, 78 %). **^{1}H NMR (500 MHz, $CDCl_3$)** δ 7.21 (H-5', t, *J* = 7.8 Hz, 1H), 6.81 – 6.72 (H-2', H-4' and H-6', m, 3H), 6.17 (NH_2, s, 2H), 5.25 (NH_2, s, 2H), 3.86 (H-10', s, 2H), 3.79 (H-7', s, 3H), 2.93 (H-9', t, *J* = 6.8 Hz, 2H), 2.81 (H-8', t, *J* = 6.8 Hz, 2H), 2.04 (NH, s, 1H), 1.93 (H-7, tt, *J* = 8.4, 4.2 Hz, 1H), 1.15 – 1.09 (cyclopropyl-H, m, 2H), 0.95 – 0.84 (cyclopropyl-H, m, 2H); **^{13}C NMR (126 MHz, $CDCl_3$)** δ 164.5 (C-6 and C-4, overlapping), 159.9 (C-2 and C-3', overlapping), 141.4 (C-1'), 129.7 (C-5'), 121.2 (C-6'), 114.8 (C-2'), 111.6 (C-4'), 103.0 (C-5), 55.3 (C-7'), 49.7 (C-10'), 45.3 (C-9'), 36.2 (C-8'), 12.6 (C-7), 8.9 (C-8); **IR (ν_{max}/cm^{-1})** 3330, 3192 (N-H); 2936, 2835 (C-H); 1602 (N-H), 1257 (C-O); **HRMS** *m/z*: calculated for : $C_{17}H_{24}N_5O$, 314.1975 found: $[M+H]^+$ 314.1966. HPLC purity: 100.00 %.

4.7.19. Synthesis of 6-cyclopropyl-5-{[(4-methoxyphenethyl)amino]methyl}pyrimidine-2,4-diamine (28y)

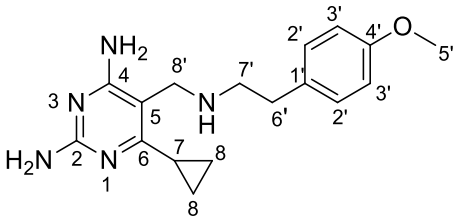

Prepared from (*E*)-6-cyclopropyl-5-{[(4-methoxyphenethyl)imino]methyl}pyrimidine-2,4-diamine **51y** (0.110 g, 0.35 mmol), 1,2-dichloroethane (3 mL), tetrahydrofuran (6 mL), sodium borohydride (0.087 g, 2.29 mmol). Pure product isolated as colourless gel (0.090 g, 82 %). **^{1}H NMR (500 MHz, $CDCl_3$)** δ 7.10 (C-2', d, *J* = 8.6 Hz, 2H), 6.84 (C-3', d, *J* = 8.5 Hz, 2H), 5.99 (NH_2, s, 2H), 4.94 (NH_2, s, 2H), 3.84 (C-8', s, 2H), 3.79 (H-5', s, 3H), 2.88 (C-7', t, *J* = 6.8 Hz, 2H), 2.75 (C-6', t, *J* = 6.8 Hz, 2H), 2.05 (NH, s, 1H), 1.93 (C-7, tt, *J* = 8.2, 4.9 Hz, 1H), 1.11 – 1.04 (cyclopropyl-H, m, 2H), 0.90 – 0.82 (cyclopropyl-H, m, 2H); **^{13}C NMR (126 MHz,**

CDCl$_3$) δ 164.4 (C-6 and C-4, overlapping), 158.3 (C-2 and C-4', overlapping), 131.8 (C-1'), 129.7 (C-2'), 114.1 (C-3'), 103.2 (C-5), 55.4 (C-5'), 50.1 (C-8'), 45.3 (C-7'), 35.3 (C-6'), 12.6 (C-7), 8.8 (C-8); **IR (ν_{max}/cm^{-1})** 3331, 3178 (N-H); 2931, 2835 (C-H); 1611 (N-H), 1243 (C-O); **HRMS** *m/z*: calculated for : $C_{17}H_{24}N_5O$, 314.1975 found: $[M+H]^+$ 314.1966. HPLC purity: 94.43 %.

4.7.20. Synthesis of 6-cyclopropyl-5-{[(2-fluorophenethyl)amino]methyl}pyrimidine-2,4-diamine (28z)

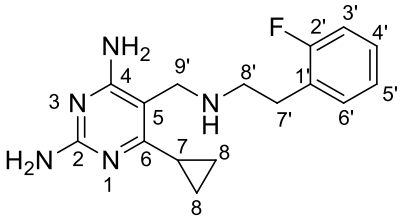

Prepared from (*E*)-6-cyclopropyl-5-{[(2-fluorophenethyl)imino]methyl}pyrimidine-2,4-diamine **51z** (0.066 g, 0.22 mmol), 1,2-dichloroethane (3 mL), tetrahydrofuran (6 mL), sodium borohydride (0.054 g, 1.43 mmol). Pure product isolate as a colourless gel (0.045 g, 68 %). **^{1}H NMR (400 MHz, CDCl$_3$)** δ 7.18 (H-4' and H-5', t, *J* = 7.0 Hz, 2H), 7.08 – 6.98 (H-3' and H-6', m, 2H), 6.04 (NH_2, s, 2H), 5.04 (NH_2, s, 2H), 3.85 (H-9', s, 2H), 2.94 – 2.88 (H-8', m, 2H), 2.88 – 2.81 (H-7', m, 2H), 2.03 (NH, s, 1H), 1.94 (H-7, tt, *J* = 8.2, 4.9 Hz, 1H), 1.06 – 1.00 (cyclopropyl-H, m, 2H), 0.87 – 0.80 (cyclopropyl-H, m, 2H); **^{13}C NMR (101 MHz, CDCl$_3$)** δ 166.1 (C-6), 164.1 (C-4), 161.37 (C-2', d, *J* = 244.7 Hz), 160.7 (C-2), 131.1 (C-6', d, *J* = 4.8 Hz), 128.2 (C-1', d, *J* = 8.1 Hz), 126.7 (C-4', d, *J* = 15.8 Hz), 124.2 (C-5', d, *J* = 3.7 Hz), 115.5 (C-3', d, *J* = 22.4 Hz), 102.9 (C-5), 48.7 (C-9'), 45.2 (C-8'), 29.5 (C-7'), 12.6 (C-7), 8.8 (C-8); **IR (ν_{max}/cm^{-1})** 3327, 3191 (N-H); 3008, 2855 (C-H); 1611 (N-H), 1227 (C-F); **HRMS** *m/z*: calculated for : $C_{16}H_{21}N_5F$, 302.1776 found: $[M+H]^+$ 302.1767. HPLC purity: 95.57 %.

4.7.21. Synthesis of 6-cyclopropyl-5-{[(3-fluorophenethyl)amino]methyl}pyrimidine-2,4-diamine (28a')

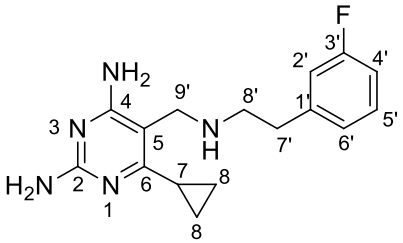

Prepared from (*E*)-6-cyclopropyl-5-{[(3-fluorophenethyl)imino]methyl}pyrimidine-2,4-diamine **51a'** (0.053 g, 0.18 mmol), 1,2-dichloroethane (3 mL), tetrahydrofuran (6 mL),

sodium borohydride (0.044 g, 1.15 mmol). Pure product isolate as a colourless gel (0.040 g, 75 %). **^{1}H NMR (300 MHz, $CDCl_3$)** δ 7.29 – 7.20 (H-5', m, 1H), 7.00 – 6.85 (H-2', H-4' and H-6', m, 3H), 6.09 (NH_2, s, 2H), 5.07 (NH_2, s, 2H), 3.84 (H-9', s, 2H), 2.90 (H-8', t, *J* = 6.1 Hz, 2H), 2.80 (H-7', t, *J* = 6.6 Hz, 2H), 2.03 (NH, s, 1H), 1.92 (H-7, tt, *J* = 8.0, 4.8 Hz, 1H), 1.04 – 0.98 (cyclopropyl-H, m, 2H), 0.88 – 0.79 (cyclopropyl-H, m, 2H); **^{13}C NMR (75 MHz, $CDCl_3$)** δ 166.6 (C-6), 164.7 (C-4), 163.0 (C-3', d, *J* = 245.9 Hz), 160.6 (C-2), 142.4 (C-1', d, *J* = 7.1 Hz), 130.1 (C-5', d, *J* = 8.2 Hz), 124.5 (C-6', d, *J* = 2.7 Hz), 115.6 (C-2', d, *J* = 20.9 Hz), 113.3 (C-4', d, *J* = 21.1 Hz), 102.6 (C-5), 49.5 (C-9'), 45.1 (C-8'), 35.9 (C-7'), 12.7 (C-7), 8.8 (C-8); **IR (ν_{max}/cm^{-1})** 3329, 3189 (N-H); 3010, 2854 (C-H); 1613 (N-H), 1248 (C-F); **HRMS** *m/z*: calculated for : $C_{16}H_{21}N_5F$, 302.1776 found: $[M+H]^+$ 302.1766. HPLC purity: 97.78 %.

4.7.22. Synthesis of 6-cyclopropyl-5-{[(4-fluorophenethyl)amino]methyl}pyrimidine-2,4-diamine (28b')

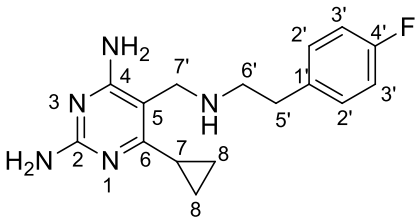

Prepared from (*E*)-6-cyclopropyl-5-{[(4-fluorophenethyl)imino]methyl}pyrimidine-2,4-diamine **51b'** (0.054 g, 0.18 mmol), 1,2-dichloroethane (3 mL), tetrahydrofuran (6 mL), sodium borohydride (0.044 g, 1.17 mmol). Pure product isolate as a colourless gel (0.040 g, 74 %). **^{1}H NMR (400 MHz, $CDCl_3$)** δ 7.16 – 7.10 (H-2', m, 2H), 7.00 – 6.94 (H-3', m, 2H), 5.96 (NH_2, s, 2H), 4.89 (NH_2, s, 2H), 3.83 (H-7', s, 2H), 2.87 (H-6', td, *J* = 6.7, 1.2 Hz, 2H), 2.77 (H-5', t, *J* = 6.8 Hz, 2H), 2.03 (NH, s, 1H), 1.92 (H-7, tt, *J* = 8.1, 4.8 Hz, 1H), 1.04 – 0.98 (cyclopropyl-H, m, 2H), 0.85 – 0.78 (cyclopropyl-H, m, 2H); **^{13}C NMR (101 MHz, $CDCl_3$)** δ 166.7 (C-6), 164.0 (C-4), 161.6 (C-4', d, *J* = 243.9 Hz), 160.9 (C-2), 135.5 (C-1', d, *J* = 2.9 Hz), 130.2 (C-2', d, *J* = 8.1 Hz), 115.4 (C-3', d, *J* = 21.3 Hz), 102.9 (C-5), 49.9 (C-7'), 45.3 (C-6'), 35.5 (C-5'), 12.7 (C-7), 8.7 (C-8); **IR (ν_{max}/cm^{-1})** 3318, 3191 (N-H); 3006, 2845 (C-H); 1620 (N-H), 1216 (C-F); **HRMS** *m/z*: calculated for : $C_{16}H_{21}N_5F$, 302.1776 found: $[M+H]^+$ 302.1764. HPLC purity: 95.25 %.

4.7.23. Synthesis of 6-cyclopropyl-5-{[(2-chlorophenethyl)amino]methyl}pyrimidine-2,4-diamine (28c')

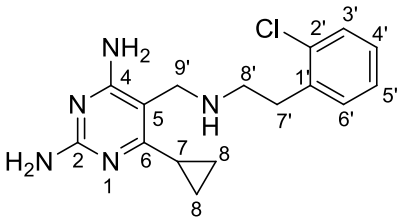

Prepared from (E)-6-cyclopropyl-5-{[(2-chlorophenethyl)imino]methyl}pyrimidine-2,4-diamine **51c'** (0.053 g, 0.27 mmol), 1,2-dichloroethane (3 mL), tetrahydrofuran (6 mL), sodium borohydride (0.041 g, 1.10 mmol). Pure product isolate as colourless gel (0.040 g, 75%). **^{1}H NMR (400 MHz, $CDCl_3$)** δ 7.36 – 7.33 (H-3', m, 1H), 7.23 – 7.12 (H-4', H-5' and H-6', m, 3H), 6.02 (NH_2, s, 2H), 4.92 (NH_2, s, 2H), 3.85 (H-9', s, 2H), 2.98 – 2.88 (H-7' and H-8', m, 4H), 2.04 (NH, s, 1H), 1.94 (H-7, tt, *J* = 8.1, 4.8 Hz, 1H), 1.04 – 0.98 (cyclopropyl-H, m, 2H), 0.86 – 0.79 (cyclopropyl-H, m, 2H); **^{13}C NMR (101 MHz, $CDCl_3$)** δ 166.8 (C-6), 163.9 (C-4), 160.8 (C-2), 137.5 (C-1), 134.2 (C-2'), 130.9 (C-3'), 129.8 (C-4'), 127.9 (C-5'), 126.9 (C-6'), 102.9 (C-5), 48.3 (C-9'), 45.3 (C-8'), 34.0 ((C-7'), 12.7 (C-7), 8.8 (C-8); **IR (ν_{max}/cm^{-1})** 3326, 3194 (N-H); 3007, 2857 (C-H); 1615 (N-H), 722 (C-Cl); **HRMS** *m/z*: calculated for : $C_{16}H_{21}N_5{}^{35}Cl$, 318.1480 found: $[M+H]^+$ 318.1468.

4.7.24. Synthesis of 6-cyclopropyl-5-{[(3-chlorophenethyl)amino]methyl}pyrimidine-2,4-diamine (28d')

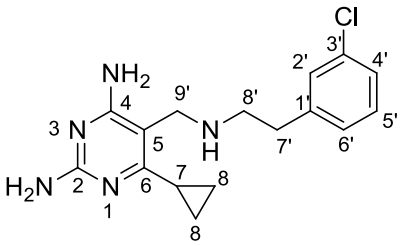

Prepared from (*E*)-6-cyclopropyl-5-{[(3-chlorophenethyl)imino]methyl}pyrimidine-2,4-diamine **51d'** (0.106 g, 0.34 mmol), 1,2-dichloroethane (3 mL), tetrahydrofuran (6 mL), sodium borohydride (0.083 g, 2.18 mmol). Pure product isolated as colourless gel (0.084 g, 79 %). **^{1}H NMR (500 MHz, $CDCl_3$)** δ 7.23 – 7.16 (H-2', H-4' and H-6' , m, 3H), 7.06 (H-5', d, *J* = 7.2 Hz, 1H), 5.80 (NH_2, s, 2H), 4.77 (NH_2, s, 2H), 3.83 (H-9', s, 2H), 2.90 (H-8', t, *J* = 6.8 Hz, 2H), 2.77 (H-7', t, *J* = 6.8 Hz, 2H), 1.97 – 1.90 (H-7, m, 1H), 1.04 – 0.98 (cyclopropyl-H, m, 2H), 0.86 – 0.77 (cyclopropyl-H, m, 2H); **^{13}C NMR (126 MHz, $CDCl_3$)** δ 164.5 (C-6, C-4 and C-2, overlapping), 141.9 (C-1'), 134.5 (C-3'), 129.9 (C-5'), 128.9 (C-2'), 127.1 (C-6'),

126.7 (C-4'), 103.1 (C-5), 49.6 (C-9'), 45.4 (C-8'), 36.0 (C-7'), 12.6 (C-7), 8.8 (C-8); **IR (ν_{max}/cm^{-1})** 3326, 3191 (N-H); 3008, 2853 (C-H); 1598 (N-H), 782 (C-Cl); **HRMS** *m/z*: calculated for : $C_{16}H_{21}N_5{}^{35}Cl$, 318.1480 found: $[M+H]^+$ 318.1462. HPLC purity: 90.00 %.

4.7.25. Synthesis of 6-cyclopropyl-5-{[(4-chlorophenethyl)amino]methyl}pyrimidine-2,4-diamine (28e')

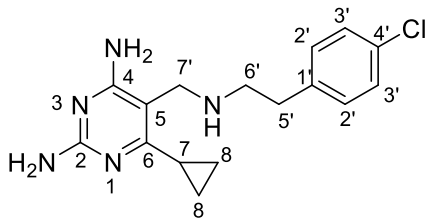

Prepared from (*E*)-6-cyclopropyl-5-{[(4-chlorophenethyl)imino]methyl}pyrimidine-2,4-diamine **51e'** (0.120 g, 0.38 mmol), 1,2-dichloroethane (3 mL), tetrahydrofuran (6 mL), sodium borohydride (0.093 g, 2.47 mmol). Pure product isolated as colourless gel (0.084 g, 70 %). **^{1}H NMR (400 MHz, CDCl$_3$)** δ 7.24 (H-3', d, *J* = 8.4 Hz, 2H), 7.10 (H-2', d, *J* = 8.4 Hz, 2H), 5.91 (NH_2, s, 2H), 4.90 (NH_2 ,s, 2H), 3.82 (H-7', s, 2H), 2.87 (H-6', t, *J* = 6.6 Hz, 2H), 2.76 (H-5', t, *J* = 6.8 Hz, 2H), 1.92 (H-7, tt, *J* = 8.1, 4.7 Hz, 1H), 1.03 – 0.97 (cyclopropyl-H, m, 2H), 0.84 – 0.78 (cyclopropyl-H, m, 2H); **^{13}C NMR (101 MHz, CDCl$_3$)** δ 166.6 (C-6), 164.3 (C-4), 161.4 (C-2), 138.5 (C-1'), 132.1 (C-4'), 130.2 (C-2'), 128.7 (C-3'), 103.1 (C-5), 49.8 (C-7'), 45.4 (C-6'), 35.8 (C-5'), 12.6 (C-7), 8.7 (C-8); **IR (ν_{max}/cm^{-1})** 3322, 3188 (N-H); 3007, 2853 (C-H); 1604 (N-H), 807 (C-Cl); **HRMS** *m/z*: calculated for : $C_{16}H_{21}N_5{}^{35}Cl$, 318.1480 found: $[M+H]^+$ 318.1466. HPLC purity: 92.16 %.

4.7.26. Synthesis of 6-cyclopropyl-5-{[(2,4-dichlorophenethyl)amino]methyl}pyrimidine-2,4-diamine (28f')

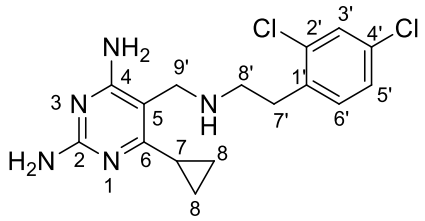

Prepared from (*E*)-6-cyclopropyl-5-{[(2,4-dichlorophenethyl)imino]methyl}pyrimidine-2,4-diamine **51f'** (0.111 g, 0.32 mmol), 1,2-dichloroethane (3 mL), tetrahydrofuran (6 mL), sodium borohydride (0.078 g, 2.06 mmol). Pure product isolated as white semi-solid (0.081 g, 73 %). **^{1}H NMR (400 MHz, CDCl$_3$)** δ 7.37 (H-3', d, *J* = 2.0 Hz, 1H), 7.18 (H-5', dd, *J* = 8.2, 2.0 Hz, 1H), 7.14 (H-6', d, *J* = 8.2 Hz, 1H) 5.95 (NH_2, s, 2H), 4.98 (NH_2, s, 2H), 3.86 (H-9', s,

2H), 2.96 – 2.86 (H-7’ and H-8’, m, 4H), 1.96 (H-7, tt, *J* = 8.2, 4.9 Hz, 1H), 1.12 – 1.04 (cyclopropyl-H, m, 2H), 0.92 – 0.84 (cyclopropyl-H, m, 2H); **^{13}C NMR (126 MHz, $CDCl_3$)** δ 164.5 (C-6, C-4 and C-2, overlapping), 136.2 (C-1’), 134.9 (C-2’), 132.9 (C-4’), 131.7 (C-6’), 129.6 (C-3’), 127.3 (C-5’), 103.1 (C-5), 48.2 (C-9’), 45.4 (C-8’), 33.6 (C-7’), 12.6 (C-7), 8.9 (C-8); **IR (ν_{max}/cm^{-1})** 3324, 3184 (N-H); 3005, 2853 (C-H); 1607 (N-H), 814 (C-Cl); **HRMS** *m/z*: calculated for : $C_{16}H_{20}N_5{}^{35}Cl_2$, 352.1090 found: $[M+H]^+$ 352.1073. HPLC purity: 87.66 %.

4.7.27. Synthesis of 6-cyclopropyl-5-{[(3,4-dichlorophenethyl)amino]methyl}pyrimidine-2,4-diamine (28g’)

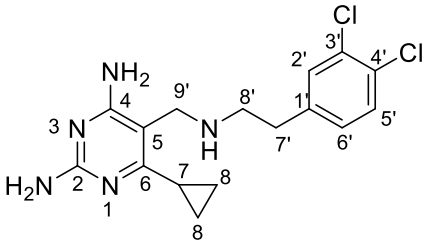

Prepared from (E)-6-cyclopropyl-5-{[(3,4-dichlorophenethyl)imino]methyl}pyrimidine-2,4-diamine **51g’** (0.080 g, 0.23 mmol), 1,2-dichloroethane (3 mL), tetrahydrofuran (6 mL), sodium borohydride (0.056 g, 1.48 mmol). Pure product isolated as colourless gel (0.067 g, 84 %). **^{1}H NMR (400 MHz, $CDCl_3$)** δ 7.35 (H-5’, d, *J* = 8.2 Hz, 1H), 7.28 (H-2’, d, *J* = 2.1 Hz, 1H), 7.02 (H-6’, dd, *J* = 8.2, 2.1 Hz, 1H), 5.79 (NH_2, s, 2H), 4.76 (NH_2, s, 2H), 3.83 (H-9’, s, 2H), 2.88 (H-8’, td, *J* = 6.8, 0.9 Hz, 2H), 2.75 (H-7’, t, *J* = 6.8 Hz, 2H), 1.94 (H-7, tt, *J* = 8.2, 4.8 Hz, 1H), 1.06 – 0.99 (cyclopropyl-H, m, 2H), 0.88 – 0.80 (cyclopropyl-H, m, 2H); **^{13}C NMR (101 MHz, $CDCl_3$)** δ 166.4 (C-6), 164.3 (C-4), 161.2 (C-2), 140.3 (C-1’), 132.5 (C-3’), 130.8 (C-4’), 130.5 (C-5’), 130.4 (C-2’), 128.3 (C-6’), 102.9 (C-5), 49.6 (C-9’), 45.4 (C-8’), 35.6 (C-7’), 12.6 (C-7), 8.8 (C-8); **IR (ν_{max}/cm^{-1})** 3322, 3193 (N-H); 3009, 2854 (C-H); 1609 (N-H), 814 (C-Cl); **HRMS** *m/z*: calculated for : $C_{16}H_{20}N_5{}^{35}Cl_2$, 352.1090 found: $[M+H]^+$ 352.1073. HPLC purity: 92.69 %.

4.8. Crystal structure and refinement

Intensity data for **compounds 51b** was collected on a either a BRUKER D8 Venture PHOTON II pixel array area detector with Mo Kα graphite monochromated sealed X-ray source (50kV, 30 mA), or a Bruker D8 Venture Bio PHOTON III diffractometer with a Mo Kα IμS DIAMOND source (50kV, 1.4 mA). The collection method involved *ω*- and *φ*-scans, with either 768 × 1024 (PHOTON II) or 1536 × 1024 (PHOTON III) bit data frames. The unit cell and full data set were collected using

APEX4[58]; *SAINT* was used to integrate the data, and *SADABS* was used to make empirical absorption corrections and scale the data. Space group assignments were made using *XPREP* on all compounds. Using *Olex2*[59], the crystal structures were solved with the *ShelXT*[60] structure solution program using Intrinsic Phasing and refined with the *ShelXL*[61] refinement package using Least Squares minimization. Non-hydrogen atoms were first refined isotropically followed by anisotropic refinement by full matrix least-squares calculations based on F^2. Professor Manuel Fernandes of the University of the Witwatersrand was responsible for carrying out these experiments.

Crystal data for 63b: $C_{20}H_{21}N_5O$ (M =347.42 g/mol): monoclinic, space group $P2_1/c$ (no. 14), a = 10.5453(5) Å, b = 24.7909(9) Å, c = 14.5962(6) Å, β = 105.268(2)°, V = 3681.2(3) Å^3, Z = 8, T = 173.00 K, μ(MoKα) = 0.081 mm^{-1}, *Dcalc* = 1.254 g/cm^3, 237890 reflections measured (4.004° ≤ 2Θ ≤ 56.728°), 9180 unique (R_{int} = 0.1123, R_{sigma} = 0.0313) which were used in all calculations. The final R_1 was 0.0441 (I > 2σ(I)) and wR_2 was 0.1199 (all data).

4.9. Enzyme preparation and inhibition assays

*Pf*DHFRs and *Hs*DHFR enzymes were expressed under T7 promotor of pET17b plasmids in *E. Coli* BL21(DE3) and purified from the crude bacterial lysate of IPTG (isopropyl-β-D-thiogalactopyranoside) induced cells by methotrexate-agarose affinity chromotography. Enzyme inhibition assay was determined in 96-well plates at 25°C using Multiskan GO microplate spectrophotometer (Thermo Scientific) and the K_i-values were calculated as previously described in a separate publication.[40]

4.10. Parasite culture, antiplasmodial and cytotoxicity testing *in vitro*.

Two *P. falciparum* strains, TM4/8.2 (wild type *Pf*DHFR) and V1/S (QM *Pf*DHFR) were cultured in human erythrocytes at 37°C under 3% CO_2 in RPMI 1640 culture media containing 25mM HEPES, 0.2% $NaHCO_3$, 40 μg/mL gentamicin and 8% human serum. *In vitro* antimalarial activity was determined by ^{3}H-hypoxanthine incorporation method. Cytotoxicity of each compound was determined against two mammalian derived cell lines, Vero (African green monkey kidney epithelial cells) and KB (human epithelial carcinoma cells) by quantitative staining of cellular proteins using sulforhodamine B protein staining.[40]

APPENDIX

^{1}H NMR spectrum of 30a

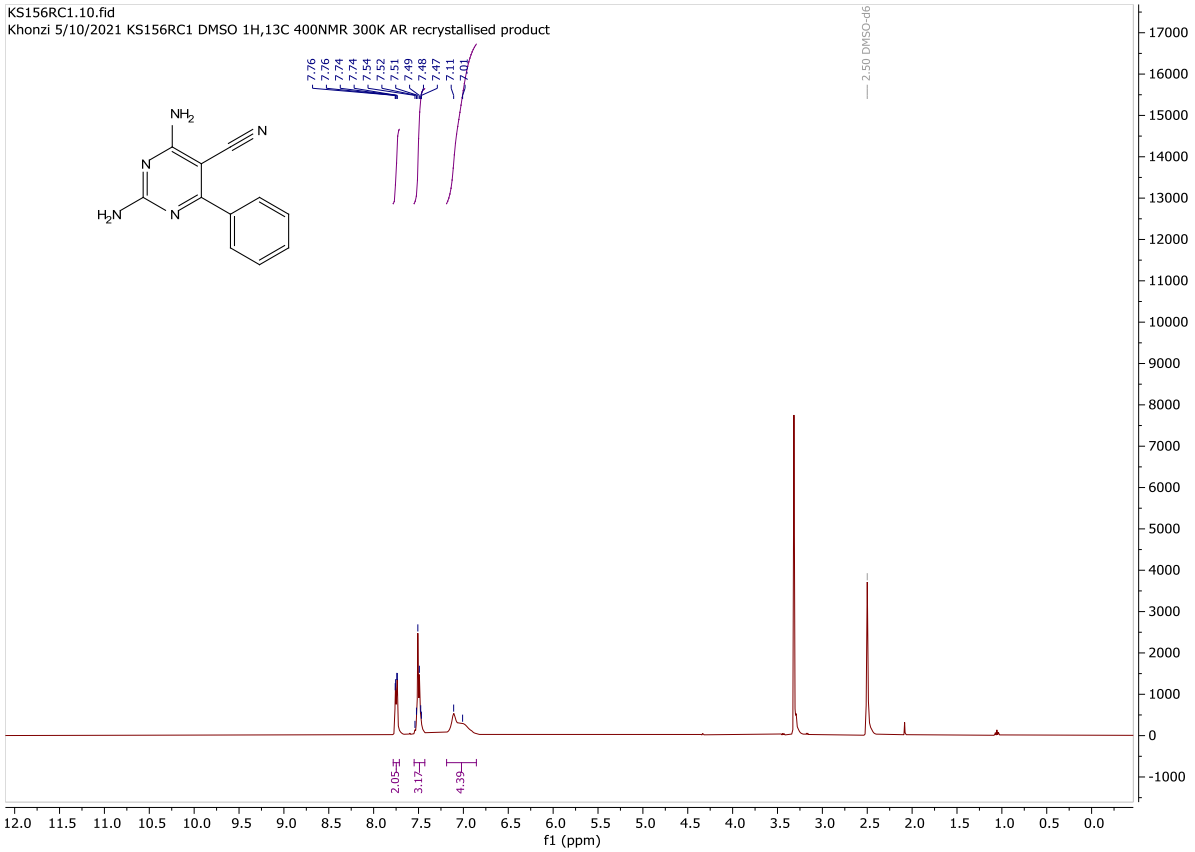

^{13}C NMR spectrum of 30a

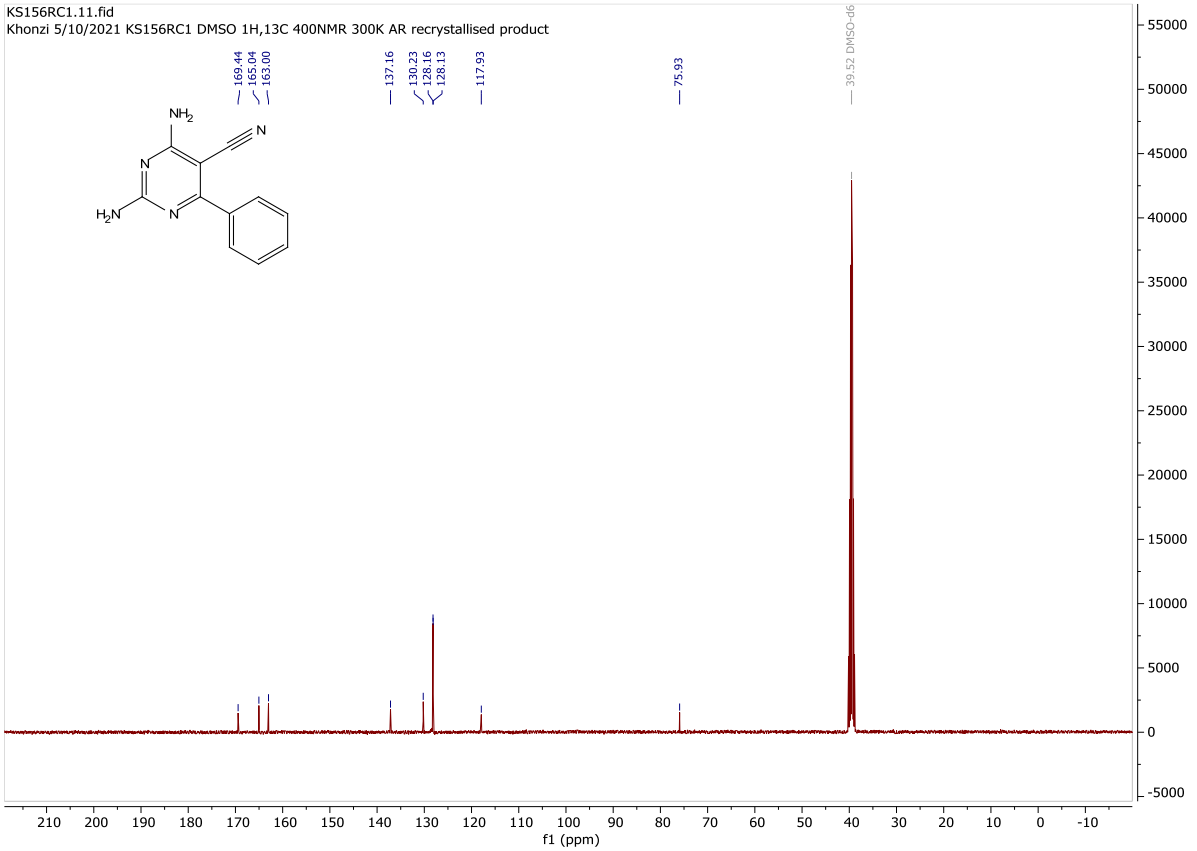

^{1}H NMR spectrum of 31a

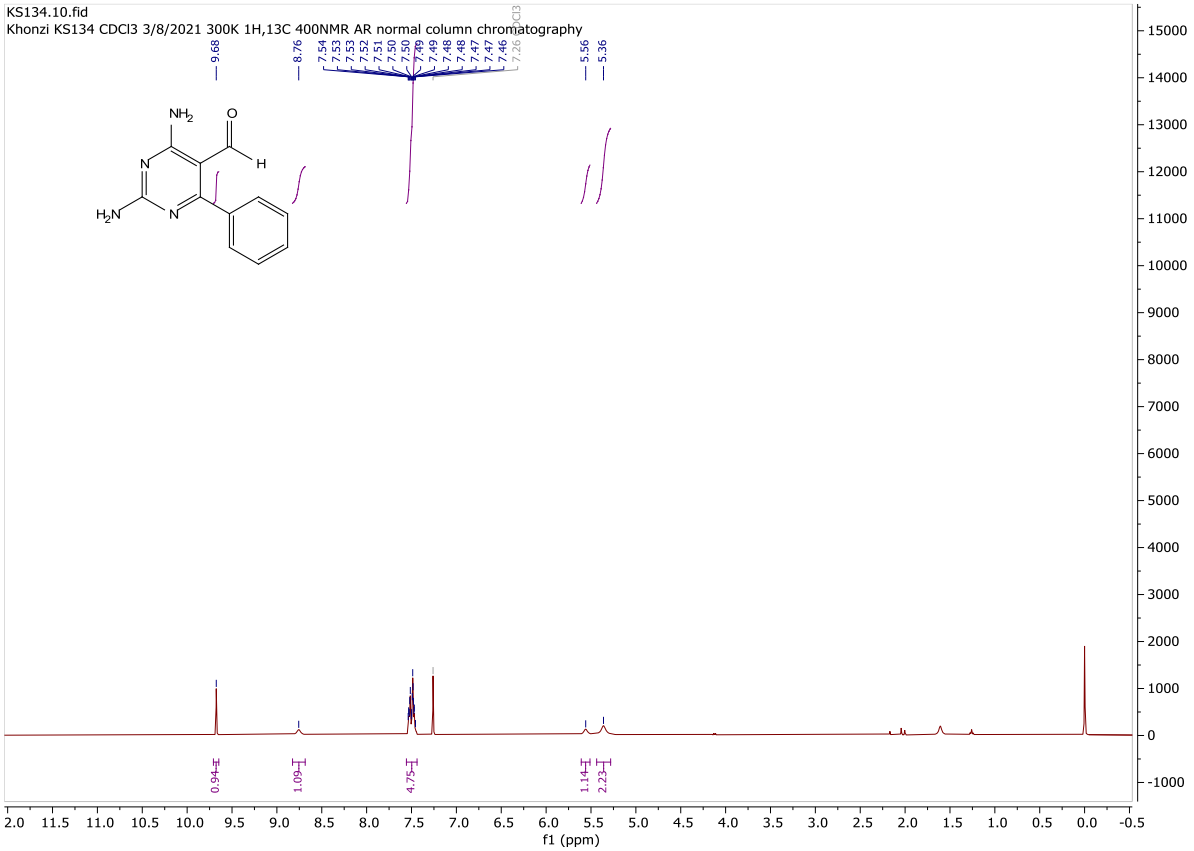

^{13}C NMR spectrum of 31a

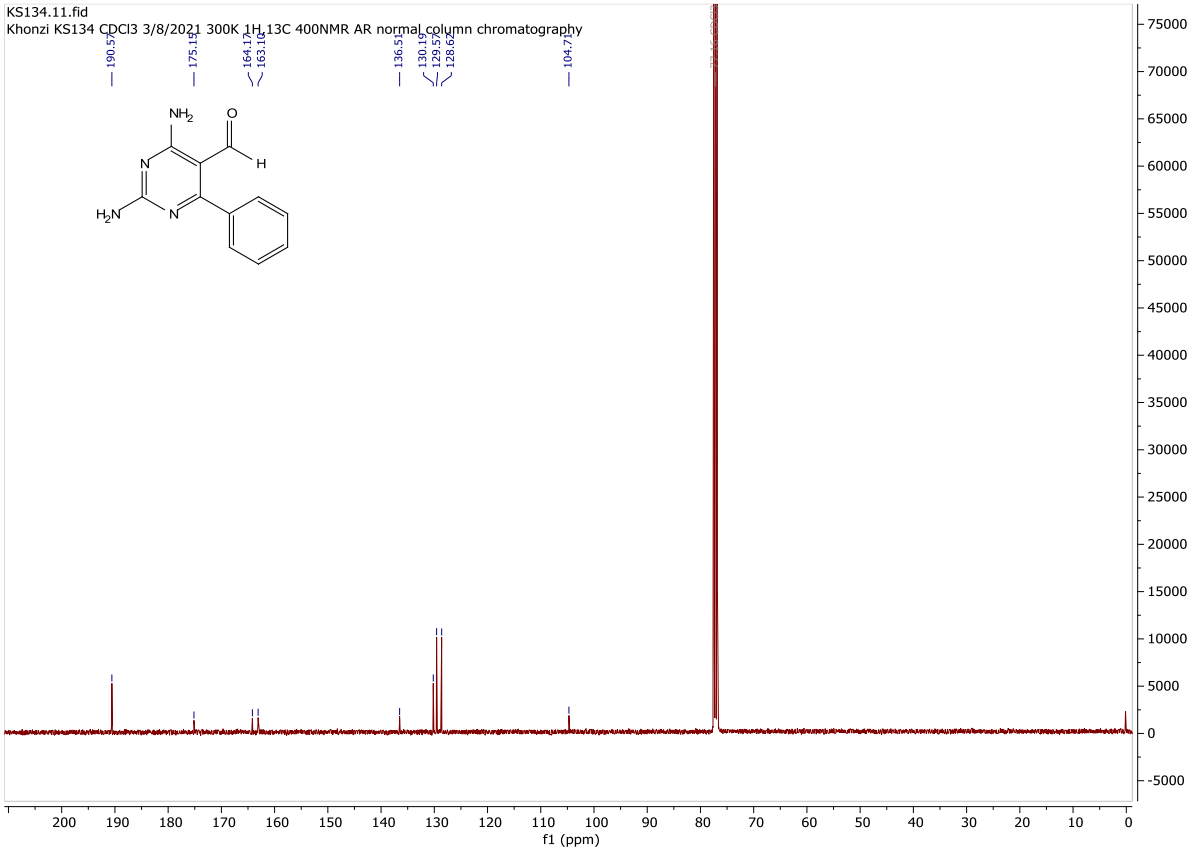

^{1}H NMR spectrum of 51c

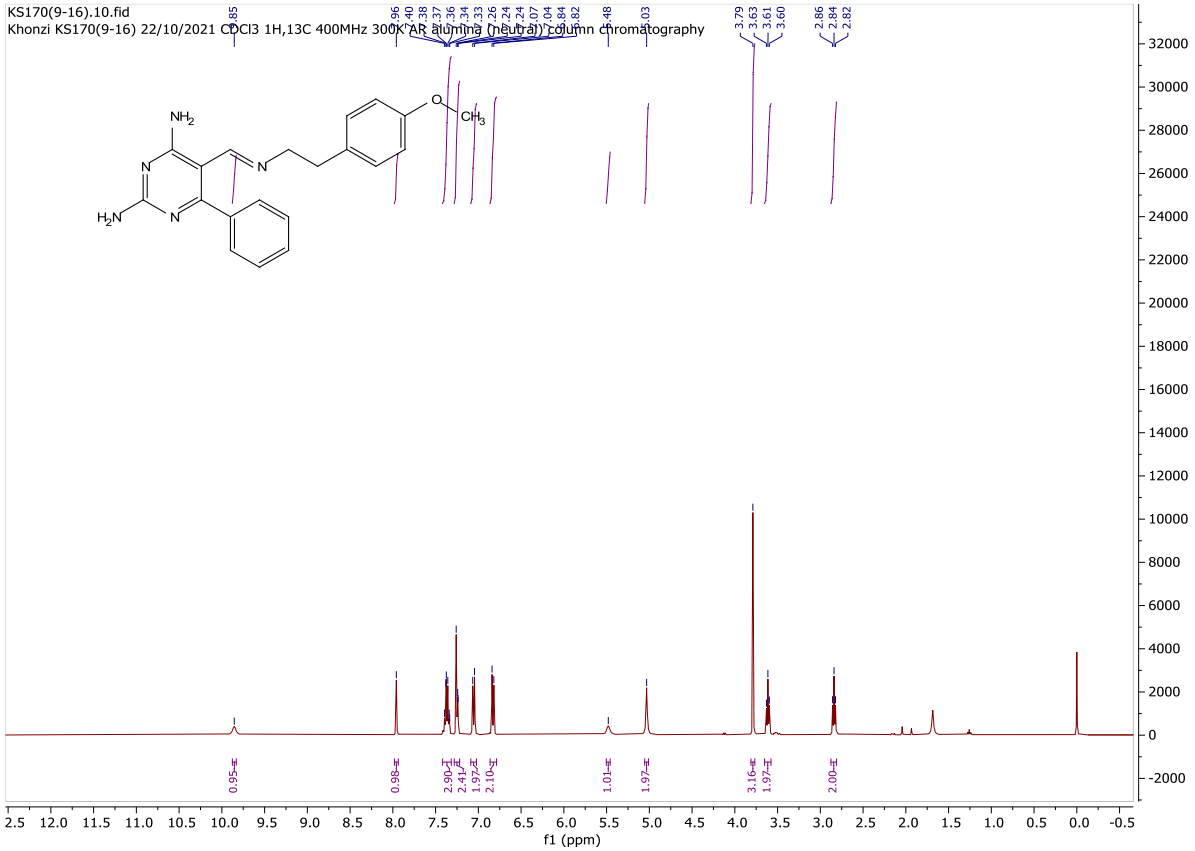

^{13}C NMR spectrum of 51c

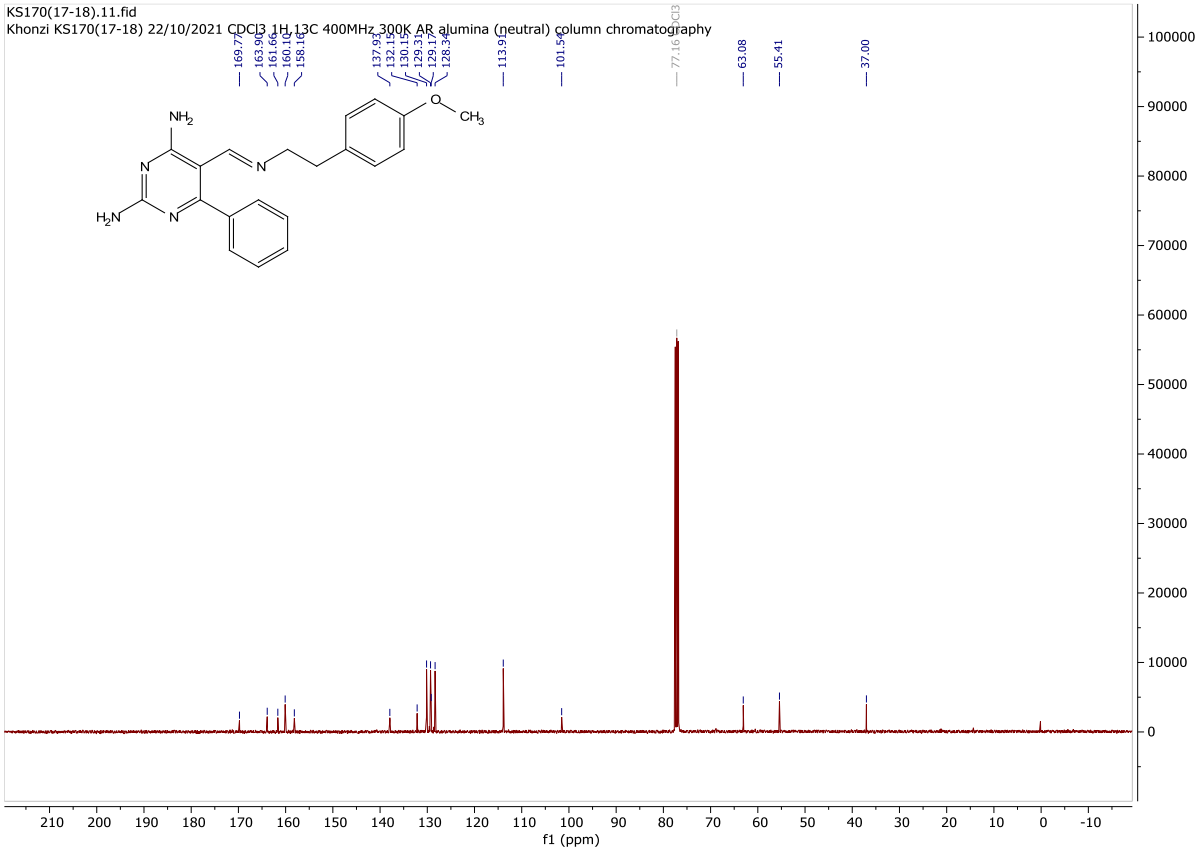

^{1}H NMR spectrum of 28c

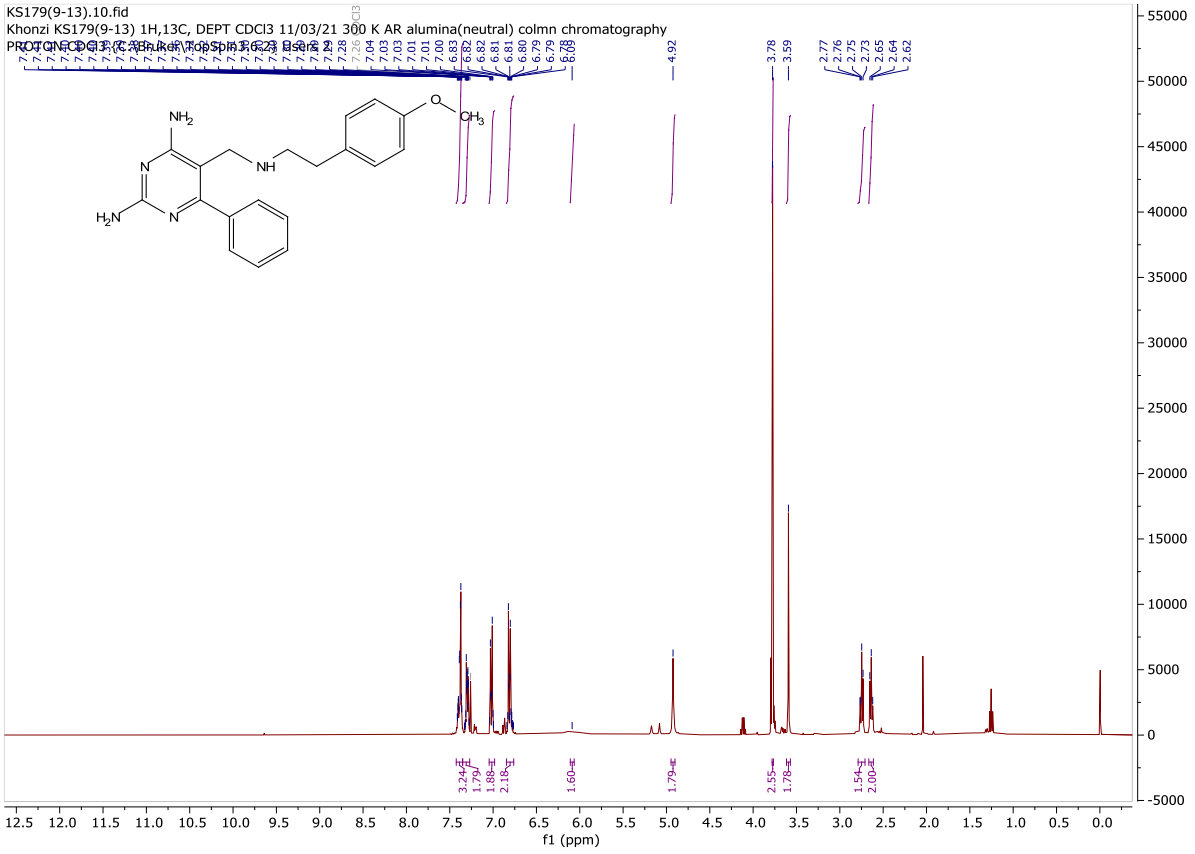

^{13}C NMR spectrum of 28c

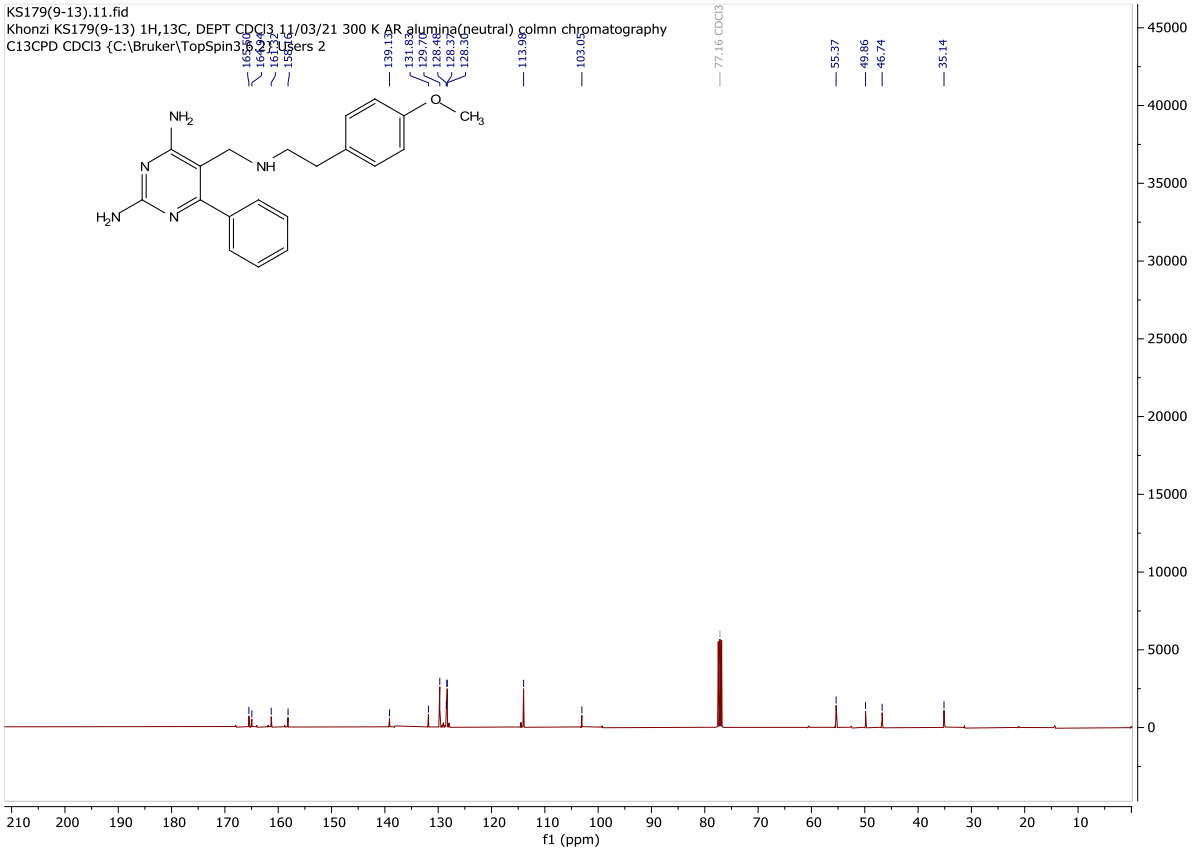

^{1}H NMR spectrum of 28u

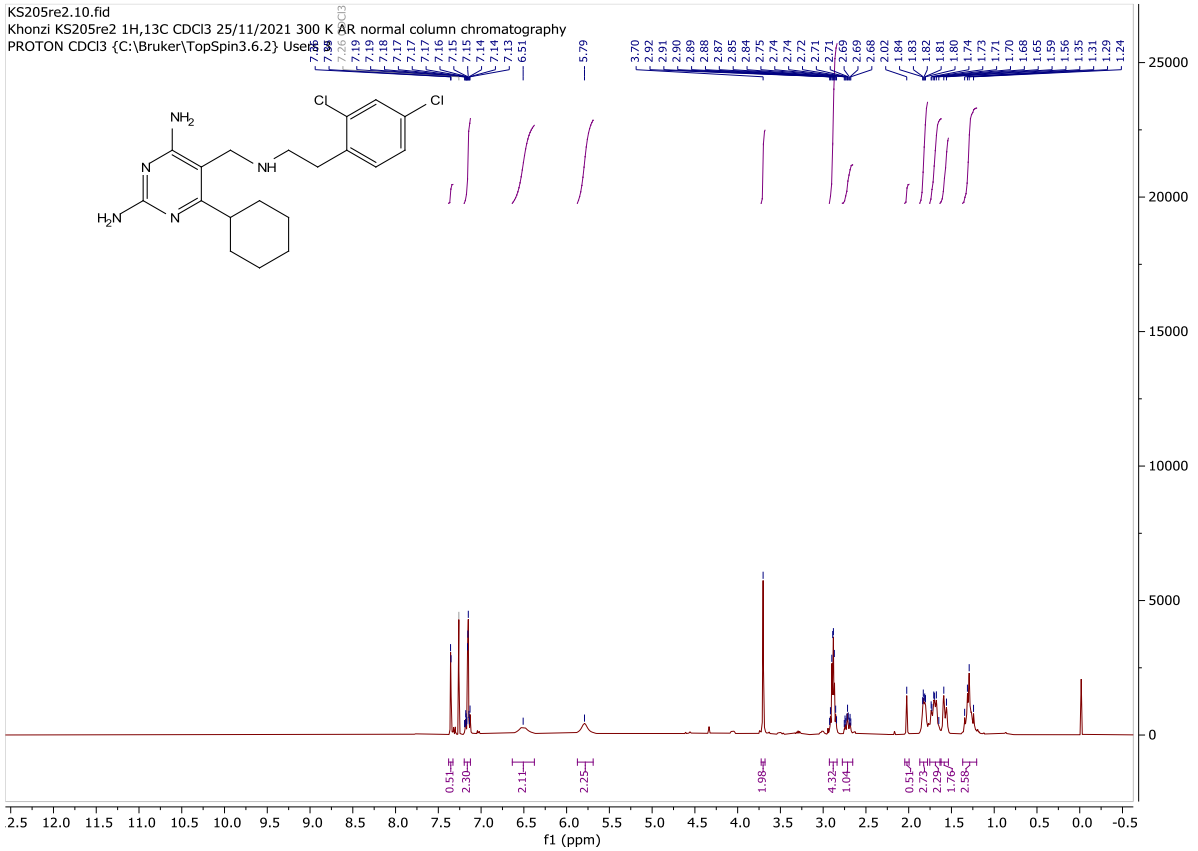

^{13}C NMR spectrum of 28u

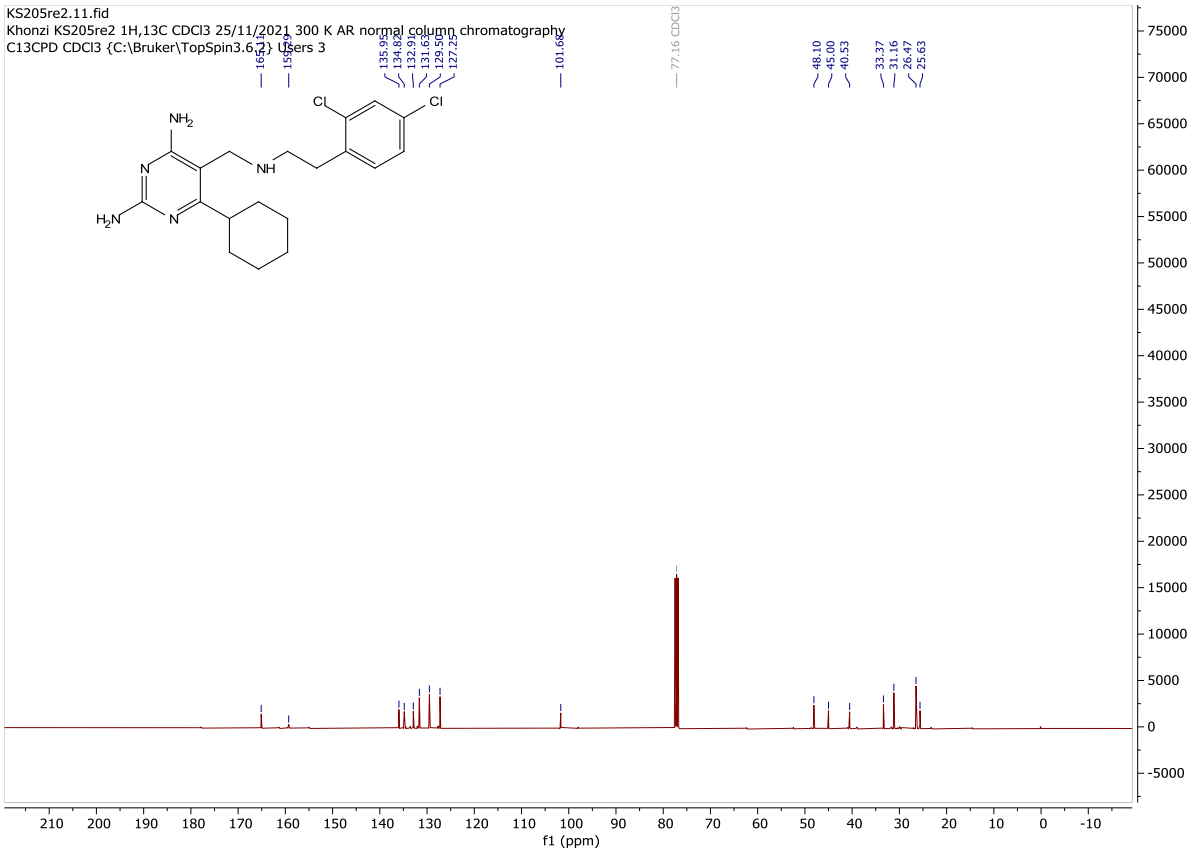

^{1}H NMR spectrum of 28b’

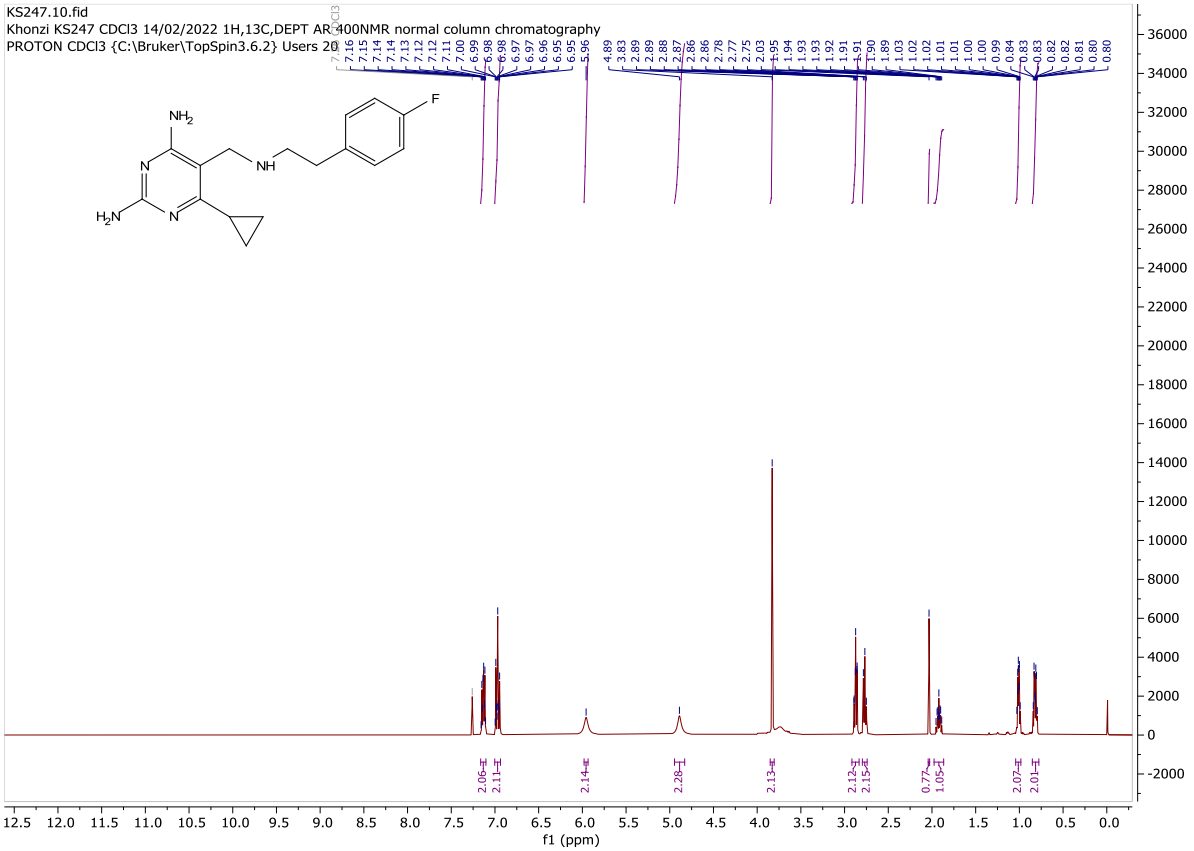

^{13}C NMR spectrum of 28b’

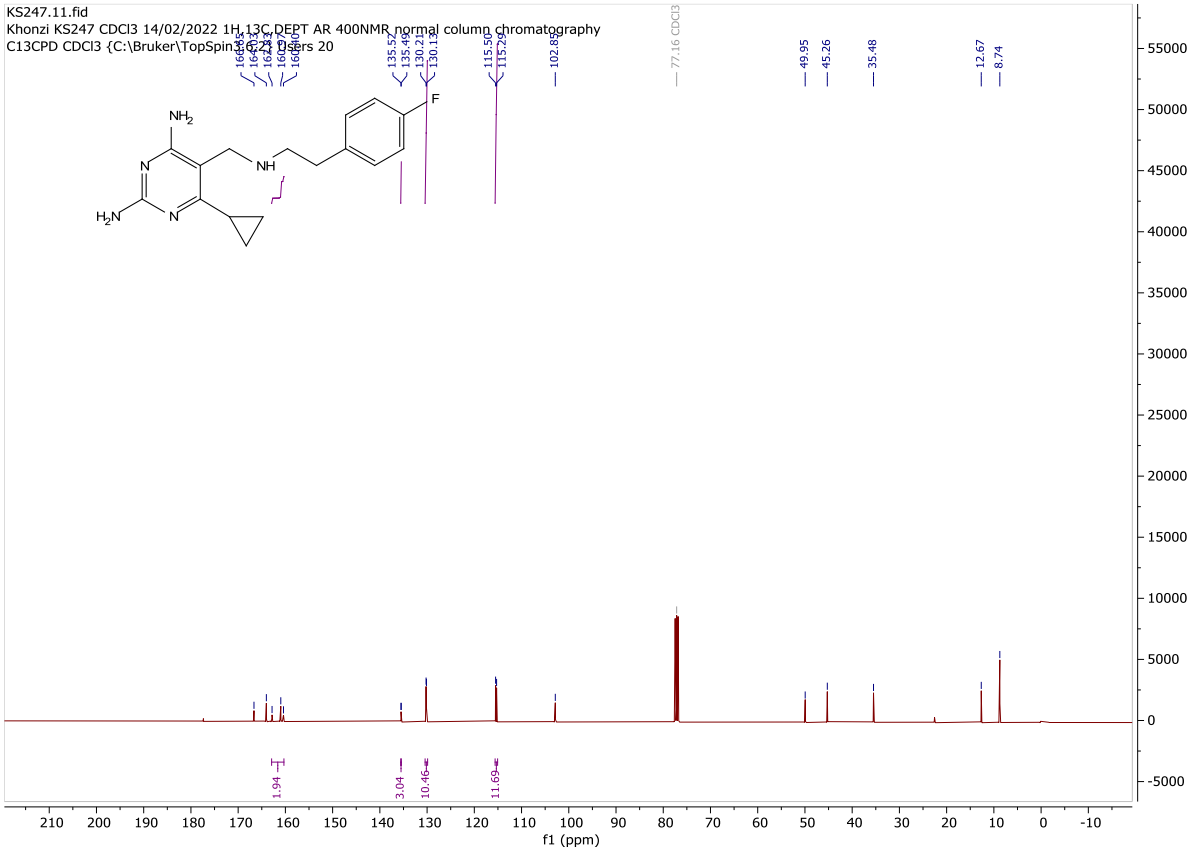

PART 2-THE TRANSMISSION STAGE

CHAPTER 5: Gametocytes and transmission-blocking agents

The second component of this research project will focus on a relatively new research area on the development of transmission-blocking antimalarials. The malaria burden can be significantly reduced by preventing parasite transmission between the human host and mosquito vector.[17] Successfully preventing human-to-mosquito transmission of the malaria parasites is a possible solution to eventually eliminate malaria as a disease.[17] For years this field was neglected, as the focus was on treating clinical symptoms in patients, which are observed due to the asexual replication of the parasite which results in the destruction of the human erythrocytes.[62] As a result, standard antimalarial drug efficacy and drug resistance assessments neglected parasitic gametocytes in their protocols.[63] However it is now known that gametocytes can be present in the bloodstream for 2-4 weeks after a patient has been declared malaria free.[64] With drug resistance spreading and with no clinically proven vaccines that are 100% effective, using drug combinations or gametocytocidal drugs possessing transmission-blocking activity is essential for malaria control and elimination.[63]

5.5. Gametocyte development

Gametocytes are the sex cells of the malaria parasite, which cause no clinical manifestations[65] but are responsible for the parasite's transmission from the human to the *Anopheles* mosquito, which is key for the continuation of the parasitic life cycle.[66] Their function in the life cycle of the parasite makes them important targets for transmission-blocking interventions.[62] A biological overview of *P. falciparum* gametocytes, focusing on gametocyte commitment, gametocyte maturation (gametocytogenesis), gametocyte metabolism and gametogenesis will be outlined.[62] Expanding our knowledge of gametocyte biology will enable the development of malaria transmission-blocking intervention strategies,[65] which include targeting gametocytes or the mosquito midgut stages by drugs or vaccines to inhibit parasite transmission from human host to the mosquito, hence, stopping malaria from spreading.[62,65]

5.1.1. Gametocyte commitment

Gametocyte commitment is the process where a switch happens from an asexual blood stage to a sexual pathway to form parasitic gametocytes, sexual precursor cells.[67] This occurs because of the asexual blood stages not being able to be transmitted to the mosquito for the continuation of the parasite's life cycle.[62]

Commitment to gametocyte development occurs before schizogony,[67] where a single schizont makes a progeny of merozoites which remain asexual blood stage parasites, continuing the erythrocytic cycle,[62] or become sexual forms, male or female gametocytes, [62,68] and persist in an infectious state until a mosquito takes a blood meal.[69] The female gametocytes appear several days before males and throughout the period of their presence, the females vastly outnumber the males.[65] Researchers have also observed that when the parasite is treated with gametocytocidal drugs, the decrease of the gametocytes in the blood is accompanied by a large decrease in male gametocytes, whilst female gametocytes persist for a longer time in the peripheral blood.[68]

Studies have shown that gametocyte commitment can also be attributed to the collaborative action of epigenetics, in which in *P. falciparum*, heterochromatin protein 1 (PfHP1) and *Pf* histone deacetylase 2 (PfHda2) showed involvement in the epigenetic regulation of gametocyte commitment. *Plasmodium* parasites depend more on the regulation of transcript stability and turnover to give sufficient gene regulation.[69] Transcriptional regulation research in *P. berghei* and *P. falciparum* showed that Apetala 2-G (AP2-G)[70], belonging to the apicomplexan AP2 DNA-binding protein family, triggers a transcription cascade which also starts off gametocyte commitment, **Figure 45**.[62,71] Additionally, stress factors like anaemia, high parasitaemia, host immune response or drug treatment with fansidar, steroid hormones and chloroquine or sulfadoxine-pyrimethamine combination therapy in particular, are believed to increase gametocyte production.[62]

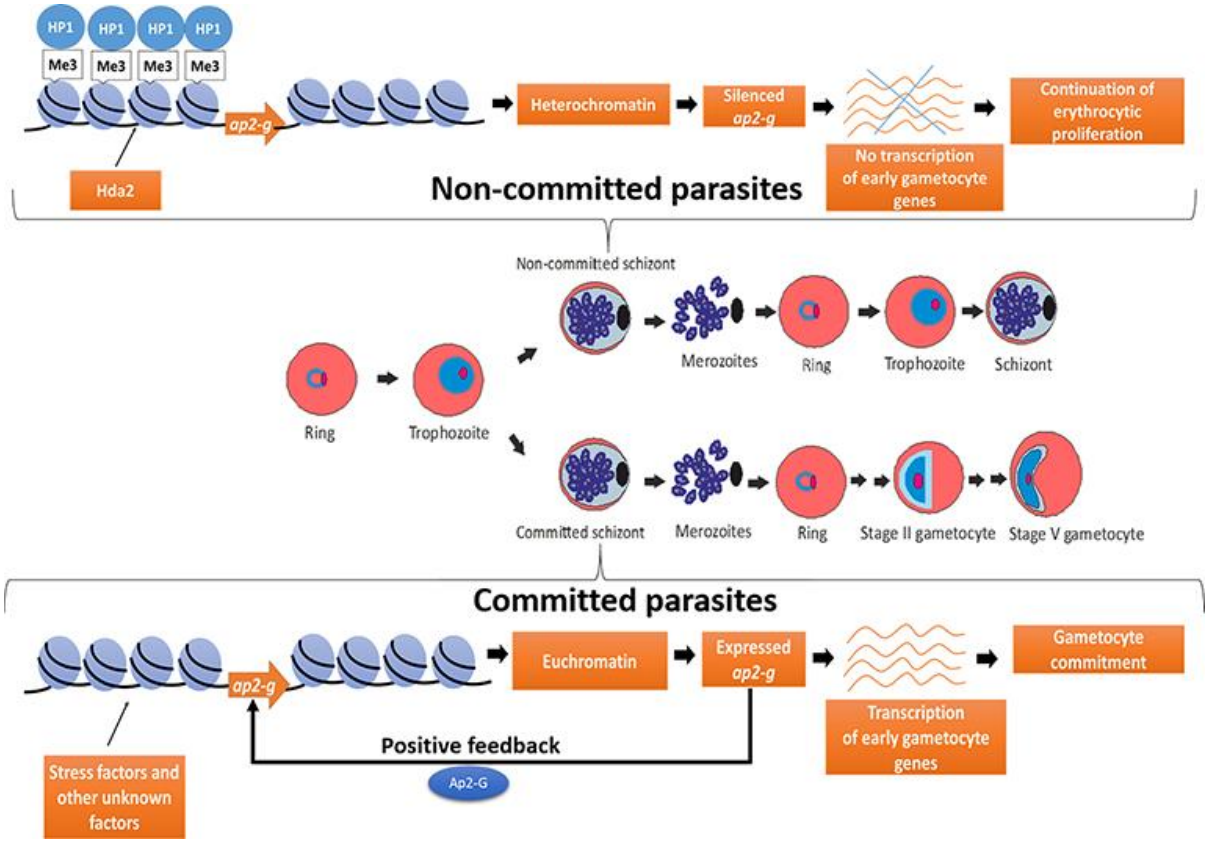

Figure 45: A proposed mechanism of gametocyte commitment. Comparing committed parasites, which differentiate to gametocytes as a result of epigenetic and transcriptional regulation working in unison with non-committed parasites.[62]

5.1.2. Gametocyte maturation

Each *Plasmodium* species has different gametocyte morphologies. When mature however, *P. falciparum* gametocytes develop a falciform or crescent shape which differs vastly from the round to oval shape of the fully developed gametocytes from *P. knowlesi, P. ovale, P. vivax* and *P. malariae*.

In *P. falciparum*, gametocyte development takes from 8–12 days.[68] There are five well defined morphological stages (I-V) that the parasite goes through in gametocyte development, of which only the mature stage V gametocytes infect mosquitoes.[66,72] Each stage has a relevant stage specific protein that has a function in the development, integrity, as well as fertilisation preparation of the gametocyte. The expression of proteins related to a specific gender assist (in later stages) with gamete fertilisation in the mosquito midgut (**Figure 46**).[62] Stages I–IV are concealed in the bone marrow and stage V circulates in the peripheral blood vessels.[73] Stage I is characterised by having rounded shape gametocytes which are difficult to distinguish from the asexual trophozoites that are still developing.[62,73] Stage IIa is characterised by its granular

distribution of pigment in several food vacuoles and has a large and round formation which distinguishes it from trophozoites. Stage IIb is where elongation of the gametocyte begins, and there is an observed D-shape. Stage III gametocytes are oval shaped with a slightly distorted red blood cell caused by further elongation of the gametocyte. Stage IV has clearly distinguishable male and female forms. Both genders are thin and elongated and have pointed tips. Stage V gametocytes have the falciform or crescent shape, which makes them the most distinguishable among all stages.[62]

Proteins expressed in early stage I–II gametocytes are Pfs16 (also expressed in all gametocyte stages), Pfg27 and the six LCCL-domain proteins, **Figure 46**. The **LCCL** domain is a conserved protein module, founded from the proteins, ***L****imulus* clotting factor **C**; cochlear protein **C**och-5b2; and lung gestation protein **L**gl1.[74] The Pfs16 protein's main function is not well understood, however it is important because disruption of this protein results in a decrease in gametocyte production[75] and the ability of the male gametocytes to exflagellate being impaired.[62] Pfg27 is also key for gametocyte production.[76] This is a phosphoprotein, which is expressed initially in stage II.[62] It is responsible for forming homodimers that function, *in vitro,* as single-stranded RNA-binding proteins[62] and the deletion of its gene causes abnormal gametocytes to form.[76] The six LCCL-domain proteins (called LAP in *P. berghei* and CCp in *P. falciparum*) have adhesive properties[77] and are initially expressed from stage II. In the gametocytes of *P. falciparum* CCp proteins are localized within the parasitophorous vacuole, however, after gametes emerge, the proteins associate with the gametes' surface.[62,77] Stage IIb initially expresses sexual stage proteins, namely, Pfs230 and Pfs48/45 as well as the osmiophilic body proteins Pfg377 and Pfmdv-1, or sexual stage-specific cytoskeletal proteins like α-tubII (tubulin II) as well as actin II.[62] The surface proteins, Pfs230 and Pfs48/45 possess adhesive properties[77] and disrupting the genes of both these proteins impair the fertility of microgametocytes. Pfg377 is associated with the formation of osmiophilic bodies in macrogametocytes of *P. falciparum*[62], therefore, disrupting the gene for this protein causes a significant decrease in fertilisation.[78] Osmiophilic bodies are membrane-bound vesicles mainly found in *Plasmodium* macrogametocytes. Their abundance increases as the gametocyte matures.[78] These vesicles are responsible for releasing their contents into the parasitophorous vacuole which assists in the escape of gametocytes from the erythrocyte following ingestion by the mosquito.[78] Protein Pfmdv-1, also called Pfpeg3, shows high expression in early gametocytes until stage V, thereafter it is expressed in low levels.[79] Pfmdv-1 is essential for maintaining membrane structures that are important for gametocyte maturation in

erythrocytes,[80] however, disrupting the encoding gene of Pfmdv-1 causes a 20-fold decrease in microgametocyte production.[62] The actin II and the α-tubulin II cytoskeletal proteins are sexual stage-specific and are both predominantly present in microgametocytes.[81] α-Tubulin II is incorporated in the axonemes (the central strand of a flagellum) of emerging male gametes,[62] while actin II, only found in *Plasmodium* species, is expressed solely in the stages where transmission to the mosquito is involved, including the gametocyte, gamete and sporozoite stages.[82] Actin II still has a function that is not well understood, however, disruption of the genes of both these proteins causes impairment of male gametogenesis.[62] The protein PfB0400w, also called PfMR5, is observed in the mature stage V microgametocyte.[62,83] Although there is still uncertainty with regards to its function, its expression in male stage V gametocytes suggests that it may be involved in the preparation of gametocytes for exflagellation.[62]

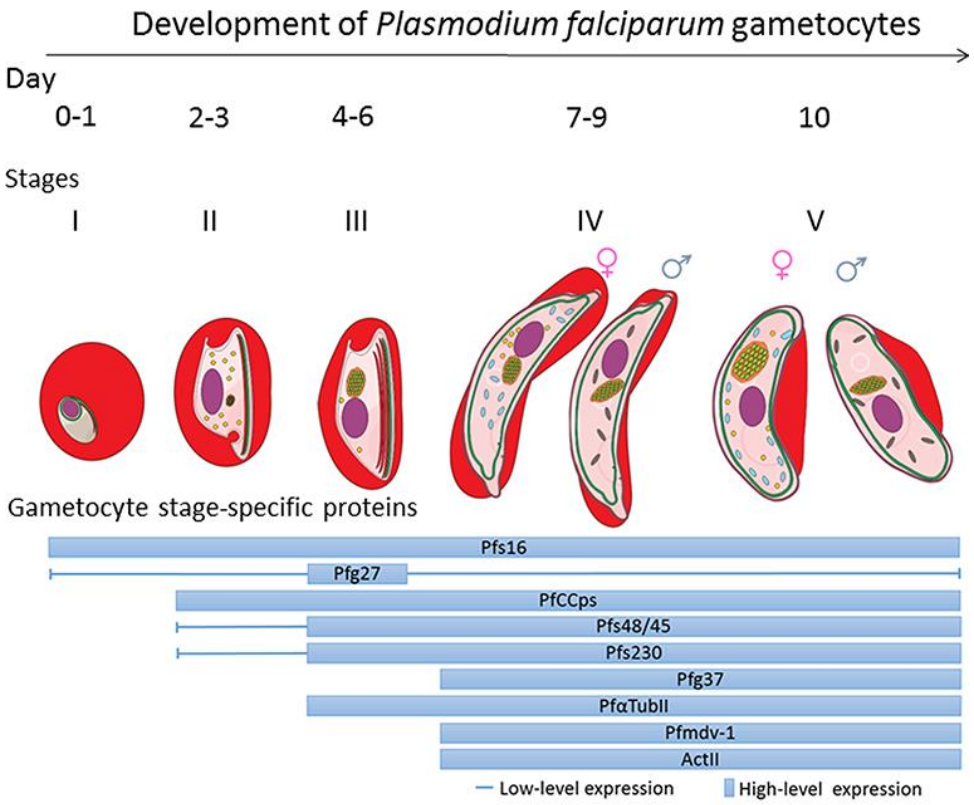

Figure 46: A representation of the stages of gametocyte development in *P. falciparum*, as well as the proteins expressed at each stage in the development of the gametocytes. Proteins that are expressed at a high level have a bar as a representation and proteins that are expressed at a low level have a full line as a representation. This figure is limited only to gene products.[62]

Stage-specific proteins are important in the development of gametocytes and hence the continuation of the malaria parasite life cycle. As discussed above, it is evident that drug design and development of potential drugs that target the disruption of these proteins, particularly stage V proteins, can serve as ideal transmission-blocking agents. Certain drugs such as trioxaquines (see later) are reported to kill stage V gametocytes however as this is a relatively new research area, their mode of action is still not well understood.

5.1.3. Gametocyte metabolism

Gametogenesis is the process of converting gametocytes to viable gametes.[84] During gametocytogenesis (the process of creating gametocytes via mitotic division of gametogenia), the parasite, *P. falciparum* experiences intense metabolic processes which include energy production[84] as well as synthesis and degradation of various molecules such as lipids and proteins.[62,85] These metabolic processes could be used to identify novel targets for drug development.

Lipids are vital multifunctional molecules, which have a role in the proliferation and growth of the parasite and other functions including energy storage, cell signalling, and membrane stability.[85] Sphingolipids are essential for both membrane structure and signalling.[85] They play a role in ceramide metabolism and undergo enrichment as gametocytes mature. Inhibiting the ceramide biosynthetic pathway could kill gametocytes,[62] hence another potential drug target.

Some researchers suggest that DNA replication occurs in male gametocytes,[86] and that this is a rapidly occurring process. It is also reported that male gametocytes will go through three rounds of DNA replication within minutes, with eight male gametes being produced.[87] This is disputed by Ngwa, *et al*. who suggest that no DNA replication occurs in gametocytes,[62] however, the synthesis of nucleic acids is solely for producing RNA.[62] RNA production decreases on about the 6th day of gametocytogenesis, therefore, the RNA and the synthesis of proteins are more vital in earlier gametocyte stages rather than later gametocyte stages.[62] Protein expression differs for each respective gender, where female gametocytes produce proteins needed for mitochondria and ribosomes, while male gametocytes solely require proteins to form axonemes, synthesise DNA and for exflagellation.[62] Therefore, although DNA replication in gametocytes is not fully understood, it is possible that ceasing either DNA or RNA production would prove a viable drug target to stop gametocyte formation.

The malaria parasites have one mitochondrion and during parasite development the gametocytes' mitochondria are longer and have more cristae than the asexual blood stage

malarial parasites.[62] This observation implies that the synthesis of ATP via the electron transport chain is primarily responsible for producing energy in gametocytes.[88] There is seven times more cytochrome b in the sexual stages as compared to the asexual blood stages.[89] The cytochrome bc1 complex creates a gradient that allows ATP synthesis by adding more protons to the electron transport chain.[62,88] Cytochrome bc1 is a key target for the antimalarial drug atovaquone **21** that inhibits ubiquinone, causing *Plasmodium* cytochrome bc1 activity to be inhibited and its mitochondrial function to be impaired, which results in gametocyte death.[90] Other drugs, namely, primaquine, **57** and its analogue bulaquine, **58**, **Figure 47**, also show gametocytocidal activities, with primaquine **57** thought to cause mitochondrion deformation.[91] The mode of action of these drugs is not well understood, however they reduce gametocytaemia in infection by *P. falciparum*.[62]

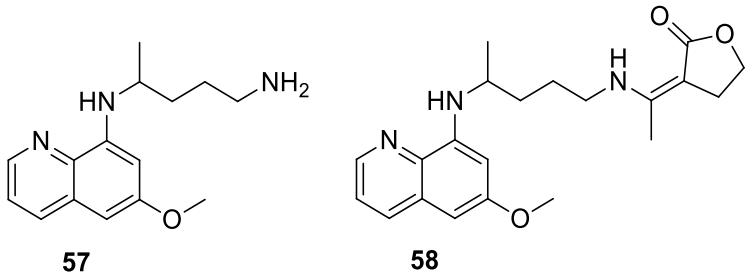

Figure 47: Structures of primaquine (57) and bulaquine (58).

5.2. Known transmission-blocking drugs

Transmission-blocking is essential to end the malaria parasite life cycle because even if a drug kills asexual parasites and resolves malaria-associated signs and symptoms, gametocytogenesis can begin after the utilisation of certain antimalarial drugs, like chloroquine **6**, pyrimethamine **7** and sulfadoxine **15** (**Figure 48**).[63] An "ideal" transmission-blocking drug is said to be a compound that acts against mature and functioning stage V gametocytes to either directly kill them or irreversibly compromise their future onward development in the mosquito.[92]

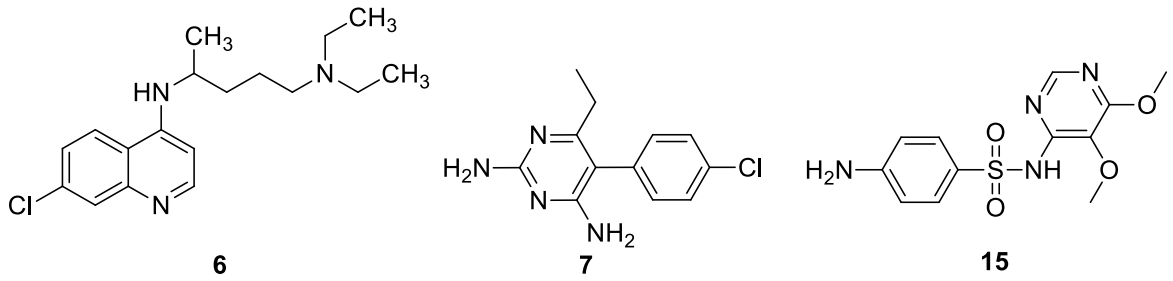

Figure 48: Structures of chloroquine (6), pyrimethamine (7) and sulfadoxine (15).

Currently, 8-aminoquinolines (primaquine **57, Figure 47** and tafenoquine (WR-238605) **59**, **Figure 49**) are the only gametocytocides with high effectiveness against gametocytes of all human malaria species, with male gametocytes showing a high sensitivity.[63,68] Primaquine **57** prevents exflagellation in the gametocytes present and therefore reduces transmissibility, however, its use is limited since it causes hemolytic anaemia in patients with glucose-6-phosphate dehydrogenase deficiency.[68,93,94]

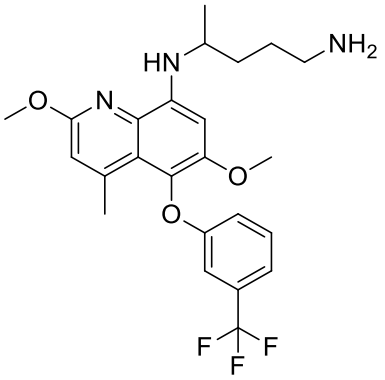

59

Figure 49: Structure of tafenoquine (59).

Artemisinin derivatives DHA **9**, artesunate **10** and artemether **60**, **Figure 50**, do not kill mature gametocytes of *P. falciparum*, they do however kill immature gametocytes and asexual erythrocytic parasites before gametogenesis by the inhibition of both the heme polymerization and haemoglobin catabolic pathway, and this indirectly inhibits gametocyte development.[63,68,95,96]

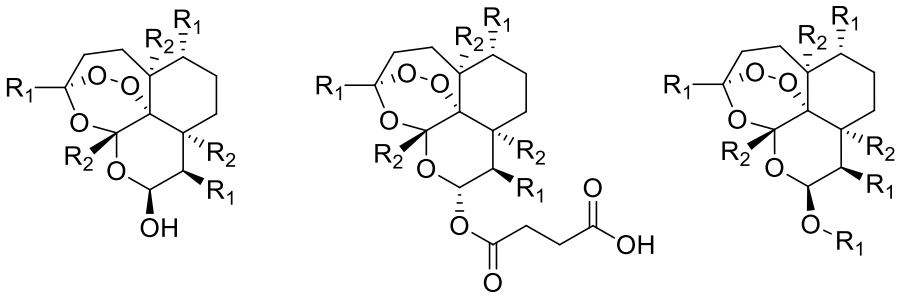

9 **10** **60**

$R_1 = CH_3$
$R_2 = H$

Figure 50: Structure of artemisinin derivatives DHA (9), artesunate (10) and artemether (60).

Artemisinin Combination Therapies (ACTs) are also employed as antimalarial agents of the sexual stage of the parasite. Common ACTs include DHA-piperaquine, artesunate-amodiaquine, artesunate-mefloquine and artemether-lumefantrine. ACTs differ with regards to gametocyte clearance, where gametocyte clearance is much slower in 4-aminoquinoline partner drugs piperaquine **61** and amodiaquine **62** than drug compounds possessing aryl-amino alcohol and related structures, such as mefloquine **63** and lumefantrine **64**, **Figure 51**.[72,94]

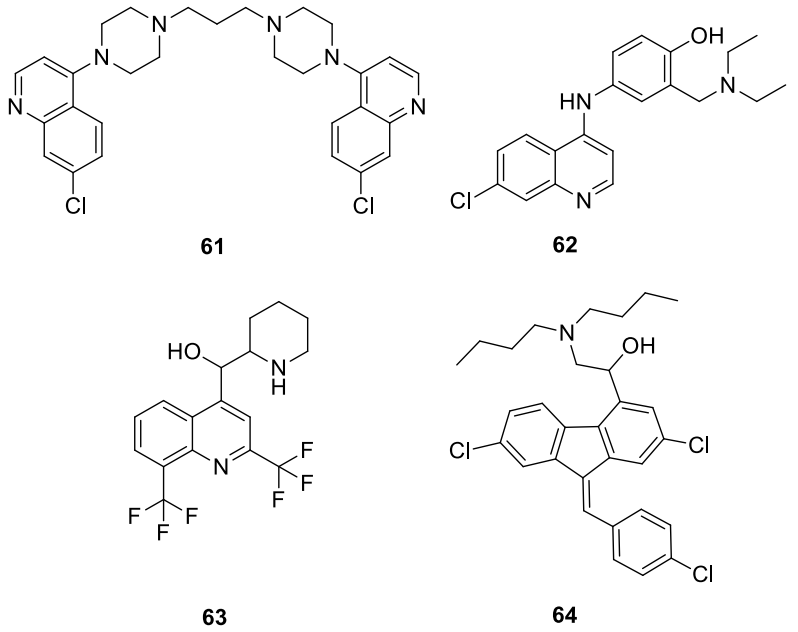

Figure 51: Structures of piperaquine (61), amodiaquine (62), mefloquine (63), lumefantrine (64).

Pyrimethamine **7** is reported to damage ookinetes. [95] This is important as this could prohibit the development of ookinetes into oocytes that later produce sporozoites, and hence disrupt the parasite life cycle and transmission.

5.3. Potential gametocytocidal drugs under development

Researchers working in this field have been hard at work in attempting to develop gametocytocidal compounds that have the potential to disrupt the malaria parasite life cycle and, in the future, completely eradicate the disease. Such compounds include tafenoquine **59**, **Figure 49** which is an 8-aminoquinoline analogue of primaquine **57** (**Figure 47**)[97] with an increased metabolic half-life (two-weeks), meaning it stays in the body for the whole period needed for asexual parasites to become mature gametocytes, and therefore facilitating clearance of all infective parasites.[95] It is unique in showing activity against liver schizonts[98] as well as all stages of the parasite and has a reduced toxicity and higher clinical effectiveness

than primaquine.[95] Tafenoquine **59** was reported to be undergoing Phase IIb/III clinical trials in 2010.[95] The drug was recently FDA approved in July 2018, as a prophylaxis and radical cure for *P.vivax* infection.[99,100] However, its *P. falciparum* transmission-blocking efficacy is unclear and clinical trials for this are still continuing.

Bulaquine (Elubaquine) **58**, is another synthetic 8-aminoquinoline analogue possessing a 2,4 dihydrofuran side chain in the 8 position of the quinoline, hence making it structurally different from primaquine **57** (**Figure 47**). It has better gametocyte clearance of *P. falciparum* than primaquine **57** in patients with acute infections over a long period (8 days).[95,101]The drug has undergone clinical trials in humans as an anti-relapse therapy against *P. vivax* and results showed that it is comparable to primaquine **58** in terms of safety and tolerability. Bulaquine was reported to be undergoing clinical trials against *P. falciparum* gametocytes in 2010.[95,102] There have been no recent reports however about the outcomes of these trials.

Trioxaquines have a hybrid nature and contain synthetic peroxides.[103] They are covalent chimeras that combine a parasite-toxic trioxane with an aminoquinoline which bioaccumulates within parasites.[95] Trioxaquine 2 (DU1302) **65**, a salt formed by the protonation of trioxaquine citric acid, **Figure 52**, is a more active version of trioxaquines and has undergone *in vitro* tests against *P. falciparum* and shows high activity against both immature gametocytes (stages II-IV) and mature gametocytes (stage V).[95,103] DU1302 **65** was observed to be effective independent of stereochemistry of the analogue, with both isomers showing equal activity. Trioxaquines have not yet undergone evaluation against *P. falciparum* in humans, but they display promise against *P. falciparum* infected humanized mice.[95]

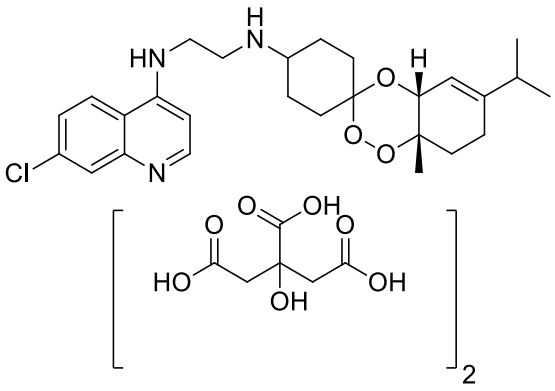

65

Figure 52: Structure of trioxaquine 2 (DU1302) (65).

Epoxomicin **66**, **Figure 53**, is a natural derivative of certain *Actinomycetes* bacterial strains and can be synthesised from spirodiepoxides.[17] The α9,β9-epoxyketone is its active moiety. It works by inhibiting proteosomes, hence it inhibits the expressions of genes responsible for encoding cysteine proteases as well as the proteosome throughout gametocytogenesis.[95] This compound reduced *P. falciparum* gametocytes by 77% within 24 hours and completely killed gametocytes after 72 hours *in vitro*.[95] Epoxomicin shows activity against the parasites throughout the asexual, sexual, and mosquito midgut stages of the life cycle, however, the viability of mouse or human cell lines (3T3 or A549, respectively) was not reduced. These findings show promise for further development and *in vivo* investigations of this compound as an antimalarial agent with transmission-blocking potential, in addition to reducing clinical symptoms caused by asexual parasites.[104]

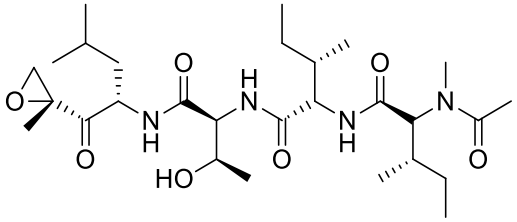

66

Figure 53: Structure of epoxomicin (66).

Methylene blue (methylthioninium chloride) **67**, **Figure 54**, when provided as a combination treatment with dihydroartemisinin-piperaquine, exhibits strong gametocytocidal activity against *P. falciparum in vivo*. [105] This combination therapy completely clears every sexual stage. It also acts against both older and younger gametocytes.[95,106] Human volunteer trials have suggested that methylene blue is safe and has a strong gametocytocidal effect when combined with dihydroartemisinin-piperaquine.[105] Limitations associated with methylene blue include vomiting and development of blue urine, which could affect patient compliance. Researchers require further studies to determine the lowest efficacious dose of methylene blue and provide a simplified treatment schedule that will enable its use as a single dose gametocytocide, similar to primaquine **57**.[105]

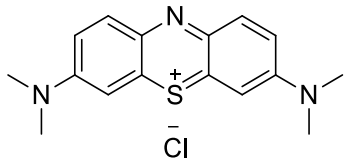

67

Figure 54: Structure of methylene blue (67).

Tipranavir **68**, **Figure 55**, a nonpeptidic HIV protease inhibitor, was found to be both gametocytocidal and an inhibitor of gametocytogenesis of the *P. falciparum* parasite.[107] Other protease inhibitors that were also found to be inhibitory include, saquinavir **69**, lopinavir **70** and darunavir **71**, **Figure 55**.[95] Hobbs *et al.* have reported that a possible limitation of their study of protease inhibitors as transmission-blocking agents, is the differential drug effect seen in *in vitro* studies versus what may occur in *in vivo* studies because of protein binding.[108] Additionally, the possibility that metabolites of these drugs may have additional effects on parasite transmission prompts the need for further studies.[108]

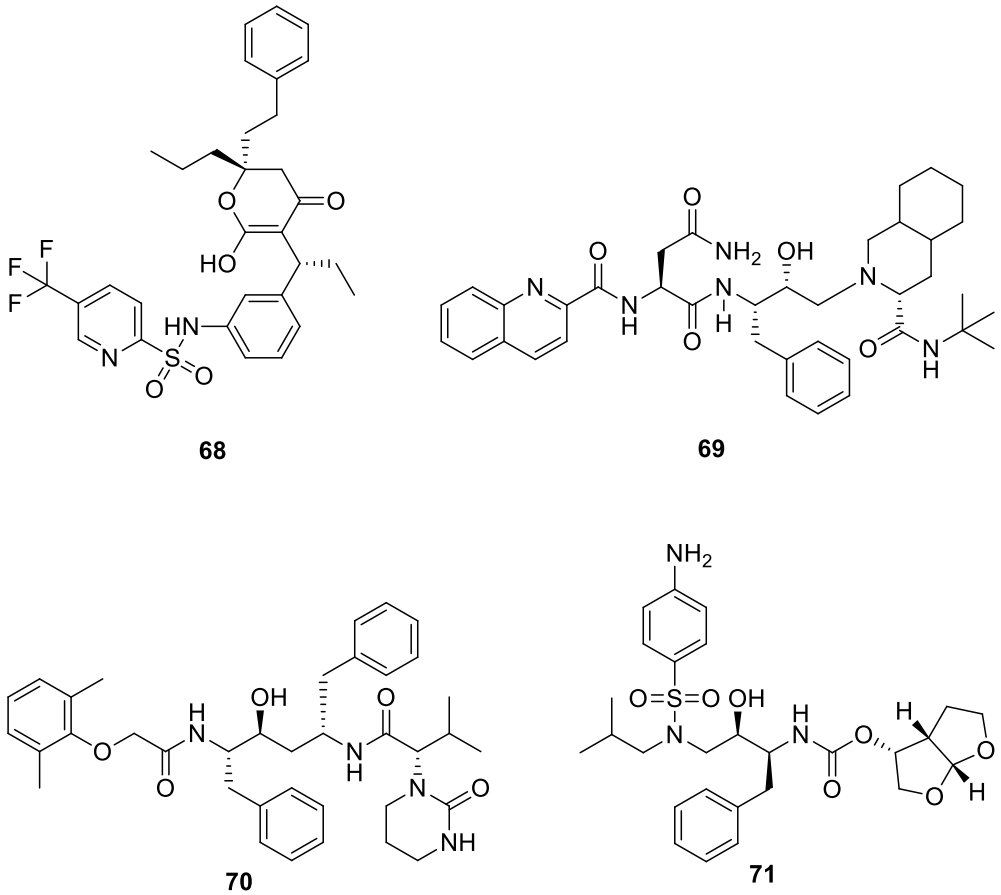

68 69 70 71

Figure 55: Structures of tipranavir (68) saquinavir (69), lopinavir (70) and darunavir (71).

Riboflavin **72**, **Figure 56** shows toxicity, *in vitro,* against *P. falciparum* gametocytes, via possible interferences with haemoglobin digestion during gametocytogenesis.[95] Its effects are on mature as well as immature gametocytes.[109] This compound also shows potential activity against asexual parasites when used in synergy with drugs like quinine **5**, pyrimethamine **7** and mefloquine **63**, showing its potential use as a drug in combination therapy.[109]

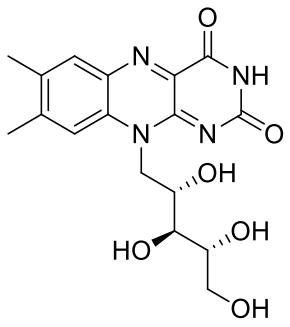

72

Figure 56: Structure of riboflavin (72).

Neem, a complex mixture of substances isolated from the *Azadirachta indica* tree native to India, is known for its insect repellent and insecticide properties.[95] However, it has now shown activity, *in vitro,* against the sexual stages of *P. falciparum* by killing more than 90% of both immature and mature gametocytes.[110] Its activity comes from several component limonoids, a class of oxygenated terpenoids, specifically: azadirachtin **73**, gedunin **74** and nimbolide **75**, **Figure 57**.[110] Azadirachtin **73** acts by stopping exflagellation by inhibiting cytoskeletal activity as well as interfering with male gametocyte endomitosis.[110] Gedunin **74** acts as a heat shock protein (Hsp) inhibitor.[111] The mode of action of nimbolide **75** is well characterised in cancer as it functions by inhibiting the proliferation of cancerous cells by inducing apoptosis, however although effective against *P. falciparum*, its function is not well characterised.[112] While neem and its components display promising activity against *P. falciparum*, its feasibility of use is limited by significant technical challenges. Limonoids have minimal bioavailability and have a short metabolic half-life and gedunin **74** is poorly absorbed in the digestive tract.[95] In addition, more research is required with regards to understanding the safety and possible interaction of neem with other drugs.[95]

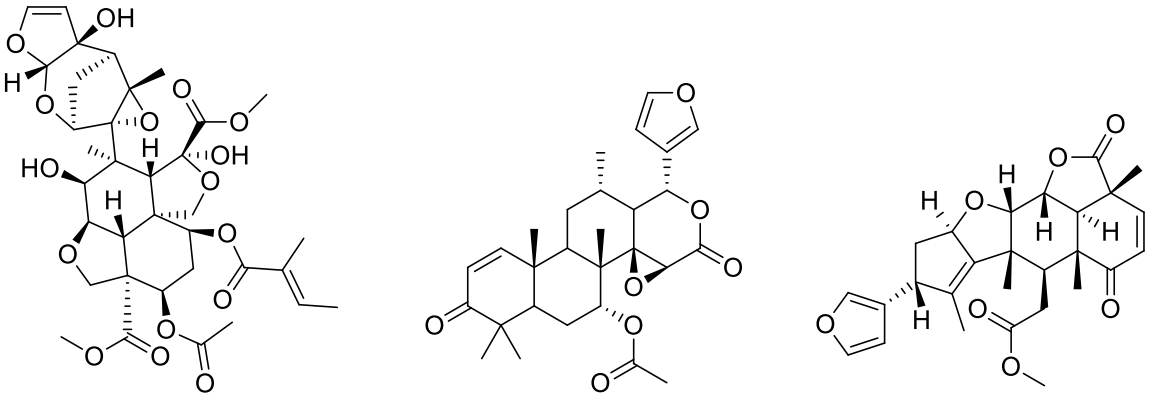

73 74 75

Figure 57: Structures of azadirachtin (73), gedunin (74) and nimbolide (75).

5.4. Approach to the synthesis of transmission-blocking hit compound MMV1581558 and derivatives

Recent research has included the investigation of the transmission-blocking ability of the compounds of the Medicines for Malaria Venture (MMV) Pandemic Response Box (PRB).[22] All compounds in the PRB were tested for either gametocytocidal activity (where compounds that are active kill the gametocyte), their ability to cause permanent damage to the gametocytes so that gamete formation cannot be completed (sterilize them), or their ability to have direct interference with the process of gamete formation once triggered (are contraceptive).[22,92]

Gametocyte activity for these MMV compounds were tested as either "carryover" or "washout". Cultured mature stage V gametocytes were exposed to the compound of interest for 24 h and then either fed to mosquitoes without removing the compound so that it enters the mosquito blood meal and can also act during vector stage development ("carryover"), or the gametocytes were washed free of compound before feeding ("washout").[92] The compounds which had undergone dose response tests in the *P. falciparum* standard membrane feeding assay (PfDGFA) showed one of three characteristics: (i) they displayed equal potency against microgametocytes and macrogametocytes, (ii) they showed activity against both sexes but higher potency against males, or (iii) they showed activity against males but no activity against females at the highest concentration tested.[92] A number of promising candidates were identified from this work.

Researchers at the University of Pretoria screened the MMV PRB and identified the hit compound MMV1581558 **76**, **Figure 58**, and observed that it is active against stage IV/V gametocytes.[22] In this research project we will focus on developing SAR data for this multistage and transmission-blocking hit compound, MMV1581558 **76**.[22] This compound was shown to have endectocide and stage-specific activity against stage IV/V gametocytes and was also gametocytocidal towards male gametes.[22] It is known to act as a G protein-coupled receptor (GPCR) inhibitor and inhibits male gamete exflagellation.[22] However, it was also observed that this compound has limited solubility and could potentially be cytotoxic. These shortcomings prompted our research to develop derivatives with potentially improved pharmacokinetics while maintaining or improving the transmission blocking activity. This part of the research is a collaboration with researchers at the University of Pretoria where an array of other MMV compounds targeting *Plasmodium* asexual and liver stage parasites, stage IV/V gametocytes, gametes, oocysts and endectocides from the MMV PRB are being studied.[22]

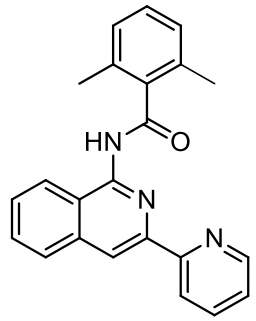

76

Figure 58: Structure of hit compound MMV1581558 (76)

5.4.1. Synthesis of substituted isoquinolines as potential transmission-blocking compounds

We aim to synthesise functional derivatives of MMV1581558 **76** to develop SAR data, and potentially improve gametocytocidal activity. We will explore variations in the isoquinoline ring substituents, X; the pyridyl functional group, Y; and the amide substituent R as shown (**77**, **Figure 59)**.

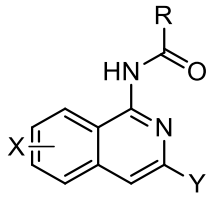

R = 2-picolinyl, nicotinyl, isonicotinyl, 2,6-dimethylphenyl, 3-methylpicolinyl
X = H, 3-F, 2-Cl, 4-Cl
Y = 2-pyridyl, 3-pyridyl, 4-pyridyl

77

Figure 59: General structure of proposed analogues of MMV1581558.

The synthesis of these compounds will primarily be achieved via a two-step reaction, as shown in **Scheme 21**. This will involve the initial formation of the isoquinoline core by reacting a substituted carbonitrile **78** with a substituted *o*-tolunitrile **79** to give the desired substituted isoquinoline amine **80**. This will be followed by the amidation of the amino functional group, achieved by reacting a substituted acyl chloride **81** with the substituted isoquinoline amine **80** to afford the desired isoquinoline amide **77**. The isoquinoline has been well researched and offers a variety of medicinal benefits which include among many others, anticancer, antifungal, antioxidant and antimalarial properties.

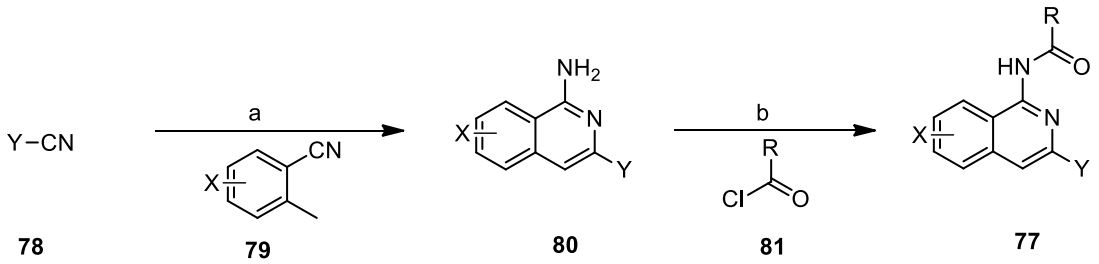

78 **79** **80** **81** **77**

Scheme 21: Proposed synthetic rout for the synthesis of compound (77).

The analogues synthesised will undergo testing against *P. falciparum* stage IV/V gametocytes to achieve structure-activity relationship (SAR) information. Our efforts in this regard will be discussed in depth in the chapter that follows.

CHAPTER 6: RESULTS AND DISCUSSION

The second component of the research project focuses on the synthesis of 3-substituted-isoquinolin-1-yl benzamides **77**, **Scheme 22** as potential transmission-blocking agents. These analogues target the sexual stage of the parasite and function by inhibiting stage IV/V gametocytes, which in turn prevents the transmission of the parasite from the human host back to the feeding mosquito.

The planned synthetic approach affords our desired analogues **77** in only two steps from relatively simple precursors. In this chapter our efforts towards the development of this synthetic route will be described.

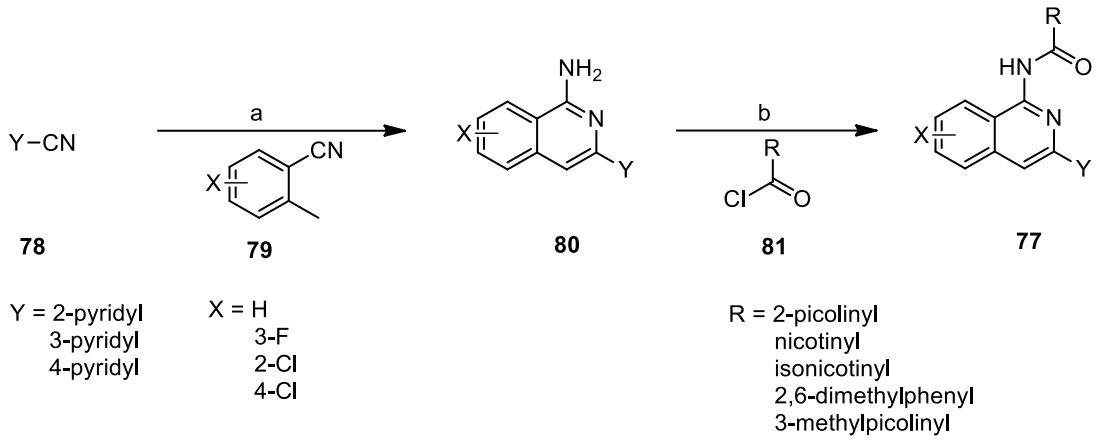

Scheme 22: *Reagents and conditions*: a) KOtBu, toluene, 110 °C; b) i) nBuLi, -10 °C ii) ArCOCl, -10 °C.

6.1. Properties of MMV1581558 and preliminary SAR data

Researchers at the University of Pretoria screened the MMV PRB and identified the multistage and transmission-blocking hit compound MMV1581558 **76**, **Figure 46**, which demonstrated promising activity against stage IV/V gametocytes (IC_{50} 130 nM).[22] At this stage the exact mode of action is not known, but mode of action studies are being considered as part of a broader project. Although active, limitations of this hit compound included a low solubility (< 5 µM at pH 6.5) as well as cytotoxicity concerns (CHO IC_{50} = 0.99 µM). The hit compound also displayed limited microsomal stability (CL_{int} = 90.7/32.2/90.4 µg/min/mg (h/r/m)). To this end, this project will focus on synthesising analogues to contribute to the development of SAR data for MMV1581558 **76** and attempt to address some of these concerns. We will explore variations in the isoquinoline ring substituents, X; the pyridyl functional group, Y; and the amide substituent R (**77**, **Scheme 22**). This is part of a larger project, where additional

variations in the X, Y and Z substituents are being considered by co-workers and will not be reported in detail here. However, preliminary data for a small subset of analogues **82** is included in **Figure 60**. Some other modifications by co-workers also included exploring structures where (X = 2,6-dimethyl, Y = 2-pyridyl and Z = MeNHC=O) and (X = H, Y = 2-pyridyl and Z = NHC=O).

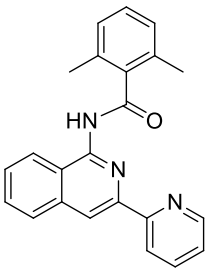

76 IC_{50} 130 nM (stage IV/V gametocytes)
Solubility pH 6.5 (μM) < 5
Cytotoxicity CHO IC50 = 0.99 μM
CLint 90.7/ 32.2/ 90.4 μg/ min/ mg (h/r/m)

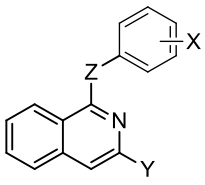

82

				(stage IV/V gametocytes)
82a	X = 2,6-dimethyl,	Y = H,	Z = NHC=O,	IC_{50} 183 nM
82b	X = 2-methyl,	Y = 2-pyridyl,	Z = NHC=O,	IC_{50} 136 nM
82c	X = 2-methyl,	Y = 2-pyridyl,	Z = MeNHC=O,	IC_{50} 264 nM
82d	X = 2,6-dimethyl,	Y = H,	Z = $NHCH_2$,	IC_{50} >4000 nM
82e	X = 2,6-dimethyl,	Y = H,	Z = $N(Me)CH_2$	IC_{50} >9000 nM

Figure 60: Structure of MMV1581558 (76) and general structures of isoquinoline derivatives (82) with IC_{50} values.

These compounds **82** were prepared in order to determine the minimum pharmacophore and this process is still underway, with additional analogues being prepared and solubility and cytotoxicity testing not completed as yet. However, the preliminary results obtained showed promising gametocyte inhibitory activity for compounds **82a-c** bearing an amide linker with IC_{50} values against stage IV/V gametocytes in the range of 183 – 264 nM (**Figure 60**). Not surprisingly, compound **82b** showed the best inhibitory activity (IC_{50} 136 nM), which is very similar to what was observed for the hit compound **76** (IC_{50} 130 nM), as **82b** and **76** differ by only one methyl group. Interestingly, compound **82a** which lacked the 2-pyridyl group still showed promising inhibitory activity (IC_{50} 183 nM) and related analogues are being considered by co-workers in our laboratory. Compounds that did not possess an amide linker (compounds **82d-e**) demonstrated a large decrease in activity (IC_{50} >4000 nM and >9000 nM respectively). This confirmed the significance of the amide linker for inhibitory activity against stage IV/V gametocytes. It must be mentioned that as this is early stage SAR we do however need more information before drawing conclusions as to what features are essential for biological activity. Early SAR not included here also showed compound **80** (where X = H and Y = 2-pyr), **Scheme 12**, as active (IC_{50} 200nM). Currently, the potential for these compounds to portray ion chelation is being conducted.

In this project therefore, we have planned to maintain the amide linker in the analogues to be synthesised (**77**) and primarily focus on variations in the isoquinoline ring substituents by introducing halogens, X (in the hope of improving microsomal stability); and introducing varying pyridyl groups for the R and Y substituents (to modify solubility) (**77**, **Scheme 22**). The compounds proposed for this project (**77**) will potentially demonstrate improved pharmacokinetic properties while maintaining good gametocidal activity.

6.2. Approaches to the synthesis of the isoquinoline core

The formation of the isoquinoline core is an important step to achieve the synthesis of the final compounds **77** (**Scheme 22**). A number of successful methods using metal catalysts to synthesise isoquinoline derivatives have been reported in literature and only a few will be highlighted herein. A method reported by Roesch *et al.* utilised two catalysts in their synthetic procedure, **Scheme 23** step *a*.

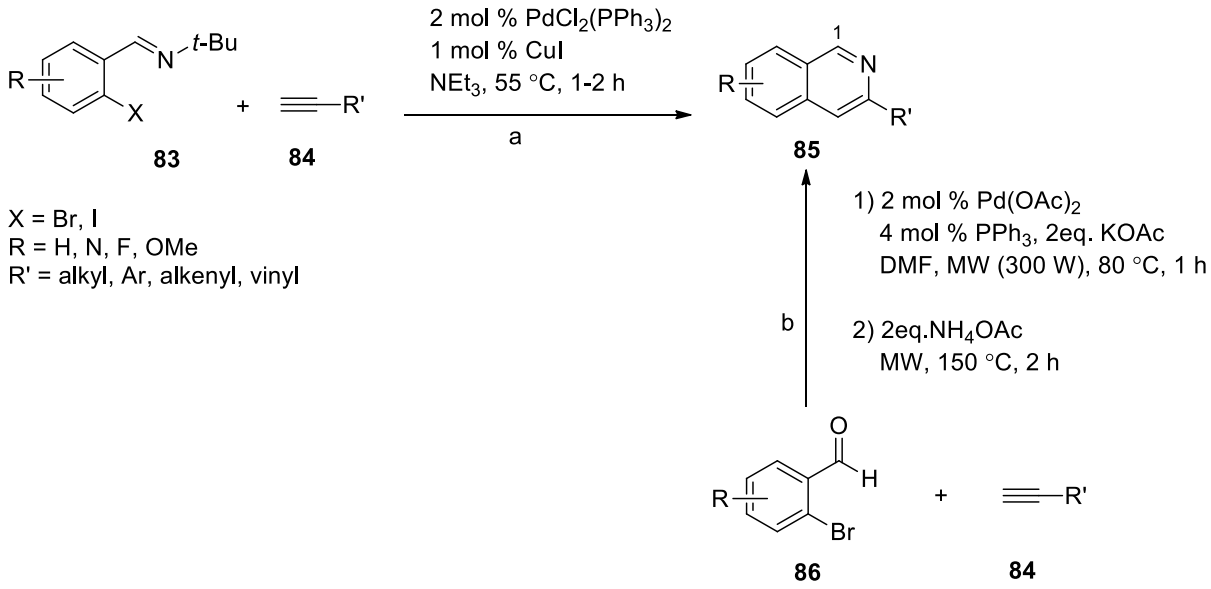

Scheme 23: Reported catalyst dependant isoquinoline synthesis.[113,114]

In their approach, a palladium-catalyzed coupling of the *tert*-butylimine **83** of *o*-iodobenzaldehyde with aryl- and alkenyl-substituted terminal acetylenes **84** is initially performed, followed by a copper-catalyzed cyclization to produce isoquinolines **85** in high yields of 72-91 % in relatively short reaction times of 1-2 hours.[113] The synthesis of compound **85** was also reported by Yang *et al.* (**Scheme 23** step *b*). In this case, sequential coupling-imination-annulation reactions of ortho-bromoarylaldehydes **86** and terminal alkynes **84** with ammonium acetate in the presence of a palladium catalyst, and under microwave irradiation,

produced various substituted isoquinolines, in moderate to good yields of 38-86 %.[114] Although the synthesis protocols described demonstrated promising results, these routes did not afford isoquinolines functionalised at C-1. Many other similar synthetic approaches can be utilised to prepare C-1 unsubstituted isoquinolines.[115–117] However, for the compounds of interest in this project, an amino substituent is required at C-1. To the best of our knowledge, there is only one method reported that introduces an amino substituent at C-1 on an already prepared isoquinoline.[118] This method by Tezuka *et al*. involves reacting a simple isoquinoline **87** with *N*-benzyloxyamine in the presence of a copper catalyst in THF to afford the 1-aminoisoquinoline compound **88** in high yields of 87 %, **Scheme 24**.

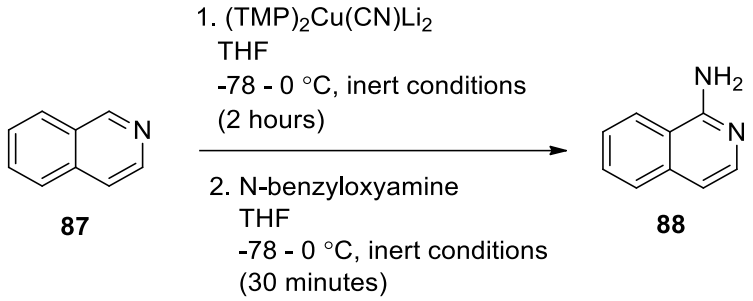

Scheme 24: 1-aminoisoquinoline synthesis.[118]

Although promising, this method has only been reported for simple isoquinolines and although this protocol may be successful in conjunction with the methodologies reported in **Scheme 23**, too many steps will be required to synthesise the substituted 1-aminoisoquinoline compounds we desire.

To achieve the synthesis of isoquinolines functionalised at C-1 with the desired amino group, alternative synthetic methods had to be considered. An approach utilized by de Zwart *et al*.[119] is shown in **Scheme 25**.

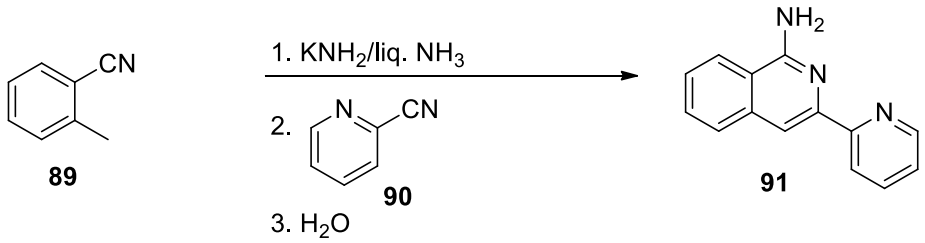

Scheme 25: Reported synthesis of 1-amino-3-(2-pyridyl)isoquinoline.[119]

In their synthetic approach potassium amide is prepared *in situ* by adding potassium metal at -33 °C to liquid ammonia. This is subsequently reacted with *o*-tolunitrile **89** followed by 2-

pyridine carbonitrile **90** to afford the 1-amino-3-(2-pyridyl)isoquinoline **91** in a 60 % yield. This approach was promising; however, our concern was with the hazards associated with the use of potassium metal, particularly should the process need to be carried out on a larger scale.

Alternatively, a method reported by Long *et al*. (**Scheme 26**) involving gold (III)-mediated domino reactions from readily available 2-alkynylbenzamides **92** and ammonium acetate in acetonitrile at reflux generated products **93** in good yields of 54-95 %.[120]

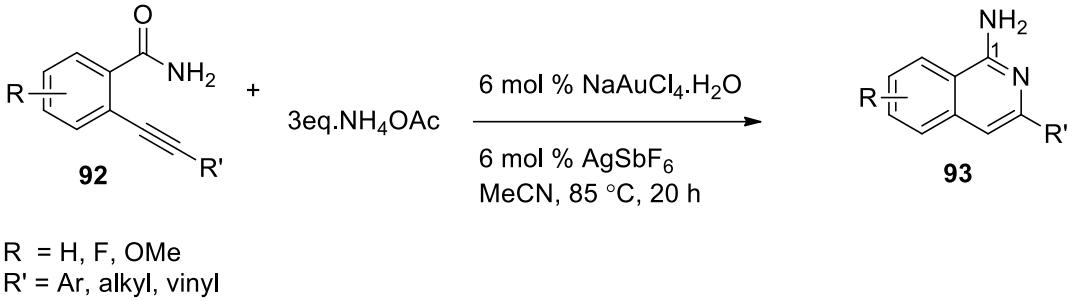

Scheme 26: Metal catalysed synthesis of 1-aminoisoquinoline.[120]

Although the reported synthesis for compound **93** yielded excellent results, the amide precursors would have to be prepared in several steps and there were concerns with the cost effectiveness of the approach. Therefore, a more direct method to yield the desired 1-aminoisoquinoline was investigated. Fortunately, a catalyst free base-mediated cyclization reaction has been reported by Feng *et al.*[121] This method, based on the original synthesis reported by de Zwart *et al.* (**Scheme 25**) involved reacting a substituted *o*-tolunitrile with a substituted benzonitrile in the presence of the base KO^{t}Bu, and afforded 1-aminoisoquinoline products in moderate to high yields of 35 – 81 % (**Scheme 27**).

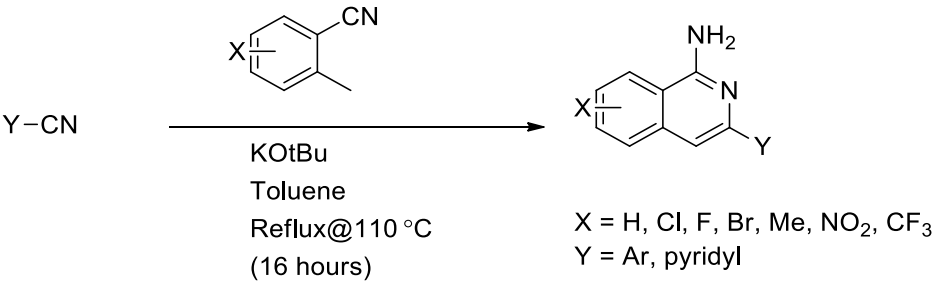

Scheme 27: Reported synthesis of substituted 1-aminoisoquinolines.[121]

This approach had also been reported by Feng and co-workers in a methodology paper for the synthesis of 1-amino-isoquinolines bearing 3- and 4-pyridyl Y substituents, however, did not include the 2-pyridyl variant. However, this method utilised readily available starting materials

in a multicomponent fashion and seemed to be a suitable option for our synthesis. The advantage of this approach is the use of multicomponent coupling reactions which are atom economical and utilise readily or commercially available starting materials.[48] Additionally, various X and Y substituents can be used in the same synthetic approach to generate a variety of products. Furthermore the use of KO^{t}Bu in place of the potassium metal used in the original synthesis (**Scheme 25**), makes this synthetic approach amenable to larger scale processes.

We therefore embarked on the synthesis of our key intermediate 1-aminoisoquinolines **80** using KO^{t}Bu in a method that was previously reported by Feng *et al*. on a set of similar analogues.[121] (**Scheme 27**).

6.3. Synthesis of 3-substituted-1-amino-isoquinolines (80)

As shown in **Scheme 28**, this base-mediated cyclization reaction between a substituted *o*-tolunitrile and a substituted benzonitrile could be used to introduce variations in both the X and Y substituents of our key 1-aminoisoquinolines **80**, **Scheme 28**.

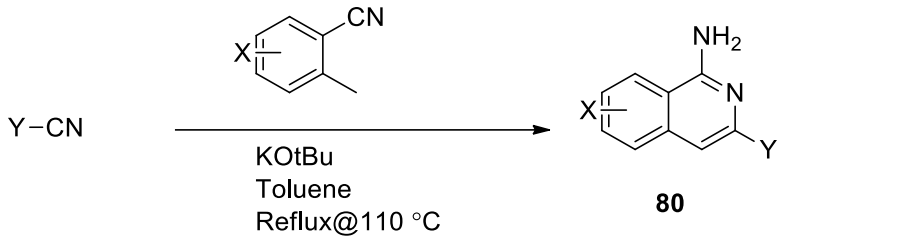

80a; X = H, Y = 2-pyridyl
80b X = 7-F, Y = 2-pyridyl
80c X = 6-Cl, Y = 2-pyridyl
80d X = 8-Cl, Y = 2-pyridyl
80e X = H, Y = 3-pyridyl
80f X = H, Y = 4-pyridyl

Scheme 28: Cyclization reaction forming 3-substituted-1-amino-isoquinoline (80).

The proposed mechanism of this reaction in relation to our compounds is illustrated in **Scheme 29**.

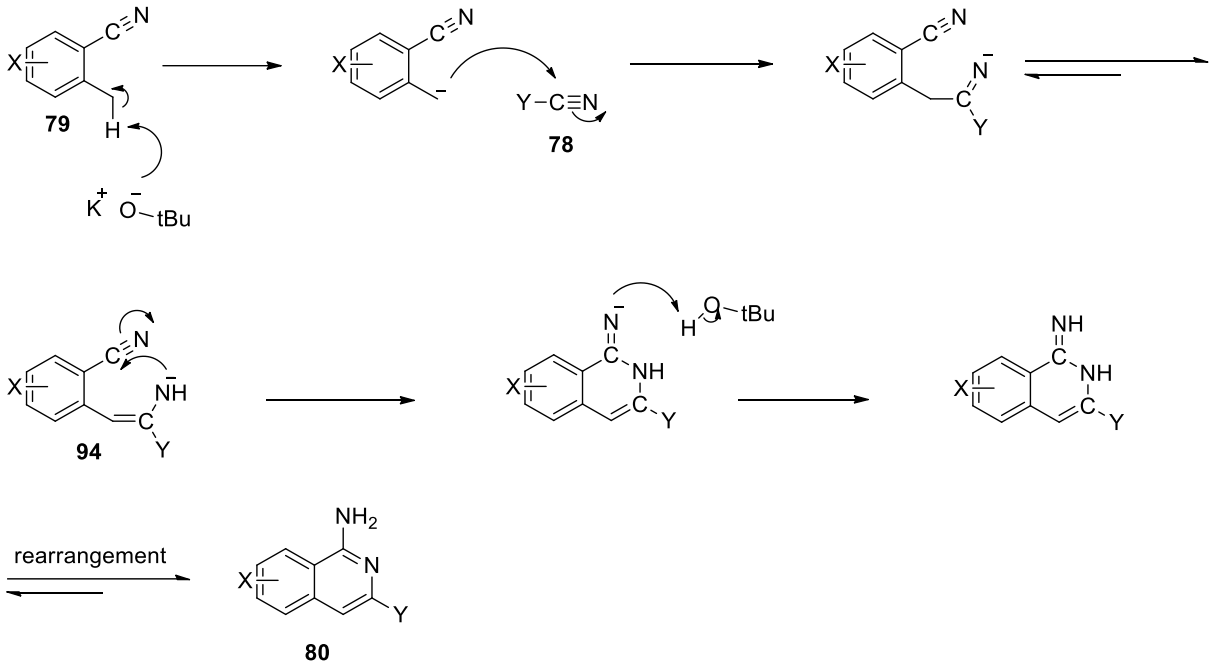

Scheme 29: Proposed mechanism of formation of 3-substituted-1-amino-isoquinoline (80), and analogues.

In the proposed mechanism, the base KO^{t}Bu deprotonates the substituted *o*-tolunitrile **79**, which then performs a nucleophilic addition on the substituted carbonitrile **78**. A substituted aminovinyl benzonitrile intermediate **94** is formed which cyclizes via an intramolecular nucleophilic attack on the carbon of the nitrile functional group, which subsequently rearranges to the desired substituted 1-aminoisoquinoline **80**.

In this project we propose to synthesise **80** where X = H, F and Cl and Y = 2-pyridyl, 3-pyridyl and 4-pyridyl and utilise theses aminoisoquinolines to prepare analogues of the hit compound **76**. Variations in these substituents may modify the pharmacokinetic properties associated with the solubility and cytotoxicity of the hit compound mentioned previously.

6.3.1. Synthesis of 3-(pyridin-2-yl)isoquinolin-1-amine and halogenated analogues[119]

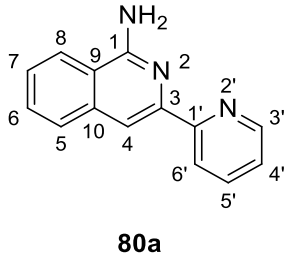

Figure 61: Structure of 3-(pyridin-2-yl)isoquinolin-1-amine (80a).

To test the cyclization reaction proposed in **Scheme 28**, 3-(pyridin-2-yl)isoquinolin-1-amine **80a** was synthesised. This compound is the precursor to the hit compound **76** which we aimed to synthesise first to test our methodology. A base-mediated cyclization reaction for the synthesis of compound **80a** was achieved by reacting 2-pyridine carbonitrile and *o*-tolunitrile under basic conditions, in distilled toluene in a pressure tube. This reaction mixture was heated to reflux for 3 hours to afford the desired compound **80a**, **Figure 61**. The reaction time was varied between 1 and 24 hours and runs were monitored by TLC in an attempt to optimise conversion to the desired product. However, it was observed that extending the reaction beyond 3 hours did not improve the product yields, hence we decided to run the reaction for 3 hours. After this time, the product was purified by recrystallisation from MeOH, isolating a brown solid with a melting point of 158-159 °C and in a 63 % yield. This methodology affords the product **80a** in a slightly improved yield to that reported by de Zwart *et al.*[119] who reported a yield of 60 % for the same product and a melting point of 152-153 °C.

In the ^{1}H NMR spectrum, all aromatic protons assigned to the isoquinoline core and 2-pyridyl substituent were observed in the aromatic region, as expected. A multiplet signal due to H-6' was observed at δ 8.64 – 8.60 ppm, while proton H-3' gave rise to a doublet signal at δ 8.29 ppm. The aromatic proton H-4 produced a singlet signal at δ 8.07 ppm, and confirmed the successful intermolecular cyclization between 2-pyridine carbonitrile and *o*-tolunitrile to form the isoquinoline core, since no alkyl CH_3 signal belonging to the *o*-tolunitrile was present in the aliphatic region. The multiplet signal at δ 7.78 – 7.67 ppm integrating for 3 protons was due to protons H-6, H-8 and H-5'. Other multiplet signals at δ 7.57 – 7.50 ppm and δ 7.43 – 7.37 ppm were assigned to protons H-5 and H-7 respectively, while proton H-4' was observed as a multiplet signal at δ 7.20 – 7.14 ppm. A characteristic singlet signal integrating for two protons was observed for NH_2 at δ 5.22 ppm. For further confirmation, the ^{13}C NMR spectrum was analysed. Carbons C-1, C-3 and C-4 gave rise to peaks at δ 156.9, 148.1 and 110.3 ppm respectively, confirming the formation of the isoquinoline core. Carbon C-1', which links the isoquinoline core to the pyridyl group was observed as a peak at δ 155.9 ppm. The remaining aromatic carbons were observed in the region of δ 149.4 to 118.1 ppm, as expected. The IR spectrum also showed the presence of the NH_2, aromatic CH, C-N and aromatic C=C with bands visible at 3309, 3055, 1378 and 1569 cm^{-1} respectively.

The reaction was repeated using conventional heating in a round-bottomed flask under a nitrogen atmosphere to see how this would affect the yield of the product. However, these conditions did not yield much success in forming the desired product, but interestingly,

favoured the formation of the homo-coupled product, 3-(*o*-tolyl)isoquinolin-1-amine **95**, **Figure 62**, which was formed by *o*-tolunitrile reacting with itself. The homo-coupled product was isolated with minor contaminants, however, ^{1}H and ^{13}C NMR spectroscopy confirmed the formation of **95** by the CH_3 signal observed as a singlet signal integrating for three protons at 2.29 ppm on the ^{1}H NMR spectrum and 21.59 ppm on the ^{13}C NMR spectrum. This side reaction has been reported by Feng *et al.* for the multicomponent reactions of *o*-tolunitrile with substituted benzonitriles.[121] Fortunately the homo-coupled product was formed in negligible quantities in our reaction carried out in a pressure tube.

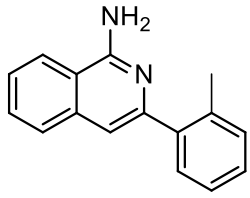

95

Figure 62: Structure of 3-(*o*-tolyl)isoquinolin-1-amine (95).

We also discovered that this reaction is sensitive to the quality of KO^{t}Bu, as cleaner reactions were obtained when freshly sublimed KO^{t}Bu was used affording higher yields of product. More by-products were observed by TLC if the base was not sublimed prior to use.

With the success of this reaction, analogues with variations in the isoquinoline ring, X, were prepared using substituted *o*-tolunitriles, while keeping the 2-pyridyl, Y, substituent constant, **Scheme 30**. Using the same reaction conditions proposed in **Scheme 28**, 1-aminoisoquinoline analogues **80b-d**, were isolated in moderate to high yields ranging from 49-78 %, **Scheme 30**.

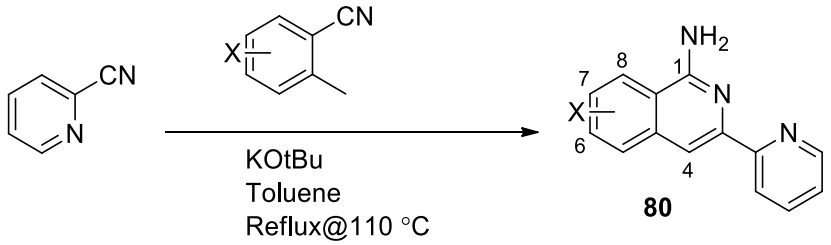

80

80b X = 7-F, 49 %
80c X = 6-Cl, 78 %
80d X = 8-Cl, 73 %

Scheme 30: Synthesis of halogenated 2-pyridyl-1-aminoisoquinolines (80b-d).

Compound **80c**, 6-chloro-3-(pyridin-2-yl)isoquinolin-1-amine, was produced in the highest yield (78 %) by this methodology.

The purified products **80b-d** were characterised using ^{1}H and ^{13}C NMR and IR spectroscopy, HRMS and melting point. **Table 11** summarises the key ^{1}H and ^{13}C NMR spectroscopic signals of these compounds. Additional characterisation data can be found in the experimental section, Chapter 8.

Table 11: Key ^{1}H NMR and ^{13}C NMR spectroscopic signals for analogues 80b-d.

Compound	NH_2 (ppm)	$^{4}\underline{H}$-C=C- (ppm)	$^{1}\underline{C}$-NH_2 (ppm)	$^{4}\underline{C}$=C (ppm)
80b	-	7.88 – 7.78 (m)	158.3	109.6
80c	5.44 (s)	8.00 (s)	156.2	109.1
80d	6.34 (s)	8.06 (s)	156.0	110.0

In the ^{1}H NMR spectra for **80c-d**, a singlet integrating for two protons for the NH_2 group was observed in each case in the regions of 5.44 ppm to 6.34 ppm. This signal was not observed for **80b** due to hydrogen-deuterium exchange with the MeOD solvent. Successful formation of the isoquinoline core was confirmed by proton H-4 in each case, which was observed as a singlet or multiplet in the region of 7.78 – 8.06 ppm in the ^{1}H NMR spectra and in the region of 109.1 to 110.0 ppm in the ^{13}C NMR spectra. The broad N-H band was also observed in a similar region of 3292 - 3360 cm^{-1} for all compounds in the IR spectra and the amine carbon ($\underline{C}$-NH_2) was observed in the characteristic region of 156.0 – 158.3 ppm in the ^{13}C NMR spectra. In each case there was no unreacted starting material observed, and although the homo-coupled product was observed on the TLC, separation of the product from the homo-coupled product was readily achieved during the purification process by silica gel column chromatography.

6.3.2. Synthesis of 3-(pyridin-3-yl)isoquinolin-1-amine (80e)[121]

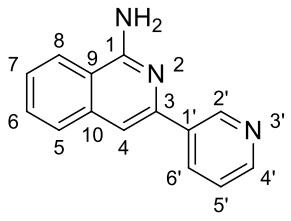

80e

Figure 63: Structure of 3-(pyridin-3-yl)isoquinolin-1-amine (80e).

Having successfully synthesised the 3-(pyridin-2-yl)isoquinolin-1-amine and its analogues with variations in the isoquinoline ring, we decided to use the same method to synthesise

aminoisoquinoline analogues **80**, **Scheme 30**, with variations in the Y substituent. To test the reaction, 3-(pyridin-3-yl)isoquinolin-1-amine **80e** was synthesised. The synthesis of the compound **80e** was achieved using the same base-mediated intermolecular cyclization described for the synthesis of **80a-d**, however, 2-pyridine carbonitrile was now replaced with 3-pyridine carbonitrile. The desired product **80e** was successfully synthesised and purified by silica gel column chromatography, isolating an orange solid in a yield of 35% with a melting point of 144-145 °C. IR spectroscopy confirmed the presence of the key functional groups NH_2, aromatic CH, C-N and aromatic C=C with bands visible at 3328, 3058, 1374 and 1562 cm^{-1} respectively.

The ^{1}H NMR spectrum for product **80e** showed a doublet at δ 9.26 ppm and a doublet of doublets at δ 8.60 ppm which were assigned to protons H-2' and H-6' respectively. Protons H-6 and H-4' gave rise to a doublet of triplets at δ 8.35 ppm and a doublet of quartets at δ 7.82 ppm respectively. A doublet of triplets signal was observed for proton H-8 at δ 7.77 ppm, while multiplet signals in the region of δ 7.68 – 7.35 ppm belonged to the pyridyl proton H-5' and the isoquinoline protons H-5, H-7 and H-4. The singlet signal oberved at δ 5.39 was chracteristic for NH_2. The ^{13}C NMR spectrum gave rise to fourteen carbon signals as expected. Carbons C-1, C-3 and C-4 were observed at δ 156.4, 146.8 and 109.3 ppm confirming the formation of the isoquinoline core. Carbon C-1', which links the isoquinoline core to the pyridyl was observed at δ 135.4 ppm. The remaining aromatic carbons were observed in the region of δ 149.2 to 117.3 ppm, as expected. HRMS gave the desired mass of 222.1143 $[M+H]^{+}$.

6.3.3. Synthesis of 3-(pyridin-4-yl)isoquinolin-1-amine (80f)[121]

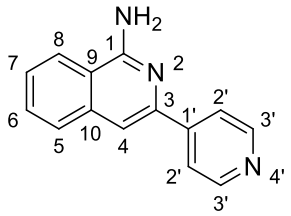

80f

Figure 64: Structure of 3-(pyridin-4-yl)isoquinolin-1-amine (80f).

The synthesis of the compound **80f** was also achieved using the synthetic protocol in **Scheme 30**, however, 4-pyridine carbonitrile was now used in place of 2-pyridine carbonitrile. Compound **80f** was successfully synthesised and purified by silica gel column

chromatography, affording a yellow solid in 33 % yield. HRMS gave rise to a molecular ion with a mass of 222.1145, which corresponds with the expected mass of $C_{14}H_{12}N_3$.

^{1}H NMR spectroscopy confirmed the synthesis of product **80f** as it showed two doublet of doublets signals at δ 8.69 and 7.96 ppm, characteristic of the pyridyl protons H-3' and H-2' respectively. A multiplet signal at δ 7.86 – 7.79 ppm was observed for protons H-6 and H-8, while protons H-5 and H-7 each gave rise to a doublet of doublet of doublets signal at δ 7.67 ppm and δ 7.54 ppm respectively. Finally, a doublet signal integrating for one proton was observed for proton H-4 at δ 7.60 ppm and the singlet signal oberved at δ 5.28 was assigned to NH_2. The ^{13}C NMR spectrum confirmed product formation by showing signals for carbons C-1, C-3 and C-4 at δ 156.3, 147.2 and 110.2 ppm respectively, again confirming that the isoquinoline core had successfully formed. Carbon C-1', which confirms the link between the isoquinoline core and the pyridyl substituent was observed at δ 146.7 ppm. The remaining aromatic carbons were observed in the region of δ 150.3 to 117.9 ppm, as expected. The NMR spectroscopic data reported by Feng *et al.*[121] also compares well with our data. The IR spectrum also showed the presence of the NH_2, aromatic CH, C-N and aromatic C=C functional groups with bands visible at 3321, 3188, 1381 and 1561 cm^{-1} respectively. A melting point of 171-172 °C was also obtained.

Compounds **80e** and **80f** were isolated in lower yields than expected (**80e**, 35 % and **80f**, 33 %) as literature reported slightly higher yields (**80e**, 49 % and **80f**, 54 %).[121] This could be due to the fact that the homo-coupled product was observed on the TLC plate and co-eluted with the majority of products **80e** and **80f** in the purification process by silica-gel column chromatography, and hence decreased yields of the pure products were observed.

In an attempt to successfully isolate **80e** and **80f**, purification by recrystallisation was explored using MeOH, EtOH or EtOAc, but unfortunately, in each case the homo-coupled product and the desired product would both crystallise out. The yields obtained however were sufficient to continue to the next step.

6.4. Synthesis of 2,6-dimethyl-*N*-3-substituted-isoquinolin-1-yl-benzamides (77a-f)

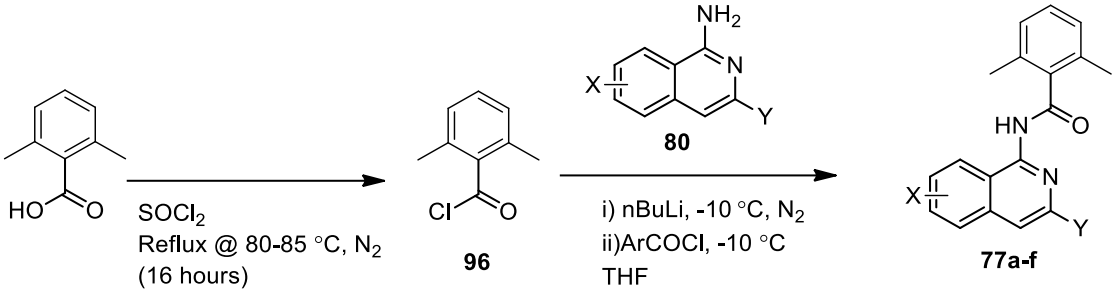

77a X = H, Y = 2-pyridyl
77b X = 7-F, Y = 2-pyridyl
77c X = 6-Cl, Y = 2-pyridyl
77d X = 8-Cl, Y = 2-pyridyl
77e X = H, Y = 3-pyridyl
77f X = H, Y = 4-pyridyl

Scheme 31: Amidation reaction forming 2,6-dimethyl-*N*-3-substituted-isoquinolin-1-yl-benzamide (77a-f)

With the isoquinoline amines **80** in hand, we were in a position to test the final step of the synthesis of our analogues **77**. This step involved an amidation reaction between the isoquinoline amine **80** and a 2,6-dimethylbenzoyl chloride **96** to afford 3-substituted-isoquinolin-1-yl benzamides **77a-f**, **Scheme 31**. As discussed previously, the amide linker plays an essential role in the inhibitory activity of the compounds against stage IV/V gametocytes, therefore this linker will remain unchanged for all the final compounds.

Amidation reactions are well researched in organic synthesis. The reactions are typically performed by reacting an activated carboxylic acid with an amine. These reactions can be achieved by metal mediated methods[122], coupling reagents[123] or by generating an acyl chloride intermediate which is subsequently reacted with an amine in the presence of a base to generate the amide.[124] Leggio *et al.*[122] reported a method that directly forms the amide via a one-pot condensation reaction achieved by reacting a carboxylic acid **97** and an amine **98**, mediated by the $TiCl_4$ in pyridine, with low to high yields of amide product **99** (9 - 98 %) generated (**Scheme 32** step *a*). A synthetic protocol reported by Sheehan *et al.*[123] involved reacting a carboxylic acid **97** and an amine **98** in the presence of the coupling reagent *N,N'*-dicyclohexylcarbodiimide (DCC), using THF as a solvent at room temperature (**Scheme 32** step *b*). A methodology used by Zhang *et al.*[124] incorporated the conversion of the carboxylic acid **97** to an acyl chloride intermediate **100** which is reacted with an amine **98** in the presence of a base. Some of the bases used in this synthetic protocol included Et_3N, Na_2HPO_4 and K_3PO_4, which produced the better results with yields up to 99 % (**Scheme 32** step *c*).

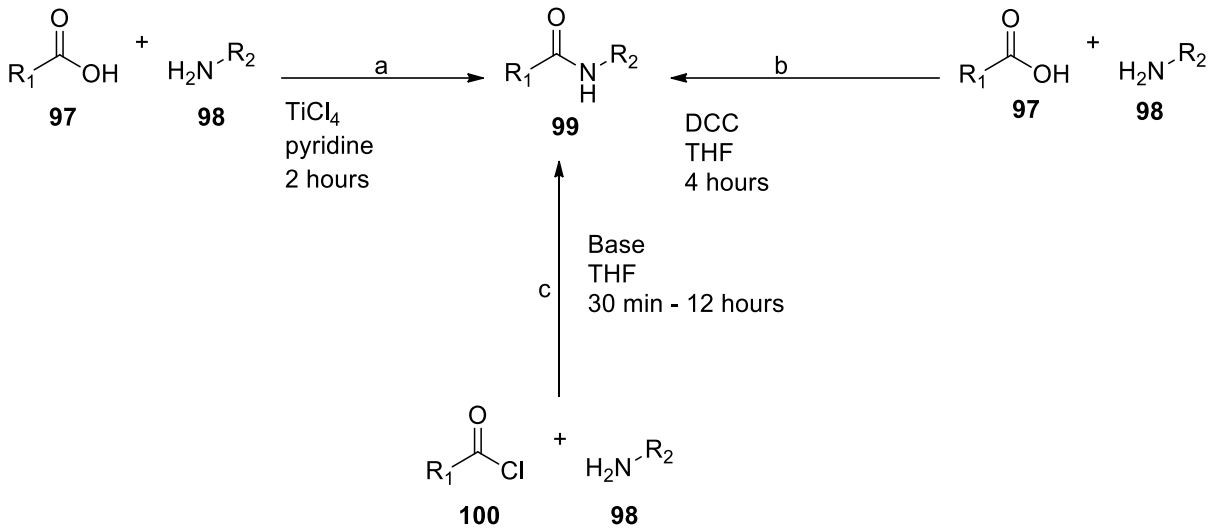

Scheme 32: Amidation synthetic protocols.

The method reported by de Zwart *et al.* in 1988 to synthesise the hit compound and similar amide analogues was similar to Zhang *et al*. in that they generated the acyl chloride intermediate of the carboxylic acid, however, they utilised n-BuLi as a base (**Scheme 31**).[119] We therefore explored and optimised this method for the synthesis of our compounds.

Scheme 33 illustrates the proposed mechanism of this amidation reaction in relation to our compounds.

In the proposed mechanism shown in **Scheme 33**, n-BuLi acts as a base and deprotonates the amine on compound **80**. This results in the amine becoming more nucleophilic and hence undergoes a nucleophilic addition to the highly electrophilic acyl chloride **81**, which eliminates a chloride to afford the amide **77**.

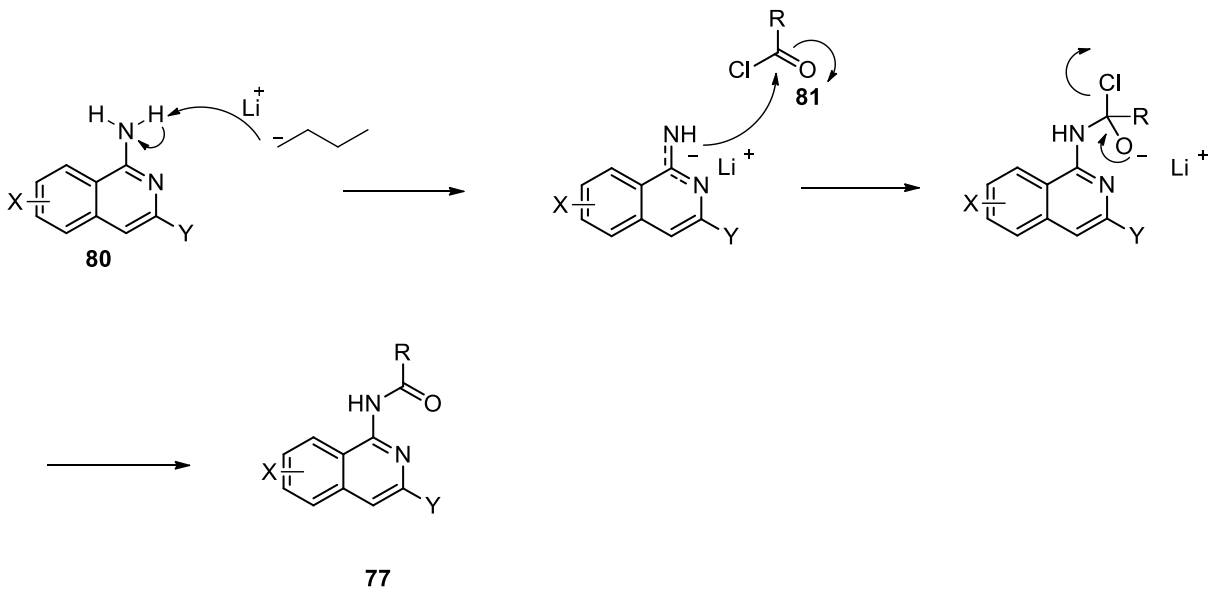

Scheme 33: Proposed mechanism for amidation reaction.

6.4.1. Synthesis of 2,6-dimethyl-*N*-(3-(pyridin-2-yl)isoquinolin-1-yl)benzamide (77a)

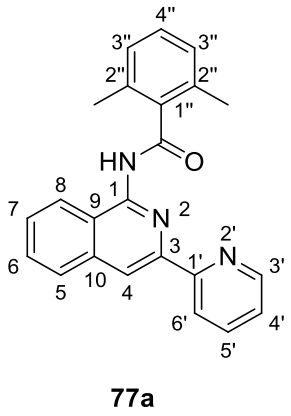

77a

Figure 65: Structure of 2,6-dimethyl-*N*-(3-(pyridin-2-yl)isoquinolin-1-yl)benzamide (52a).

To test the proposed amidation reaction, the hit compound **77a** was synthesised from **80a** and 2,6-dimethylbenzoyl chloride. We first formed the 2,6-dimethylbenzoyl chloride by dissolving 2,6-dimethylbenzoic acid in excess thionyl chloride and running the reaction at reflux overnight under a nitrogen atmosphere. After this time, the remaining thionyl chloride was removed *in vacuo* to isolate the 2,6-dimethylacyl chloride. In a separate, three-necked, round bottomed flask, the isoquinoline amine **80a** was dissolved in THF and the reaction mixture subsequently cooled to -10 °C. This was followed by the addition of n-BuLi to the reaction and left to stir for 10 minutes. Following the method reported by de Zwart *et al.*[119] the 2,6-dimethylbenzoyl chloride was dissolved in THF, added to the reaction mixture and was left to stir at -10 °C for

1 hour. The desired product was isolated and purified by recrystallisation from MeOH, yielding 9 % of a pale brown solid product **77a** with a melting point of 232-233 °C. This low yield corresponded with that reported in the literature (9 %) and the melting point reported in literature was 232-233 °C.[119] Fortunately, we were able to optimise this yield by adding the neat acyl chloride directly to the amine/THF solution, which improved the yield to 22 %.

The NMR spectra obtained for compound **77a** were unsatisfactory when run at room temperature, as peaks in the ^{1}H NMR spectrum were not resolved, and the required ^{13}C NMR spectroscopic signals were not visible. We postulated that this is likely due to restricted rotation about the amide bond. To confirm product formation, we therefore assessed the sample using HRMS of which the expected product mass of 354.1555 $[M+H]^{+}$ was found. We then obtained a crystal structure by single crystal X-ray diffraction, **Figure 66**, for further confirmation. To our delight, the crystal structure clearly showed our desired product in the geometric conformation of a *cis*-amide.

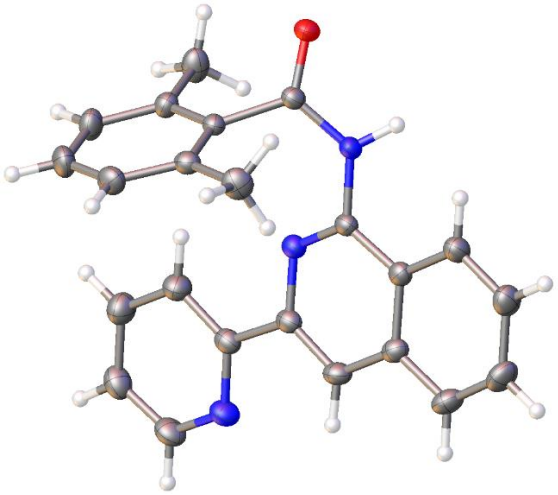

Figure 66: Crystal structure of synthesised hit compound (77a).

After this confirmation we then utilised variable temperature NMR spectroscopy to determine if there was indeed restricted rotation about the amide bond. Spectra were obtained using eight different temperatures, ranging from 30 °C to 100 °C to achieve the best resolution. It was then observed that temperatures of 70 - 100 °C were required in order to obtain spectra with good resolution. **Figure 67** shows the difference in resolution in the ^{1}H NMR spectra run at 30 °C (**Figure 67_4**), 40 °C (**Figure 67_3**), 70 °C (**Figure 67_2**) and 100 °C (**Figure 67_1**).

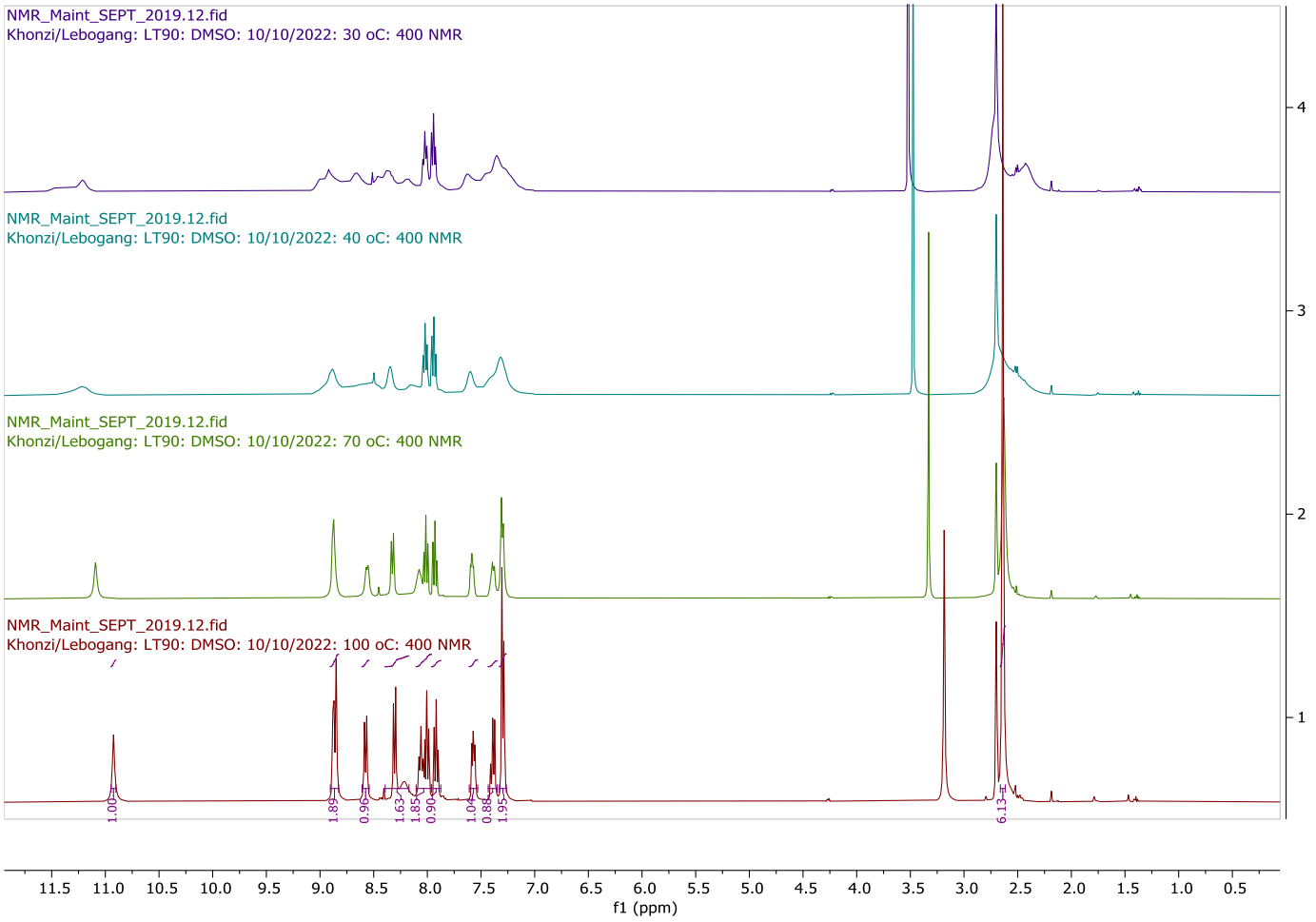

Figure 67: ^{1}H NMR spectra at 30 °C (_4), 40 °C (_3), 70 °C (_2) and 100 °C (_1) for compound 77a.

As a result of the amide rotating on an NMR time scale, the formation of two sets of NMR signals are observed at room temperature affording a *cis* and *trans* conformer of the product **77a**.[125] The consequence of this is seen in the ^{1}H NMR spectrum at 30 °C (**Figure 67_4**) where there are two singlet signals in the region of 11.0 ppm to 11.5 ppm due to the NH proton of the two isomers. This becomes more apparent in the aromatic region from 7.0 ppm to 9.5 ppm with the presence of the highly unresolved signals (**Figure 67_4** and **Figure 67_3**). At high temperatures (**Figure 67_2** and **Figure 67_1**) however, this is not the case because the rotation increases therefore making the signals non-distinguishable on an NMR time scale [125] hence producing a spectrum with better resolution.

The high temperature ^{1}H NMR spectrum of **77a** showed a singlet signal integrating for one proton at δ 10.72 ppm, this was characteristic of the NH group. This was a key signal to observe as this confirmed the successful formation of the amide bond. The other important signal we observed that confirmed product formation was the singlet signal at δ 2.44 ppm which integrated for six protons and confirmed the presence of the two CH_3 substituents. A multiplet signal at δ 8.71 – 8.60 ppm integrating for two protons was assigned to H-8 and H-5'. The pyridyl protons H-6' and H-3' each gave rise to two doublet signals at 8.38 ppm and 8.11 ppm respectively. A singlet signal observed at δ 8.02 ppm belonged to proton H-4, while the multiplet signal at δ 7.90 – 7.77 ppm from protons H-6 and H-7 was also observed. A doublet of doublets of doublets signal due to H-5 was visible at δ 7.72 ppm and multiplet signals at δ 7.41 – 7.33 ppm and δ 7.23 – 7.16 ppm were assigned to protons H-4'' and H-4' respectively. The equivalent protons H-3'' gave rise to a doublet signal which was observed at δ 7.10 ppm. The ^{13}C NMR spectrum showed the key C=O signal at δ 172.1 ppm confirming successful product formation. Furthermore, the two CH_3 groups gave rise to a signal in the aliphatic region at δ 18.5 ppm as expected. Carbons C-1, C-3 and C-4 were observed as peaks at δ 169.6, 147.2, 120.2 ppm respectively, confirming that the isoquinoline core had been maintained. Although a shift was observed for C-1'owing to the amidation, the signal for C-1' was observed at δ 148.8 ppm. Each pair of equivalent carbons, C-2'' and C-3'' gave rise to signals observed at δ 148.7 ppm and δ 126.6 ppm respectively. The remaining aromatic carbons were observed in the region of δ 155.0 to 114.9 ppm, as expected. IR spectroscopy further confirmed the formation of the product by displaying NH, aromatic CH, C-N, aromatic C=C and importantly, C=O bands at 3290, 3056, 1255, 1596 and 1646 cm^{-1} respectively.

In an attempt to improve the yields further, longer reactions times were explored and different bases, Et_3N and K_2CO_3 were used (from the method reported by Zhang *et al.*[124]) as they were readily available. This was not successful however as by-products formed in each case which made purification challenging and offered undesirable yields. Significantly, the reaction does not go to completion, and a large portion of the isoquinoline amine **80** remains unreacted as observed by TLC and can be recovered during purification by column chromatography. The reason for this could be attributed to the low nucleophilicity of this amine and the bulkiness of the 2,6-dimethylbenzoyl chloride which is potentially causing steric hindrance.

The success of this reaction however, enabled us to apply this method to the synthesis of the remaining analogues bearing a 2,6-dimethylbenzamide substituent, **77b-f**. These analogues were also prepared in moderate yields (14 – 24 %) and were purified by either recrystallisation

or column chromatography. Compound **77b** was recrystallised from EtOAc, while compounds **77c** and **77d** were recrystallised from MeOH and EtOH respectively. Compounds **77e-f** were purified by silica gel column chromatography using 50 % EtOAc/hexane as the eluent.

The characterisation of the purified products **77b-f** was performed using ^{1}H and ^{13}C NMR spectroscopy, IR spectroscopy, HRMS and melting point. **Table 12** summarises key ^{1}H and ^{13}C NMR spectroscopic signals for compounds **77b-f**. These compounds **77b-f**, are all novel as none have been reported in literature. Additional characterisation data can be found in the experimental section, Chapter 8.

As illustrated in **Table 12**, in each case, the NH protons produce a singlet signal in the expected region of 10.38 – 11.02 ppm in the ^{1}H NMR spectra. Furthermore all compounds **77b-f** produce a singlet signal integrating for 6 protons in the region of 2.40 – 2.43 ppm in the ^{1}H NMR spectra characteristic of the two CH_3 groups. The ^{13}C NMR spectra show a peak in the region of 169.1 – 169.7 ppm for all compounds **77b-f** and this was assigned to the carbonyl carbon (<u>*C*</u>=O) of the compounds. All the compounds were high melting solids in the range of 196 - 268 °C, with compound **77b** having the highest melting point of 267 – 268 °C.

Table 12: Yields and key ^{1}H and ^{13}C NMR spectroscopic signals for novel compounds 77b-f.

Compound	Temp. (°C)	Structure	NH (ppm)	2 x C<u>*H*₃</u> (ppm)	<u>*C*</u>=O	Yield (%)
77b	90	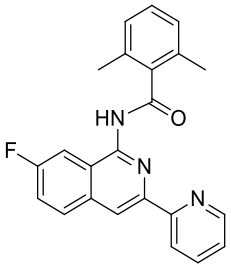	10.81 (s)	2.43 (s)	169.6	24
77c	90	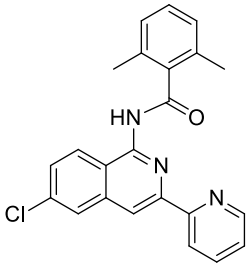	10.84 (s)	2.42 (s)	169.7	22
77d	90	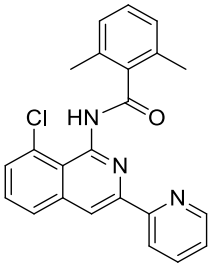	10.38 (s)	2.44 (s)	169.1	14
77e	90	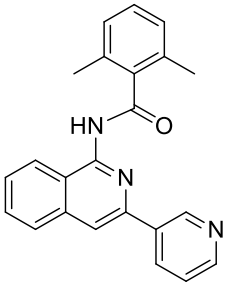	10.87 (s)	2.40 (s)	169.6	17
77f	70	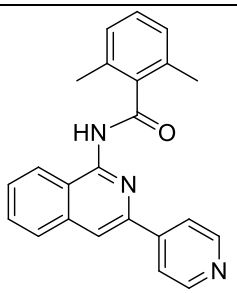	11.02 (s)	2.40 (s)	169.6	14

6.4.2. Synthesis of 3-methyl-*N*-(3-(pyridin-2-yl)isoquinolin-1-yl)picolinamide (77g)

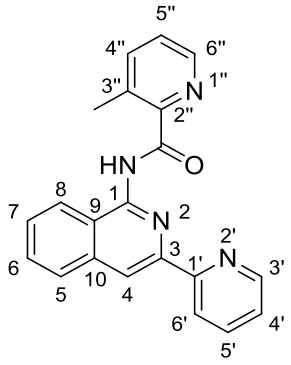

77g

Figure 68: Structure of 3-methyl-*N*-(3-(pyridin-2-yl)isoquinolin-1-yl)picolinamide (77g).

Following the successful synthesis of the novel 2,6-dimethylbenzamide analogues **77a-f**, we explored synthesising other novel analogues that bear a nitrogen heteroatom in the benzamide R-group. First we explored the synthesis of the monomethylated analogue bearing a nitrogen heteroatom, 3-methyl-*N*-(3-(pyridin-2-yl)isoquinolin-1-yl)picolinamide **77g** (**Figure 68**). The synthesis of compound **77g** was achieved using the same optimised conditions and procedures for the amidation reaction described in **Scheme 31**. A successful reaction between 3-methylipicolinic acyl chloride and the aminoisoquinoline **80a** afforded the desired product, 3-methyl-*N*-(3-(pyridin-2-yl)isoquinolin-1-yl)picolinamide **77g**. Compound **77g** was purified by silica gel column chromatography, affording a yellow solid in a 23% yield. This was confirmed by IR spectroscopic bands of the NH, aromatic CH, C=N, aromatic C=C and C=O functional groups being observed at 3338, 3048, 1624, 1565 and 1686 cm^{-1} respectively as expected in the IR spectrum. The molecular ion $[M+H]^+$ observed by HRMS had the desired mass of 341.1409.

In the ^1H NMR spectrum, overlapping signals of NH and proton H-6' gave rise to a multiplet observed at δ 8.70 – 8.64 ppm therefore confirming successful amide bond formation. Another key signal observed was a singlet at δ 2.80 ppm which integrated for three protons, which was characteristic of the CH_3 group. A multiplet signal integrating for two protons observed at δ 8.59-8.49 ppm was assigned to protons H-4 and H-6'', while doublet signals were observed for protons H-8 and H-3' at δ 8.14 ppm and δ 7.94 ppm respectively. Proton H-4'' gave rise to a triplet signal at δ 7.83 ppm, while a multiplet signal was also observed at δ 7.70 – 7.63 ppm for protons H-5 and H-5'. Two triplet signals due to each of the protons H-5'' and H-7 were observed at δ 7.59 ppm δ 7.28 ppm respectively. A doublet of doublets observed at δ 7.38 ppm

was characteristic of proton H-6. Proton H-4' gave rise to a multiplet at δ 7.22 – 7.16 ppm. The ^{13}C NMR spectrum provided further confirmation of a successful synthesis as the C=O signal was observed at δ 164.4 ppm. Furthermore, the signal observed at δ 21.1 ppm was characteristic of the CH_3 group. Carbons C-1, C-3 and C-4 were observed at δ 155.6, 146.7 and 116.4 ppm respectively, confirming that the isoquinoline core was still maintained. The signal due to carbon C-1' was observed at the expected value of δ149.4 ppm. The remaining aromatic carbons were observed in the region of δ 148.7 to 120.5 ppm, as expected. A melting point of 128-129 °C was obtained.

6.4.3. Attempted synthesis of *N*-(3-(pyridin-2-yl)isoquinolin-1-yl)picolinamide (77h)

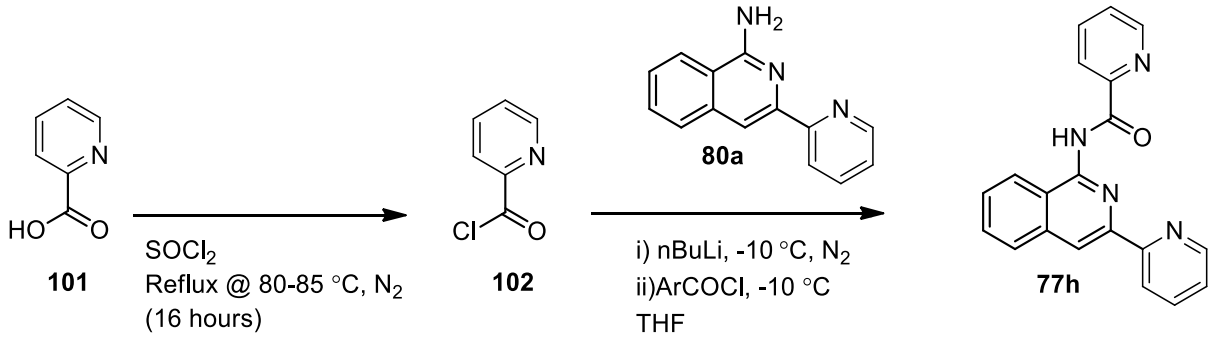

Scheme 34: Attempted synthesis of *N*-(3-(pyridin-2-yl)isoquinolin-1-yl)picolinamide (77h)

A successful synthesis of novel compound **77g** prompted us to continue with the same synthetic protocol to synthesise a variety of pyridyl containing amides. To test the reaction, 2-picolinic acid **101** was converted to 2-picolinoyl chloride **102** which was reacted with the aminoisoquinoline **80a** to afford the novel compound *N*-(3-(pyridin-2-yl)isoquinolin-1-yl)picolinamide **77h**. The reaction was successful but low yielding (12 %). This was concerning because higher yields were expected due to this compound not having a methyl substituent ortho to the acyl chloride to cause steric hindrance as was observed for compounds **77a-f** bearing the 2,6-dimethylbenzamide and for **77g** bearing a single methyl substituent. Purification of the final compound also proved challenging.

This result prompted us to look for an alternative way to synthesise the desired compound **77h**. Many coupling agents have been used for the formation of amide bonds directly from carboxylic acids. One such approach uses the well-known *N,N'*-dicyclohexylcarbodiimide (DCC) **103** initially reported by Sheehan *et al.*[123] in 1955. This approach uses DCC **103** to activate the carbonyl of a carboxylic acid **97**, which is subsequently reacted with an amine **98**

to afford the desired amide product **99**. **Scheme 35** shows the proposed general mechanism for this reaction.

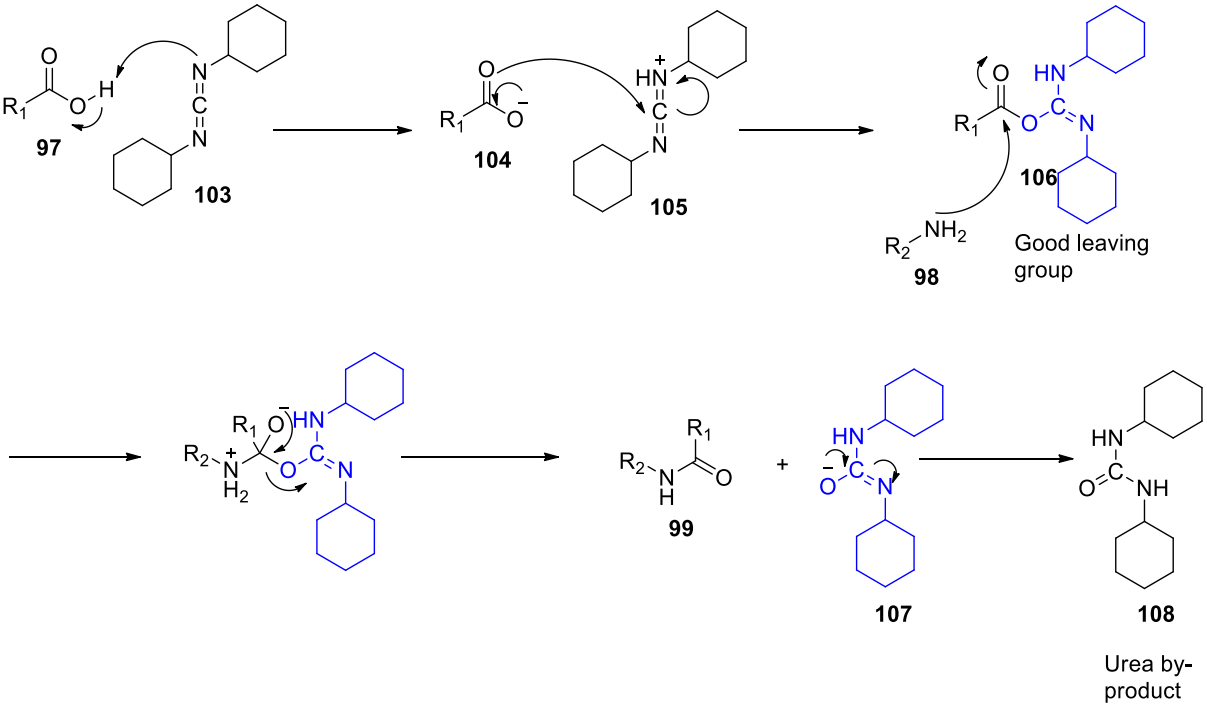

Scheme 35: Proposed mechanism for amidation reaction using DCC coupling agent.

In the proposed mechanism, a proton transfer from the carboxylic acid **97** to DCC **103** takes place. This produces a nucleophilic carboxylate ion **104** and DCC bearing an iminium ion **105**, which in turn activates the iminium carbon by making it more electrophilic. Compound **104** then performs a nucleophilic addition on **105** which affords the intermediate **106**. The *N*,*N*′-dicyclohexylcarbamimidyl group (highlighted in blue) is a good leaving group which makes the carbonyl of the carboxylic acid more electrophilic and susceptible to a nucleophilic addition by the amine **98**. The amide product **99** is afforded via the elimination of the *N*,*N*′-dicyclohexylcarbamimidate ion **107** which in turn forms the urea by-product **108**.

6.4.4. Attempted synthesis of *N*-(3-(pyridin-2-yl)isoquinolin-1-yl)picolinamide (77h) using DCC protocol.

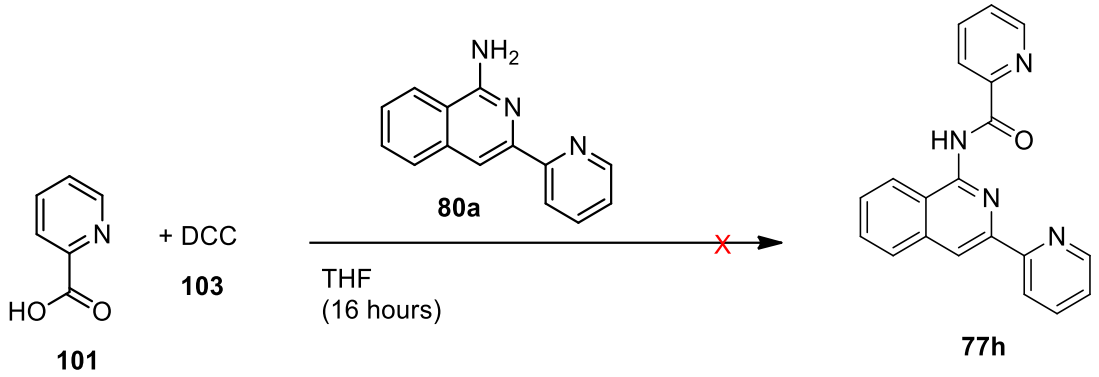

Scheme 36: Attempted synthesis of *N*-(3-(pyridin-2-yl)isoquinolin-1-yl)picolinamide (77h)

In an attempt to synthesise compound **77h** using the DCC protocol, 2-picolinic acid **101** was dissolved in THF and subsequently reacted with DCC **103**. The reaction was allowed to run for 1 hour at room temperature. After this time the isoquinoline amine **55a** was added and the reaction was left to stir for 16 hours at room temperature under a nitrogen atmosphere. After isolation by work up, the crude product was purified by silica gel column chromatography. Unfortunately, the reaction did not produce the desired product. Interestingly however, the intermediate, (*E*)-*N*,*N'*-dicyclohexylcarbamimidic picolinic anhydride **109**, **Figure 55**, was recovered. To try to get the reaction to progress further reflux temperatures 80-85 °C were used, however, compound **109** did not react further. These findings suggest that the intermediate shown in **Figure 55** is possibly too sterically crowded to interact with the bulky isoquinoline amine **80a**, and hence the reaction does not progress beyond the formation of the intermediate **109**.

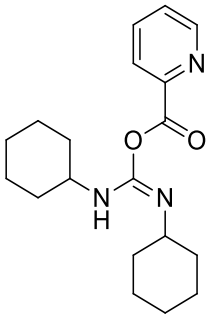

109

Figure 69: Structure of (*E*)-*N*,*N'*-dicyclohexylcarbamimidic picolinic anhydride.

We attempted the modified approach of the DCC protocol which was reported by Cocco *et al.*[126] This method uses DCC and *N*-hydroxysuccinimide (NHS) **110** to essentially convert the carboxylic acid to an activated ester **111**, which makes it more susceptible to nucleophilic attack. **Scheme 37** shows the proposed mechanism for this reaction.

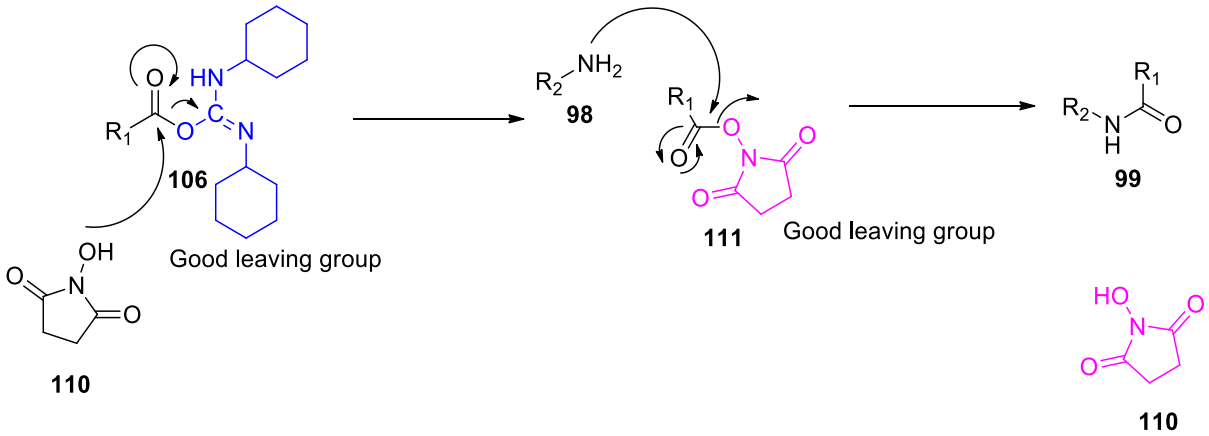

Scheme 37: Proposed amidation mechanism for DCC/NHS protocol.

In the proposed mechanism, compound **106** is produced in a similar manner as shown in **Scheme 15**. NHS **110** then performs a nucleophilic addition on the activated carbonyl of **106**, affording the intermediate **111**. Again the intermediate **111** possesses a good leaving group (highlighted in pink), which is eliminated when the amine **98** performs a nucleophilic addition on the electrophilic carbonyl of **111**. The amide product **99** is subsequently formed and the NHS **110** is regenerated.

The DCC/NHS protocol was carried out in a similar manner as shown in **Scheme 36**, where 2-picolinic acid **101** was dissolved in THF and subsequently treated with DCC **103** and NHS **110**. The reaction was run for 1 hour at room temperature and after this time the isoquinoline amine **80a** was added and the reaction was left to stir for 16 hours at room temperature under

a nitrogen atmosphere. We had anticipated that this DCC/NHS protocol may yield better results since the ester intermediate **111** possess a leaving group which is less bulky than the intermediate **106** afforded by the protocol that only uses DCC, **Scheme 36**. To our surprise however, the intermediate **109**, **Figure 55**, was also isolated in this reaction and persisted even when reflux temperatures were used to run the reaction.

We therefore considered alternative, less hindered coupling agents to synthesise the analogues of interest and considered the use of 1,1'-carbonyldiimidazole (CDI). CDI containing reactions have been previously used by Baucom *et al.* to mediate coupling and cyclization to generate [1,2,4]triazolo[4,3-*a*]pyridines **112** in high yields, **Scheme 38**.[127]

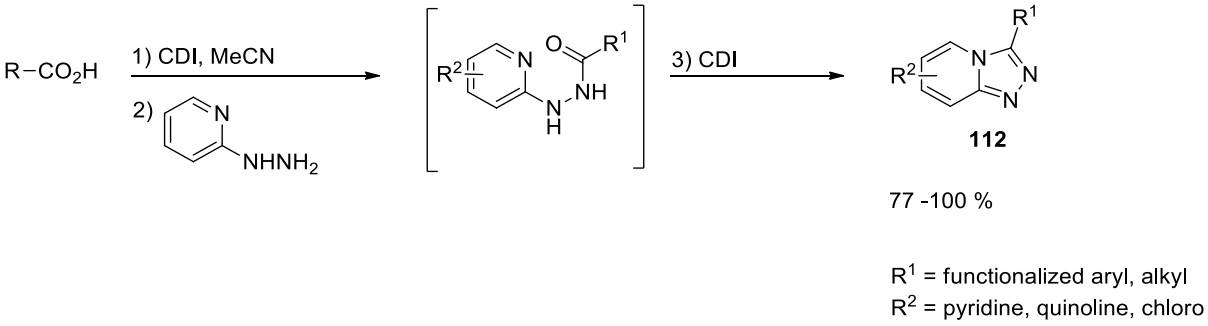

Scheme 38: CDI mediated coupling affording [1,2,4]triazolo[4,3-*a*]pyridines.

Similarly, Usachova *et al.*[128] also reported a CDI mediated amidation reaction. In this publication, amides were isolated and used as precursors for the synthesis of hydroxamic acids.[128] In their methodology, one of their approaches included reacting 2-(*o*-tolyl)acetic acid **113** and hydroxylamine hydrochloride **114** in THF and in the presence of CDI to afford the desired *N*-hydroxy-2-(*o*-tolyl)acetamide **115** in high yields (96 %), **Scheme 39**.

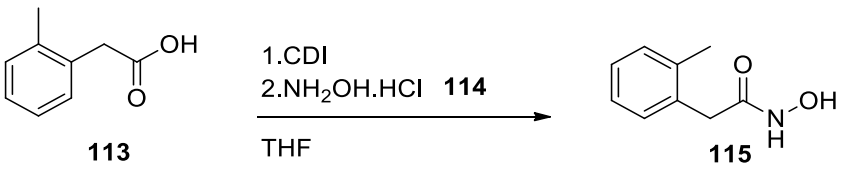

Scheme 39: CDI mediated amidation reaction affording *N*-hydroxy-2-(*o*-tolyl)acetamide (115).

Scheme 40 illustrates the proposed mechanism of this reaction in relation to our compounds.

In the proposed mechanism for CDI mediated amidation; CDI **116** deprotonates the substituted carboxylic acid **117**, affording a carboxylate ion **118**. Compound **118** then performs a nucleophilic attack on the carbonyl of the charged CDI intermediate which via multiple steps

generates the (*1H*-imidazol-1-yl)ketone **119**. The carbonyl carbon of **119** is highly electrophilic due to the imidazole that acts as a good leaving group. This would enable our poorly nucleophilic amine **80a** to perform a nucleophilic addition on compound **119**, to afford the desired final compounds **77**.

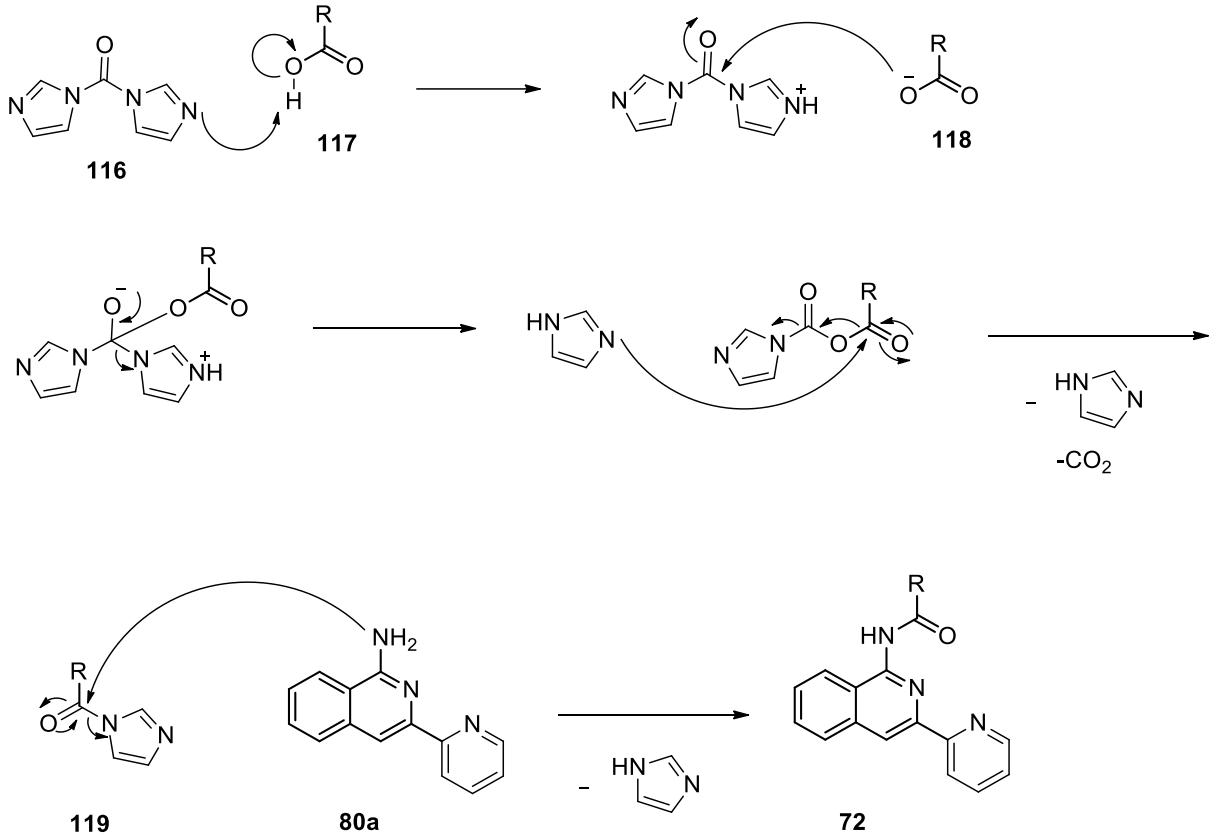

Scheme 40: Proposed mechanism for CDI mediated coupling.

6.4.5. Synthesis of *N*-(3-(pyridin-2-yl)isoquinolin-1-yl)-picolinamide (77h)

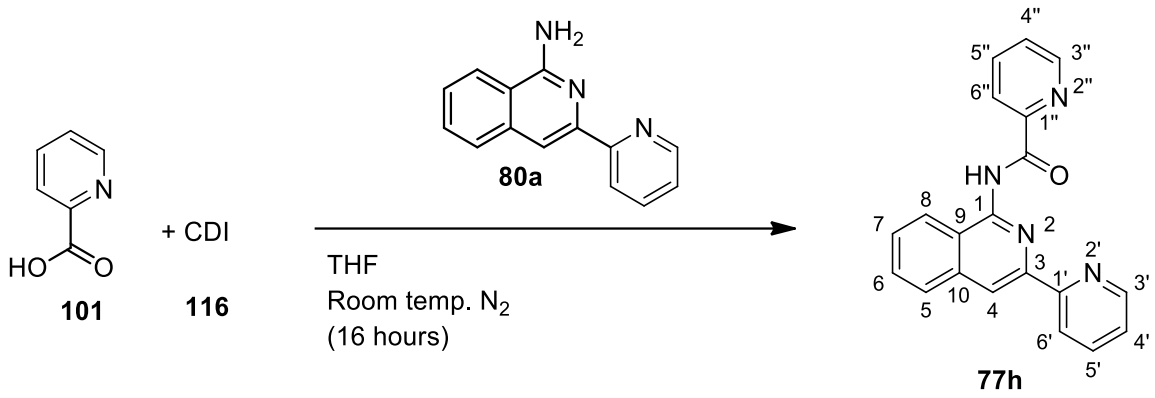

Scheme 41: Synthesis of *N*-(3-(pyridin-2-yl)isoquinolin-1-yl)pyridyl amides (77h).

We therefore explored and optimised the methodology reported by Usachova *et al.*[128] in relation to our compounds, **Scheme 41**. The reaction proposed in **Scheme 41** was tested by synthesising *N*-(3-(pyridin-2-yl)isoquinolin-1-yl)picolinamide **77h**. This coupling method is advantageous in that it avoids the limitations posed by the acyl chloride **81**, which serves as an intermediate in the previous method employed, **Scheme 33**. Furthermore the CDI is a less hindered coupling agent which will avoid the steric limitations such as that posed by DCC or DCC/NHS used previously (**Scheme 36**). Our test reaction was achieved by dissolving 2-picolinic acid **101** in THF in the presence of CDI, which was left to stir at room temperature for an hour to form the (*1H*-imidazol-1-yl)(pyridin-2-yl)methanone intermediate. The imidazole is a good leaving group which is essential as it enhances the electrophilic nature of the carbonyl carbon of 2-picolinic acid and hence makes it more susceptible to nucleophilic attack by the isoquinoline amine **80a**, which was subsequently added. The reaction mixture was left to stir for 16 hours at room temperature under a nitrogen atmosphere. After this time a new product had formed by TLC, and the resulting mixture was diluted with 5% $KHSO_4$ (aq.) and the organic layer was extracted with DCM. The role of the 5% $KHSO_4$ (aq.) is to hydrolyse the excess CDI, and to protonate the imidazole and the unreacted isoquinoline amine **80a** to keep them in the aqueous layer to enable separation of the desired product. In cases where the desired product became protonated and remained in the aqueous layer, this was diluted further with water and neutralised using solid $NaHCO_3$ and then extracted again using DCM. Purification was achieved by recrystallisation using DCM/hexane. The product **77h** was isolated as a yellow solid in a 58 % yield which melts at 162-164 °C.

The ^{1}H NMR spectrum was run using MeOD, and therefore the key signal belonging to the NH group was not observed due to hydrogen-deuterium exchange with the MeOD solvent. The ^{1}H NMR spectrum however did integrate for thirteen protons which matched the structure **77h**. A multiplet signal at δ 8.82 – 8.76 ppm was characteristic of the pyridyl proton H-6'. A doublet signal was observed for proton H-3'' at δ 8.66 ppm and a singlet was observed for proton H-4 at δ 8.63 ppm. Three doublet signals were observed at δ 8.51 ppm, δ 8.29 ppm and δ 8.14 ppm belonging to H-6'', H-8, and H-5, respectively. A multiplet signal at δ 8.11 – 8.03 was observed for protons H-6 and H-3'. Three triplet signals at δ 7.94 ppm, δ 7.80 ppm and δ 7.42 ppm were assigned to protons H-7, H-5'' and H-4', respectively. A multiplet signal for H-5' and H-4'' was observed at δ 7.73 – 7.65 ppm. The ^{13}C NMR spectrum showed the key C=O signal at δ 165.8 ppm, confirming successful product formation. The isoquinoline core was maintained and this was confirmed by carbons C-1, C-3 and C-4 observed at δ 157.1, 149.2 and 118.1 ppm

respectively. Carbon C-1', gave rise to a peak observed at δ 150.8 ppm, while the remaining aromatic carbons were observed in the region of δ 150.4 to 123.1 ppm, as expected. The IR spectrum confirmed the presence of the NH, aromatic CH, C=N, aromatic C=C and C=O functional groups with bands visible at 3335, 3055, 1626, 1566 and 1693 cm^{-1} respectively. HRMS also confirmed formation of the product with the molecular ion observed with the desired mass of 327.1201.

The success of this reaction enabled us to apply this method to the synthesis of the remaining novel analogues **77i** and **77j**.

6.4.6. Synthesis of *N*-(3-(pyridin-2-yl)isoquinolin-1-yl)nicotinamide (77i)

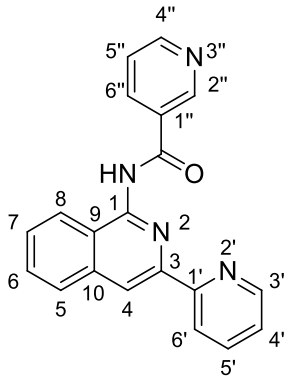

Figure 70: Structure of *N*-(3-(pyridin-2-yl)isoquinolin-1-yl)nicotinamide (77i).

Compound **77i** was synthesised using the same method described for the preparation of compound **77h** (**Scheme 41**), starting from nicotinic acid. Using this method, the desired product **77i** was successfully synthesised and purified by silica gel column chromatography, affording a brown solid in 53 % yield. IR spectroscopy confirmed the presence of the important functional groups NH, aromatic CH, C=N, aromatic C=C and C=O by displaying bands at 3202, 3066, 1665, 1569 and 1601 cm^{-1} respectively.

The ^{1}H NMR spectrum for compound **77i** showed a singlet signal observed at δ 9.37 ppm which was characteristic for proton H-2''. A doublet signal was observed for proton H-6' at δ 8.77 ppm, while a multiplet signal at δ 8.66 – 8.52 ppm was assigned to protons H-3', H-4'' and H-6''. A doublet signal observed at δ 8.07 ppm was due to H-8. A multiplet signal at δ 7.89 – 7.78 ppm was assigned to H-4 and H-5', while the multiplet at δ 7.77 – 7.65 ppm was assigned to H-5 and H-5''. Two additional multiplets at δ 7.61 – 7.51 ppm and δ 7.49 – 7.41 ppm were characteristic of H-6 and H-7 respectively. Finally, proton H-4' gave rise to a triplet signal observed at δ 7.34 ppm. The ^{13}C NMR spectrum showed the key C=O signal at δ 176.8

ppm. Carbons C-1, C-3 and C-4 were observed at δ 158.3, 136.2 and 111.6 ppm respectively, confirming that the isoquinoline core has been maintained. Carbon C-1' appeared as a signal at δ 149.8 ppm, as expected. The remaining aromatic carbons on compound **52i** gave rise to signals in the region of δ 152.0 to 121.2 ppm, as expected. A melting point of 150-151 °C was obtained and a molecular ion of mass 327.1190 $[M+H]^+$ was observed by HRMS.

6.4.7. Synthesis of *N*-(3-(pyridin-2-yl)isoquinolin-1-yl)isonicotinamide (77j)

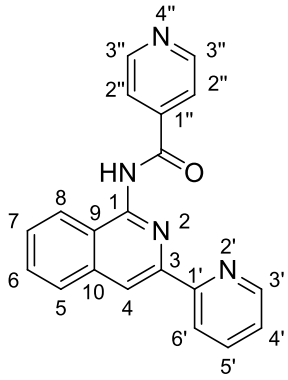

Figure 71: Structure of *N*-(3-(pyridin-2-yl)isoquinolin-1-yl)isonicotinamide (77j).

Similarly, compound **77j** was synthesised using the CDI mediated coupling reaction described in **Scheme 41**, employing isonicotinic acid. The desired product **77j** was successfully synthesised and purified by silica gel column chromatography, affording a pale brown solid in a 63 % yield. HRMS confirmed the presence of the desired product with a molecular ion of the desired mass of 327.1207 being observed.

The ^{1}H NMR spectrum confirmed the formation of compound **77j** by doublet signals being observed at δ 8.72 ppm and δ 8.31 ppm which were assigned to equivalent protons H-3'' and protons H-2'' respectively. This was significant as it confirmed the presence of the isonicotinamide substituent. A doublet signal was observed for proton H-6' at δ 8.96 ppm, while proton H-3' gave rise to a multiplet signal at δ 8.84 – 8.77 ppm. A doublet signal for H-8 and a singlet signal for H-4 were observed at δ 8.24 ppm and δ 8.05 ppm respectively. Three triplet signals at δ 7.98 ppm, δ 7.72 ppm and δ 7.49 ppm were observed for protons H-5', H-7 and H-4' respectively. Protons H-5 and H-6 gave rise to a multiplet signal at δ 7.94 – 7.81 ppm. In the ^{13}C NMR spectrum the key C=O signal was observed at δ 176.7 ppm as expected. A confirmation of the isoquinoline core was provided by the presence of C-1, C-3 and C-4 signals observed at δ 151.2, 149.9, 112.0 ppm respectively. The signal at δ 150.7 ppm was characteristic of carbon C-1'. Each pair of equivalent carbons, C-2'' and C-3'' were observed

as peaks at δ 124.6 ppm and δ 150.5 ppm respectively. As expected, the remaining aromatic carbons were observed in the region of δ 151.2 to 121.3 ppm. The melting point obtained was 208-209 °C. The IR spectrum confirmed the presence of the NH, aromatic CH, C=N, aromatic C=C and C=O functional groups with bands visible at 3084, 3036, 1628, 1569 and 1601 cm^{-1} respectively.

The success of using CDI as a coupling agent encouraged us to test the same method for the synthesis of the 2,6-dimethyl benzamides prepared previously to potentially increase the yield of product. To this end, the same protocol shown in **Scheme 41** was used for the synthesis of the hit compound **76**, in order to test the methodology. A new product formed which was initially subjected to HRMS analysis as the high temperature NMR spectroscopic analysis had to be scheduled. Interestingly, when characterising the purified product by HRMS, we did not observe the desired mass of 354.1555 $[M+H]^+$, instead, we predominantly saw the mass of the isoquinoline amine starting material **80a** (222.1126 $[M+H]^+$). Following this, NMR spectroscopy was used for further confirmation of our findings. Interestingly, the spectrum observed closely, but not exactly, matched that of the desired product. This encouraged us to obtain an X-ray crystal structure of the product. The crystal structure confirmed that the desired product had not been formed, but that we had isolated a salt instead. The crystal structure clearly showed the H-bonding between our acid and amine starting materials; isolated as co-crystals (**Figure 72**). This suggests that in this reaction the isoquinoline amine **80a** instead acts as a base and deprotonates the 2,6-dimethylbenzoic acid forming a 2,6-dimethylcarboxylate anion, which forms an intermolecular hydrogen bond with the isoquinoline amine. Presumably the acid is too bulky to undergo a reaction with CDI.

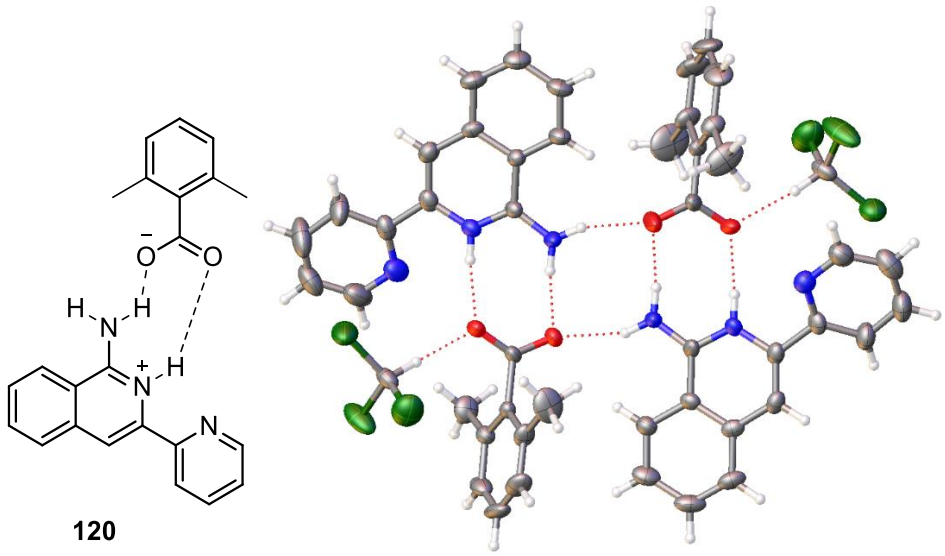

120

Figure 72: (Left) General structure (120) showing formation of co-crystals of 2,6-dimethylbenzoic acid and 1-aminoisoquinoline 80a. (Right) Crystal structure showing formation of co-crystals between 2,6-dimethylbenzoic acid and compound 1-aminoisoquinoline 80a.

The same reaction, using a different isoquinoline amine, 6-chloro-3-(pyridin-2-yl)isoquinolin-1-amine **80c**, was tested to see if the results would be consistent with what was previously observed. This reaction also resulted in the formation of the salt, as evidenced by the X-ray crystal structure clearly showing the co-crystal, **Figure 73**.

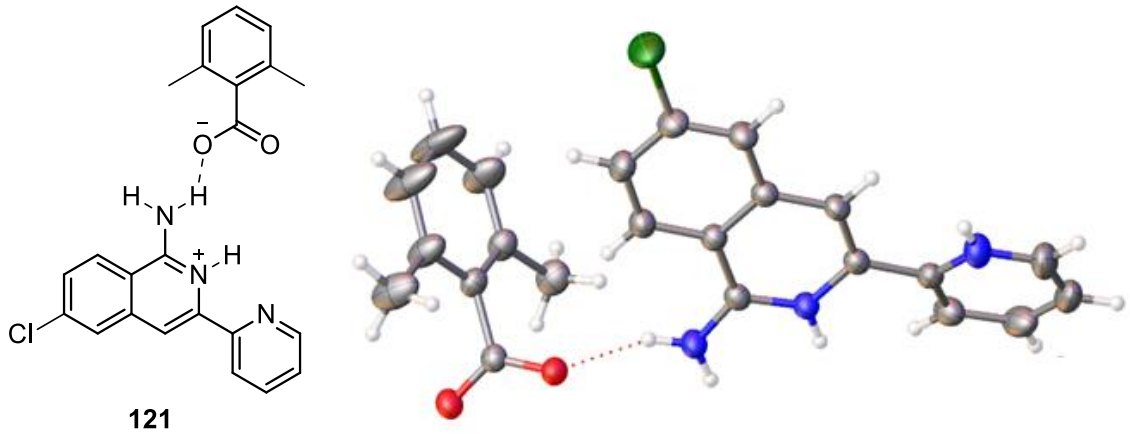

121

Figure 73: (Left) General structure (121) and (right) crystal structure showing formation of co-crystals between 2,6-dimethylbenzoic acid and compound 80c.

The undesirable outcome for these reactions clearly indicated that the use of the CDI coupling reagents in the formation of our hindered amides from non-nucleophilic amines would not be feasible.

We did however also attempt to synthesise the monomethylated, 3-methyl-*N*-(3-(pyridin-2-yl)isoquinolin-1-yl)picolinamide **77g** using the CDI method and fortunately this was successful. The yield of product obtained (26 %) however was similar to that obtained using the earlier method employing n-BuLi and 2,6-dimethylbenzoyl chloride **Scheme 31**.

6.5. Synthesis of 2-(3-(pyridin-2-yl)isoquinolin-1-yl)isoindoline-1,3-dione (122)

The final variation in our analogue synthesis involved replacing the amide linker with a symmetrical 1,3-dione linker to determine what effect this would have on biological activity. To this end, we embarked on the synthesis of the final novel analogue **122** (**Scheme 42**).

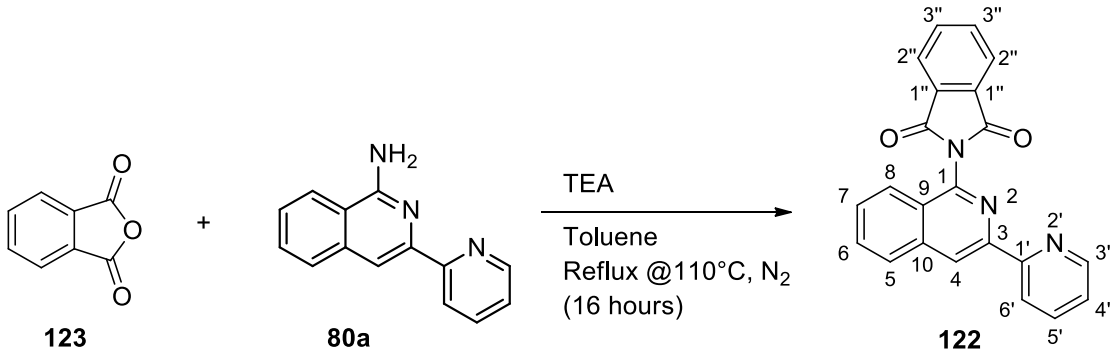

Scheme 42: Synthesis of 2-(3-(pyridin-2-yl)isoquinolin-1-yl)isoindoline-1,3-dione (122).

This was achieved by dissolving the isoquinoline amine **80a** in toluene, reacting it with triethylamine (TEA) and thereafter leaving the reaction mixture to stir at room temperature under a nitrogen atmosphere for 10 minutes. After this time, phthalic anhydride **123** was added, and the reaction mixture was heated to reflux and stirred overnight under a nitrogen atmosphere. The reaction mixture was then left to cool to room temperature and upon cooling the crude product precipitated out of solution. The precipitate was filtered and purified by recrystallisation from EtOAc, isolating the desired product **122** in a yield of 72 %.

In the ^{1}H NMR spectrum, a singlet signal integrating for one proton was observed at δ 8.42 ppm, which was characteristic of the proton H-4. A multiplet signal at δ 7.34 – 7.24 ppm was observed for protons H-2'' and H-3'', confirming the presence of the isoindoline group. A multiplet signal at δ 8.20 – 8.14 ppm was assigned to H-6', while a doublet signal for proton

H-3' was observed at δ 7.92 ppm. A multiplet signal integrating for three protons was observed at δ 7.55 – 7.43 ppm and assigned to H-5, H-8 and H-5'. Three triplet signals at δ 7.19 ppm, δ 7.05 ppm and δ 6.76 ppm were characteristic of protons H-6, H-7 and H-4'. The ^{13}C NMR spectrum provided further evidence of product formation as the two carbonyl groups gave rise to a signal at δ 167.5 ppm, an important signal confirming successful product formation. Each pair of equivalent carbons, C-1'', C-2'' and C-3'' were observed at δ 134.8, 124.3 and 132.3 ppm respectively, hence confirming the presence of the isoindoline group. The presence of the isoquinoline core was evidenced by peaks for C-1, C-3 and C-4 observed at δ 155.4, 148.9, 119.8 ppm respectively. Carbon C-1', was observed as a signal at δ 149.1 ppm. The remaining aromatic carbons were observed in the region of δ 145.0 to 122.1 ppm, as expected. HRMS analysis gave a molecular ion of the expected mass of 352.1085 $[M+H]^+$. IR spectroscopy showed the aromatic CH, C-N, aromatic C=C and C=O functional groups as bands at 3064, 1317, 1562 and 1720 cm^{-1} respectively. A melting point of 267-268 °C was also obtained.

A successful synthesis of compounds **77a-j** and compound **122** meant that these compounds could be sent for a series of biological assays where their inhibitory capabilities against *P.faliciparum* stage IV/V gametocytes could be assessed in order to determine key structure-activity relationships (SAR). Solubility, microsomal stability, and cytotoxicity will also be determined in order to ascertain if any of the variations introduced have favourably modified these properties.

Compounds **77a-j** and compound **122** all had their purity assessed by means of HPLC prior to biological assessment. All compounds showed a purity > 93 %, with compound **77d** showing the highest purity of 100.00 % and the resynthesized hit compound **77a** showing a purity of 98.20 %. The individual purities of the compounds **77a-j** and **122** are reported in the experimental section in chapter 8.

6.6. Biological Assay Data

The isoquinoline analogues **77** and **122**, were submitted to our collaborators at the University of Pretoria for biological assessment where several assays are being performed on the analogues (**Figure 61**). These include assays against *P. falciparum* stage IV/V gametocytes as well as a whole cell assay against the asexual blood stages of *P. falciparum*; microsomal stability, (using microsomes from the livers of humans, rats and monkeys to assess the rate of clearance of the analogues over time); and finally cytotoxicity (CHO assay) and solubility, which were the major concerns with the hit compound **76**. The biological assays are being

performed at the University of Pretoria and the CSIR by a team led by Professor L-M. Birkholtz and Dr M. van der Watt.

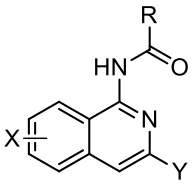

77

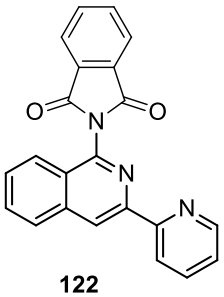

122

77a	R = 2,6-diMe phenyl	X = H	Y = 2-pyridyl
77b	R = 2,6-diMe phenyl	X = 7-F	Y = 2-pyridyl
77c	R = 2,6-diMe phenyl	X = 6-Cl	Y = 2-pyridyl
77d	R = 2,6-diMe phenyl	X = 8-Cl	Y = 2-pyridyl
77e	R = 2,6-diMe phenyl	X = H	Y = 3-pyridyl
77f	R = 2,6-diMe phenyl	X = H	Y = 4-pyridyl
77g	R = 3-methylpicolinyl	X = H	Y = 2-pyridyl
77h,	R = 2-picolinyl	X = H	Y = 2-pyridyl
77i	R = nicotinyl	X = H	Y = 2-pyridyl
77j	R = isonicotinyl	X = H	Y = 2-pyridyl

Figure 74: Analogues submitted for biological assays.

Unfortunately, the biological assays are still underway and only the asexual blood stage (ABS) data is available and is included in **Table 13**. Compounds were assessed for antiplasmodial activity in a whole cell *P. falciparum* screen against the NF54 strain for activity against the blood stages of the parasite.

From the ABS assay data received we observed a two-fold difference in the IC_{50} values of the original hit compound **76** (IC_{50} 3.92 µM) and the resynthesised analogue **77a** (IC_{50} 1.18 µM), at this stage the reasons for this are unclear. Factors that could contribute to the difference could be the percentage purity of the compounds. The percentage purity of compound **77a** was assessed using HPLC and a 98.20 % purity was observed for this compound, we do not however have this information with regards to the hit compound **76**. For compounds with a TCP-5 profile, the compounds should be selective for gametocytes and not be active against the asexual blood stages. In general, most compounds have activities in the micromolar range (IC_{50} 1.18 – 7 µM) except for compounds **77b** (IC_{50} 400 nM), **77i** (IC_{50} 500 nM) and **77j** (IC_{50} 300 nM). These compounds may potentially act as dual inhibitors. However, few conclusions can be drawn at this stage with the limited data available. We are hopeful that some of the modifications made in this work could be of benefit for the development of a transmission blocking agent derived from the hit compound MMV1581558.

Table 13: A comparison of the asexual blood stage inhibitory activity data of compounds 77 and 122 vs the hit compound 76.

Entry	Structure	ABS IC_{50} (µM)[a]
76 (original hit compound)	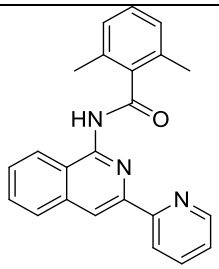	3.92
77a (resynthesized analogue)	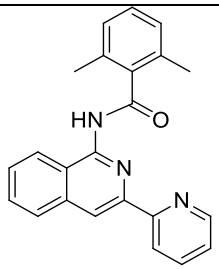	1.18
77b	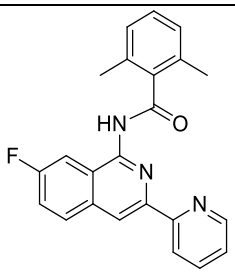	0.4
77c	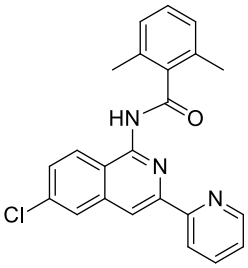	1.4

[a] NF54

Table 13: A comparison of the asexual blood stage inhibitory activity data of compounds 77 and 122 vs the hit compound 76 continued.

Entry	Structure	ABS IC_{50} (µM)[a]
77d	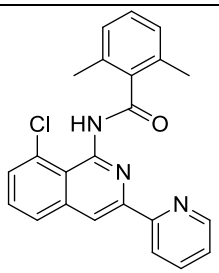	>3
77e	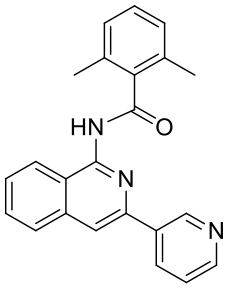	7
77f	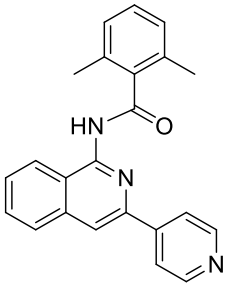	4.4
77g	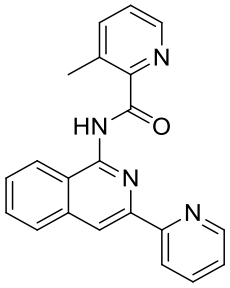	1.2

[a] NF54

Table 13: A comparison of the asexual blood stage inhibitory activity data of compounds 77 and 122 vs the hit compound 76 continued.

Entry	Structure	ABS IC_{50} (µM)[a]
77h	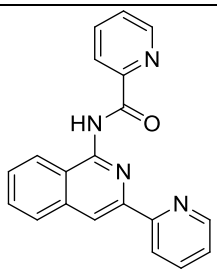	2.0
77i	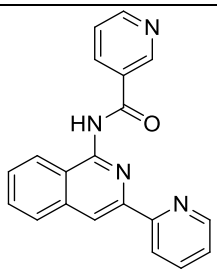	0.5
77j	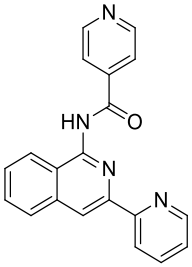	0.3
122	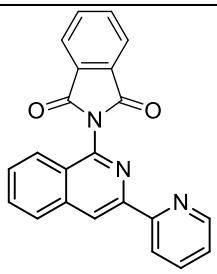	>3

[a] NF54

CHAPTER 7: CONCLUSIONS AND FUTURE WORK

7.1. Conclusions

The aim of the second part of the research project was to synthesise analogues of the hit compound MMV1581558 (**76**) that potentially possess gametocytocidal activity against stage IV/V gametocytes. A small collection of isoquinoline derivatives with this potential was synthesised. A successful synthetic protocol was developed and comprised of primarily two steps to afford the substituted isoquinolin-1-yl benzamides **77a-j**, **Scheme 43**.

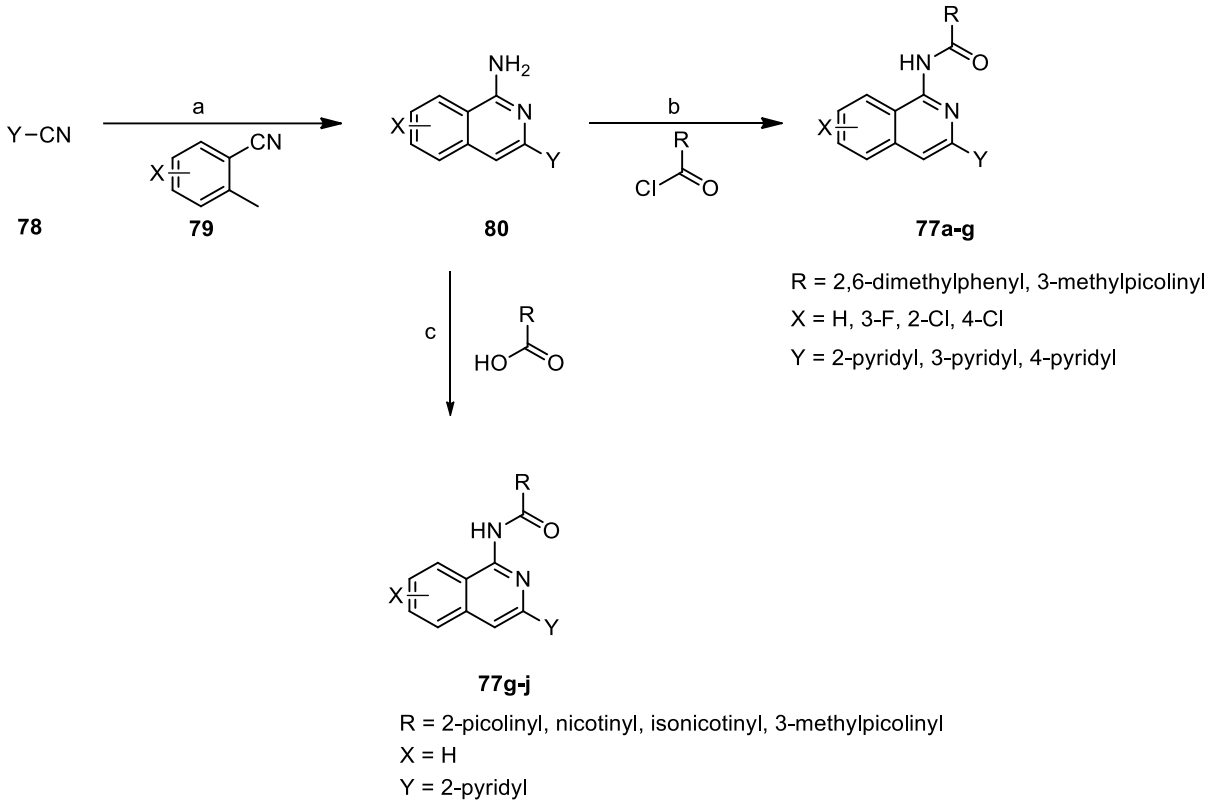

Scheme 43: Complete synthesis of substituted isoquinolin-1-yl benzamides (77). Reagents and conditions: a) KO^{t}Bu, toluene, 110 °C; b) i) n-BuLi, -10 °C; ii) ArCOCl, -10 °C; c) CDI, THF room temperature.

Substituted 1-aminoisoquinolines **80** were synthesised from benzonitriles as shown in step *a*. A base-mediated intermolecular cyclization reaction between a substituted carbonitrile and a substituted *o*-tolunitrile using KO^{t}Bu was utilised. The reaction afforded moderate to high yields (33-78 %) of the intermediate 1-aminoisoquinolines **80**. A limitation of this reaction was that a side product was generated by homocoupling of *o*-tolunitrile to itself, which affected the yield significantly in some cases. The second step differed with respect to the reagents used. The synthesis of 2,6-dimethylbenzamides **77a-f** was achieved as shown in step *b*, however this

reaction was low yielding (14-22 %) because the reaction did not go to completion, which we believe was caused by steric hindrance due to the bulkiness of the 2,6-dimethylbenzoyl chloride. By comparison, the synthesis of the pyridyl amides **77h-j**, was achieved as shown in step *c* by making use of a coupling agent, CDI. This reaction showed improved yields of 53-68 %. Interestingly, the 3-methylpicolinic benzamide **77g** could be prepared by either method, step *b* or *c*, with each method giving similar yields of product (23-26 %). When comparing the yields of the compounds **77a-g** bearing a monomethylated or dimethylated R substituent in an *ortho* position vs the compounds bearing pyridyl R substituents **77h-j** it was clear that the methyl in this position significantly reduces the reactivity between the compound **80** and the respective methylated benzoyl chloride. Although the synthesis of amides **77a-f** was not high yielding, this method offers an advantage of being inexpensive and efficient as only two steps are required to afford the final compound. The final variation in the synthesis involved replacing the amide linker with the 1,3-dione linker (**Scheme 22**) by synthesising 2-(3-(pyridin-2-yl)isoquinolin-1-yl)isoindoline-1,3-dione **122** in relatively high yield of 72 %.

All compounds were submitted for biological assessment to obtain information about the analogues' inhibitory capabilities against *P. falciparum* stage IV/V gametocytes in order to determine key structure-activity relationships. Furthermore solubility, microsomal stability and cytotoxicity will also be determined in order to ascertain if any of the variations will improve the pharmacokinetic properties of the hit compound **76**. Thus far we have only received the results of the asexual blood stage (ABS) activity assay. Most analogues were found to display only moderate activity in the low micromolar ranges against the asexual blood stages of *P. falciparum* (NF54; IC_{50} 1.18 – 7 µM), except for compounds **77b** (NF54; IC_{50} 400 nM), **77i** (NF54; IC_{50} 500 nM) and **77j** (NF54; IC_{50} 300 nM) which were slightly more potent. No conclusions regarding these compounds can be made as yet, as the majority of the biological data is not yet available.

7.2. Future Work

Future work will include a thorough interpretation of the biological assay data once a complete set of results has been received. As we have established that the amide linker is key for the inhibitory activity of the analogues, the biological assay results received will give information about which variations are essential in improving the other pharmacokinetic properties, that is, solubility, cytotoxicity and microsomal stability. This data will therefore direct us as to the next generation of analogues to synthesise.

As discussed previously, there were concerns with the first step of the synthetic scheme (**Scheme 43** step *a*) as *o*-tolunitrile coupled with itself which significantly affected the yields at times. Possible future work will include revisiting the traditional methods of synthesising isoquinolines which included the use of catalysts. A method reported by Long *et al.* (**Scheme 44**) involving gold (III) catalysed reactions may be explored and modified to fit our needs. Although this may be a slightly more expensive alternative, the potential yields (54-95 %) that might result from these reactions may make this route more desirable.

Scheme 44: Metal catalysed synthesis of 1-aminoisoquinoline.[120]

The second step of the reaction (**Scheme 43** step *b*) produced compounds in low yields (23 – 26 %). To try and improve the yields, future work could include using a highly versatile amidation method reported by Sabatini *et al.* which uses a borate ester catalyst, which produces products with moderate to high yields of 66 – 96 % (**Scheme 45**).[129]

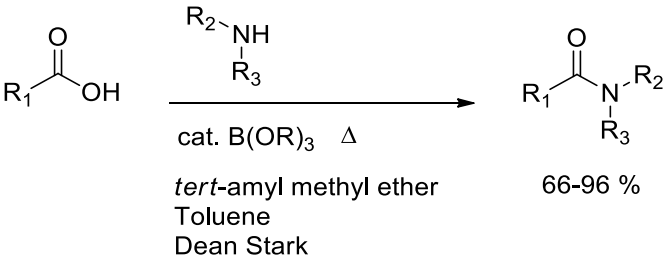

Scheme 45: Amidation using Borate ester catalyst.[129]

This method is advantageous in that it avoids using molecular sieves since a Dean-Stark apparatus is used for water removal to avoid hydrolysis of the ester. In addition, safe solvents, *tert*-amyl-methyl ether and toluene are used and finally a low cost catalyst is used.

CHAPTER 8: EXPERIMENTAL-PART 2

8.1. General procedure for synthesis of 3-substituted-1-amino-isoquinoline and analogues (80)

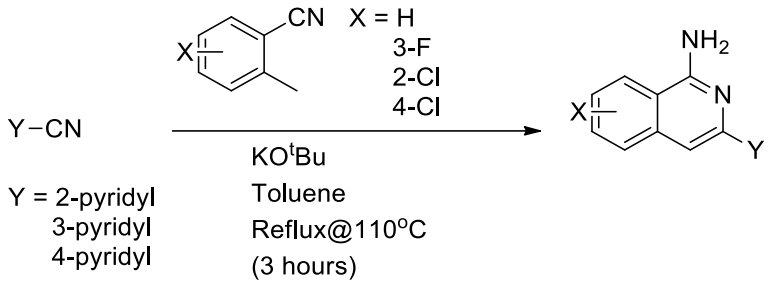

In a pressure tube, the substituted benzonitrile (500 mg, 1.0 eq) was dissolved in toluene (20-30 mL) in the presence of a magnetic stirrer bar. Upon dissolution, the substituted *o*-tolunitrile (1.5 eq) was added and the mixture was stirred at room temperature. Freshly sublimed KO^{t}Bu (2.0 eq) was then added. The mixture was heated to reflux with stirring for 3 hours. When the reaction was complete, the crude product was purified by silica gel column chromatography and/or recrystallisation. The eluent used for column chromatography was gradient elution 50-100 % ethyl acetate/hexane. The solvent used for recrystallisation was methanol. The following compounds were prepared by this method:

8.1.1. Synthesis of 3-(pyridin-2-yl)isoquinolin-1-amine (80a)[119]

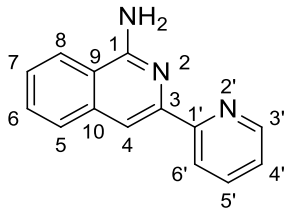

Prepared from 2-pyridine carbonitrile (0.500 g, 4.80 mmol), *o*-tolunitrile (0.85 mL, 7.2 mmol) and KO^{t}Bu (1.08 g, 9.60 mmol). Isolated as a brown solid (0.663 g, 62.5 %). m.p. 158-159 °C; **^{1}H NMR (400 MHz, CDCl$_3$)** δ 8.64 – 8.60 (H-6', m, 1H), 8.29 (H-3', d, *J* = 8.0 Hz, 1H), 8.07 (H-4, s, 1H), 7.78 – 7.67 (H-6, H-8 and H-5', m, 3H), 7.57 – 7.50 (H-5, m, 1H), 7.43 – 7.37 (H-7, m, 1H), 7.20 – 7.14 (H-4', m, 1H), 5.22 (NH$_2$, s, 2H); **^{13}C NMR (101 MHz, CDCl$_3$)** δ 156.9 (C-1), 155.9 (C-1'), 149.4 (C-3'), 148.1 (C-3), 138.3 (C-10), 136.9 (C-5'), 130.4 (C-6), 128.4 (C-5), 126.6 (C-7), 123.1 (C-8), 122.7 (C-4'), 121.2 (C-6'), 118.1 (C-9), 110.3 (C-4); **IR (ν_{max}/cm^{-1})** 3309 (N-H); 3055 (=C-H); 1378 (C-N); 1569 (Ar-C=C), **HRMS** *m/z*: calculated for: $C_{14}H_{12}N_3$, 222.1026 found: $[M+H]^+$ 222.1126.

8.1.2. Synthesis of 7-fluoro-3-(pyridin-2-yl)isoquinolin-1-amine (80b)

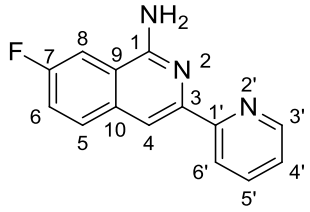

Prepared from 2-pyridine carbonitrile (0.500 g, 4.80 mmol), 5-fluoro-2-methylbenzonitrile (974 mg, 7.20 mmol) and KO^{t}Bu (1.08 g, 9.60 mmol). Isolated as an orange solid (0.56 g, 49%). m.p. 131-132 °C; **^{1}H NMR (400 MHz, MeOD)** δ 8.61 – 8.52 (H-6', m, 1H), 8.24 (H-3', d, *J* = 8.0 Hz, 1H), 7.88 – 7.78 (H-4, H-5, H-8 and H-5', m, 4H), 7.42 (H-6, t, *J* = 8.9 Hz, 1H), 7.36 – 7.29 (H-4', m, 1H); **^{13}C NMR (101 MHz, MeOD)** δ 162.2 (C-7, d, J_{C-F} = 245.8 Hz), 158.3 (C-1, d, J_{C-F} = 4.8 Hz), 158.0 (C-1'), 149.8 (C-3'), 148.4 (C-10, d, J_{C-F} = 2.9 Hz), 138.5 (C-5'), 136.3 (C-3), 131.5 (C-5, d, J_{C-F} = 8.4 Hz), 124.3 (C-4'), 122.7 (C-6'), 121.2 (C-6, d, J_{C-F} = 24.9 Hz), 119.9 (C-9, d, J_{C-F} = 8.1 Hz), 109.6 (C-4, d, J_{C-F} = 1.8 Hz), 108.9 (C-8, d, J_{C-F} = 22.4 Hz); **IR (ν_{max}/cm^{-1})** 3360, 3312 (N-H); 3061 (=C-H); 1419 (C-F); 1562 (Ar-C=C), **HRMS** *m/z*: calculated for: $C_{14}H_{11}FN_3$, 240.0932 found: $[M+H]^+$ 240.0903.

8.1.3. Synthesis of 6-chloro-3-(pyridin-2-yl)isoquinolin-1-amine (80c)

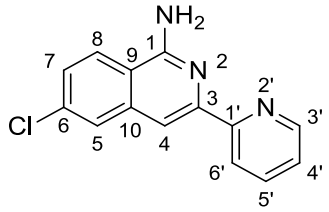

Prepared from 2-pyridine carbonitrile (0.500 g, 4.80 mmol), 4-chloro-2-methylbenzonitrile (1.09 g, 7.20 mmol) and KO^{t}Bu (1.08 g, 9.60 mmol). Isolated as a yellow solid (0.960 g, 78.0 %). m.p. 142-143 °C; **^{1}H NMR (400 MHz, CDCl$_3$)** δ 8.72 – 8.66 (H-6', m, 1H), 8.32 (H-3', d, *J* = 7.9 Hz, 1H), 8.00 (H-4, s, 1H), 7.80 – 7.63 (H-5, H-8 and H-5', m, 3H), 7.35 – 7.28 (H-7, m, 1H), 7.25 (H-4', t, *J* = 6.2 Hz, 1H), 5.44 (NH_2, s, 2H); **^{13}C NMR (101 MHz, CDCl$_3$)** δ 156.2 (C-1), 155.9 (C-1'), 149.3 (C-3'), 149.2 (C-3), 139.2 (C-10), 136.9 (C-5'), 136.4 (C-6), 127.1 (C-5), 126.9 (C-7), 124.5 (C-4'), 123.3 (C-8), 121.2 (C-6'), 116.1 (C-9), 109.1 (C-4); **IR (ν_{max}/cm^{-1})** 3443, 3292 (N-H); 3161 (=C-H); 667 (C-Cl); 1567 (Ar-C=C), **HRMS** *m/z*: calculated for: $C_{14}H_{11}N_3{}^{35}Cl$, 256.0636 found: $[M+H]^+$ 256.0611.

8.1.4. Synthesis of 8-chloro-3-(pyridin-2-yl)isoquinolin-1-amine (80d)

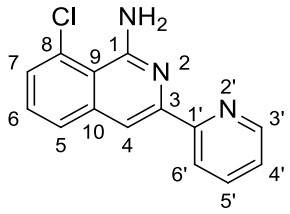

Prepared from 2-pyridine carbonitrile (0.250 g, 2.40 mmol), 2-chloro-6-methylbenzonitrile (0.250 g, 3.60 mmol) and KO^{t}Bu (0.538 g 4.80 mmol). Isolated as an orange solid (0.447 g, 72.8 %). m.p. 141-142 °C; **^{1}H NMR (400 MHz, CDCl$_3$)** δ 8.75 – 8.68 (H-6', m, 1H), 8.37 (H-3', d, *J* = 8.0 Hz, 1H), 8.06 (H-4, s, 1H), 7.80 (H-5', t, *J* = 7.8 Hz, 1H), 7.70 (H-5, d, *J* = 7.4 Hz, 1H), 7.49 – 7.37 (H-7 and H-6, m, 2H), 7.28 (H-4', t, *J* = 6.6 Hz, 1H), 6.34 (NH_2, s, 2H); **^{13}C NMR (101 MHz, CDCl$_3$)** δ 156.0 (C-1), 155.5 (C-1'), 149.3 (C-3'), 148.5 (C-3), 141.7 (C-10), 136.9 (C-5'), 130.5 (C-8), 129.9 (C-6), 128.8 (C-7), 128.0 (C-5), 123.4 (C-4'), 121.2 (C-6'), 115.5 (C-9), 110.0 (C-4); **IR (ν_{max}/cm^{-1})** 3510, 3323 (N-H); 3048 (=C-H); 667 (C-Cl); 1550 (Ar-C=C), **HRMS** *m/z*: calculated for: $C_{14}H_{11}N_3{}^{35}Cl$, 256.0636 found: $[M+H]^+$ 256.0603.

8.1.5. Synthesis of 3-(pyridin-3-yl)isoquinolin-1-amine (80e)[121]

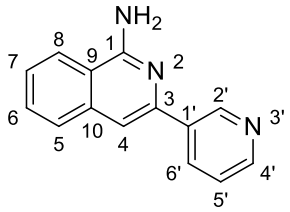

Prepared from 3-pyridine carbonitrile (0.500 g, 4.80 mmol), *o*-tolunitrile (0.85 mL, 7.2 mmol) and KO^{t}Bu (1.08 g, 9.60 mmol). Isolated as an orange solid (0.367 g, 34.6 %). m.p. 144-145 °C; **^{1}H NMR (400 MHz, CDCl$_3$)** δ 9.26 (H-2', d, *J* = 2.3 Hz, 1H), 8.60 (H-6', dd, *J* = 4.8, 1.7 Hz, 1H), 8.35 (H-6, dt, *J* = 7.9, 1.8 Hz, 1H), 7.82 (H-4', dq, *J* = 8.3, 0.9 Hz, 1H), 7.77 (H-8, dt, *J* = 8.2, 0.8 Hz, 1H) 7.68 – 7.60 (H-5', m, 1H), 7.52 – 7.47 (H-5 and H-7, m, 2H), 7.40 – 7.35 (H-4, m, 1H), 5.39 (NH_2, s, 2H); **^{13}C NMR (101 MHz, CDCl$_3$)** δ 156.4 (C-1), 149.2 (C-4'), 148.4 (C-2'), 146.8 (C-3), 138.1 (C-10), 135.4 (C-1'), 134.3 (C-6'), 130.7 (C-6), 127.8 (C-5), 126.6 (C-7), 123.6 (C-8), 122.8 (C-5'), 117.3 (C-9), 109.3 (C-4); **IR (ν_{max}/cm^{-1})** 3328 (N-H); 3058 (=C-H); 1374 (C-N); 1562 (Ar-C=C), **HRMS** *m/z*: calculated for: $C_{14}H_{12}N_3$, 222.1026 found: $[M+H]^+$ 222.1143.

8.1.6. Synthesis of 3-(pyridin-4-yl)isoquinolin-1-amine (80f)[121]

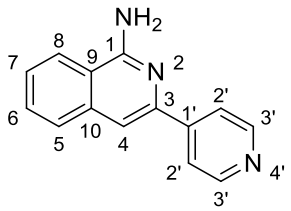

Prepared from 4-pyridine carbonitrile (0.500 g, 4.80 mmol), *o*-tolunitrile (0.85 mL, 7.2 mmol) and KO^{t}Bu (1.08 g, 9.60 mmol). Isolated as a yellow solid (0.345 g, 32.5 %). m.p. 171-172 °C; **^{1}H NMR (400 MHz, CDCl$_3$)** δ 8.69 (H-3', dd, *J* = 4.7, 1.6 Hz, 2H), 7.96 (H-2', dd, *J* = 4.6, 1.7 Hz, 2H), 7.86 – 7.79 (H-6 and H-8, m, 2H), 7.67 (H-5, ddd, *J* = 8.1, 6.9, 1.2 Hz, 1H), 7.60 (H-4, d, *J* = 1.0 Hz, 1H), 7.54 (H-7, ddd, *J* = 8.2, 6.9, 1.3 Hz, 1H), 5.28 (NH_2, s, 2H); **^{13}C NMR (101 MHz, CDCl$_3$)** δ 156.3 (C-1), 150.3 (C-3'), 147.2 (C-3), 146.7 (C-1'), 137.9 (C-10), 130.7 (C-6), 128.1 (C-5), 127.1 (C-7), 122.8 (C-8), 121.1 (C-2'), 117.9 (C-9), 110.2 (C-4); **IR (ν_{max}/cm^{-1})** 3321 (N-H); 3188 (=C-H); 1381 (C-N); 1561 (Ar-C=C), **HRMS** *m/z*: calculated for: $C_{14}H_{12}N_3$, 222.1026 found: $[M+H]^+$ 222.1145.

8.2. General procedure for synthesis of substituted-isoquinolin-1-yl benzamides (77)

The amide synthesis was achieved using two methods, method A and method B. Method A was used primarily for synthesising the 2,6-dimethylbenzamides. Method B was used to synthesise the nitrogen containing benzamides.

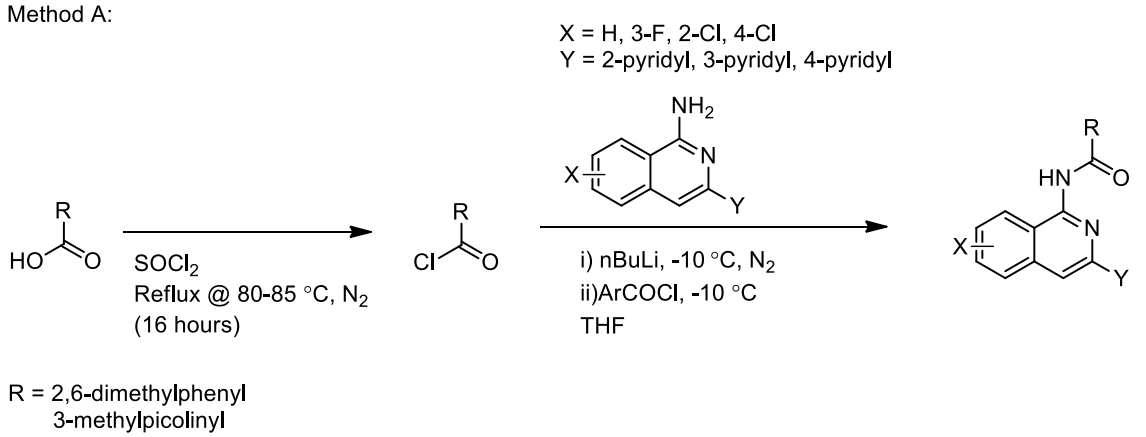

Scheme A: Synthesis of compounds 77a-g.

Method A: 2,6-dimethylbenzoic acid (170 mg, 1 eq) was dissolved in excess thionyl chloride in a two-neck round bottomed flask in the presence of a magnetic stirrer bar and refluxed overnight under a nitrogen atmosphere. After this time, the remaining thionyl chloride was

removed under high vacuum to isolate the 2,6-dimethylbenzoyl chloride (1eq). In a separate three-neck round bottomed flask, in the presence of a magnetic stirrer bar, the amine (1 eq) was dissolved in THF (3 - 4 mL). The solution was then cooled to -10 °C. Once at the desired temperature, n-butyllithium (n-BuLi) (6.8 eq) was added slowly, and the solution was left to stir for 10 minutes, a deep brick-red colour was observed. After 10 minutes, the 2,6-dimethylbenzoyl chloride was added to the reaction mixture and was left to stir at -10 °C for 1 hour. After an hour the reaction was left to warm to room temperature, the n-BuLi was quenched with water (50 mL) and the organic product extracted into DCM (3 x 100 mL). The organic layer was dried using anhydrous potassium carbonate and concentrated *in vacuo*. The desired product was purified by recrystallisation. Solvents used for recrystallisation differed according to analogues, solvents included methanol, ethanol and ethyl acetate. It is important to note that the NMR spectra obtained for the 2,6-dimethylbenzamides were unsatisfactory when run at room temperature. High temperature NMR spectroscopy at 70 - 100 °C was required to get desirable spectra. The following compounds were prepared by this method:

8.2.1. Synthesis of 2,6-dimethyl-*N*-(3-(pyridin-2-yl)isoquinolin-1-yl)benzamide (77a)[119]

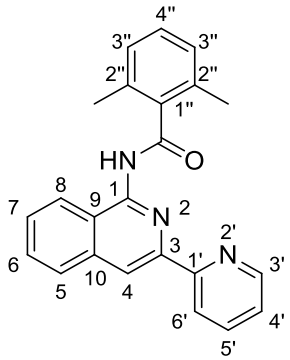

Prepared from 2,6-dimethylbenzoic acid (0.170 g, 1.13 mmol), 3-(pyridin-2-yl)isoquinolin-1-amine **80a** (0.251 g, 1.13 mmol) n-BuLi (0.71 mL, 7.7 mmol), $SOCl_2$ (3-4 mL) and THF (3-4 mL). Isolated as a pale brown solid (0.087 g, 22 %). m.p. 232-233 °C; **^{1}H NMR (400 MHz, DMSO-*d*$_6$)** δ 10.72 (NH, s, 1H), 8.71 – 8.60 (H-8 and H-5', m, 2H), 8.38 (H-6', d, *J* = 8.4 Hz, 1H), 8.11 (H-3', d, *J* = 8.2 Hz, 1H), 8.02 (H-4, s, 1H), 7.90 – 7.77 (H-6 and H-7, m, 2H), 7.72 (H-5, ddd, *J* = 8.3, 6.9, 1.3 Hz, 1H), 7.41 – 7.33 (H-4'', m, 1H), 7.23 – 7.16 (H-4', m, 1H), 7.10 (H-3'', d, *J* = 7.5 Hz, 2H), 2.44 (2 x CH_3, s, 6H); **^{13}C NMR (101 MHz, DMSO-*d*$_6$)** δ 172.1 (C=O), 169.6 (C-1), 155.0 (C-3'), 148.8 (C-1'), 148.7 (C-2''), 147.2 (C-3), 137.9 (C-10), 137.6 (C-1''), 136.2 (C-5'), 133.2 (C-6), 130.3 (C-4''), 127.5 (C-5), 127.4 (C-7), 127.2 (C-8), 126.6 (C-3''), 124.5 (C-4'), 122.9 (C-6'), 120.2 (C-4), 114.9 (C-9), 18.5 (2 x CH_3); **IR**

(ν_{max}/cm^{-1}) 3290 (N-H); 3056 (=C-H); 1255 (C-N); 1596 (Ar-C=C), 1646 (C=O) **HRMS** *m/z*: calculated for: $C_{23}H_{20}N_3O$, 354.1601 found: $[M+H]^+$ 354.1555. HPLC purity: 98.20 %.

8.2.2. Synthesis of *N*-(7-fluoro-3-(pyridin-2-yl)isoquinolin-1-yl)-2,6-dimethylbenzamide (77b)

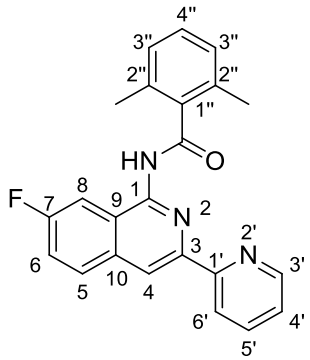

Prepared from 2,6-dimethylbenzoic acid (0.170 g, 1.13 mmol), 7-fluoro-3-(pyridin-2-yl)isoquinolin-1-amine **80b** (0.251 g, 1.13 mmol) n-BuLi (0.71 mL, 7.7 mmol), $SOCl_2$ (3-4 mL) and THF (3-4 mL). Isolated as a pale pink solid (0.100 g, 24 %). m.p. 267-268 °C; **^{1}H NMR (300 MHz, DMSO-*d*$_6$)** δ 10.81 (NH, s, 1H), 8.70 – 8.64 (H-4 and H-6', m, 2H), 8.22 (H-3', dd, *J* = 5.7, 9.1 Hz, 1H), 8.13 – 7.91 (H-5 and H-4'', m, 2H), 7.93 – 7.80 (H-5', m, 1H), 7.77 – 7.64 (H-8, m, 1H), 7.37 (H-4', td, *J* = 2.5, 5.2 Hz, 1H), 7.20 (H-6, dd, *J* = 6.5, 8.5 Hz, 1H), 7.10 (H-3'', d, *J* = 7.5 Hz, 2H), 2.43 (2 x CH_3, s, 6H); **^{13}C NMR (75 MHz, DMSO-*d*$_6$)** δ 169.6 (C=O), 160.3 (C-7, d, J_{C-F} = 247.4 Hz), 154.8 (C-1), 148.7 (C-2''), 148.4 (C-1'), 146.9 (C-3'), 137.8 (C-3), 136.3 (C-1''), 134.9 (C-10), 133.2 (C-3''), 130.7 (C-6, d, J_{C-F} = 8.8 Hz), 127.6 (C-4''), 126.8 (C-5, d, J_{C-F} = 2.8 Hz), 122.9 (C-4'), 120.8 (C-6'), 120.5 (C-6), 120.2 (C-9), 114.6 (C-4), 108.3 (C-8, d, J_{C-F} = 20.5 Hz), 18.6 (2 x CH_3); **IR (ν_{max}/cm^{-1})** 3187 (N-H); 3054 (=C-H); 1412 (C-F); 1565 (Ar-C=C), 1646 (C=O) **HRMS** *m/z*: calculated for: $C_{23}H_{19}FN_3O$, 372.1507 found: $[M+H]^+$ 372.1452. HPLC purity: 93.71 %.

8.2.3. Synthesis of *N*-(6-chloro-3-(pyridin-2-yl)isoquinolin-1-yl)-2,6-dimethylbenzamide (77c)

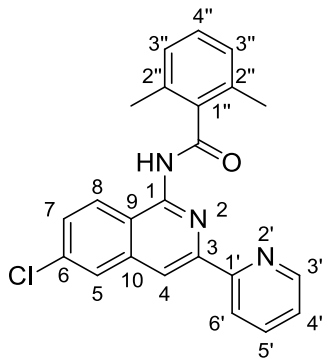

Prepared from 2,6-dimethylbenzoic acid (0.170 g, 1.13 mmol), 6-chloro-3-(pyridin-2-yl)isoquinolin-1-amine **80c** (0.290 g, 1.13 mmol) n-BuLi (0.71 mL, 7.7 mmol), $SOCl_2$ (3-4 mL) and THF (3-4 mL). Isolated as a brown solid (0.097 g, 22 %). m.p. 227-228 °C; **^{1}H NMR (300 MHz, DMSO-*d*$_6$)** δ 10.84 (NH, s, 1H), 8.76 – 8.61 (H-3' and H-6', m, 2H), 8.62 (H-4, s, 1H), 8.38 (H-8, d, *J* = 9.0 Hz, 1H), 8.22 (H-5, d, *J* = 2.1 Hz, 1H), 7.88 (H-5', td, *J* = 7.7, 1.8 Hz, 1H), 7.71 (H-7, dd, *J* = 9.0, 2.1 Hz, 1H), 7.45 – 7.34 (H-4'', m, 1H), 7.20 (H-4', dd, *J* = 8.5, 6.5 Hz, 1H), 7.10 (H-3'', d, *J* = 7.5 Hz, 2H), 2.42 (2 x CH_3, s, 6H), **^{13}C NMR (75 MHz, DMSO-*d*$_6$)** δ 169.7 (C=O), 163.2 (C-1), 157.8 (C-1'), 154.5 (C-3'), 148.8 (C-2''), 148.3 (C-3), 138.7 (C-10), 137.8 (C-1''), 136.4 (C-5'), 135.5 (C-6), 133.19 (C-3'' and C-4'', overlapping), 127.6 (C-5), 126.9 (C-7), 126.7 (C-4'), 126.1 (C-8), 123.3 (C-6'), 120.4 (C-9), 113.9 (C-4), 18.6 (2 x CH_3); **IR (ν_{max}/cm^{-1})** 3290 (N-H); 3183 (=C-H); 645 (C-Cl); 1566 (Ar-C=C), 1648 (C=O) **HRMS** *m/z*: calculated for: $C_{23}H_{19}N_3O^{35}Cl$, 388.1211 found: [M+H]+ 388.1152. HPLC purity: 95.65 %.

8.2.4. Synthesis of *N*-(8-chloro-3-(pyridin-2-yl)isoquinolin-1-yl)-2,6-dimethylbenzamide (77d)

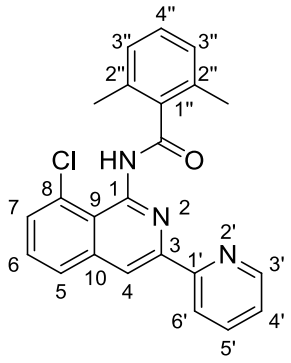

Prepared from 2,6-dimethylbenzoic acid (0.170 g, 1.13 mmol), 8-chloro-3-(pyridin-2-yl)isoquinolin-1-amine **80d** (0.290 g, 1.13 mmol) n-BuLi (0.71 mL, 7.7 mmol), $SOCl_2$ (3-4 mL) and THF (3-4 mL). Isolated as a brown solid (0.062 g, 14 %). m.p. 196-198 °C; **^{1}H NMR (300 MHz, DMSO-*d*$_6$)** δ 10.38 (NH, s, 1H), 8.72 – 8.64 (H-4 and H-6', m, 2H), 8.11 (H-3', dd, *J* = 8.0, 1.5 Hz, 1H), 7.94 – 7.83 (H-5' and H-4'', td, *J* = 8.0, 2.1 Hz, 2H), 7.82 – 7.68 (H-5 and H-7, m, 2H), 7.40 (H-4', ddd, *J* = 6.7, 4.7, 1.7 Hz, 1H), 7.18 (H-6, dd, *J* = 8.4, 6.6 Hz, 1H), 7.08 (H-3'', d, *J* = 7.5 Hz, 2H), 2.44 (2 x CH_3, s, 6H); **^{13}C NMR (75 MHz, DMSO-*d*$_6$)** δ 169.1 (C=O), 154.2 (C-1), 148.8 (C-1'), 147.4 (C-3), 146.8 (C-3'), 140.6 (C-2''), 137.5 (C-10), 136.4 (C-1''), 133.5 (C-3'' and C-4'', overlapping), 130.3 (C-5'), 129.1 (C-6), 127.6 (C-5), 126.9 (C-7), 126.8 (C-8), 123.3 (C-4'), 120.4 (C-6'), 119.6 (C-9), 115.3 (C-4), 18.6 (2 x CH_3); **IR (ν_{max}/cm^{-1})** 3323 (N-H); 3055 (=C-H); 637 (C-Cl); 1552 (Ar-C=C), 1653 (C=O) **HRMS** *m/z*: calculated for: $C_{23}H_{19}N_3O^{35}Cl$, 388.1211 found: $[M+H]^+$ 388.1140. HPLC purity: 100.00 %.

8.2.5. Synthesis of 2,6-dimethyl-*N*-(3-(pyridin-3-yl)isoquinolin-1-yl)benzamide (77e)

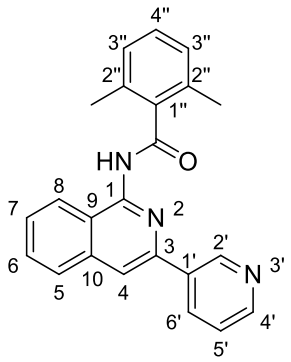

Prepared from 2,6-dimethylbenzoic acid (0.170 g, 1.13 mmol), 3-(pyridin-3-yl)isoquinolin-1-amine **80e** (0.251 g, 1.13 mmol) n-BuLi (0.71 mL, 7.7 mmol), $SOCl_2$ (3-4 mL) and THF (3-4

mL). Isolated as a brown solid (0.069 g, 17 %). m.p. 208-209 °C; **^{1}H NMR (300 MHz, DMSO-*d*$_6$)** δ 10.87 (NH, s, 1H), 9.20 (H-2', s, 1H), 8.74 (H-6', dd, *J* = 5.2, 1.5 Hz, 1H), 8.67 – 8.55 (H-4', m, 1H), 8.46 – 8.36 (H-8 and H-4'', m, 2H), 8.22 – 8.02 (H-5', m, 1H), 7.88 – 7.69 (H-5, H-6 and H-7, m, 3H), 7.25 – 7.12 (H-4, m, 1H), 7.13 – 6.98 (H-3'', m, 2H), 2.40 (2 x CH_3, s, 6H); **^{13}C NMR (75 MHz, DMSO-*d*$_6$)** δ 169.6 (C=O), 149.4 (C-1), 144.4 (C-4'), 143.4 (C-2'), 142.9 (C-3), 137.8 (C-10), 137.6 (C-2''), 135.4 (C-1''), 133.2 (C-3''), 133.1 (C-1'), 130.8 (C-6'), 127.7 (C-6), 127.1 (C-4''), 126.8 (C-5), 126.8 (C-7), 124.9 (C-8), 124.6 (C-5'), 121.7 (C-9), 115.6 (C-4), 18.6 (2 x CH_3); **IR (ν_{max}/cm^{-1})** 3204 (N-H); 3070 (=C-H); 1340 (C-N); 1597 (Ar-C=C), 1676 (C=O), **HRMS** *m/z*: calculated for: $C_{23}H_{20}N_3O$, 354.1601 found: $[M+H]^+$ 354.1601. HPLC purity: 97.18 %.

8.2.6. Synthesis of 2,6-dimethyl-*N*-(3-(pyridin-4-yl)isoquinolin-1-yl)benzamide (77f)

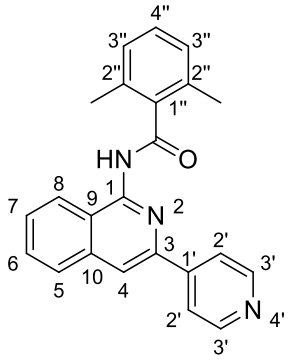

Prepared from 2,6-dimethylbenzoic acid (0.170 g, 1.13 mmol), 3-(pyridin-4-yl)isoquinolin-1-amine **80f** (0.251 g, 1.13 mmol) n-BuLi (0.71 mL, 7.7 mmol), $SOCl_2$ (3-4 mL) and THF (3-4 mL). Isolated as a brown solid (0.056 g, 14 %). m.p. 244-246 °C; **^{1}H NMR (300 MHz, DMSO-*d*$_6$)** δ 11.02 (NH, s, 1H), 9.27 – 9.13 (H-8, m, 1H), 8.78 (H-6, dd, *J* = 1.4, 5.3 Hz, 1H), 8.49 (H-4, s, 1H), 8.41 (H-5, d, *J* = 8.4 Hz, 1H), 8.07 (H-4'', d, *J* = 8.1 Hz, 1H), 7.96 – 7.81 (H-3'', m, 2H), 7.78 (H-7, ddd, *J* = 1.4, 6.9, 8.2 Hz, 1H), 7.26 – 6.99 (H-2' and H-3', m, 4H), 2.40 (2 x CH_3, s, 6H); **^{13}C NMR (75 MHz, DMSO-*d*$_6$)** δ 169.6 (C=O), 149.4 (C-3'), 149.3 (C-1), 145.2 (C-3), 145.1 (C-2''), 137.9 (C-1'), 137.6 (C-3''), 133.2 (C-2'), 130.6 (C-10), 127.6 (C-1''), 127.2 (C-6), 126.8 (C-4''), 126.7 (C-5), 124.6 (C-7), 122.1 (C-8), 120.1 (C-9), 115.6 (C-4), 18.6 (2 x CH_3); **IR (ν_{max}/cm^{-1})** 3115 (N-H); 3065 (=C-H); 1319 (C-N); 1570 (Ar-C=C), 1625 (C=O), **HRMS** *m/z*: calculated for: $C_{23}H_{20}N_3O$, 354.1601 found: $[M+H]^+$ 354.2016. HPLC purity: 99.02 %.

8.2.7. Synthesis of 3-methyl-*N*-(3-(pyridin-2-yl)isoquinolin-1-yl)picolinamide (77g)

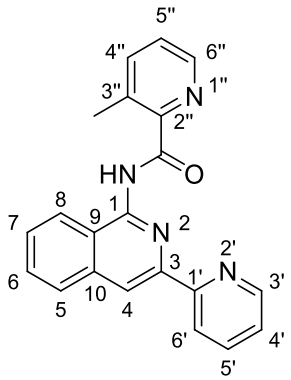

Prepared from 3-methylpyridine-2-carboxylic acid (0.155 g, 1.13 mmol), 3-(pyridin-2-yl)isoquinolin-1-amine **80a** (0.251 g, 1.13 mmol), n-BuLi (0.71 mL, 7.7 mmol), $SOCl_2$ (3-4 mL) and THF (3-4 mL). Isolated as a yellow solid (0.090 g, 23 %). m.p. 128-129 °C; **^{1}H NMR (400 MHz, $CDCl_3$)** δ 8.70 – 8.64 (NH and H-6', m, 2H), 8.59 – 8.49 (H-4 and H-6'', m, 2H), 8.14 (H-8, d, *J* = 8.4 Hz, 1H), 7.94 (H-3', d, *J* = 8.2 Hz, 1H), 7.83 (H-4'', t, *J* = 7.9 Hz, 1H), 7.70 -7.63 (H-5 and H-5', m, 2H), 7.59 (H-5'', t, *J* = 7.7 Hz, 1H), 7.38 (H-6, dd, *J* = 8.1, 4.2 Hz, 1H), 7.28 (H-7, t, *J* = 6.5 Hz, 1H), 7.22 – 7.16 (H-4', m, 1H), 2.80 (CH_3, s, 3H); **^{13}C NMR (101 MHz, $CDCl_3$)** δ 164.4 (C=O), 155.6 (C-1), 149.4 (C-1'), 148.7 (C-2''), 146.7 (C-3), 145.7 (C-3'), 141.6 (C-6''), 138.8 (C-3''), 137.9 (C-10), 136.9 (C-5'), 130.9 (C-4''), 128.5 (C-6), 127.9 (C-5), 126.6 (C-7), 124.9 (C-5''), 123.7 (C-8), 122.8 (C-4'), 122.1 (C-6'), 120.5 (C-9), 116.4 (C-4), 21.1 (CH_3); **IR (ν_{max}/cm^{-1})** 3338 (N-H); 3048 (=C-H); 1624 (C=N); 1565 (Ar-C=C), 1686 (C=O) **HRMS** *m/z*: calculated for: $C_{21}H_{17}N_4O$, 341.1397 found: $[M+H]^+$ 341.1409. HPLC purity: 95.27 %.

Method B:

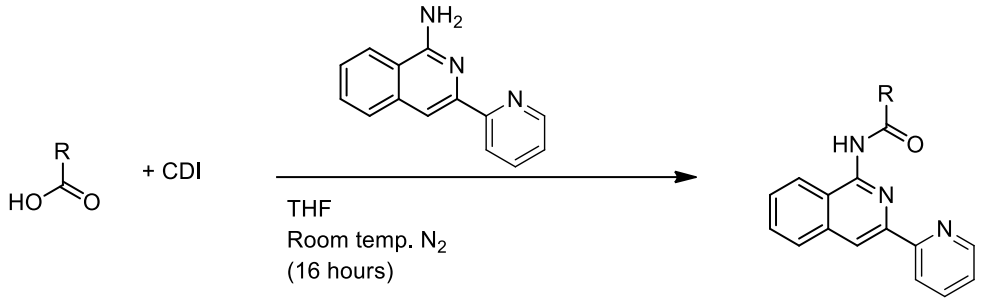

R = 2-picolinyl
nicotinyl
isonicotinyl

Scheme B: Synthesis of compounds 77h-j

Method B: The carboxylic acid (40 mg, 1eq) was dissolved in THF (2 mL), in a round bottomed flask in the presence of a magnetic stirrer bar. Upon dissolution, carbonyldiimidazole (CDI) (2 eq) was added and the reaction mixture was left to stir at room temperature for 1 hour. After 1 hour, the amine (2 eq) was then added, and the reaction mixture was left to stir for 16 hours at room temperature under a nitrogen atmosphere. When the reaction was complete, the resulting mixture was diluted with 5% $KHSO_4$ (aq) (12.5 mL) and the organic layer was extracted with DCM (100 mL). In cases where the desired product remained in the aqueous layer, the 5% $KHSO_4$ (aq) layer was diluted further with water (50 mL) and neutralised using $NaHCO_3$ and the organic layer was extracted using DCM (2 x 100 mL). The organic layer was dried using $MgSO_4$/Na_2SO_4, filtered and concentrated *in vacuo* to get the crude product. Purification was achieved using silica gel column using chromatography 50% EtOAc/hexane as the eluent or by recrystallisation using DCM/hexane or MeOH. The following compounds were prepared by this method:

8.2.8. Synthesis of *N*-(3-(pyridin-2-yl)isoquinolin-1-yl)picolinamide (77h)

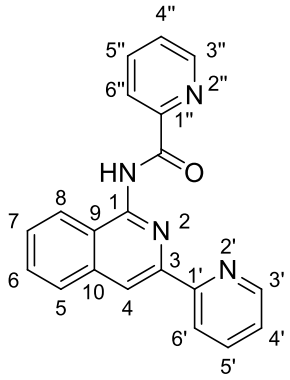

Prepared from 2-picolinic acid (0.0300 g, 0.244 mmol), 3-(pyridin-2-yl)isoquinolin-1-amine **80a** (0.108 g, 0.487 mmol), CDI (0.079 g, 0.49 mmol) and THF (2 mL). Isolated as a yellow solid (0.046 g, 58 %). m.p. 162-164 °C; **^{1}H NMR (400 MHz, MeOD)** δ 8.82 – 8.76 (H-6', m, 1H), 8.66 (H-3'', d, *J* = 4.8 Hz, 1H), 8.63 (H-4, s, 1H), 8.51 (H-6'', d, *J* = 8.1 Hz, 1H), 8.29 (H-8, d, *J* = 7.9 Hz, 1H), 8.14 (H-5, d, *J* = 8.5 Hz, 1H), 8.11 – 8.03 (H-6 and H-3', m, 2H), 7.94 (H-7, t, *J* = 7.9 Hz, 1H), 7.80 (H-5'', t, *J* = 7.6 Hz, 1H), 7.73 – 7.65 (H-5' and H-4'', m, 2H), 7.42 (H-4', t, *J* = 6.4 Hz, 1H); **^{13}C NMR (101 MHz, MeOD)** δ 165.8 (C=O), 157.1 (C-1), 150.8 (C-1'), 150.4 (C-1''), 150.2 (C-3'), 150.0 (C-3''), 149.2 (C-3), 140.1 (C-10), 139.2 (C-5''), 138.8 (C-5'), 132.3 (C-6), 129.3 (C-5), 129.2 (C-4'), 128.5 (C-7), 126.2 (C-8), 125.0 (C-5'), 124.8 (C-9), 123.8 (C-6''), 123.1 (C-6'), 118.1 (C-4); **IR (ν_{max}/cm^{-1})** 3335 (N-H); 3055 (=C-H); 1626 (C=N); 1566 (Ar-C=C), 1693 (C=O) **HRMS** *m/z*: calculated for: $C_{20}H_{15}N_4O$, 327.1240 found: $[M+H]^+$ 327.1201. HPLC purity: 99.44 %.

8.2.9. Synthesis of *N*-(3-(pyridin-2-yl)isoquinolin-1-yl)nicotinamide (77i)

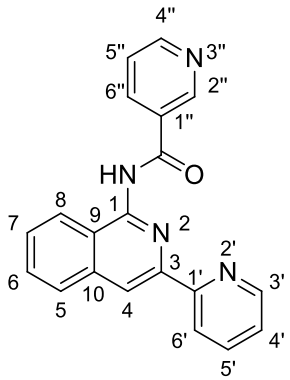

Prepared from nicotinic acid (0.0400 g, 0.325 mmol), 3-(pyridin-2-yl)isoquinolin-1-amine **80a** (0.144 g, 0.650 mmol), CDI (0.105 g, 0.650 mmol) and THF (2 mL). Isolated as a pale brown solid (0.056 g, 53 %). m.p. 150-151 °C; **^{1}H NMR (300 MHz, MeOD)** δ 9.37 (H-2'', s, 1H), 8.77 (H-6', d, *J* = 8.2 Hz, 1H), 8.66 – 8.52 (H-3', H-4'' and H-6'', m, 3H), 8.07 (H-8, d, *J* =

8.1 Hz, 1H), 7.89 – 7.78 (H-4 and H-5', m, 2H), 7.77 – 7.65 (H-5 and H-5'', m, 2H), 7.61 – 7.51 (H-6, m, 1H), 7.49 – 7.41 (H-7, m, 1H), 7.34 (H-4', t, *J* = 6.4 Hz, 1H); **^{13}C NMR (101 MHz, MeOD)** δ 176.8 (C=O), 158.3 (C-1), 152.0 (C-3'), 151.3 (C-2''), 150.6 (C-4''), 149.8 (C-1'), 138.9 (C-5'), 138.8 (C-6''), 136.2 (C-3), 135.8 (C-10), 134.8 (C-6), 129.7 (C-5), 128.7 (C-7), 128.3 (C-5''), 126.9 (C-1''), 125.7 (C-8), 124.9 (C-4'), 122.8 (C-9), 121.2 (C-6'), 111.6 (C-4); **IR (ν_{max}/cm^{-1})** 3202 (N-H); 3066 (=C-H); 1665 (C=N); 1569 (Ar-C=C), 1601 (C=O) **HRMS** *m/z*: calculated for: $C_{20}H_{15}N_4O$, 327.1240 found: $[M+H]^+$ 327.1190. HPLC purity: 99.36 %.

8.2.10. Synthesis of *N*-(3-(pyridin-2-yl)isoquinolin-1-yl)isonicotinamide (77j)

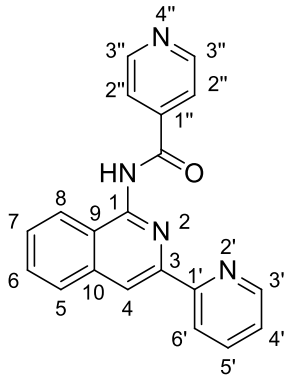

Prepared from isonicotinic acid (0.0400 g, 0.325 mmol), 3-(pyridin-2-yl)isoquinolin-1-amine **80a** (0.144 g, 0.650 mmol), CDI (0.105 g, 0.650 mmol) and THF (2 mL). Isolated as a pale brown solid (0.066 g, 63 %). m.p. 208-209 °C; **^{1}H NMR (400 MHz, MeOD)** δ 8.96 (H-6', d, *J* = 8.3 Hz, 1H), 8.84 – 8.77 (H-3', m, 1H), 8.72 (H-3'', d, *J* = 5.3 Hz, 2H), 8.31 (H-2'', d, *J* = 6.0 Hz, 2H), 8.24 (H-8, d, *J* = 8.1 Hz, 1H), 8.05 (H-4, s, 1H), 7.98 (H-5', t, *J* = 7.8 Hz, 1H), 7.94 – 7.81 (H-5 and H-6, m, 2H), 7.72 (H-7, t, *J* = 7.6 Hz, 1H), 7.49 (H-4', t, *J* = 6.3 Hz, 1H); **^{13}C NMR (126 MHz, MeOD)** δ 176.7 (C=O), 151.2 (C-1), 150.7 (C-1'), 150.5 (C-3''), 149.9 (C-3), 148.0 (C-1''), 139.1 (C-10), 138.9 (C-5'), 135.0 (C-3'), 129.8 (C-6), 128.8 (C-5), 128.4 (C-7), 126.9 (C-8) 125.8 (C-4'), 124.6 (C-2''), 123.5 (C-6') 121.3 (C-9), 112.0 (C-4); **IR (ν_{max}/cm^{-1})** 3084 (N-H); 3036 (=C-H); 1628 (C=N); 1569 (Ar-C=C), 1601 (C=O) **HRMS** *m/z*: calculated for: $C_{20}H_{15}N_4O$, 327.1240 found: $[M+H]^+$ 327.1207. HPLC purity: 98.72 %.

8.3. Synthesis of 2-(3-(pyridin-2-yl)isoquinolin-1-yl)isoindoline-1,3-dione (122)

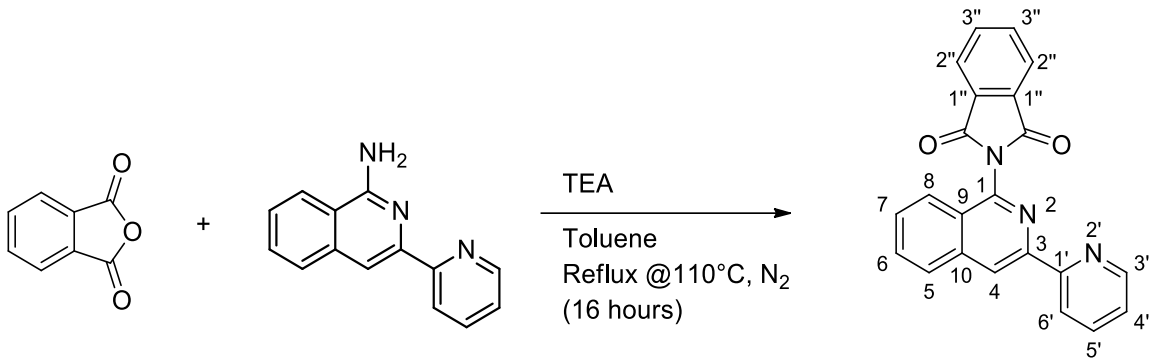

The 3-(pyridin-2-yl)isoquinolin-1-amine (0.150 g, 0.678 mmol) was dissolved in toluene (3 mL) in a round bottomed flask in the presence of a magnetic stirrer bar. Upon dissolution, 0.14 mL of triethylamine (TEA) was added and the reaction mixture was left to stir at room temperature under a nitrogen atmosphere for 10 minutes. After 10 minutes, phthalic anhydride (0.100 g, 0.678 mmol) was added, and the reaction mixture was heated to reflux and stirred overnight under a nitrogen atmosphere. After this time, the reaction mixture was cooled to room temperature and upon cooling the crude product precipitated out of solution. The precipitate was filtered and purified by recrystallisation from EtOAc to afford a white solid (0.171 g, 71.8 %), with a melting point of 267-268 °C and a percentage purity of 97.90 % which was determined on the HPLC.

^{1}H NMR (400 MHz, $CDCl_3$) δ 8.42 (H-4, s, 1H), 8.20 – 8.14 (H-6', m, 1H), 7.92 (H-3', d, *J* = 8.0 Hz, 1H), 7.55 – 7.43 (H-5, H-8 and H-5', m, 3H), 7.34 – 7.24 (H-2'' and H-3'', m, 4H), 7.19 (H-6, t, *J* = 7.7 Hz, 1H), 7.05 (H-7, t, *J* = 7.7 Hz, 1H), 6.76 (H-4', t, *J* = 6.2 Hz, 1H); **^{13}C NMR (101 MHz, $CDCl_3$)** δ 167.5 (2 x C=O), 155.4 (C-1), 149.1 (C-1'), 148.9 (C-3), 145.0 (C-10), 139.1 (C-3'), 137.6 (C-5'), 134.8 (C-1''), 132.3 (C-3''), 131.3 (C-6), 128.9 (C-5), 128.6 (C-7), 126.1 (C-8), 124.7 (C-4'), 124.3 (C-2''), 123.8 (C-6'), 122.1 (C-9), 119.8 (C-4); **IR (ν_{max}/cm^{-1})** 3064 (=C-H); 1317 (C-N); 1562 (Ar-C=C), 1720 (C=O) **HRMS** *m/z*: calculated for: $C_{22}H_{14}N_3O_2$, 352.1081 found: $[M+H]^+$ 352.1085.

8.4. Crystal structure and refinement

Similarly, the intensity data for **compounds 77a**, **120 and 121** was collected on a either a BRUKER D8 Venture PHOTON II pixel array area detector with Mo Kα graphite monochromated sealed X-ray source (50kV, 30 mA), or a Bruker D8 Venture Bio PHOTON III diffractometer with a Mo Kα IμS DIAMOND source (50kV, 1.4 mA). The collection method involved ω- and φ-scans, with either 768 × 1024 (PHOTON II) or 1536 × 1024 (PHOTON III) bit data frames. The unit cell and full data set were collected using *APEX4*[58]; *SAINT* was used to integrate the data, and *SADABS* was used to make empirical absorption corrections and scale the data. Space group assignments were made using *XPREP* on all compounds. Using *Olex2*[59], the crystal structures were solved with the *ShelXT*[60] structure solution program using Intrinsic Phasing and refined with the *ShelXL*[61] refinement package using Least Squares minimization. Non-hydrogen atoms were first refined isotropically followed by anisotropic refinement by full matrix least-squares calculations based on F^2. Professor Manuel Fernandes of the University of the Witwatersrand was responsible for carrying out these experiments.

Crystal data for 77a: $C_{23}H_{19}N_3O$ (M =353.41 g/mol): triclinic, space group P-1 (no. 2), a = 8.1633(4) Å, b = 10.6567(4) Å, c = 11.0665(5) Å, α = 106.069(2)°, β = 93.853(2)°, γ = 102.484(2)°, V = 894.91(7) Å^3, Z = 2, T = 173.00 K, μ(MoKα) = 0.082 mm^{-1}, *Dcalc* = 1.312 g/cm^3, 35934 reflections measured (3.866° ≤ 2Θ ≤ 56.692°), 4454 unique (R_{int} = 0.0622, R_{sigma} = 0.0384) which were used in all calculations. The final R_1 was 0.0446 (I > 2σ(I)) and wR_2 was 0.1327 (all data).

Crystal data for 120: $C_{24}H_{22}Cl_3N_3O_2$ (M =490.79 g/mol): monoclinic, space group $P2_1/n$ (no. 14), a = 10.0459(4) Å, b = 8.6792(4) Å, c = 30.5163(13) Å, β = 99.2608(11)°, V = 2626.0(2) Å^3, Z = 4, T = 173.0 K, μ(MoKα) = 0.373 mm^{-1}, *Dcalc* = 1.241 g/cm^3, 69824 reflections measured (5.29° ≤ 2Θ ≤ 53.996°), 5699 unique (R_{int} = 0.0267, R_{sigma} = 0.0144) which were used in all calculations. The final R_1 was 0.0760 (I > 2σ(I)) and wR_2 was 0.1995 (all data).

Crystal data for 121: $C_{23}H_{20}ClN_3O_2$ (M =405.87 g/mol): monoclinic, space group $P2_1/c$ (no. 14), a = 13.2658(6) Å, b = 7.2631(3) Å, c = 20.9559(10) Å, β = 90.894(2)°, V = 2018.87(16) Å^3, Z = 4, T = 173.0 K, μ(MoKα) = 0.214 mm^{-1}, *Dcalc* = 1.335 g/cm^3, 69402 reflections measured (3.888° ≤ 2Θ ≤ 56.646°), 5018 unique (R_{int} = 0.0899, R_{sigma} = 0.0378) which were used in all calculations. The final R_1 was 0.0521 (I > 2σ(I)) and wR_2 was 0.1455 (all data).

APPENDIX

^{1}H NMR spectrum of 80a

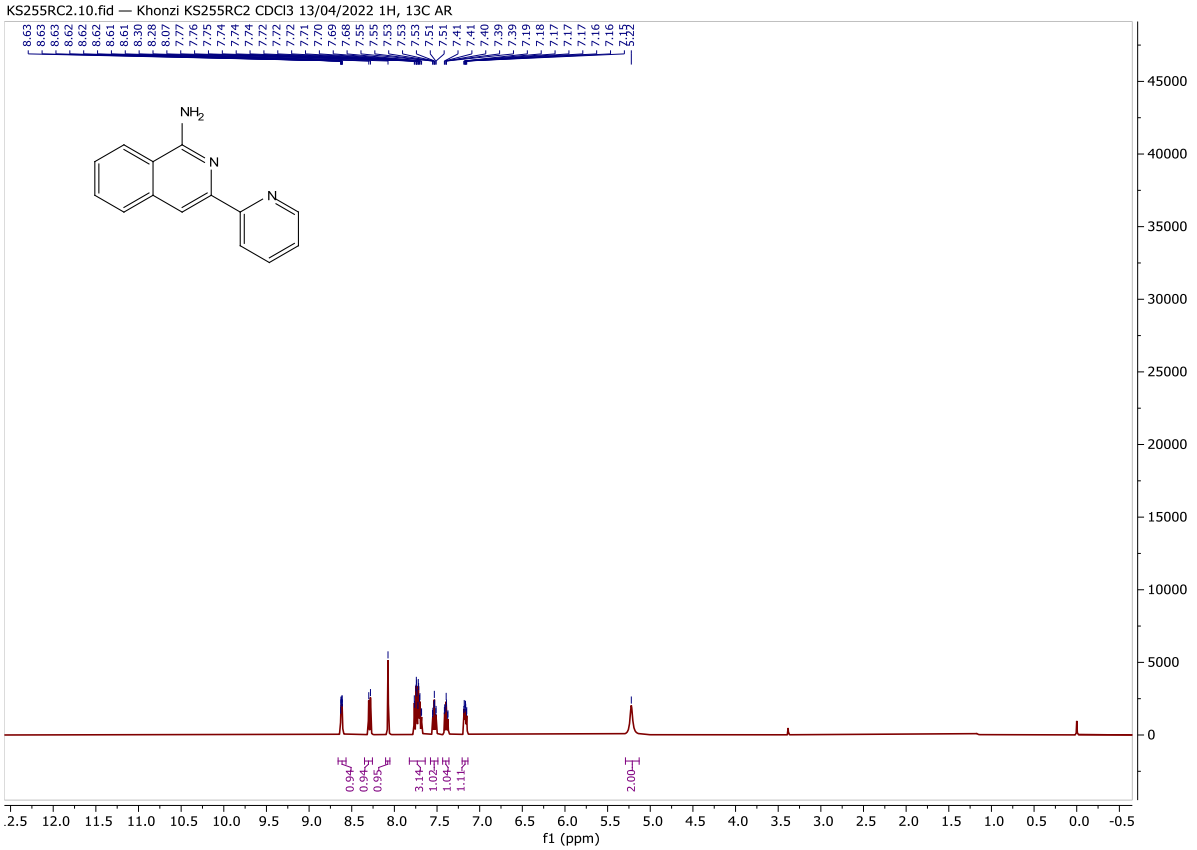

^{13}C NMR spectrum of 80a

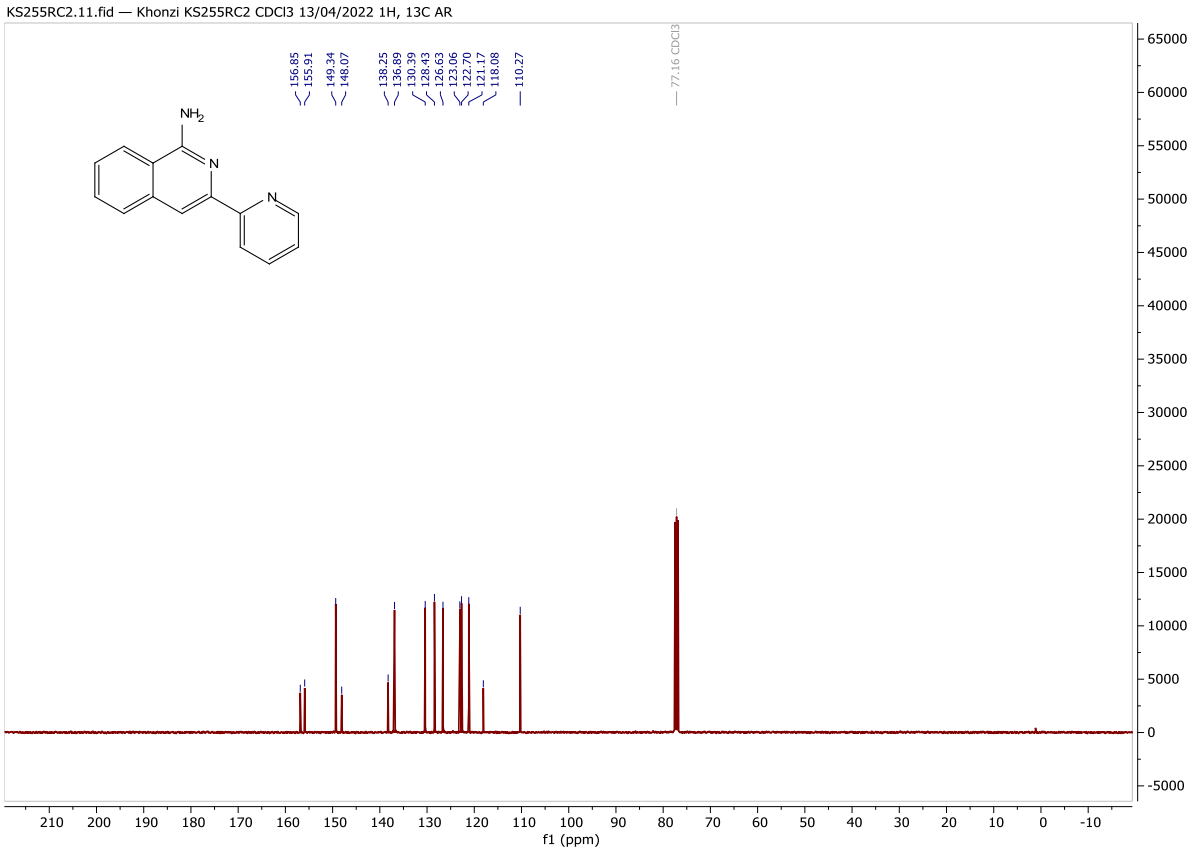

^{1}H NMR spectrum of 77a (high temperature NMR at 100 °C)

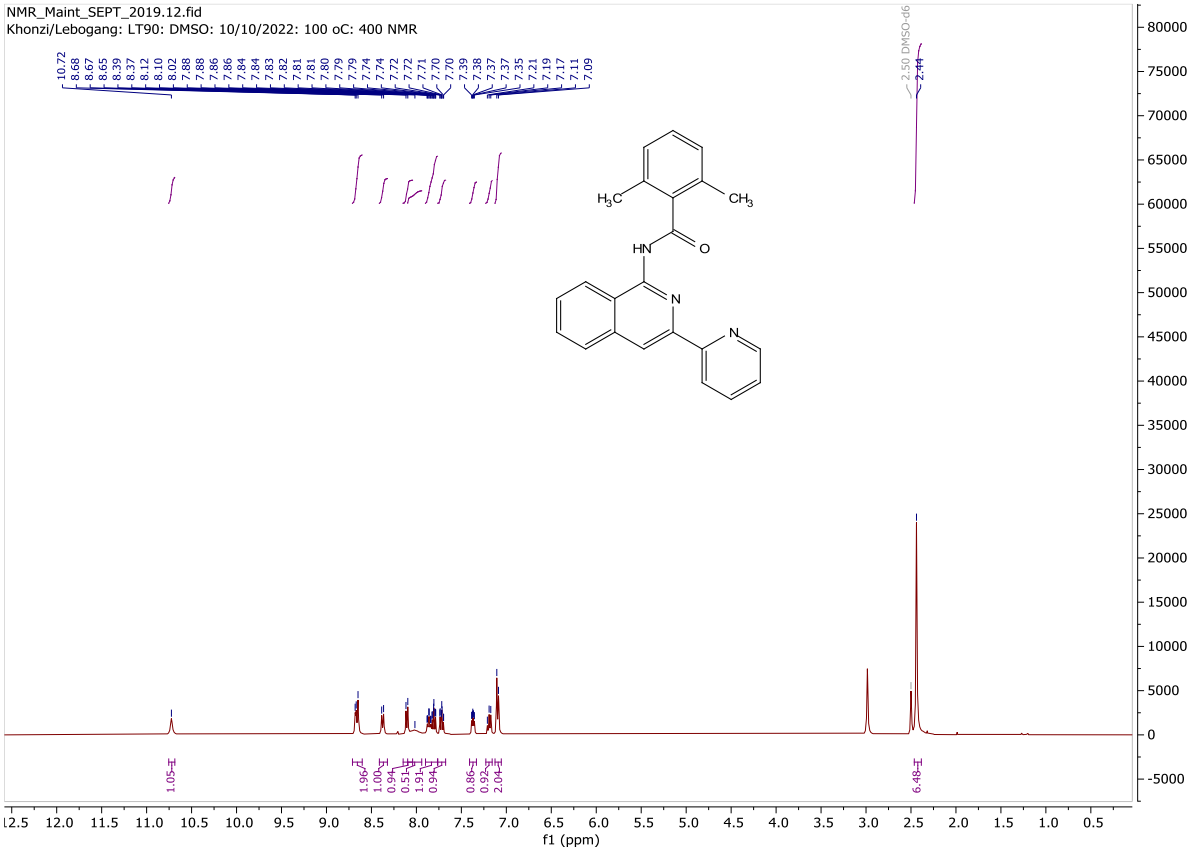

^{13}C NMR spectrum of 77a (high temperature NMR at 100 °C)

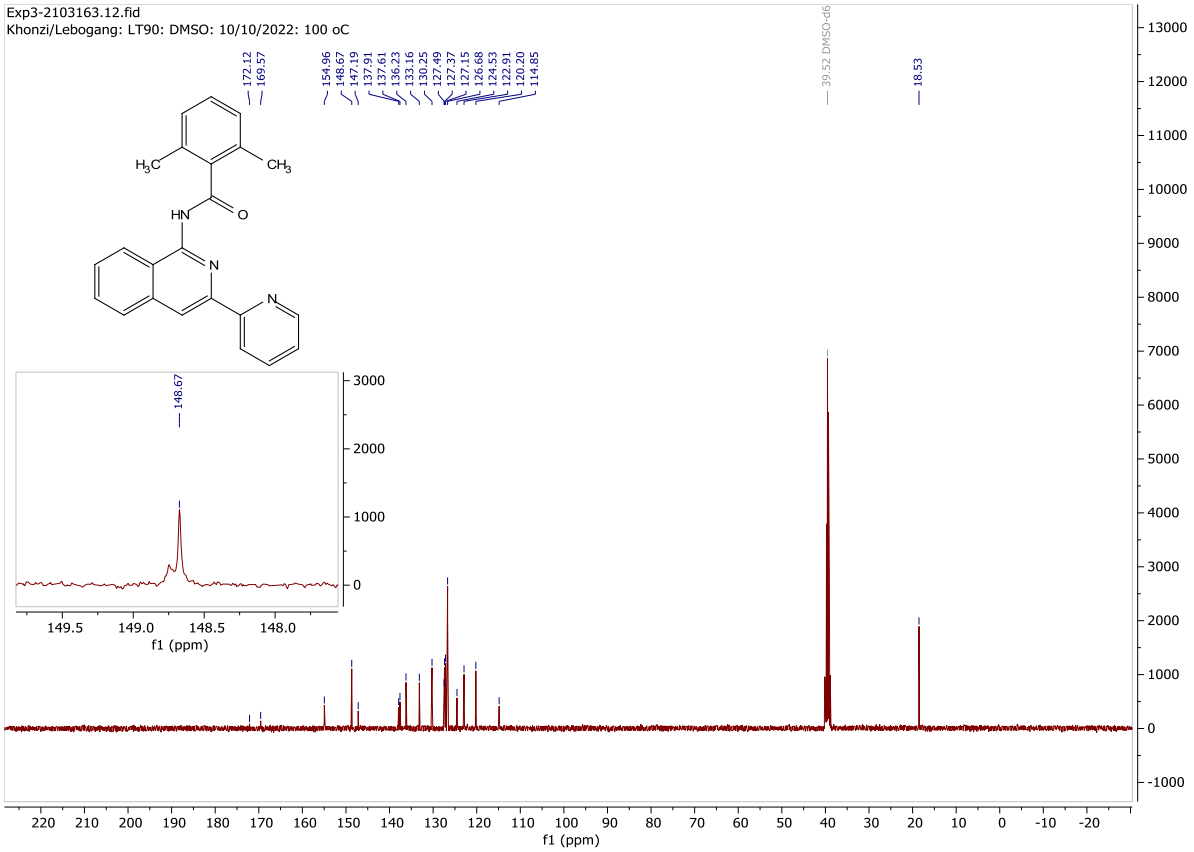

^{1}H NMR spectrum of 77d (high temperature NMR at 90 °C)

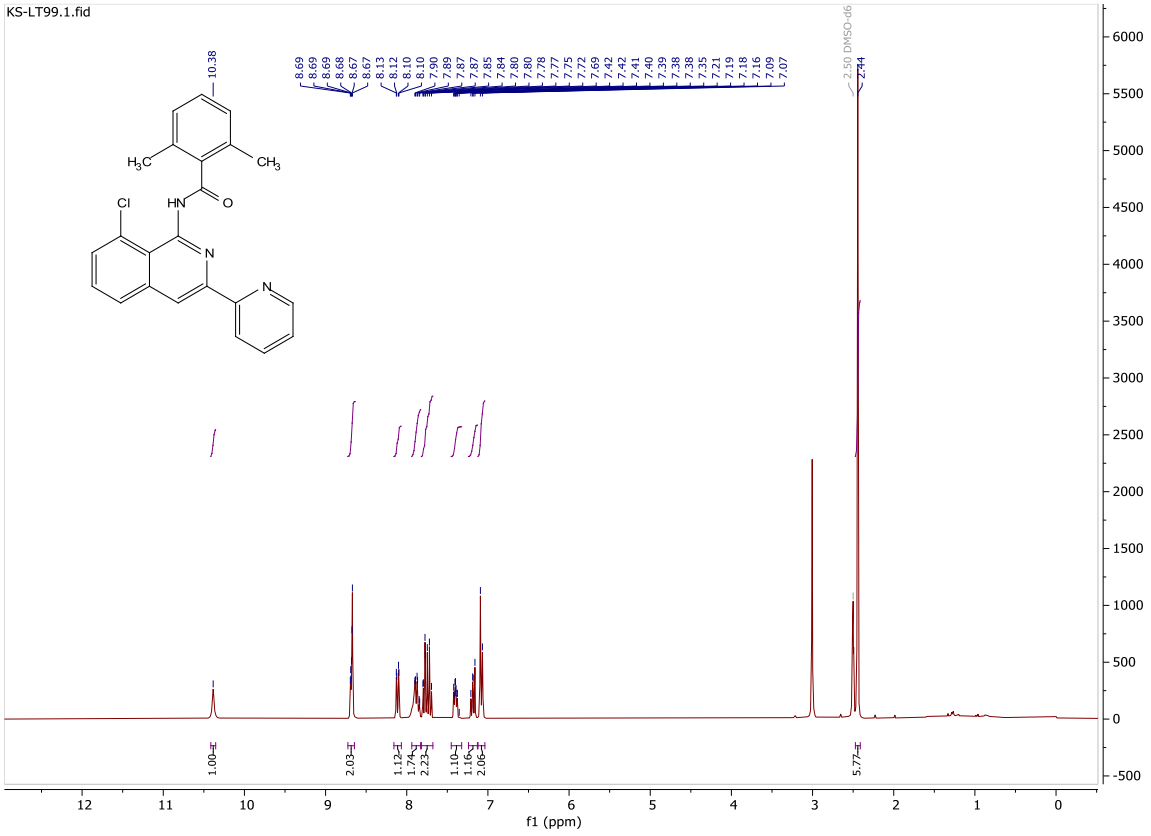

^{13}C NMR spectrum of 77d (high temperature NMR at 90 °C)

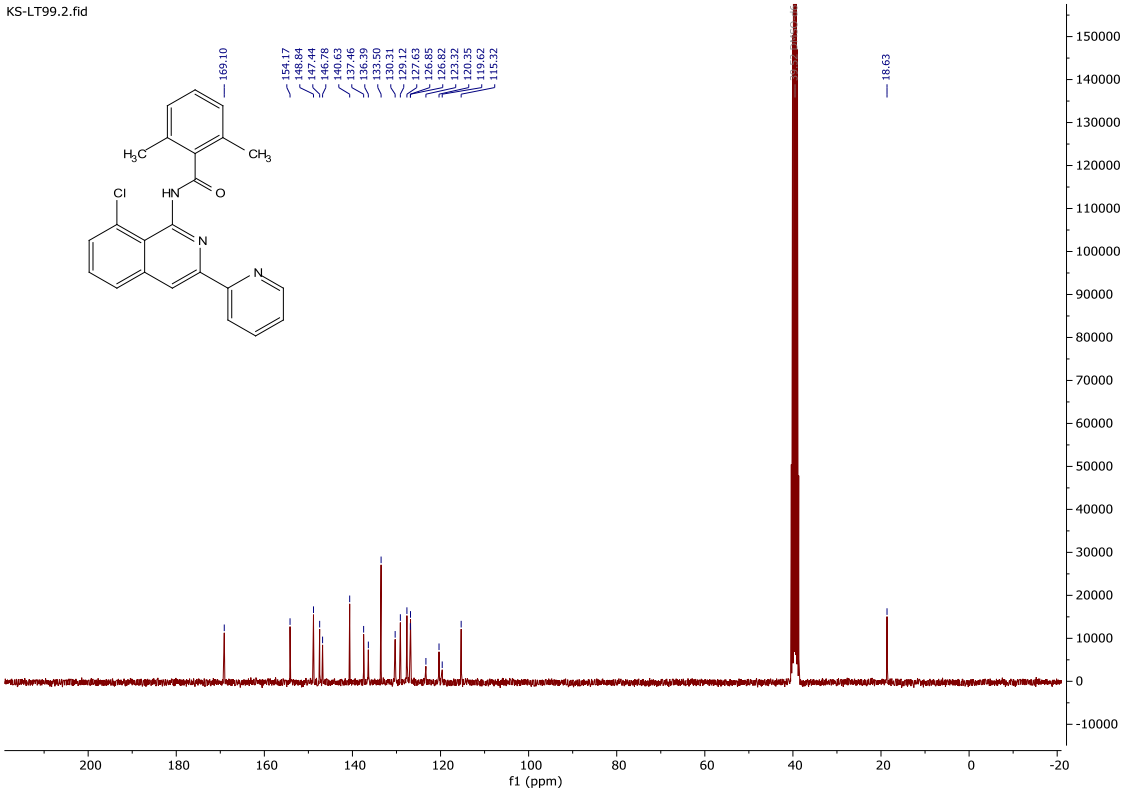

^{1}H NMR spectrum of 77g

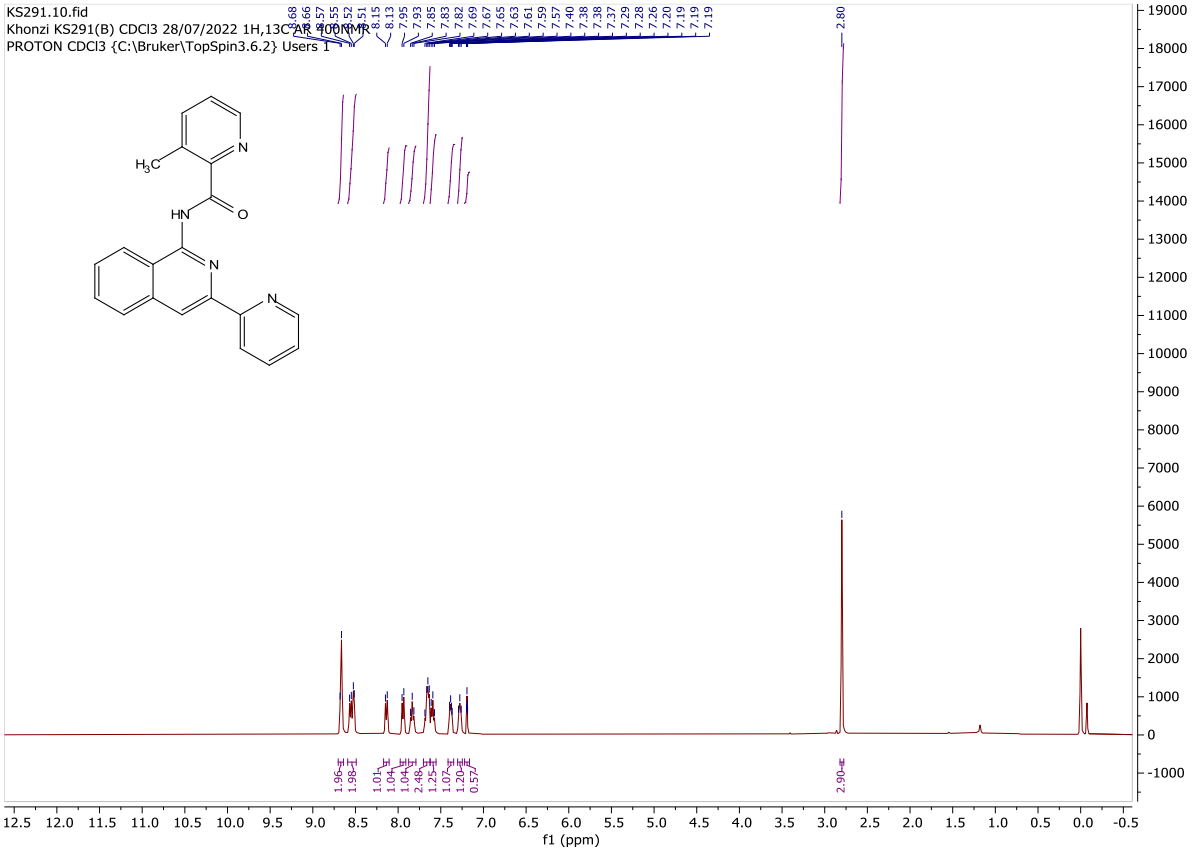

^{13}C NMR spectrum of 77g

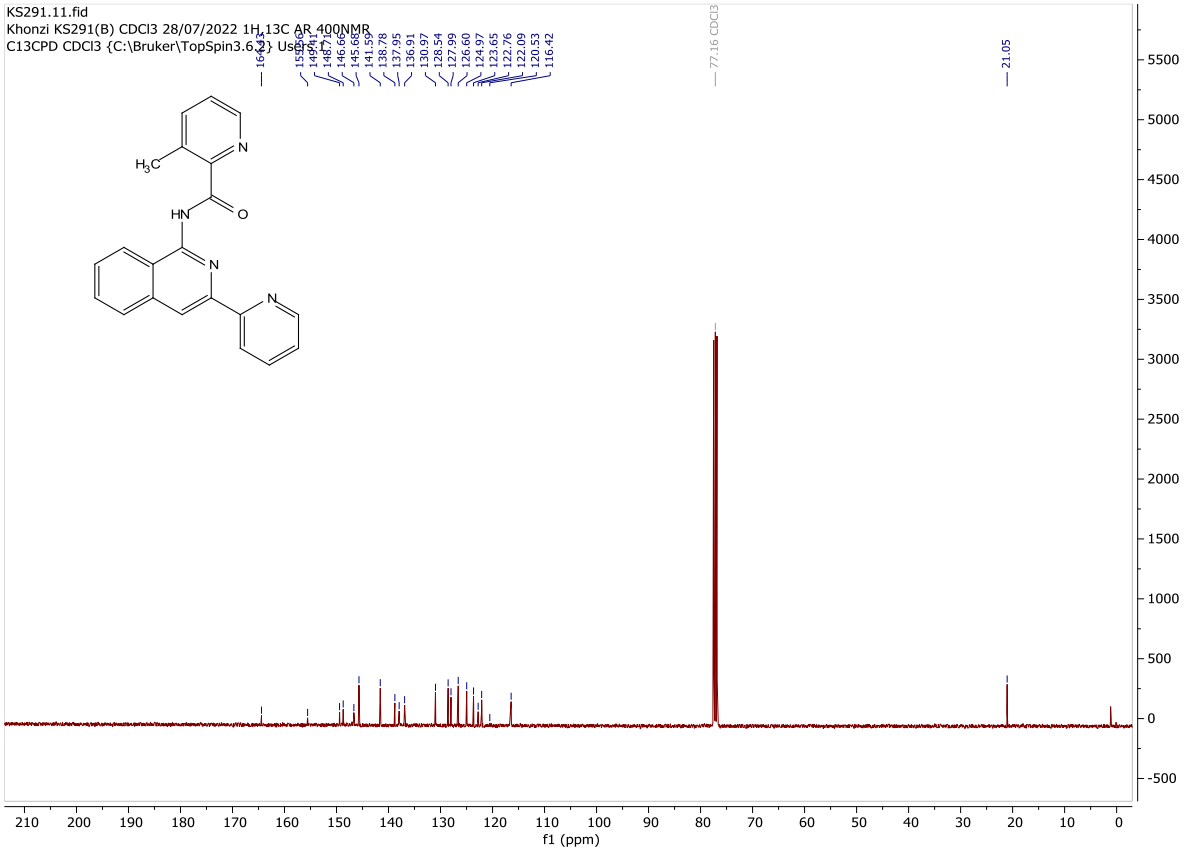

^{1}H NMR spectrum of 77h

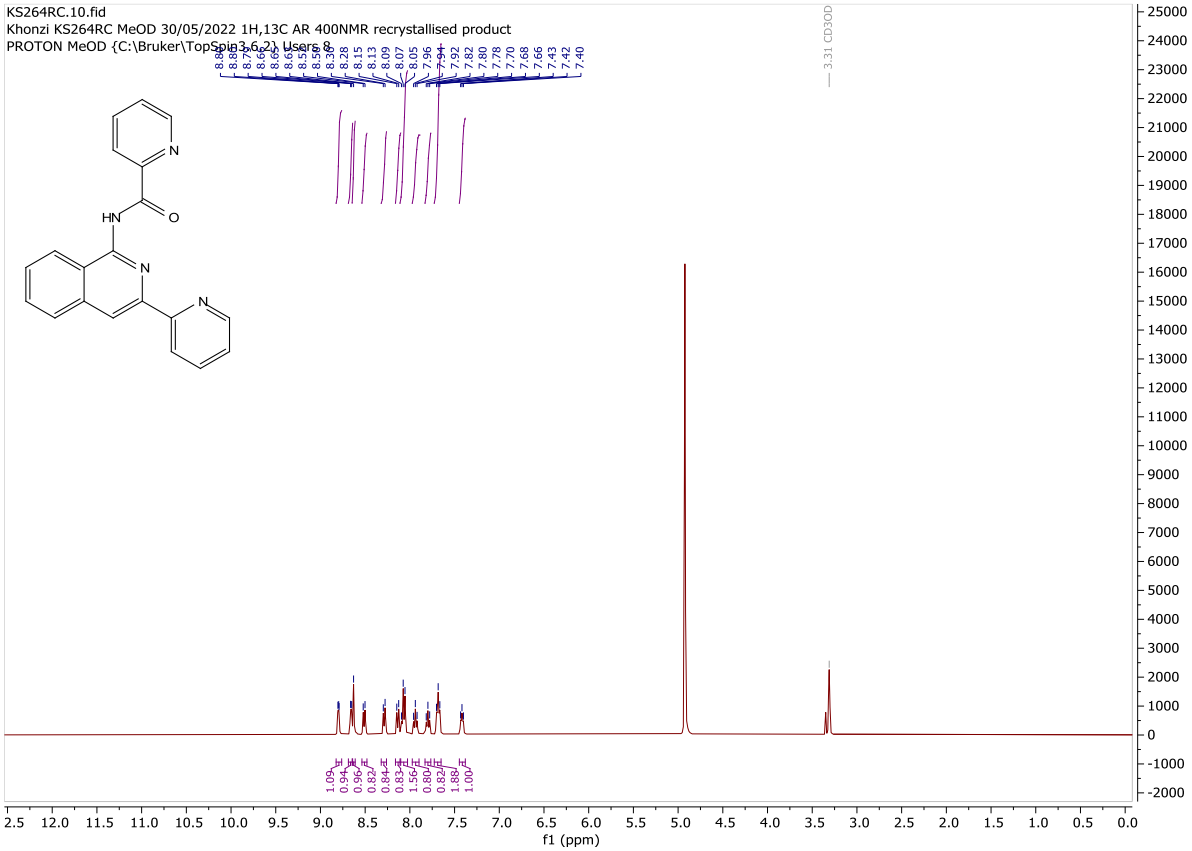

^{13}C NMR spectrum of 77h

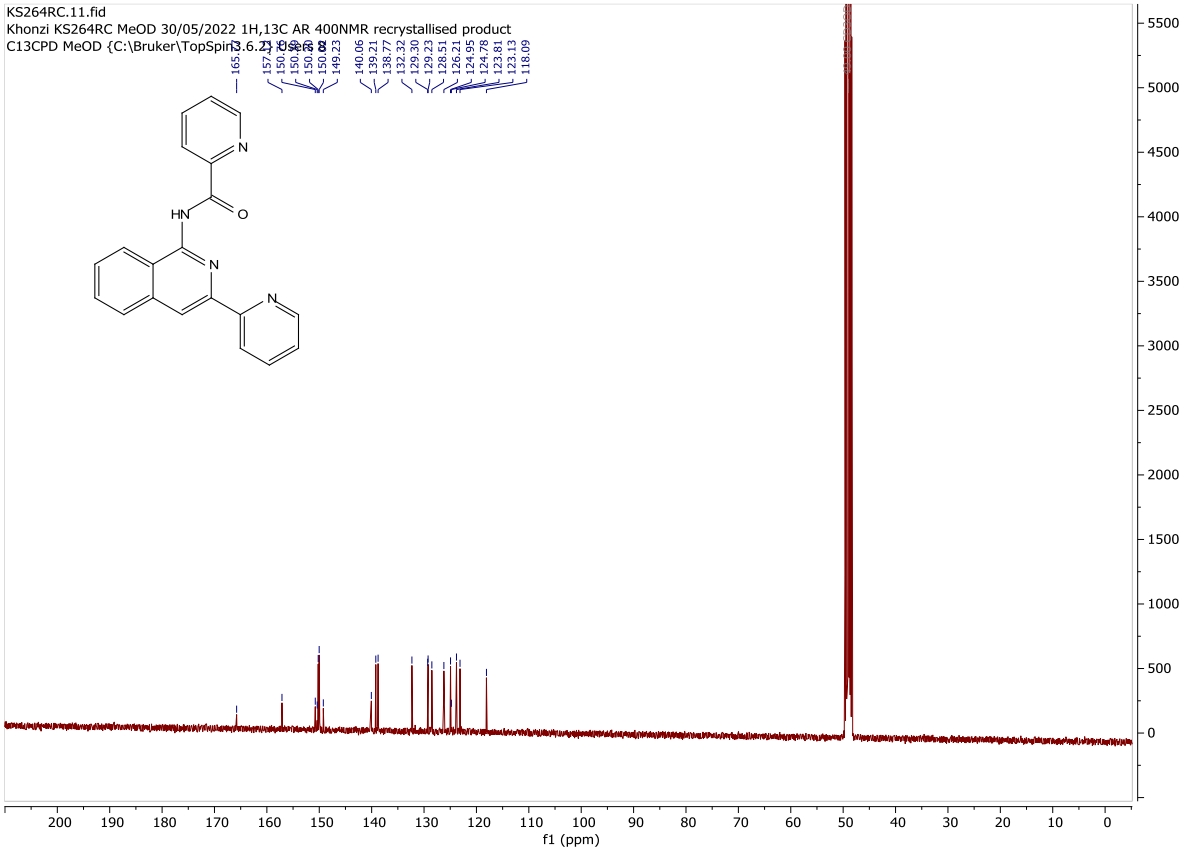

^{1}H NMR spectrum of 122

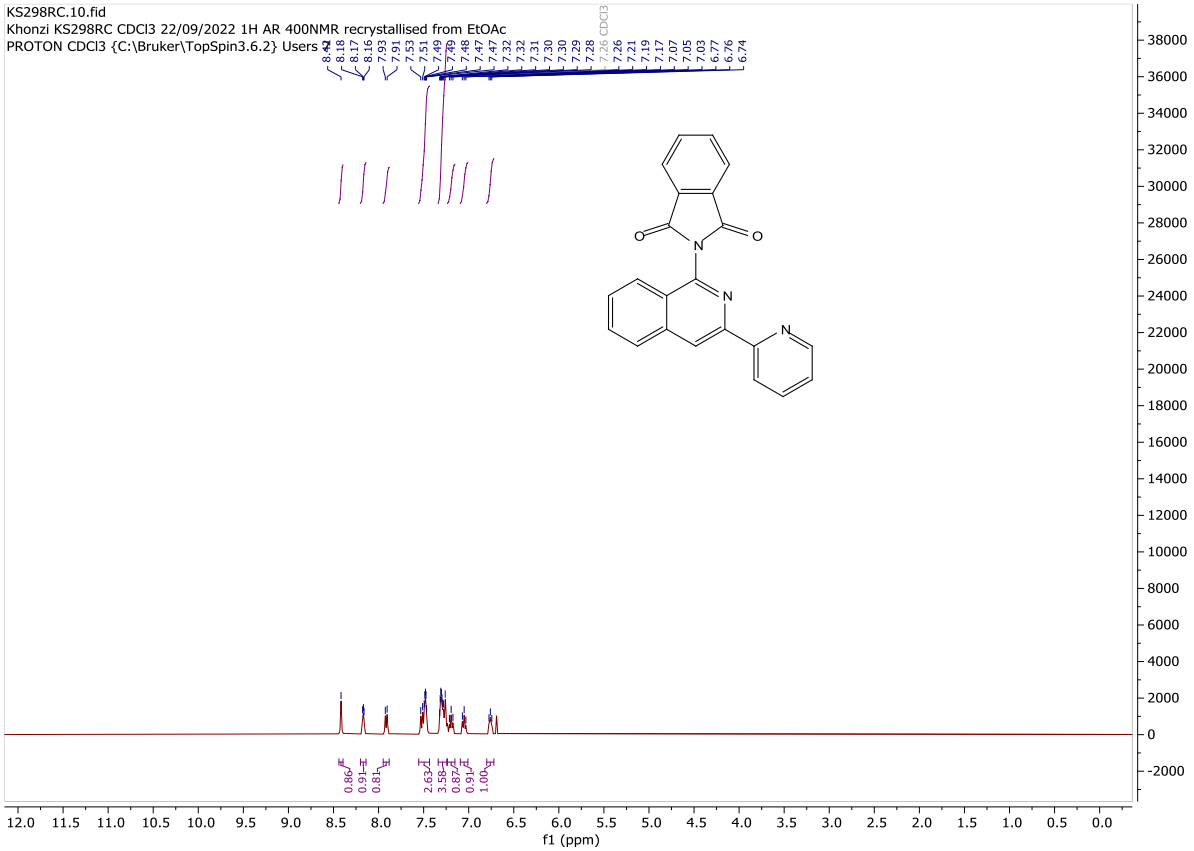

^{13}C NMR spectrum of 122

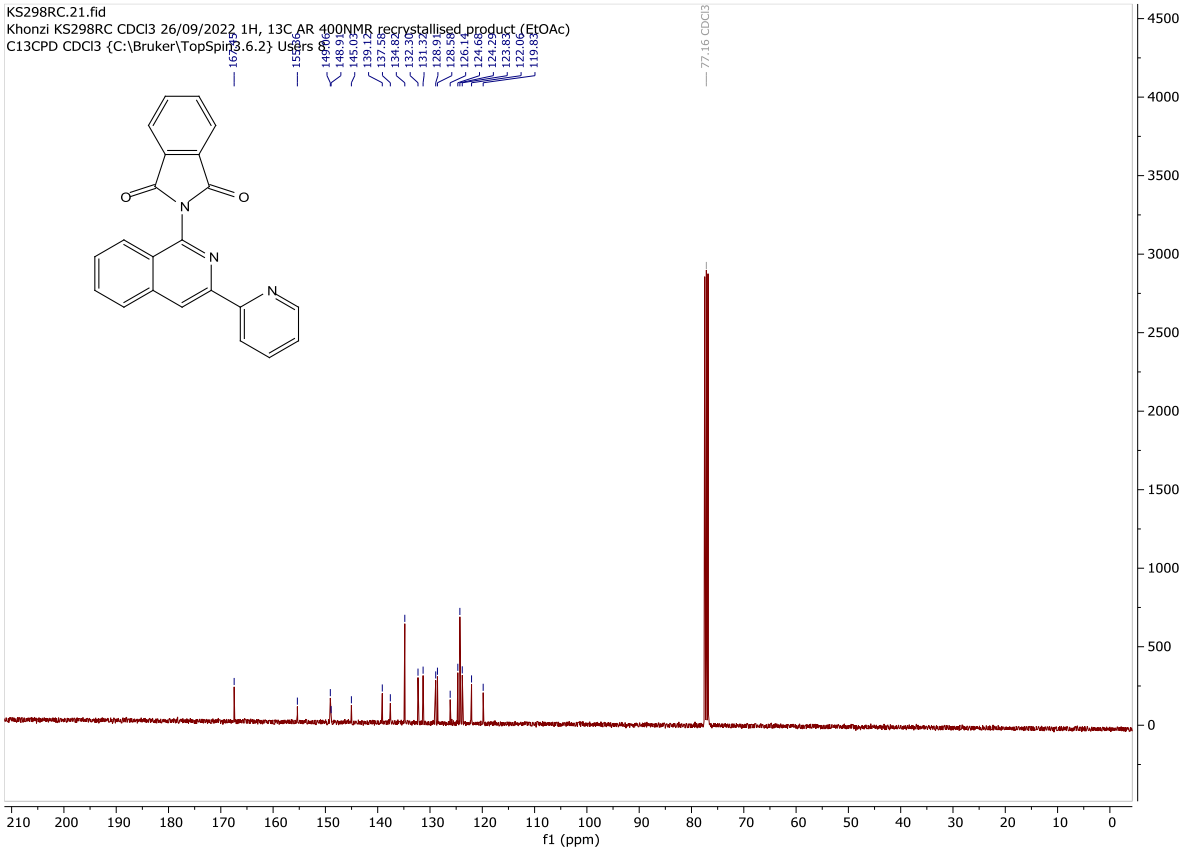

REFERENCES

(1) *World Health Organisation (2021)*. https://www.who.int/news-room/fact-sheets (accessed 2023-01-13).

(2) Arrow, K.; Panosian, C.; Gelband, H. Antimalarial Drugs and Drug Resistance. In *Saving Lives, Buying Time: Economics of Malaria Drugs in an Age of Resistance*; Arrow, K., Panosian, C., Gelband, H., Eds.; National Academies Press (US): Washington DC, 2004; Vol. 1, pp 1–2.

(3) Jagannathan, P.; Kakuru, A. Malaria in 2022: Increasing Challenges, Cautious Optimism. *Nat Commun* **2022**, *13* (1), 2678. https://doi.org/10.1038/s41467-022-30133-w.

(4) Roser, M. *Malaria: One of the leading causes of child deaths, but progress is possible and you can contribute to it*. Our World in Data. https://ourworldindata.org/malaria-introduction (2022-10-27)

(5) Beck, T. Will Malaria Soon Be a Thing of the Past?The Potential of Recombinant Protein Vaccines to Control One of the World's Most Deadly Diseases. In *Coffee Break: Tutorials for NCBI Tools*; Dean, L., McEntyre, J., Eds.; National Center for Biotechnology Information (US): Bethesda (MD), 2006.

(6) Okumu, F. O.; Moore, S. J. Combining Indoor Residual Spraying and Insecticide-Treated Nets for Malaria Control in Africa: A Review of Possible Outcomes and an Outline of Suggestions for the Future. *Malar. J.* **2011**, *10* (1), 208. https://doi.org/10.1186/1475-2875-10-208.

(7) Pryce, J.; Medley, N.; Choi, L. Indoor Residual Spraying for Preventing Malaria in Communities Using Insecticide-Treated Nets. *CDSR*. **2022**, *2022* (1). https://doi.org/10.1002/14651858.CD012688.pub3.

(8) Turusov, V.; Rakitsky, V.; Tomatis, L. Dichlorodiphenyltrichloroethane (DDT): Ubiquity, Persistence, and Risks. *Environ. Health Perspect.* **2002**, *110* (2), 125–128. https://doi.org/10.1289/ehp.02110125.

(9) Soderlund, D. M. Molecular Mechanisms of Pyrethroid Insecticide Neurotoxicity: Recent Advances. *Arch. Toxicol.* **2012**, *86* (2), 165–181. https://doi.org/10.1007/s00204-011-0726-x.

(10) Global Insecticide Use for Vector-Borne Disease Control, 6th ed.; World Health Organisation: Geneva, 2021. pp 8-34.

(11) Laurens, M. B. RTS,S/AS01 Vaccine (Mosquirix^{TM}): An Overview. *Hum Vaccin Immunother* **2020**, *16* (3), pp 480–489. https://doi.org/10.1080/21645515.2019.1669415.

(12) Datoo, M. S.; Natama, M. H.; Somé, A.; Traoré, O.; Rouamba, T.; Bellamy, D.; Yameogo, P.; Valia, D.; Tegneri, M.; Ouedraogo, F.; Soma, R.; Sawadogo, S.; Sorgho, F.; Derra, K.; Rouamba, E.; Orindi, B.; Ramos Lopez, F.; Flaxman, A.; Cappuccini, F.; Kailath, R.; Elias, S.; Mukhopadhyay, E.; Noe, A.; Cairns, M.; Lawrie, A.; Roberts, R.; Valéa, I.; Sorgho, H.; Williams, N.; Glenn, G.; Fries, L.; Reimer, J.; Ewer, K. J.; Shaligram, U.; Hill, A. V. S.; Tinto, H. Efficacy of a Low-Dose Candidate Malaria Vaccine, R21 in Adjuvant Matrix-M, with Seasonal Administration to Children in Burkina Faso: A Randomised Controlled Trial. *Lancet.* **2021**, *397* (10287), 1809–1818. https://doi.org/10.1016/S0140-6736(21)00943-0.

(13) R21/Matrix-M^{TM} malaria vaccine developed by University of Oxford receives regulatory clearance for use in Ghana. https://www.thecable.ng/oxford-malaria-vaccine-gets-clearance-for-use-in-ghana#:~:text=A%20malaria%20vaccine%20called%20R21,percent%20effective%20in%20preventing%20malaria (accessed 2023-04-18)

(14) Rosenthal, P. J. Artemisinin Resistance Outside of Southeast Asia. *Am. J. Trop. Med. Hyg.* **2018**, *99* (6), 1357–1359. https://doi.org/10.4269/ajtmh.18-0845.

(15) Ocan, M.; Akena, D.; Nsobya, S.; Kamya, M. R.; Senono, R.; Kinengyere, A. A.; Obuku, E. A. Persistence of Chloroquine Resistance Alleles in Malaria Endemic Countries: A Systematic Review of Burden and Risk Factors. *Malar. J.* **2019**, *18* (1), 76. https://doi.org/10.1186/s12936-019-2716-z.

(16) Heinberg, A.; Kirkman, L. The Molecular Basis of Antifolate Resistance in *Plasmodium Falciparum* : Looking beyond Point Mutations. *Ann. N. Y. Acad. Sci.* **2015**, *1342* (1), 10–18. https://doi.org/10.1111/nyas.12662.

(17) Birkholtz, L.-M.; Alano, P.; Leroy, D. Transmission-Blocking Drugs for Malaria Elimination. *Trends Parasitol.* **2022**, *38* (5), 390–403. https://doi.org/10.1016/j.pt.2022.01.011.

(18) Product Development Partnerships (PDPs). Collaborations in Global Health. https://www.gesundheitsforschung-bmbf.de/en/product-development-partnerships-pdps-8692.php (accessed 2023-01-12)

(19) Mahoney, R. T. Product Development Partnerships: Case Studies of a New Mechanism for Health Technology Innovation. *Health Res. Policy Syst.* **2011**, *9* (1), 33. https://doi.org/10.1186/1478-4505-9-33.

(20) Williamson, A. E.; Ylioja, P. M.; Robertson, M. N.; Antonova-Koch, Y.; Avery, V.; Baell, J. B.; Batchu, H.; Batra, S.; Burrows, J. N.; Bhattacharyya, S.; Calderon, F.; Charman, S. A.; Clark, J.; Crespo, B.; Dean, M.; Debbert, S. L.; Delves, M.; Dennis, A. S. M.; Deroose, F.; Duffy, S.; Fletcher, S.; Giaever, G.; Hallyburton, I.; Gamo, F.-J.; Gebbia, M.; Guy, R. K.; Hungerford, Z.; Kirk, K.; Lafuente-Monasterio, M. J.; Lee, A.; Meister, S.; Nislow, C.; Overington, J. P.; Papadatos, G.; Patiny, L.; Pham, J.; Ralph, S. A.; Ruecker, A.; Ryan, E.; Southan, C.; Srivastava, K.; Swain, C.; Tarnowski, M. J.; Thomson, P.; Turner, P.; Wallace, I. M.; Wells, T. N. C.; White, K.; White, L.; Willis, P.; Winzeler, E. A.; Wittlin, S.; Todd, M. H. Open Source Drug Discovery: Highly Potent Antimalarial Compounds Derived from the Tres Cantos Arylpyrroles. *ACS. Cent. Sci.* **2016**, *2* (10), 687–701. https://doi.org/10.1021/acscentsci.6b00086.

(21) Visentin, M.; Zhao, R.; Goldman, I. D. The Antifolates. *Hematol. Oncol. Clin. North Am.* **2012**, *26* (3), 629–648. https://doi.org/10.1016/j.hoc.2012.02.002.

(22) Reader, J.; van der Watt, M. E.; Taylor, D.; le Manach, C.; Mittal, N.; Ottilie, S.; Theron, A.; Moyo, P.; Erlank, E.; Nardini, L.; Venter, N.; Lauterbach, S.; Bezuidenhout, B.; Horatscheck, A.; van Heerden, A.; Spillman, N. J.; Cowell, A. N.; Connacher, J.; Opperman, D.; Orchard, L. M.; Llinás, M.; Istvan, E. S.; Goldberg, D. E.; Boyle, G. A.; Calvo, D.; Mancama, D.; Coetzer, T. L.; Winzeler, E. A.; Duffy, J.; Koekemoer, L. L.; Basarab, G.; Chibale, K.; Birkholtz, L.-M. Multistage and Transmission-Blocking Targeted Antimalarials Discovered from the Open-Source MMV Pandemic Response Box. *Nat. Commun.* **2021**, *12* (1), 269. https://doi.org/10.1038/s41467-020-20629-8.

(23) Bailey, L. B.; Gregory, J. F. Folate Metabolism and Requirements. *J. Nutr.* **1999**, *129* (4), 779–782. https://doi.org/10.1093/jn/129.4.779.

(24) Yuthavong, Y.; Kamchonwongpaisan, S.; Leartsakulpanich, U.; Chitnumsub, P. Folate Metabolism as a Source of Molecular Targets for Antimalarials. *Future Microbiol* **2006**, *1* (1), 113–125. https://doi.org/10.2217/17460913.1.1.113.

(25) Zheng, Y.; Cantley, L. C. Toward a Better Understanding of Folate Metabolism in Health and Disease. *J. Exp. Med.* **2019**, *216* (2), 253–266. https://doi.org/10.1084/jem.20181965.

(26) Hyde, J. E. Exploring the Folate Pathway in Plasmodium Falciparum. *Acta. Trop.* **2005**, *94* (3), 191–206. https://doi.org/10.1016/j.actatropica.2005.04.002.

(27) Liu, C. T.; Hanoian, P.; French, J. B.; Pringle, T. H.; Hammes-Schiffer, S.; Benkovic, S. J. Functional Significance of Evolving Protein Sequence in Dihydrofolate Reductase from Bacteria to Humans. *Proc. Natl. Acad. Sci.* **2013**, *110* (25), 10159–10164. https://doi.org/10.1073/pnas.1307130110.

(28) Volpato, J. P.; Yachnin, B. J.; Blanchet, J.; Guerrero, V.; Poulin, L.; Fossati, E.; Berghuis, A. M.; Pelletier, J. N. Multiple Conformers in Active Site of Human Dihydrofolate Reductase F31R/Q35E Double Mutant Suggest Structural Basis for Methotrexate Resistance. *J. Biol. Chem.* **2009**, *284* (30), 20079–20089. https://doi.org/10.1074/jbc.M109.018010.

(29) Nzila, A. The Past, Present and Future of Antifolates in the Treatment of Plasmodium Falciparum Infection. *J. Antimicrob. Chemother.* **2006**, *57* (6), 1043–1054. https://doi.org/10.1093/jac/dkl104.

(30) Antony, H.; Parija, S. Antimalarial Drug Resistance: An Overview. *Trop. Parasitol.* **2016**, *6* (1), 30. https://doi.org/10.4103/2229-5070.175081.

(31) Mikomangwa, W. P.; Minzi, O.; Mutagonda, R.; Baraka, V.; Mlugu, E. M.; Aklillu, E.; Kamuhabwa, A. A. R. Effect of Sulfadoxine-Pyrimethamine Doses for Prevention of Malaria during Pregnancy in Hypoendemic Area in Tanzania. *Malar. J.* **2020**, *19* (1), 160. https://doi.org/10.1186/s12936-020-03234-4.

(32) Jiang, T.; Chen, J.; Fu, H.; Wu, K.; Yao, Y.; Eyi, J. U. M.; Matesa, R. A.; Obono, M. M. O.; Du, W.; Tan, H.; Lin, M.; Li, J. High Prevalence of Pfdhfr–Pfdhps Quadruple Mutations Associated with Sulfadoxine–Pyrimethamine Resistance in Plasmodium

Falciparum Isolates from Bioko Island, Equatorial Guinea. *Malar. J.* **2019**, *18* (1), 101. https://doi.org/10.1186/s12936-019-2734-x.

(33) Kohn, K. W. Drugs Against Cancer: Stories of Discovery and the Quest for a Cure. National Cancer Institute Bethesda, Maryland. pp 1-14.

(34) Proguanil. *In LiverTox: Clinical and Research Information on Drug-Induced Liver Injury*; National Institute of Diabetes and Digestive and Kidney Diseases: Bethesda (MD), 2017. https://www.ncbi.nlm.nih.gov/books/NBK548239/ (accessed: 2022-10-25)

(35) Knight, D. J.; Peters, W. The Antimalarial Activity of N-Benzyloxydihydrotriazines. *Ann. Trop. Med. Parasitol.* **1980**, *74* (4), 393–404. https://doi.org/10.1080/00034983.1980.11687360.

(36) Gerum, A. B.; Ulmer, J. E.; Jacobus, D. P.; Jensen, N. P.; Sherman, D. R.; Sibley, C. H. Novel *Saccharomyces Cerevisiae* Screen Identifies WR99210 Analogues That Inhibit *Mycobacterium Tuberculosis* Dihydrofolate Reductase. *Antimicrob. Agents Chemother.* **2002**, *46* (11), 3362–3369. https://doi.org/10.1128/AAC.46.11.3362-3369.2002.

(37) Winstanley, P. A.; Mberu, E. K.; Szwandt, I. S.; Breckenridge, A. M.; Watkins, W. M. In Vitro Activities of Novel Antifolate Drug Combinations against Plasmodium Falciparum and Human Granulocyte CFUs. *Antimicrob. Agents Chemother.* **1995**, *39* (4), 948–952. https://doi.org/10.1128/AAC.39.4.948.

(38) Friesen, J.; Borrmann, S.; Matuschewski, K. Induction of Antimalaria Immunity by Pyrimethamine Prophylaxis during Exposure to Sporozoites Is Curtailed by Parasite Resistance. *Antimicrob. Agents Chemother.* **2011**, *55* (6), 2760–2767. https://doi.org/10.1128/AAC.01717-10.

(39) Falco, E. A.; Goodwin, L. G.; Hitchings, G. H.; Rollo, I. M.; Russell, P. B. 2:4-Diaminopyrimidines-a new series of antimalarials. *Br. J. Pharmacol. Chemother.* **1951**, 6 (2), 185–200. https://doi.org/10.1111/j.1476-5381.1951.tb00634.x.

(40) Somandi, K.; Seanego, T. D.; Dlamini (née Molatsane), T.; Maree, M.; de Koning, C. B.; Vanichtanankul, J.; Rattanajak, R.; Saeyang, T.; Yuthavong, Y.; Kamchonwongpaisan, S.; Rousseau, A. Molecular Docking Studies, Synthesis and Biological Evaluation of Substituted Pyrimidine-2,4-diamines as Inhibitors of

Plasmodium Falciparum Dihydrofolate Reductase. *ChemMedChem* **2022**. https://doi.org/10.1002/cmdc.202200418.

(41) Japrung, D.; Leartsakulpanich, U.; Chusacultanachai, S.; Yuthavong, Y. Conflicting Requirements of *Plasmodium Falciparum* Dihydrofolate Reductase Mutations Conferring Resistance to Pyrimethamine-WR99210 Combination. *Antimicrob. Agents Chemother.* **2007**, *51* (12), 4356–4360. https://doi.org/10.1128/AAC.00577-07.

(42) Yuvaniyama, J.; Chitnumsub, P.; Kamchonwongpaisan, S.; Vanichtanankul, J.; Sirawaraporn, W.; Taylor, P.; Walkinshaw, M. D.; Yuthavong, Y. Insights into Antifolate Resistance from Malarial DHFR-TS Structures. *Nat. Struct. Mol. Biol.* **2003**, *10* (5), 357–365. https://doi.org/10.1038/nsb921.

(43) *Schrödinger Release 2021-1: Induced Fit Docking*; Schrödinger, LLC: New York, 2021. https://www.schrodinger.com (accessed 2022-10-25).

(44) Lourens, A. C. U.; Gravestock, D.; van Zyl, R. L.; Hoppe, H. C.; Kolesnikova, N.; Taweechai, S.; Yuthavong, Y.; Kamchonwongpaisan, S.; Rousseau, A. L. Design, Synthesis and Biological Evaluation of 6-Aryl-1,6-Dihydro-1,3,5-Triazine-2,4-Diamines as Antiplasmodial Antifolates. *Org. Biomol. Chem.* **2016**, *14* (33), 7899–7911. https://doi.org/10.1039/C6OB01350C.

(45) Seanego, T. D.; Klein, H. F.; van Vuuren, N. C. J.; Zyl, R. L. van; Rousseau, A. L. Pyrimidine-2,4-Diamines as Antiplasmodial Antifolates. *Arkivoc* **2020**, *2020* (5), 1–16. https://doi.org/10.24820/ark.5550190.p011.315.

(46) Tse, E. G.; Houston, S. D.; Williams, C. M.; Savage, G. P.; Rendina, L. M.; Hallyburton, I.; Anderson, M.; Sharma, R.; Walker, G. S.; Obach, R. S.; Todd, M. H. Nonclassical Phenyl Bioisosteres as Effective Replacements in a Series of Novel Open-Source Antimalarials. *J. Med. Chem.* **2020**, *63* (20), 11585–11601. https://doi.org/10.1021/acs.jmedchem.0c00746.

(47) Yuvaniyama, J.; Chitnumsub, P.; Kamchonwongpaisan, S.; Vanichtanankul, J.; Sirawaraporn, W.; Taylor, P.; Walkinshaw, M. D.; Yuthavong, Y. Insights into Antifolate Resistance from Malarial DHFR-TS Structures. *Nat. Struct. Mol. Biol.* **2003**, *10* (5), 357–365. https://doi.org/10.1038/nsb921.

(48) Paprocki, D.; Madej, A.; Koszelewski, D.; Brodzka, A.; Ostaszewski, R. Multicomponent Reactions Accelerated by Aqueous Micelles. *Front. Chem.* **2018**, *6*. https://doi.org/10.3389/fchem.2018.00502.

(49) Wang, X.; Sathunuru, R.; Melendez, V.; Kozar, M. P.; Lin, A. J. Facile Synthesis of 2,4-Diamino-6-Alkyl- or 6-Aryl-Pyrimidine Derivatives. *J. Heterocycl. Chem.* **2010**, *47* (5), 1056–1061. https://doi.org/10.1002/jhet.419.

(50) Deshmukh, M. B.; Anbhule, P. v; Jadhav, S. D.; Jagtap, S. S.; Patil, D. R.; Salunkhe, S. M.; Sankpal, S. A. A Novel and Environmental Friendly, One-Step Synthesis of 2,6-Diamino-4-Phenyl Pyrimidine-5-Carbonitrile Using Potassium Carbonate in Water. *Indian J. Chem.* **2008**; 47B (5), 792–795.

(51) Raghuvanshi, D. S.; Singh, K. N. Microwave-Assisted One-Pot Synthesis of Functionalized Pyrimidines Using Ionic Liquid. *J. Heterocycl. Chem.* **2011**, *48* (3), 582–585. https://doi.org/10.1002/jhet.540.

(52) Sheibani, H.; Saljoogi, A. S.; Bazgir, A. Three-Component Process for the Synthesis of 4-Amino-5- Pyrimidinecarbonitriles under Thermal Aqueous Conditions or Microwave Irradiation. *Arkivoc* **2008**, *2008* (2), 115–123. https://doi.org/10.3998/ark.5550190.0009.213.

(53) Rong, L.; Han, H.; Gao, L.; Dai, Y.; Cao, M.; Tu, S. Efficient and Facile Synthesis of 2,4-Diamino-6-Arylpyrimidine-5-Carbonitrile Under Solvent-Free Conditions. *Synth. Commun.* **2010**, *40* (4), 504–509. https://doi.org/10.1080/00397910902987784.

(54) Lok, C. M. The 2014 Murray Raney Award Lecture: Architecture and Preparation of Supported Nickel Catalysts. *Top. Catal.* **2014**, *57* (17–20), 1318–1324. https://doi.org/10.1007/s11244-014-0298-0.

(55) Staskun, B.; van Es, T. The Reduction of Nitriles to Aldehydes: Applications of Raney Nickel/Sodium Hypophosphite Monohydrate, of Raney Nickel/Formic Acid, or of Raney(Ni/Al)Alloy/Formic Acid, Respectively. *S. Afr. J. Chem.* **2008**; Vol. 61.

(56) Abdel-Magid, A. F.; Carson, K. G.; Harris, B. D.; Maryanoff, C. A.; Shah, R. D. Reductive Amination of Aldehydes and Ketones with Sodium Triacetoxyborohydride. Studies on Direct and Indirect Reductive Amination Procedures. *J. Org. Chem.* **1996** *61* (11), 3849-3862. doi: 10.1021/jo960057x

(57) Hamada, Y. Role of Pyridines in Medicinal Chemistry and Design of BACE1 Inhibitors Possessing a Pyridine Scaffold. In *Pyridine*; InTech, Ed; Pandey, P. P. 2018. https://doi.org/10.5772/intechopen.74719.

(58) Bruker. *APEX4version 2021.4-1 data collection software which includes SAINT version 8.40B, SADABS-2016/2 and XPREP version 2014/2* Bruker AXS Inc., Madison, Wisconsin, USA.

(59) Dolomanov, O. v.; Bourhis, L. J.; Gildea, R. J.; Howard, J. A. K.; Puschmann, H. *OLEX2* : A Complete Structure Solution, Refinement and Analysis Program. *J. Appl. Crystallogr.* **2009**, *42* (2), 339–341. https://doi.org/10.1107/S0021889808042726.

(60) Sheldrick, G. M. *SHELXT* – Integrated Space-Group and Crystal-Structure Determination. *Acta. Crystallogr. A Found. Adv.* **2015**, *71* (1), 3–8. https://doi.org/10.1107/S2053273314026370.

(61) Sheldrick, G. M. Crystal Structure Refinement with *SHELXL*. *Acta. Crystallogr. C. Struct. Chem.* **2015**, *71* (1), 3–8. https://doi.org/10.1107/S2053229614024218.

(62) Ngwa, C. J.; Rosa, T. F. de A.; Pradel, G. The Biology of Malaria Gametocytes. In *Current Topics in Malaria*; InTech, Ed; Rodriguez-Morales, AJ. 2016. https://doi.org/10.5772/65464.

(63) Abdul-Ghani, R.; Basco, L. K.; Beier, J. C.; Mahdy, M. A. K. Inclusion of Gametocyte Parameters in Anti-Malarial Drug Efficacy Studies: Filling a Neglected Gap Needed for Malaria Elimination. *Malar. J.* **2015**, *14* (1), 413. https://doi.org/10.1186/s12936-015-0936-4.

(64) Gebru, T.; Lalremruata, A.; Kremsner, P. G.; Mordmüller, B.; Held, J. Life-Span of in Vitro Differentiated Plasmodium Falciparum Gametocytes. *Malar. J.* **2017**, *16* (1), 330. https://doi.org/10.1186/s12936-017-1986-6.

(65) Delves, M. J.; Ruecker, A.; Straschil, U.; Lelièvre, J.; Marques, S.; López-Barragán, M. J.; Herreros, E.; Sinden, R. E. Male and Female Plasmodium Falciparum Mature Gametocytes Show Different Responses to Antimalarial Drugs. *Antimicrob. Agents Chemother.* **2013**, *57* (7), 3268–3274. https://doi.org/10.1128/AAC.00325-13.

(66) Demanga, C. G.; Eng, J. W. L.; Gardiner, D. L.; Roth, A.; Butterworth, A.; Adams, J. H.; Trenholme, K. R.; Dalton, J. P. The Development of Sexual Stage Malaria

Gametocytes in a Wave Bioreactor. *Parasit. Vectors* **2017**, *10* (1), 216. https://doi.org/10.1186/s13071-017-2155-z.

(67) Josling, G. A.; Llinás, M. Commitment Isn't for Everyone. *Trends Parasitol.* **2019**, *35* (6), 381–383. https://doi.org/10.1016/j.pt.2019.03.012.

(68) White, N. J.; Ashley, E. A.; Recht, J.; Delves, M. J.; Ruecker, A.; Smithuis, F. M.; Eziefula, A. C.; Bousema, T.; Drakeley, C.; Chotivanich, K.; Imwong, M.; Pukrittayakamee, S.; Prachumsri, J.; Chu, C.; Andolina, C.; Bancone, G.; Hien, T. T.; Mayxay, M.; Taylor, W. R.; von Seidlein, L.; Price, R. N.; Barnes, K. I.; Djimdé, A.; ter Kuile, F.; Gosling, R.; Chen, I.; Dhorda, M. J.; Stepniewska, K.; Guérin, P.; Woodrow, C. J.; Dondorp, A. M.; Day, N. P.; Nosten, F. H. Assessment of Therapeutic Responses to Gametocytocidal Drugs in Plasmodium Falciparum Malaria. *Malar. J.* **2014**, *13* (1), 483. https://doi.org/10.1186/1475-2875-13-483.

(69) Hart, K. J.; Oberstaller, J.; Walker, M. P.; Minns, A. M.; Kennedy, M. F.; Padykula, I.; Adams, J. H.; Lindner, S. E. Plasmodium Male Gametocyte Development and Transmission Are Critically Regulated by the Two Putative Deadenylases of the CAF1/CCR4/NOT Complex. *PLoS. Pathog.* **2019**, *15* (1), e1007164. https://doi.org/10.1371/journal.ppat.1007164.

(70) Iwanaga, S.; Kaneko, I.; Kato, T.; Yuda, M. Identification of an AP2-Family Protein That Is Critical for Malaria Liver Stage Development. *PLoS. One* **2012**, *7* (11), e47557. https://doi.org/10.1371/journal.pone.0047557.

(71) Tadesse, F. G.; Meerstein-Kessel, L.; Gonçalves, B. P.; Drakeley, C.; Ranford-Cartwright, L.; Bousema, T. Gametocyte Sex Ratio: The Key to Understanding Plasmodium Falciparum Transmission? *Trends Parasitol.* **2019**, *35* (3), 226–238. https://doi.org/10.1016/j.pt.2018.12.001.

(72) Karunajeewa, H. A.; Mueller, I. How Important Is Gametocyte Clearance after Malaria Therapy? *BMC Med.* **2016**, *14* (1), 93. https://doi.org/10.1186/s12916-016-0641-3.

(73) Venugopal, K.; Hentzschel, F.; Valkiūnas, G.; Marti, M. Plasmodium Asexual Growth and Sexual Development in the Haematopoietic Niche of the Host. *Nat. Rev. Microbiol.* **2020**, *18* (3), 177–189. https://doi.org/10.1038/s41579-019-0306-2.

(74) Tremp, A. Z.; Sharma, V.; Carter, V.; Lasonder, E.; Dessens, J. T. LCCL Protein Complex Formation in Plasmodium Is Critically Dependent on LAP1. *Mol. Biochem. Parasitol.* **2017**, *214*, 87–90. https://doi.org/10.1016/j.molbiopara.2017.04.005.

(75) Kongkasuriyachai, D.; Fujioka, H.; Kumar, N. Functional Analysis of Plasmodium Falciparum Parasitophorous Vacuole Membrane Protein (Pfs16) during Gametocytogenesis and Gametogenesis by Targeted Gene Disruption. *Mol. Biochem. Parasitol.* **2004**, *133* (2), 275–285. https://doi.org/10.1016/j.molbiopara.2003.10.014.

(76) Olivieri, A.; Camarda, G.; Bertuccini, L.; van de Vegte-Bolmer, M.; Luty, A. J. F.; Sauerwein, R.; Alano, P. The *Plasmodium Falciparum* Protein Pfg27 Is Dispensable for Gametocyte and Gamete Production, but Contributes to Cell Integrity during Gametocytogenesis. *Mol. Microbiol.* **2009**, *73* (2), 180–193. https://doi.org/10.1111/j.1365-2958.2009.06762.x.

(77) Bennink, S.; Kiesow, M. J.; Pradel, G. The Development of Malaria Parasites in the Mosquito Midgut. *Cell Microbiol.* **2016**, *18* (7), 905–918. https://doi.org/10.1111/cmi.12604.

(78) de Koning-Ward, T. F.; Olivieri, A.; Bertuccini, L.; Hood, A.; Silvestrini, F.; Charvalias, K.; Berzosa Díaz, P.; Camarda, G.; McElwain, T. F.; Papenfuss, T.; Healer, J.; Baldassarri, L.; Crabb, B. S.; Alano, P.; Ranford-Cartwright, L. C. The Role of Osmiophilic Bodies and Pfg377 Expression in Female Gametocyte Emergence and Mosquito Infectivity in the Human Malaria Parasite Plasmodium Falciparum. *Mol. Microbiol.* **2007**, *67* (2), 278–290. https://doi.org/10.1111/j.1365-2958.2007.06039.x.

(79) Silvestrini, F.; Lasonder, E.; Olivieri, A.; Camarda, G.; van Schaijk, B.; Sanchez, M.; Younis Younis, S.; Sauerwein, R.; Alano, P. Protein Export Marks the Early Phase of Gametocytogenesis of the Human Malaria Parasite Plasmodium Falciparum. *Mol. Cell Proteomics* **2010**, *9* (7), 1437–1448. https://doi.org/10.1074/mcp.M900479-MCP200.

(80) Xu, Y.; Qiao, D.; Wen, Y.; Bi, Y.; Chen, Y.; Huang, Z.; Cui, L.; Guo, J.; Cao, Y. PfAP2-G2 Is Associated to Production and Maturation of Gametocytes in Plasmodium Falciparum via Regulating the Expression of PfMDV-1. *Front. Microbiol.* **2021**, *11*. https://doi.org/10.3389/fmicb.2020.631444.

(81) Schwank, S.; Sutherland, C. J.; Drakeley, C. J. Promiscuous Expression of α-Tubulin II in Maturing Male and Female Plasmodium Falciparum Gametocytes. *PLoS. One* **2010**, *5* (12), e14470. https://doi.org/10.1371/journal.pone.0014470.

(82) Hliscs, M.; Millet, C.; Dixon, M. W.; Siden-Kiamos, I.; McMillan, P.; Tilley, L. Organization and Function of an Actin Cytoskeleton in *P Lasmodium Falciparum* Gametocytes. *Cell Microbiol.* **2015**, *17* (2), 207–225. https://doi.org/10.1111/cmi.12359.

(83) Eksi, S.; Williamson, K. C. Male-Specific Expression of the Paralog of Malaria Transmission-Blocking Target Antigen Pfs230, PfB0400w. *Mol. Biochem. Parasitol.* **2002**, *122* (2), 127–130. https://doi.org/10.1016/S0166-6851(02)00091-9.

(84) Dash, M.; Sachdeva, S.; Bansal, A.; Sinha, A. Gametogenesis in Plasmodium: Delving Deeper to Connect the Dots. *Front. Cell Infect. Microbiol.* **2022**, *12*. https://doi.org/10.3389/fcimb.2022.877907.

(85) Gulati, S.; Ekland, E. H.; Ruggles, K. V.; Chan, R. B.; Jayabalasingham, B.; Zhou, B.; Mantel, P.-Y.; Lee, M. C. S.; Spottiswoode, N.; Coburn-Flynn, O.; Hjelmqvist, D.; Worgall, T. S.; Marti, M.; Di Paolo, G.; Fidock, D. A. Profiling the Essential Nature of Lipid Metabolism in Asexual Blood and Gametocyte Stages of Plasmodium Falciparum. *Cell Host Microbe* **2015**, *18* (3), 371–381. https://doi.org/10.1016/j.chom.2015.08.003.

(86) Liu, Z.; Miao, J.; Cui, L. Gametocytogenesis in Malaria Parasite: Commitment, Development and Regulation. *Future Microbiol.* **2011**, *6* (11), 1351–1369. https://doi.org/10.2217/fmb.11.108.

(87) Matthews, H.; Duffy, C. W.; Merrick, C. J. Checks and Balances? DNA Replication and the Cell Cycle in Plasmodium. *Parasit. Vectors* **2018**, *11* (1), 216. https://doi.org/10.1186/s13071-018-2800-1.

(88) Evers, F.; Cabrera-Orefice, A.; Elurbe, D. M.; Kea-te Lindert, M.; Boltryk, S. D.; Voss, T. S.; Huynen, M. A.; Brandt, U.; Kooij, T. W. A. Composition and Stage Dynamics of Mitochondrial Complexes in Plasmodium Falciparum. *Nat. Commun.* **2021**, *12* (1), 3820. https://doi.org/10.1038/s41467-021-23919-x.

(89) Talman, A. M.; Domarle, O.; McKenzie, F.; Ariey, F.; Robert, V. Gametocytogenesis : The Puberty of Plasmodium Falciparum. *Malar. J.* **2004**, *3* (1), 24. https://doi.org/10.1186/1475-2875-3-24.

(90) Jacobsen, L.; Husen, P.; Solov'yov, I. A. Inhibition Mechanism of Antimalarial Drugs Targeting the Cytochrome Bc_1 Complex. *J. Chem. Inf. Model.* **2021**, *61* (3), 1334–1345. https://doi.org/10.1021/acs.jcim.0c01148.

(91) Lalève, A.; Vallières, C.; Golinelli-Cohen, M.-P.; Bouton, C.; Song, Z.; Pawlik, G.; Tindall, S. M.; Avery, S. v.; Clain, J.; Meunier, B. The Antimalarial Drug Primaquine Targets Fe–S Cluster Proteins and Yeast Respiratory Growth. *Redox Biol.* **2016**, *7*, 21–29. https://doi.org/10.1016/j.redox.2015.10.008.

(92) Ruecker, A.; Mathias, D. K.; Straschil, U.; Churcher, T. S.; Dinglasan, R. R.; Leroy, D.; Sinden, R. E.; Delves, M. J. A Male and Female Gametocyte Functional Viability Assay To Identify Biologically Relevant Malaria Transmission-Blocking Drugs. *Antimicrob. Agents Chemother.* **2014**, *58* (12), 7292–7302. https://doi.org/10.1128/AAC.03666-14.

(93) Sun, W.; Tanaka, T. Q.; Magle, C. T.; Huang, W.; Southall, N.; Huang, R.; Dehdashti, S. J.; McKew, J. C.; Williamson, K. C.; Zheng, W. Chemical Signatures and New Drug Targets for Gametocytocidal Drug Development. *Sci. Rep.* **2015**, *4* (1), 3743. https://doi.org/10.1038/srep03743.

(94) Burrows, J. N.; Duparc, S.; Gutteridge, W. E.; Hooft van Huijsduijnen, R.; Kaszubska, W.; Macintyre, F.; Mazzuri, S.; Möhrle, J. J.; Wells, T. N. C. New Developments in Anti-Malarial Target Candidate and Product Profiles. *Malar. J.* **2017**, *16* (1), 26. https://doi.org/10.1186/s12936-016-1675-x.

(95) Kiszewski, A. E. Blocking Plasmodium Falciparum Malaria Transmission with Drugs: The Gametocytocidal and Sporontocidal Properties of Current and Prospective Antimalarials. *Pharmaceuticals* **2010**, *4* (1), 44–68. https://doi.org/10.3390/ph4010044.

(96) Hastings, I. M. Gametocytocidal Activity in Antimalarial Drugs Speeds the Spread of Drug Resistance. *Trop. Med. Int. Health* **2006**, *11* (8), 1206–1217. https://doi.org/10.1111/j.1365-3156.2006.01668.x.

(97) Haston, J. C.; Hwang, J.; Tan, K. R. Guidance for Using Tafenoquine for Prevention and Antirelapse Therapy for Malaria — United States, 2019. *Morb. Mortal. Wkly. Rep.* **2019**, *68* (46), 1062–1068. https://doi.org/10.15585/mmwr.mm6846a4.

(98) Ebstie, Y. A.; Abay, S. M.; Tadesse, W. T.; A.Ejigu, D. Tafenoquine and Its Potential in the Treatment and Relapse Prevention of Plasmodium Vivax Malaria: The Evidence to Date. *Drug Des. Devel. Ther.* **2016**, Vol. 10, 2387–2399. https://doi.org/10.2147/DDDT.S61443.

(99) Stone, W.; Mahamar, A.; Smit, M. J.; Sanogo, K.; Sinaba, Y.; Niambele, S. M.; Sacko, A.; Keita, S.; Dicko, O. M.; Diallo, M.; Maguiraga, S. O.; Samake, S.; Attaher, O.; Lanke, K.; ter Heine, R.; Bradley, J.; McCall, M. B. B.; Issiaka, D.; Traore, S. F.; Bousema, T.; Drakeley, C.; Dicko, A. Single Low-Dose Tafenoquine Combined with Dihydroartemisinin–Piperaquine to Reduce Plasmodium Falciparum Transmission in Ouelessebougou, Mali: A Phase 2, Single-Blind, Randomised Clinical Trial. *Lancet Microbe.* **2022**, *3* (5), e336–e347. https://doi.org/10.1016/S2666-5247(21)00356-6.

(100) Styka, A.; Savitz DA. Assessment of Long-Term Health Effects of Antimalarial Drugs When Used for Prophylaxis. In *National Academies of Sciences, Engineering, and Medicine; Health and Medicine Division; Committee to Review Long-Term Health Effects of Antimalarial Drugs; Board on Population Health and Public Health Practice*; Styka, A., Savitz DA, Eds.; National Academies Press (US): Washington (DC), 2020; Vol. 5.

(101) Gogtay, N.; Kamtekar, K.; Dalvi, S.; Mehta, S.; Chogle, A.; Aigal, U.; Kshirsagar, N. A Randomized, Parallel Study of the Safety and Efficacy of 45 Mg Primaquine versus 75 Mg Bulaquine as Gametocytocidal Agents in Adults with Blood Schizonticide-Responsive Uncomplicated Falciparum Malaria [ISCRTN50134587]. *BMC Infect. Dis.* **2006**, *6* (1), 16. https://doi.org/10.1186/1471-2334-6-16.

(102) Gogtay, N. J.; Kamtekar, K. D.; Dalvi, S. S.; Chogle, A. R.; Aigal, U.; Kshirsagar, N. A. Preliminary Report of the Evaluation of the Gametocytocidal Action of Bulaquine, in Adult Patients with Acute, *Plasmodium Falciparum* Malaria. *Ann. Trop. Med. Parasitol.* **2004**, *98* (5), 525–528. https://doi.org/10.1179/000349804225003541.

(103) Odhiambo, O. C.; Wamakima, H. N.; Magoma, G. N.; Kirira, P. G.; Malala, B. J.; Kimani, F. T.; Muregi, F. W. Efficacy and Safety Evaluation of a Novel Trioxaquine in

the Management of Cerebral Malaria in a Mouse Model. *Malar. J.* **2017**, *16* (1), 268. https://doi.org/10.1186/s12936-017-1917-6.

(104) Czesny, B.; Goshu, S.; Cook, J. L.; Williamson, K. C. The Proteasome Inhibitor Epoxomicin Has Potent *Plasmodium Falciparum* Gametocytocidal Activity. *Antimicrob. Agents Chemother.* **2009**, *53* (10), 4080–4085. https://doi.org/10.1128/AAC.00088-09.

(105) Dicko, A.; Roh, M. E.; Diawara, H.; Mahamar, A.; Soumare, H. M.; Lanke, K.; Bradley, J.; Sanogo, K.; Kone, D. T.; Diarra, K.; Keita, S.; Issiaka, D.; Traore, S. F.; McCulloch, C.; Stone, W. J. R.; Hwang, J.; Müller, O.; Brown, J. M.; Srinivasan, V.; Drakeley, C.; Gosling, R.; Chen, I.; Bousema, T. Efficacy and Safety of Primaquine and Methylene Blue for Prevention of Plasmodium Falciparum Transmission in Mali: A Phase 2, Single-Blind, Randomised Controlled Trial. *Lancet Infect. Dis.* **2018**, *18* (6), 627–639. https://doi.org/10.1016/S1473-3099(18)30044-6.

(106) Wadi, I.; Pillai, C. R.; Anvikar, A. R.; Sinha, A.; Nath, M.; Valecha, N. Methylene Blue Induced Morphological Deformations in Plasmodium Falciparum Gametocytes: Implications for Transmission-Blocking. *Malar. J.* **2018**, *17* (1), 11. https://doi.org/10.1186/s12936-017-2153-9.

(107) Azevedo, R.; Mendes, A. M.; Prudêncio, M. The Impact of Antiretroviral Therapy on Malaria Parasite Transmission. *Front. Microbiol.* **2020**, *10*. https://doi.org/10.3389/fmicb.2019.03048.

(108) Hobbs, C. v.; Tanaka, T. Q.; Muratova, O.; van Vliet, J.; Borkowsky, W.; Williamson, K. C.; Duffy, P. E. HIV Treatments Have Malaria Gametocyte Killing and Transmission Blocking Activity. *J. Infect. Dis.* **2013**, *208* (1), 139–148. https://doi.org/10.1093/infdis/jit132.

(109) Akompong, T.; Eksi, S.; Williamson, K.; Haldar, K. Gametocytocidal Activity and Synergistic Interactions of Riboflavin with Standard Antimalarial Drugs against Growth of *Plasmodium Falciparum* In Vitro. *Antimicrob. Agents Chemother.* **2000**, *44* (11), 3107–3111. https://doi.org/10.1128/AAC.44.11.3107-3111.2000.

(110) Lucantoni, L.; Yerbanga, R. S.; Lupidi, G.; Pasqualini, L.; Esposito, F.; Habluetzel, A. Transmission Blocking Activity of a Standardized Neem (Azadirachta Indica) Seed

Extract on the Rodent Malaria Parasite Plasmodium Berghei in Its Vector Anopheles Stephensi. *Malar. J.* **2010**, *9* (1), 66. https://doi.org/10.1186/1475-2875-9-66.

(111) Braga, T. M.; Rocha, L.; Chung, T. Y.; Oliveira, R. F.; Pinho, C.; Oliveira, A. I.; Morgado, J.; Cruz, A. Biological Activities of Gedunin—A Limonoid from the Meliaceae Family. *Molecules* **2020**, *25* (3), 493. https://doi.org/10.3390/molecules25030493.

(112) Sophia, J.; Kowshik, J.; Dwivedi, A.; Bhutia, S. K.; Manavathi, B.; Mishra, R.; Nagini, S. Nimbolide, a Neem Limonoid Inhibits Cytoprotective Autophagy to Activate Apoptosis via Modulation of the PI3K/Akt/GSK-3β Signalling Pathway in Oral Cancer. *Cell Death Dis.* **2018**, *9* (11), 1087. https://doi.org/10.1038/s41419-018-1126-4.

(113) Roesch, K. R.; Larock, R. C. Synthesis of Isoquinolines and Pyridines by the Palladium- and Copper-Catalyzed Coupling and Cyclization of Terminal Acetylenes. *Org. Lett.* **1999**, *1* (4), 553–556. https://doi.org/10.1021/ol990067v.

(114) Yang, D.; Burugupalli, S.; Daniel, D.; Chen, Y. Microwave-Assisted One-Pot Synthesis of Isoquinolines, Furopyridines, and Thienopyridines by Palladium-Catalyzed Sequential Coupling–Imination–Annulation of 2-Bromoarylaldehydes with Terminal Acetylenes and Ammonium Acetate. *J. Org. Chem.* **2012**, *77* (9), 4466–4472. https://doi.org/10.1021/jo300494a.

(115) Huang, Q.; Hunter, J. A.; Larock, R. C. Synthesis of Isoquinolines and Naphthyridines by Electrophilic Ring Closure of Iminoalkynes. *Org. Lett.* **2001**, *3* (19), 2973–2976. https://doi.org/10.1021/ol010136h.

(116) Chu, H.; Xue, P.; Yu, J.-T.; Cheng, J. Rhodium-Catalyzed Annulation of Primary Benzylamine with α-Diazo Ketone toward Isoquinoline. *J. Org. Chem.* **2016**, *81* (17), 8009–8013. https://doi.org/10.1021/acs.joc.6b01378.

(117) Li, H.; Liao, L.; Zhao, X. Organoselenium-Catalyzed Aza-Wacker Reactions: Efficient Access to Isoquinolinium Imides and an Isoquinoline N-Oxide. *Synlett.* **2019**, *30* (14), 1688–1692. https://doi.org/10.1055/s-0039-1690103.

(118) Tezuka, N.; Shimojo, K.; Hirano, K.; Komagawa, S.; Yoshida, K.; Wang, C.; Miyamoto, K.; Saito, T.; Takita, R.; Uchiyama, M. Direct Hydroxylation and Amination of Arenes

via Deprotonative Cupration. *J. Am. Chem. Soc.* **2016**, *138* (29), 9166–9171. https://doi.org/10.1021/jacs.6b03855.

(119) De Zwart, M. A. H.; Van der Goot, H.; Timmerman, H. Synthesis and Copper-Dependent Antimycoplasmal Activity of 1-Amino-3-(2-Pyridyl)Isoquinoline Derivatives. 1. Amides. *J. Med. Chem.* **1988**, *31* (4), 716–722. https://doi.org/10.1021/jm00399a005.

(120) Long, Y.; She, Z.; Liu, X.; Chen, Y. Synthesis of 1-Aminoisoquinolines by Gold(III)-Mediated Domino Reactions from 2-Alkynylbenzamides and Ammonium Acetate. *J. Org. Chem.* **2013**, *78* (6), 2579–2588. https://doi.org/10.1021/jo302794z.

(121) Feng, J.-B.; Wu, X.-F. Potassium *Tert* -Butoxide-Promoted Synthesis of 1-Aminoisoquinolines from 2-Methylbenzonitriles and Benzonitriles under Catalyst-Free Conditions. *Adv. Synth. Catal.* **2016**, *358* (13), 2179–2185. https://doi.org/10.1002/adsc.201600169.

(122) Leggio, A.; Bagalà, J.; Belsito, E. L.; Comandè, A.; Greco, M.; Liguori, A. Formation of Amides: One-Pot Condensation of Carboxylic Acids and Amines Mediated by TiCl4. *Chem. Cent. J.* **2017**, *11* (1), 87. https://doi.org/10.1186/s13065-017-0318-9.

(123) Sheehan, J. C.; Hess, G. P. A New Method of Forming Peptide Bonds. *J. Am. Chem. Soc.* **1955**, *77* (4), 1067–1068. https://doi.org/10.1021/ja01609a099.

(124) Zhang, L.; Wang, X. jun; Wang, J.; Grinberg, N.; Krishnamurthy, D. K.; Senanayake, C. H. An Improved Method of Amide Synthesis Using Acyl Chlorides. *Tetrahedron Lett.* **2009**, *50* (24), 2964–2966. https://doi.org/10.1016/j.tetlet.2009.03.220.

(125) Quintanilla-Licea, R.; Colunga-Valladares, J.; Caballero-Quintero, A.; Rodríguez-Padilla, C.; Tamez-Guerra, R.; Gómez-Flores, R.; Waksman, N. NMR Detection of Isomers Arising from Restricted Rotation of the C-N Amide Bond of N-Formyl-o-Toluidine and N,N'-Bis-Formyl-o-Tolidine. *Molecules* **2002**, *7* (8), 662–673. https://doi.org/10.3390/70800662.

(126) Cocco, M.; Miglio, G.; Giorgis, M.; Garella, D.; Marini, E.; Costale, A.; Regazzoni, L.; Vistoli, G.; Orioli, M.; Massulaha-Ahmed, R.; Détraz-Durieux, I.; Groslambert, M.; Py, B. F.; Bertinaria, M. Design, Synthesis, and Evaluation of Acrylamide Derivatives as

Direct NLRP3 Inflammasome Inhibitors. *ChemMedChem* **2016**, *11* (16), 1790–1803. https://doi.org/10.1002/cmdc.201600055.

(127) Baucom, K. D.; Jones, S. C.; Roberts, S. W. 1,1′-Carbonyldiimidazole (CDI) Mediated Coupling and Cyclization To Generate [1,2,4]Triazolo[4,3- *a*]Pyridines. *Org. Lett.* **2016**, *18* (3), 560–563. https://doi.org/10.1021/acs.orglett.5b03589.

(128) Usachova, N.; Leitis, G.; Jirgensons, A.; Kalvinsh, I. Synthesis of Hydroxamic Acids by Activation of Carboxylic Acids with N,N'-Carbonyldiimidazole: Exploring the Efficiency of the Method. *Synth. Commun.* **2010**, *40* (6), 927–935. https://doi.org/10.1080/00397910903026723.

(129) Sabatini, M. T.; Boulton, L. T.; Sheppard, T. D. Borate Esters: Simple Catalysts for the Sustainable Synthesis of Complex Amides. *Sci. Adv.* **2017**, *3* (9). https://doi.org/10.1126/sciadv.1701028.